P-08-79

Investigations of post-glacial faulting in the Lansjärv area, northern Sweden

Svensk Kärnbränslehantering AB

November 2008

Svensk Kärnbränslehantering AB
Swedish Nuclear Fuel
and Waste Management Co
Box 250, SE-101 24 Stockholm
Tel +46 8 459 84 00

ISSN 1651-4416
SKB P-08-79

Investigations of post-glacial faulting in the Lansjärv area, northern Sweden

Svensk Kärnbränslehantering AB

November 2008

Förord

I Lansjärv bedrevs under senare delen av 1980-talet och början 1990-talet ett projekt med syfte att klargöra neotektoniska rörelser. En förkastningslinje i Lansjärv undersöktes ingående. Mycket av resultaten finns sammanfattade i SKB:s tekniska rapporter. Denna sammanläggning av arbetsrapporter görs för att göra en del basmaterial refererbart.

Contents

Supplementary investigations of post-glacial faulting in the Lansjärv area, northern Sweden, 1990–1992

Lars O Ericsson (ed)

Roy Stanfors (ed)

May 1993

Contents

ABSTRACT

Post-glacial faults have been recognized in the northern Baltic shield for several decades.

It is important to evaluate whether such neotectonic movements can lead to new fracturing or decisively alter the geohydrological or geohydrochemical situation around a final repository for spent nuclear fuel.

The post-glacial Lansjärv fault was chosen for a interdisciplinary study because of its relative accessibility.

The goals of the study were to assess the mechanisms that caused present day scarps, to clarify the extent of any recent fracturing and to clarify the extent of any ongoing movements. All these objectives were reasonably met through a series of studies, which have been performed by SKB during 1986-1992 in two phases.

This report describes achievements that have been gained during the second phase of the study, mainly comprising seismic refraction, core drilling and displacement measurements at the Molberget fault area. One of the major conclusions is that the Lansjärv post-glacial fault reactivated pre-existing old structures and that the causes of the post-glacial movement is a combination of plate tectonics and deglaciation.

ABSTRACT (in Swedish)

Förmodade postglaciala förkastningar har under de senaste årtiondena beskrivits och undersökts på ett flertal ställen i norra delen av Baltiska skölden.

Ur SKB:s synpunkt är det viktigt att fastställa huruvida neotektoniska rörelser av detta slag kan åstadkomma sprickbildning i hela bergplintar och eventuellt ändra de geohydrologiska eller grundvattenkemiska förhållandena i anslutning till ett slutförvar för använt kärnbränsle.

Lansjärv valdes som undersökningsområde bl a med hänsyn till den relativa lättillgängligheten.

Målet för undersökningarna var i första hand att utvärdera de mekanismer som kan ha orsakat de postglaciala förkastningarna och att fastställa omfattningen av eventuell recent sprickbildning och pågående rörelser längs dessa.

Resultaten av den första etappens fältundersökningar redovisas i en rapport 1989.

I denna rapport redovisas resultat av kompletterande undersökningar som utfördes 1990-1992 främst i anslutning till Molbergsförkastningen.

1. INTRODUCTION

As any extension of the first phase of the Lansjärv study /Bäckblom, Stanfors, 1989/ it was decided to make a more detailed investigation of one of the faults.

In the period 1990-1992 a supplementary investigation programme was performed in connection to the Molberget fault, c. 10 km S of Lansjärv.

A supplementary study of seismically deformed sediments in the Lansjärv area was also carried out.

2. SUPPLEMENTARY INVESTIGATIONS AT THE MOLBERGET FAULT AREA

2.1 SEISMIC REFRACTION SURVEY

In order to prepare for more detailed investigations it was decided to excavate some trenches across the Molberget faults in the near vicinity of the trench earlier described by Lagerbäck. The exact location of the new trenches were based on seismic refraction data.

Four refraction seismic profiles were measured across the fault (Fig. 2.1). The position of the fault scarp was clearly indicated by 10-20 metres wide low-velocity sections in all the profiles, and by depressions in the bedrock surface in profiles 90-03 and 90-04 (Fig. 2.2).

2.2 EXCAVATION OF TRENCHES

Based on the results from the seismic investigation two trenches were excavated across the fault (Fig. 2.3). Later also the trench excavated 1987 was re-excavated in between the two first trenches. The location of the trenches is shown in Figures 2.1 and 2.4. Fotographs from the excavated trenches are shown in Figures 2.3, 2.5-2.11.

2.3 CORE DRILLING

Guided by the results from the excavated trenches that indicated a steeply dipping fracture zone, a core drilling program was set up.

Three boreholes were core drilled across the fault. Borehole KM001 was located at the upper eastern block scarp closely to the trench in Profile 1 and KM002 was located at the downer western block. The boreholes were drilled towards each other with an

overlap and the summarized results from the boreholes showed that the fracture zone strikes N020 and dips 80W. The third core drilled borehole, KM003, located closely to Profile 3 confirmed the orientation of the fracture zone at Molberget (Fig. 2.4).

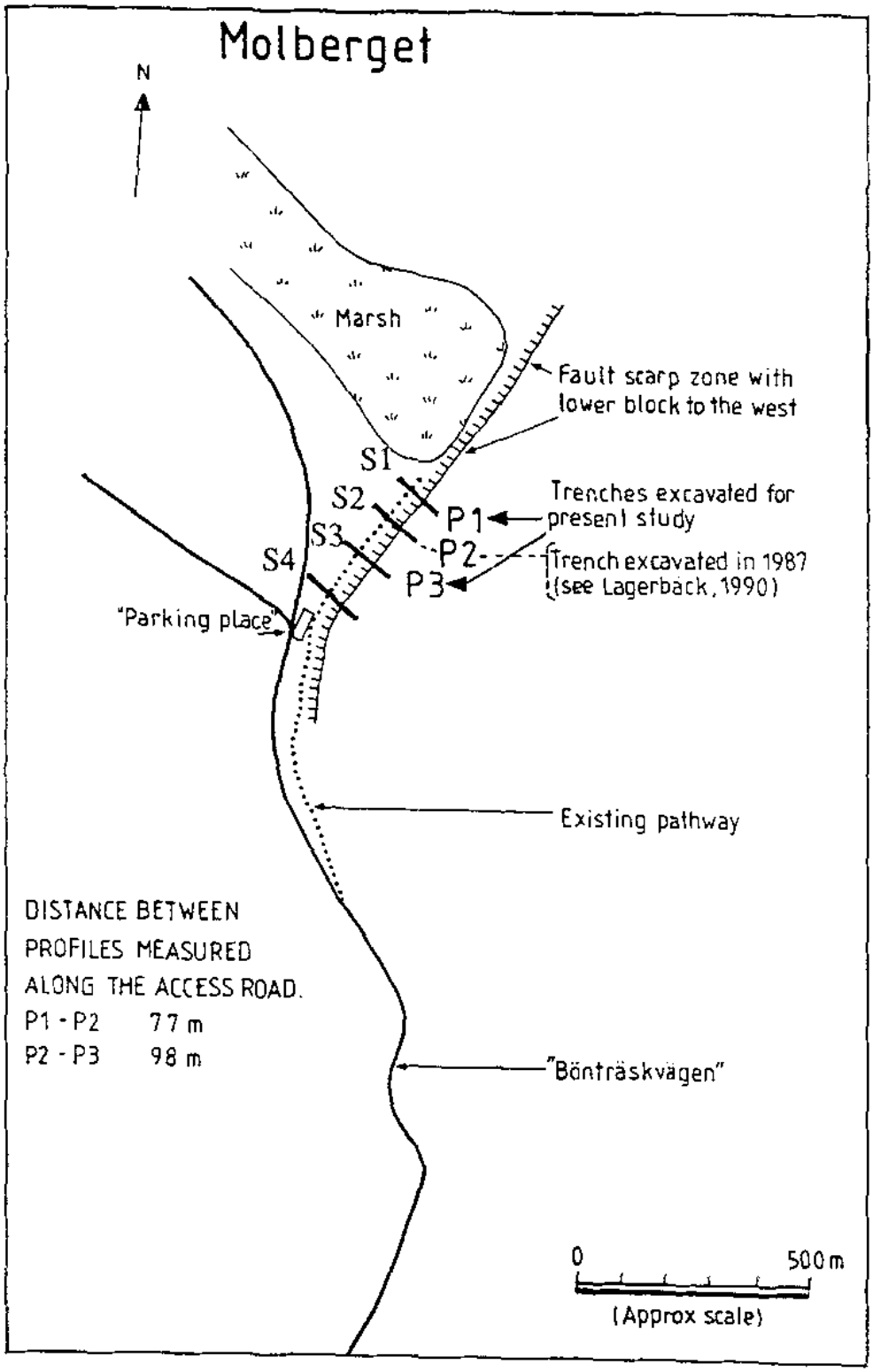

Figure 2.1 *Schematic map showing the localities of trenched profiles P1, P2 and P3 at Molberget in the Lansjärv area. S1 to S4 correspond to performed seismic refraction seismic lines (cf. Fig. 2.2).*

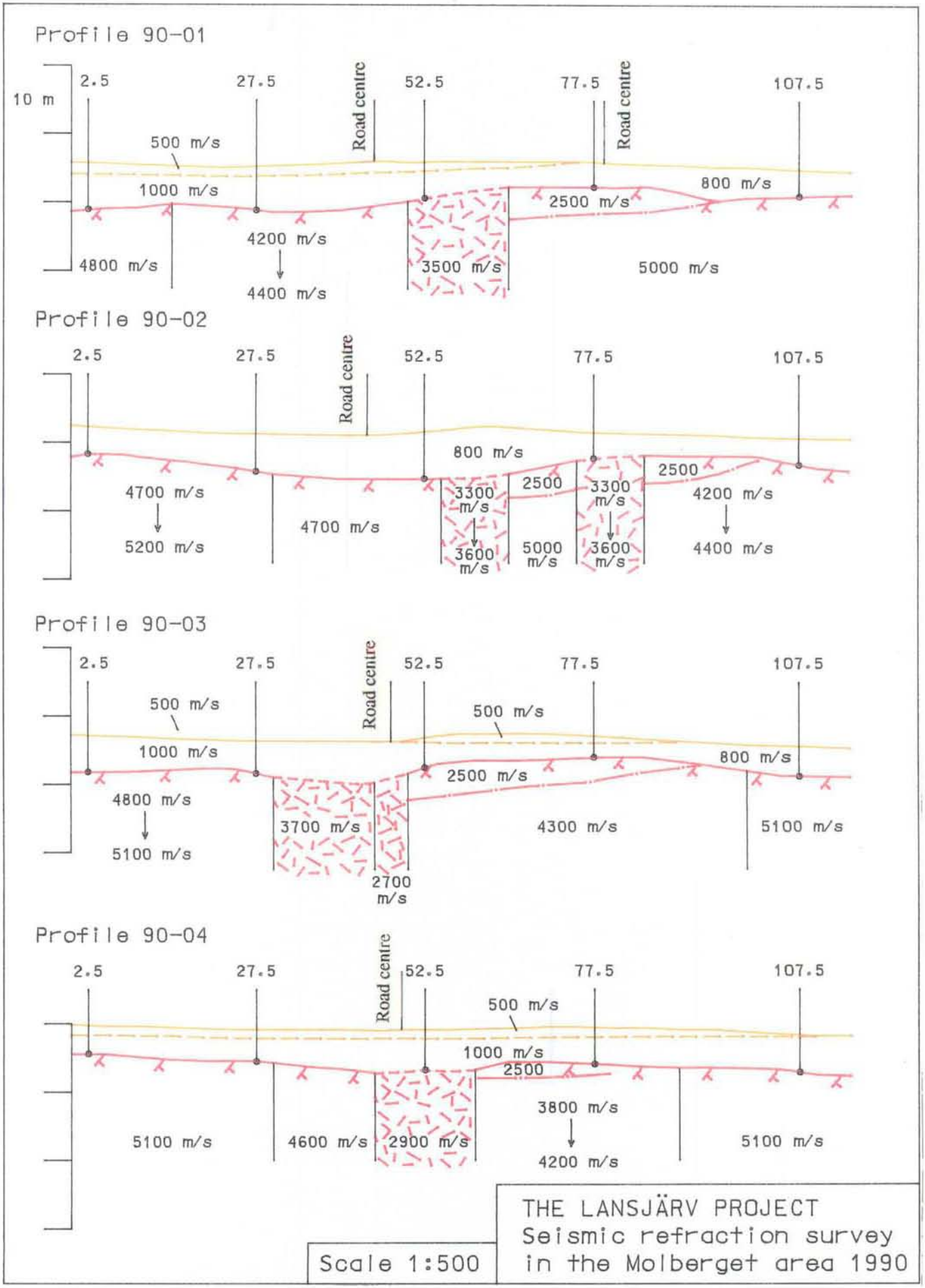

Figure 2.2 ***Seismic refraction surveys S1-S4 (90-01 to 90-04).***

Figure 2.3 *Photograph of trench in profile 1 at Molberget site showing ongoing activities of excavation and cleaning of the bedrock surface. The vertical displacement is 5.7 m. Photo G. Nilsson.*

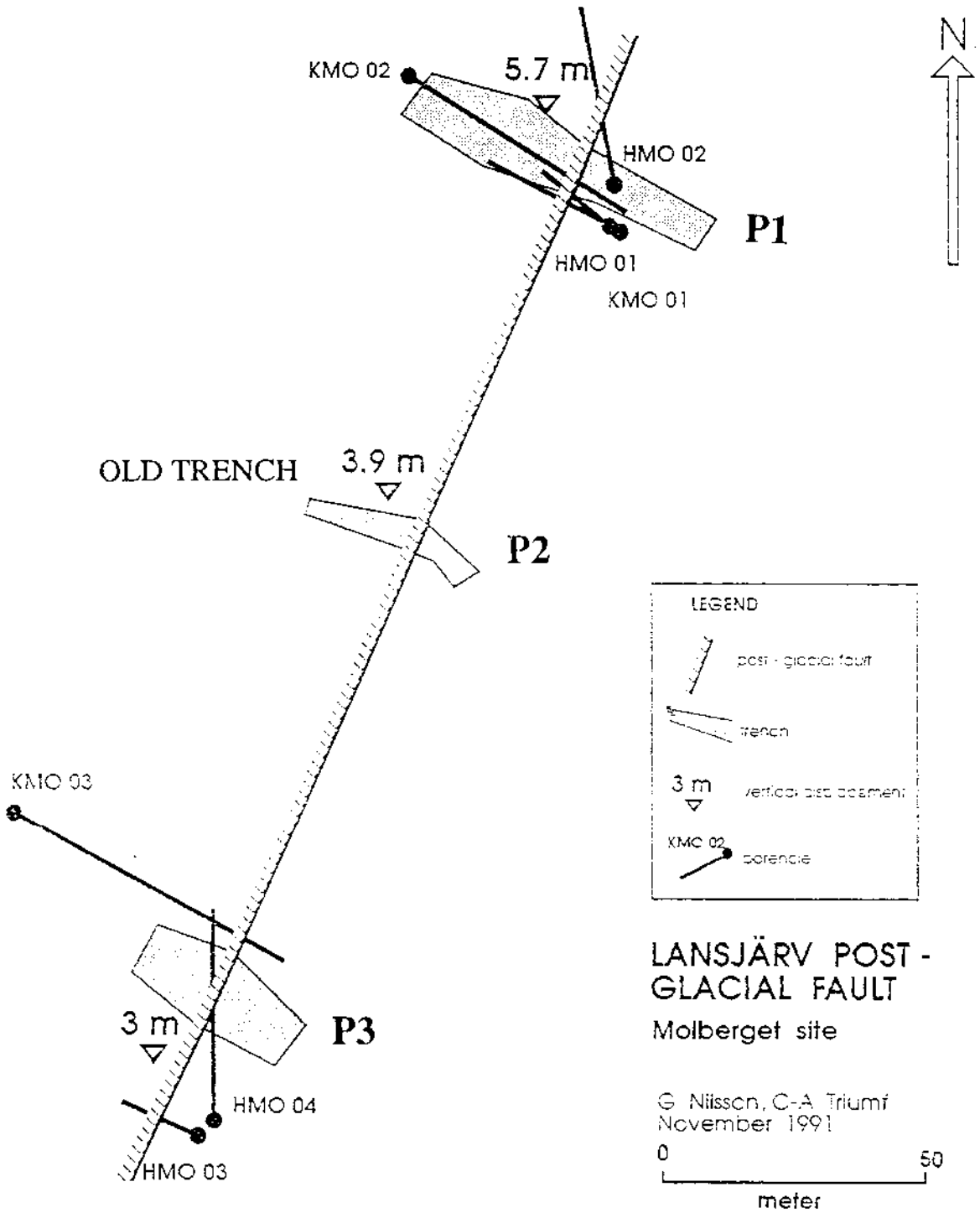

Figure 2.4. Location and outline of trenches and boreholes at Molberget site.

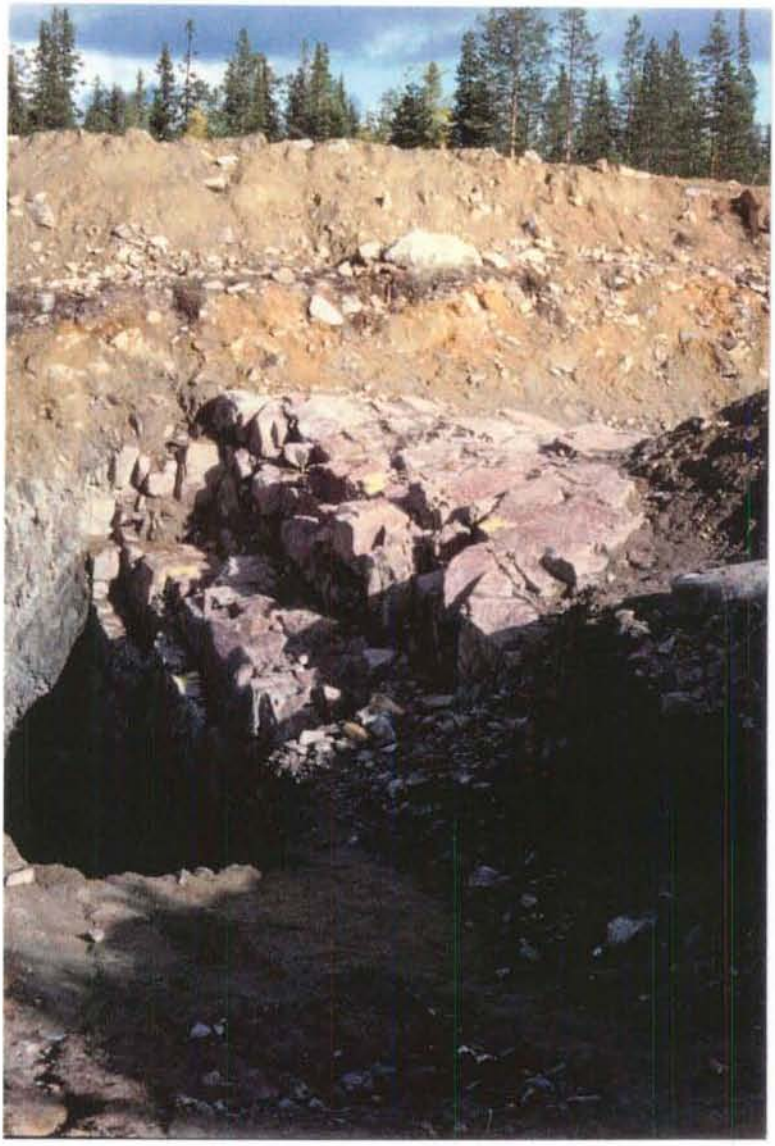

Figure 2.5 *Trench 1. Overview of the bedrock surface on the eastern side of the scarp. Height of the fault scarp is c:a 7 m. Photo R. Munier.*

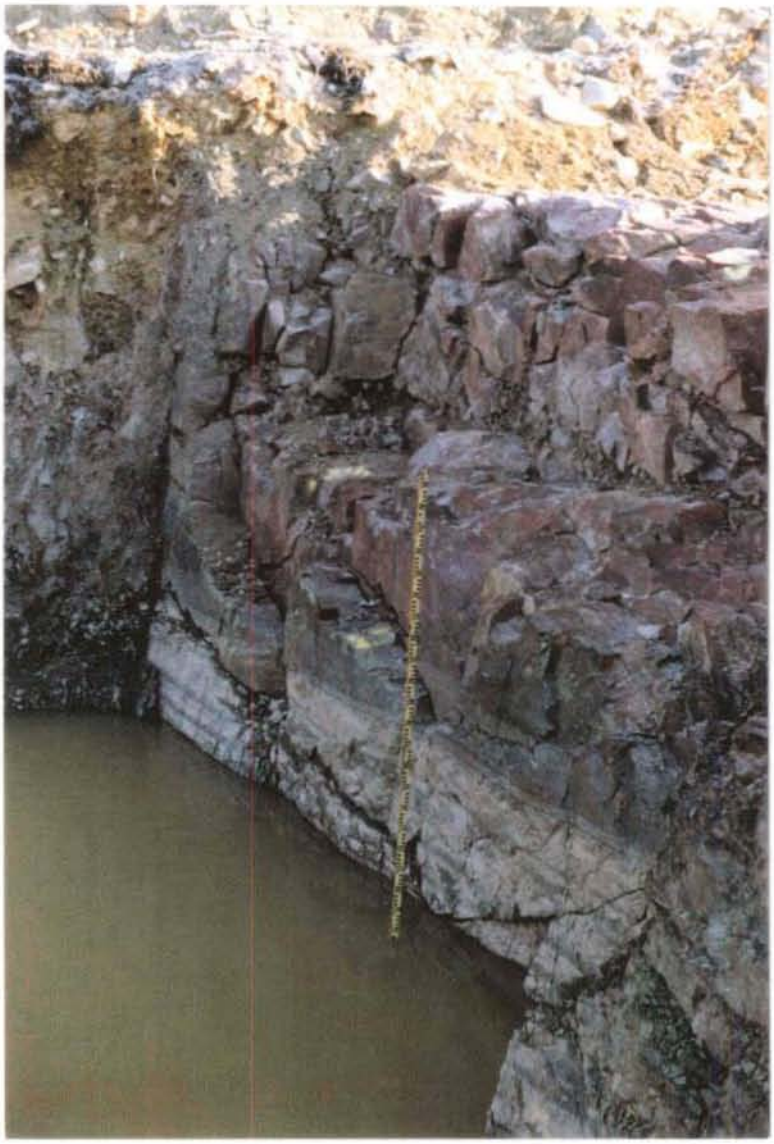

Figure 2.6 *Trench 1. View of the scarp. Photo G. Nilsson.*

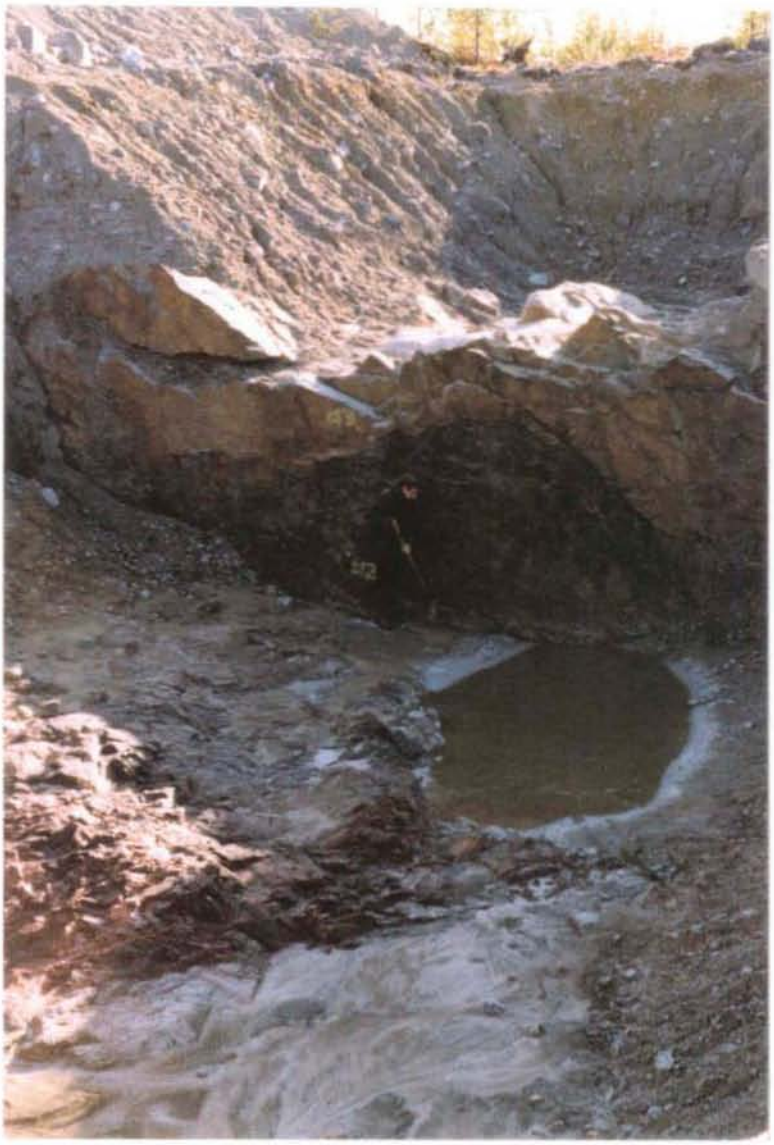

Figure 2.7 *Trench 3. Overview of the scarp. Photo G. Nilsson.*

Figure 2.8 *Trench 3. Photograph showing subhorizontal grooves on the main fault. Small scale subhorizontal slickenlines are superimposed and parallel the pencil. Photo R. Munier.*

Figure 2.9 *Trench 3. Crush zone in granite close to the western downthrown side of the scarp. Photo G. Nilsson.*

Figure 2.10 *Trench 3. Fracture zone close to the fault scarp composed of several subparallel NE-striking faults. Photo R. Munier*

Figure 2.11 *Trench 3. Detail of Fig. 2.10 Ductile precursor of the fault zone. The foliation is intensified an distorted into parallelism to the repeatedly reactivated shear zone. Photo R. Munier.*

After detailed mapping of the trenches and the drill core rock samples were selected for a mineralogical study with the primary purpose to provide information and the thermo-tectonic history of the fault zone.

2.4 MINERALOGICAL STUDIES

The aim of this investigation was to identify and describe textural and mineralogical alterations in the wall rock and within the fracture zone at the Molberget site. The character of the alterations (i.e. low- or high temperature, brittle or ductile deformation structures etc.) provides information on the thermo-tectonic history of the fault zone.

The investigation was performed by Eva-Lena Tullborg, Thomas Eliasson and John Smellie /Eliasson et al, 1991/.

2.5 A PROFILE MOUNT OF SEISMICALLY DEFORMED SEDIMENTS, SOUTHEAST OF MOLBERGET (Tore Påsse)

A profile mount was prepared of the quaternary deposits from one of the trench walls which was visited during the field excursion in Lapland in June 1991. The site chosen for the profile is the southern part of the lowermost trench southeast of Molberget, (Fig. 2.1). This site is very close to the fault (Fig. 2.12-2.13). The height of the profile is 130 cm and the width is 90 cm. The stratigraphy of the section comprises an uppermost layer of horizontally laminated postglacial beach gravel, partly encrusted by iron oxide. Below this there is a stratum of laminated sand and silt which is strongly deformed into convolutions structures. The main part of the cast comprises this stratum. The deformation is due to seismic activity according to Lagerbäck. In the lowermost part of the profile there is a homogeneous layer of silt and a layer of till. Fig. 2.14 shows a photo taken at the site before the work with the cast started.

The procedure for preparing the cast started with cleaning the vertical wall. The profile was then repeatedly sprayed with diluted lacquer. Water soluble lacquer was used with a dilution of 50/50. This step was finished two hours after midnight during the first day of work. This is mentioned just to point out the advantage of field working near the arctic circle during July. When the lacquer was dry a layer of gauze was suspended over the wall and then attached by lacquer. This step was repeated with a thin cloth. After several days

of drying a last layer was attached. This layer was composed of tape reinforced with glass-fibre.

At the after-treatment the cast was glued upon a chip board whereafter the edges were sawed off. The lacquer surface was brushed with a wire-brush in order to bring out the structures. The cast was finally sprayed with a protecting layer of varnish.

2.6 DISPLACEMENT MEASUREMENTS

In order to clarify the extent of any ongoing movements in the Lansjärv area a monitoring programme based on measurements with the Sliding Micrometer Instrument was performed at the Molberget site by JAA AB (Fig. 2.15). The result of this study is presented in the report "Displacement measurements in the post-glacial fault at the Molberget site, Lansjärv area, 1992" by Göran Nilsson (Appendix 1 in this report).

Figure 2.12. *Location of the casts (white) in the southern part of the lowermost trench at Molberget. Photo T. Påsse.*

Figure 2.13. *Location of the casts. The major cast is illustrated in Fig 2.14 prior to performing the cast. Photo T. Påsse.*

Figure 2.14. *Laminated sand and silt strongly deformed into convolution structures. The photo taken prior to the cast work. Photo T. Påsse.*

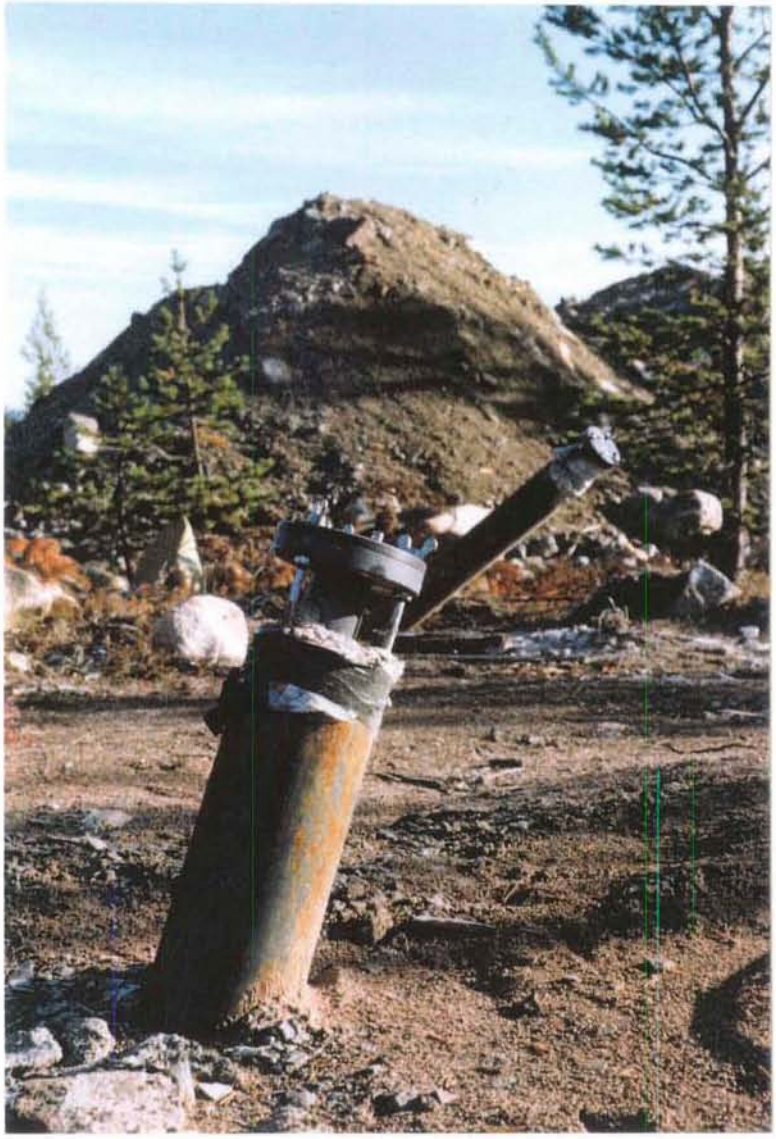

Figure 2.15. *Borehole configuration for the displacement measurements in trench 3. The photo show the 50 m long percussion drilled boreholes HMO03 and HMO04 boreholes in which displacement measurements have been carried out until January -92. Photo G. Nilsson.*

3. SEISMICALLY DEFORMED SEDIMENT IN THE LANSJÄRV AREA

In 1990 Robert Lagerbäck continued his study of the seismically induced deformations occurring in different types of deposits in the Lansjärv area. Trenches or minor pits were dug in different types of sediments and environments and at varying distances from the fault-scarp set. Included in his report are also some sites examined during previous investigations. The report presents an exposition of different sediment deformations met with and attempts to asses which of these are of seismic origin.

The results are presented by Robert Lagerbäck in an internal SKB Technical Report (TR 91-17).

REFERENCES

- **Bäckblom, G., Stanfors, R.**
1989
Interdisciplinary study of post-glacial faulting in the Lansjärv area, Northern Sweden 1986-1988.
SKB Technical Report TR 89-31, Stockholm.

- **Eliasson, T., Smellie, J. and Tullborg, E-L.**
1991.
Mineralogical studies of the "post-glacial" fault exposed at Molberget, Lansjärv area, Northern Sweden. SKB Arbetsrapport 91-14.

- **Lagerbäck, R.**
1991
Seismically deformed sediments in the Lansjärv area, Northern Sweden.
SKB Technical Report TR 91-17, Stockholm.

APPENDIX 1

DISPLACEMENT MEASUREMENTS IN THE POST-GLACIAL FAULT AT THE MOLBERGET SITE, LANSJÄRV AREA, 1991

DISPLACEMENT MEASUREMENTS IN THE POST-GLACIAL FAULT AT THE MOLBERGET SITE, LANSJÄRV AREA

by

GÖRAN NILSSON
JAA AB, Luleå

March 1992

Contents

1. INTRODUCTION

An important study within the programme on bedrock stability is the analysis of possible post-glacial fault, (PGF) movements in the Lansjärv area. The Molberget site, located near the end of a 17 km long trending fault sharp was chosen to investigate possible movements.

During 1990 two trenches were excavated across the fault and three boreholes were core drilled. The location of the trenches are shown in Figure 1.1. Later a third trench was excavated in between the two first. The subvertical bedrock scarp in the profiles varies between 3-5.6 m. The result from the investigation performed shows the major fault to be trending N20°E and dipping approx. 80°W.

One objective of the study of the bedrock stability is "to clarify the extent of any ongoing movements", (Bäckblom and Stanfors, 1989). For this purpose a monitoring programme based on measurements with the Sliding Micrometer instrument was initiated.

A total number of four, ø115 mm in diameter, boreholes were percussion drilled. The four boreholes were arranged in two separate configurations with two boreholes in each configuration to measure the any vertical or horizontal movement in the fault. In three boreholes, HMO02, HMO03 and HMO04 casings with measuring marks were installed. In borehole HMO01 it was not possible to make any installation because of borehole collapse. In borehole HMO02 the casings was installed, however measurements ceased in May-91 due to failure of the casing. The casing might very well have been subjected to gross displacement which resulted in

casing rapture. Borehole HM002 has been disregarded in the further analysis.

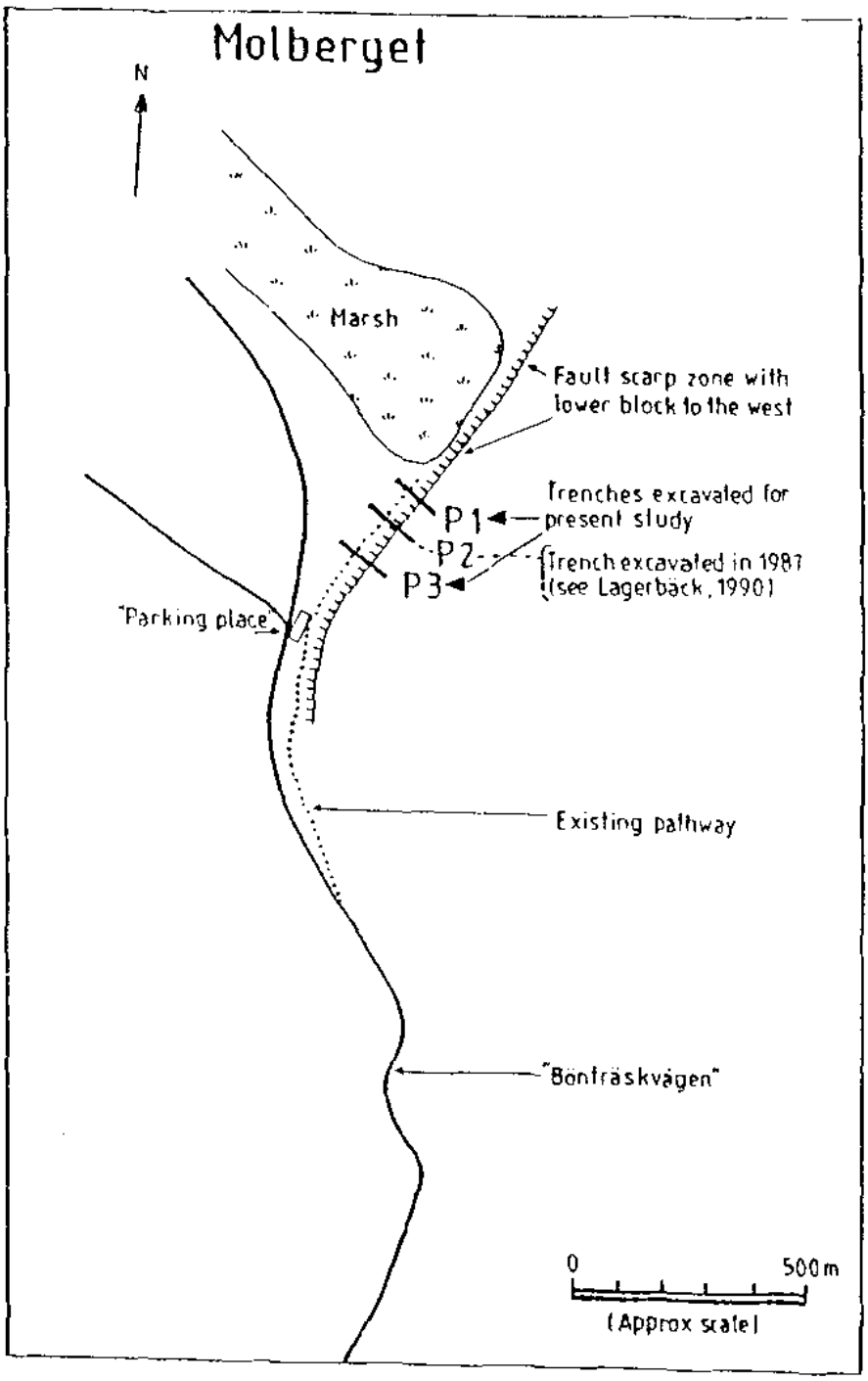

Figure 1.1. Schematic map showing the location of trenched profiles at the Molberget site. The location of the two borehole configurations approximately coincide with trenches P1 and P3.

2 TEST SITE

The fault located at the Molberget site has been identified as a postglacial fault. The differential displacements of the fault is 3-5.6 meters at Molberget. On surface investigations and investigations of the three core drilled boreholes penetrating the zone, show that the zone strike N20° E and dips 80° W. Guided by the results from these investigations the starting position of the four percussion drilled holes were located in the upper (eastern) block of the fault scarp. The borehole configuration makes it possible to measure movements both in the near-vertical as well as near-horizontal direction.

Boreholes HMO01 and HMO02 are located in Profile 1 (P1) and boreholes HMO03 and HMO04 are located in Profile 3 (P3), see also Figure 2.1. The distance between P1 and P3 is approx. 150 meter.

The borehole configurations is schematically illustrated in Figure 2.2.

2.1 Installation

In the boreholes casings with measuring marks for the Sliding Micrometer were installed. The bronze metallic measuring marks were located at 1 meter interval. The casings with the measuring marks were cement grouted in the three boreholes HMO01, HMO03 and HMO04. The measuring marks are located in the following borehole sections:

Borehole HMO 01	5.5 - 47.5
Borehole HMO 03	6.5 - 47.5 m
Borehole HMO 04	11.5- 48.5 m.

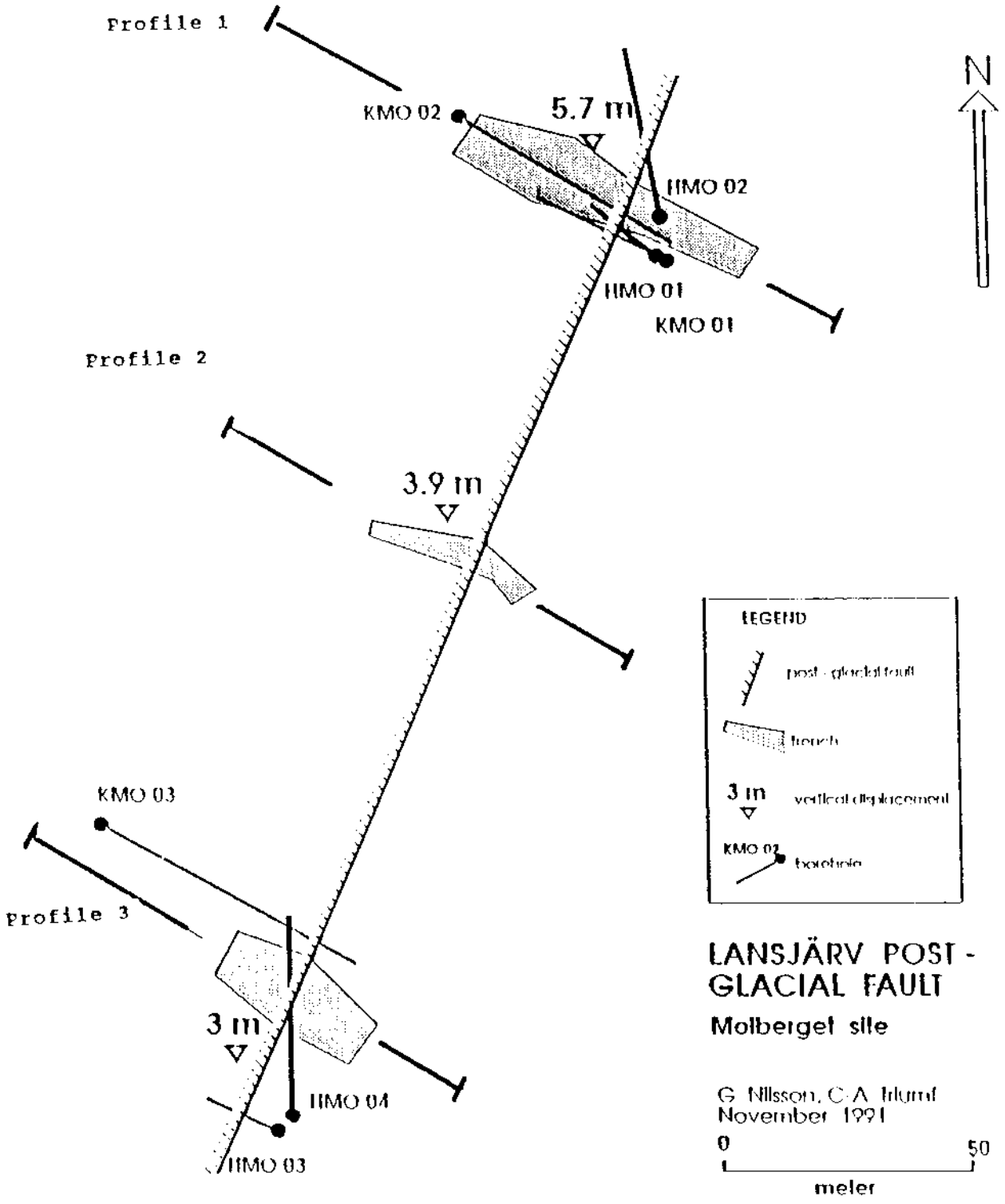

Figure 2.1 Profile 1-3 as well as the location and extent of the trenches at Molberget site.

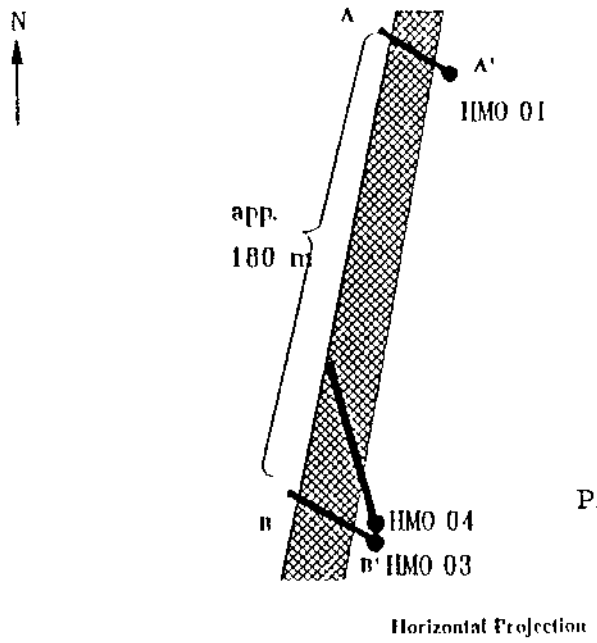

Profile 1.

Profile 3.

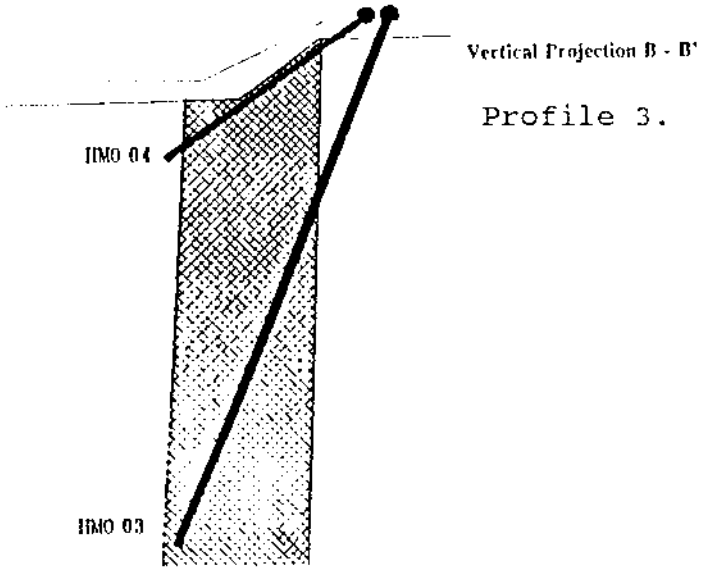

Profile 3.

LANSJÄRV
POST-GLACIAL FAULT

The Molleryet Site
Schematic Map over
Boreholes in the Program
of Displacement Monitoring

Figure 2.2 Schematic map over boreholes in the displacement monitoring program.

3 MEASUREMENT ARRANGEMENT

3.1 Sliding Micrometer

The Sliding Micrometer is a portable high precision instrument which measures the relative displacement between two measuring marks. The measurement direction is coaxial with the borehole direction. The measuring probe and the measuring principle are shown in Figure 3.1. The measuring probe is fitted with two measuring heads, in the form of incomplete spheres, at a spacing of 1 m. The measuring heads are interconnected by an invar steel rod, including a telescopic with the relative positions variable. A spring arrangement ensures that the two halves of the instrument are kept together. The relative, axial movement between the two measuring heads is recorded by a LVDT-arrangement placed inside the probe. A temperature sensor is also fitted inside the probe. The device is designed to be watertight up to external pressures of 1 MPa.

The Sliding Micrometer device includes a portable calibration frame, used to ensure the proper functioning and long term stability of the instrument. The borehole device as well as the calibration frame is designed to be self-compensating with respect to temperature effects.

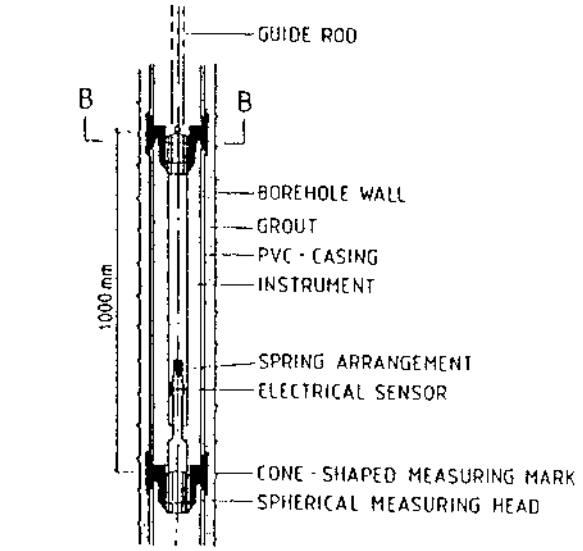

Figure 3.1 Detailed view of the Sliding Micrometer, measuring probe.

3.2 Measurements

The Sliding Micrometer is a manually operated instrument, see Figure 3.2. It requires two operators, one doing the measurement while the other records the readings.

Measurements have been performed systematically since start in November 1990 to January 1992. The results from these measurements are summarized in section 4.

In summary, the measurement cycle included the following steps:

- Instrument calibration prior to measurement.
- Readings were taken every 1 meter interval down the hole.
- Repeated instrument calibration to be compared with the one before measurement to check for instrument error.

The Sliding Micrometer measurements produce readings of the absolute distance between two measuring marks, at a accuracy of ±3 μm. The relative displacement, the change of distance between two measuring marks, is calculated as the difference between two readings.

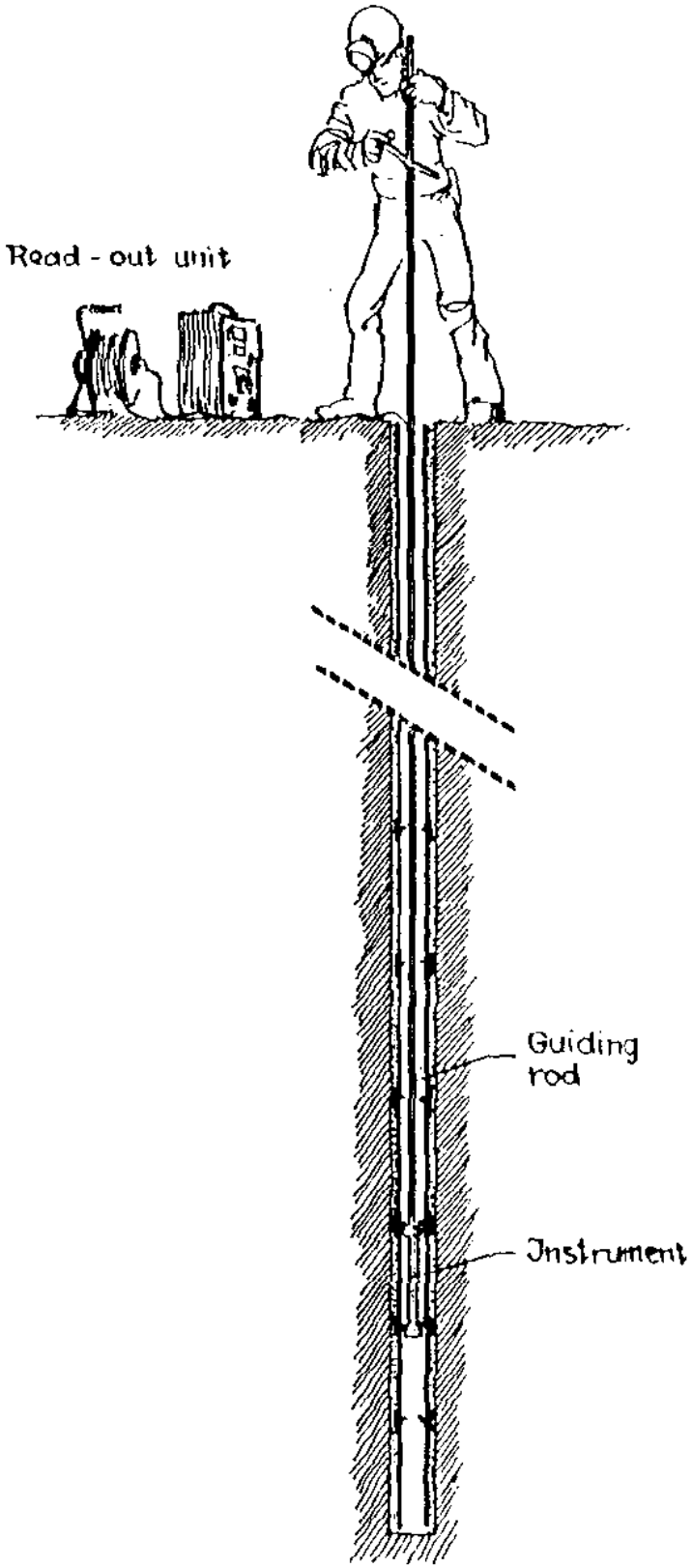

Figure 3.2 Sliding Micrometer measurement technique.

In order to support the measurements taken at one month interval as a part of the PGF study and to investigate any short term variations in readings during one and the same day a series of five repeated measurements were done in borehole HMO04. The measurements were conducted every approximate second hour starting at 8.00 in the morning.

The results of this series of five repeated measurements at two hours interval over one day show a small but significant time related variation in readings, see Figure 3.3. The only phenomenon that offers a possible explanation to this time dependent variations in readings is the tide. It becomes however apparent from this investigation that time related variations in readings over the day, although significant are small compared to the displacement figures recorded over the timeperiod of the PGF-study.

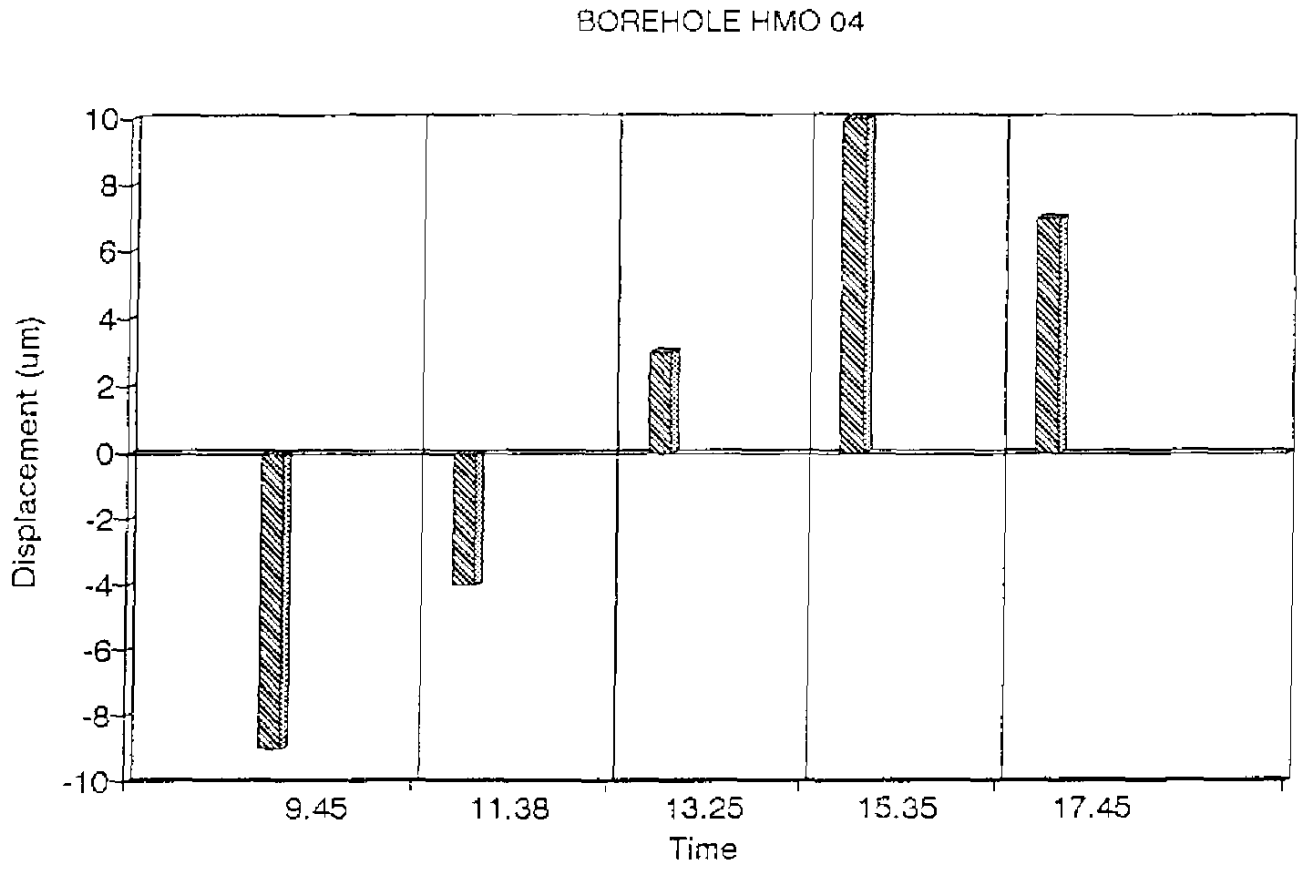

Figure 3.3 Time dependent readings taken in borehole HMO04. Each column represents the reading difference (last measuring mark movement relative first, (near surface) measuring mark) at the time of the measurements relative an initial reading taken at 08.00 am.

4. RESULTS

Displacement measurements were carried out according to the time schedule below. A total number of 13 measurements have been performed since start in November 1990.

Date	**Days**
November 10, 1990	0
December 8, 1990	28
January 10, 1991	61
March 9, 1991	119
April 7, 1991	148
May 25, 1991	196
June 27, 1991	229
July 25, 1991	257
August 28, 1991	291
October 4, 1991	328
November 9, 1991	364
December 14, 1991	399
January 25, 1992	439

4.1 Borehole HMO 03 (near vertical)

Borehole data

Orientation:	320°
Inclination:	70° (from horizontal, positive downwards)
Length:	50 m
Measured section:	6-48 m

The results from the measurements performed in borehole HMO 03 are shown in Figures 4.1-4.2.

The borehole movements in the section 6-9 meter (near ground surface) is shown in Figure 4.1.

As can be seen there is a general trend of expansion, upheave of the rock near the surface however there are variations in the readings over time. The general variation can not easily be explained. However, the drop in readings as of October-91 can possible explained by the fact that the boreholes are located close to the trenches and the field activities in September -91 included filling the trenches with soil. The total volume of the soil masses which were replaced back in the trench near the HMO03 borehole was approx. 3000 m^3. This volume has a weight of about 6000 tons which was moved by a 30-tonne excavator. Measurements elsewhere, not reported here have shown the same effect, a drop in readings as a result of dead weight loading.

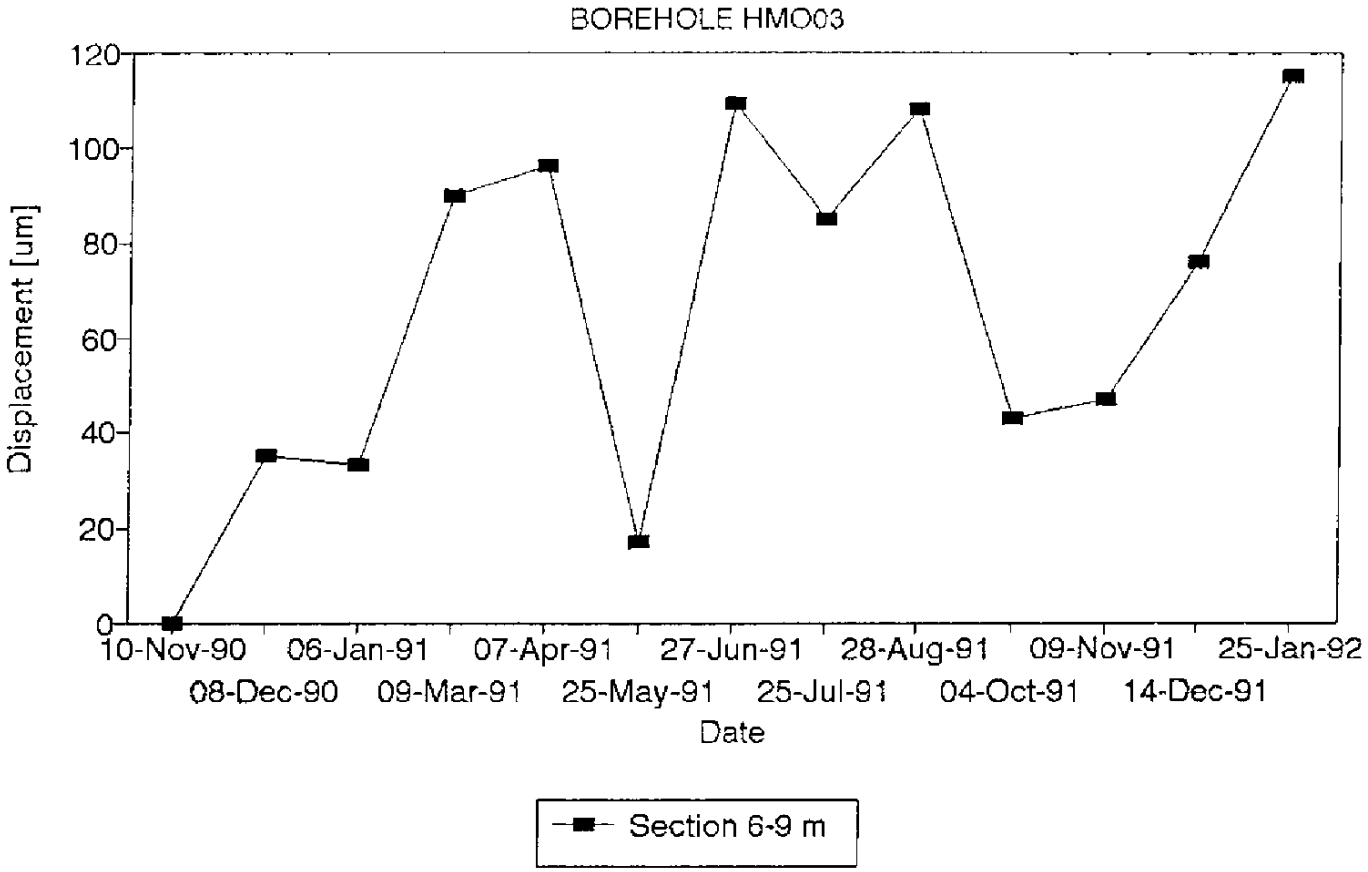

Figure 4.1 Measured displacement versus time, borehole section 6-9 meter, (the displacement of the 9 meter measuring mark relative the 6 meter measuring mark).

In Figure 4.2 the total borehole length has been divided into three sections and the rock displacements have been calculated for the three sections.

Borehole section 6-9 meter has been reviewed and comment upon in Figure 4.1. Section 9-43 meter shows a general trend to increase in length. The final measurement in January-92 indicate a rock expansion of approx. 110 μm.

Section 43-48 meter, located in the lower (western) rockblock towards the borehole end shows a general trend to decrease in length during the measuring period. In January-92 the 5 meter long section has become approx. 290 μm shorter compared with the measurement in November-90.

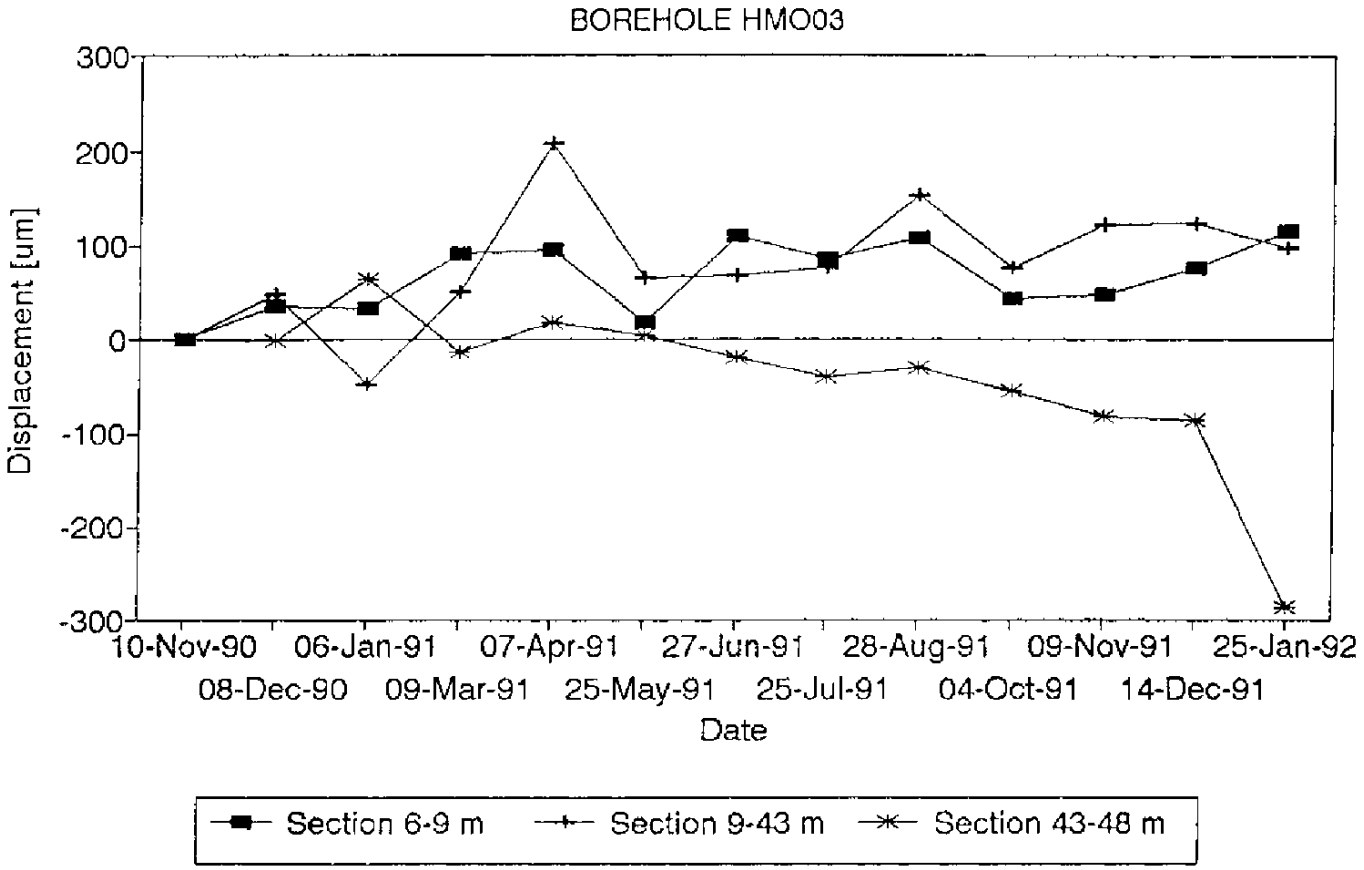

Figure 4.2 Measured displacement versus time, borehole section 6-9 m, 9-43 m and 43-48 m, (the displacement of the 6 m, 9 m and 43 m measuring marks relative the 9 m, 43 m and 48 m measuring marks, respectively).

4.2 Borehole HMO 04 (near horizontal)

Borehole data

Orientation:	350°
Inclination:	30° (from horizontal, positive downwards)
Length:	50 m
Measured section:	11-49 meter

The results from the measurements performed in borehole HMO 04 are shown in Figures 4.3-4.4.

The movements from the upper borehole section 11-13 meter is shown in Figure 4.3.

As can be seen there is a significant increase in borehole length versus time. Since the measurement started in November 1990 the section has expanded 340 μm. As the borehole direction is near horizontal this shows that there is a horizontal expansion of the rock close to the surface, section 11-13 meter in near horizontal borehole.

The borehole section 11-13 meter in borehole HMO 04 has approx. the same vertical elevation as the 6-9 meter section in borehole HMO 03. This means that the rock near the surface is expanding, both in the vertical and horizontal direction.

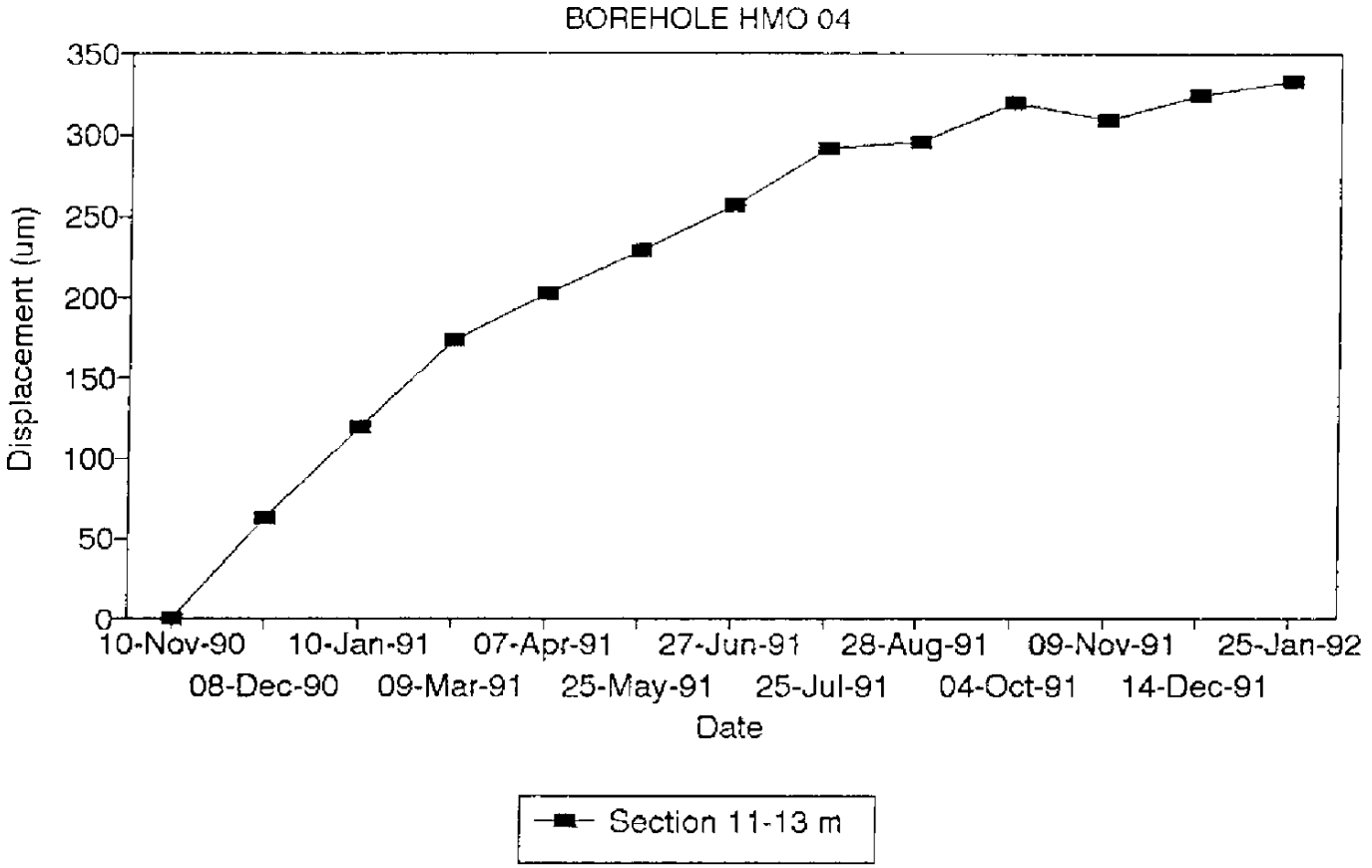

Figure 4.3 Measured displacement versus time, borehole section 11-13 meter (the displacement of the 13 meter measuring mark relative the 11 meter measuring mark).

The borehole movements in the section 13-49 meter is shown in Figure 4.4.

As can be seen the displacement has a cyclic appearance with a periodicity of one year. The maximal expansion seems to take place during winter and in January-92 with a displacement of approx. 250 μm. One year earlier in 1990 the expansion was approx. 200 μm.

Minima over the measuring period is recorded in August-91 with a borehole compression of 160 μm.

The maximum difference is 410 μm between the lowest and highest value recorded.

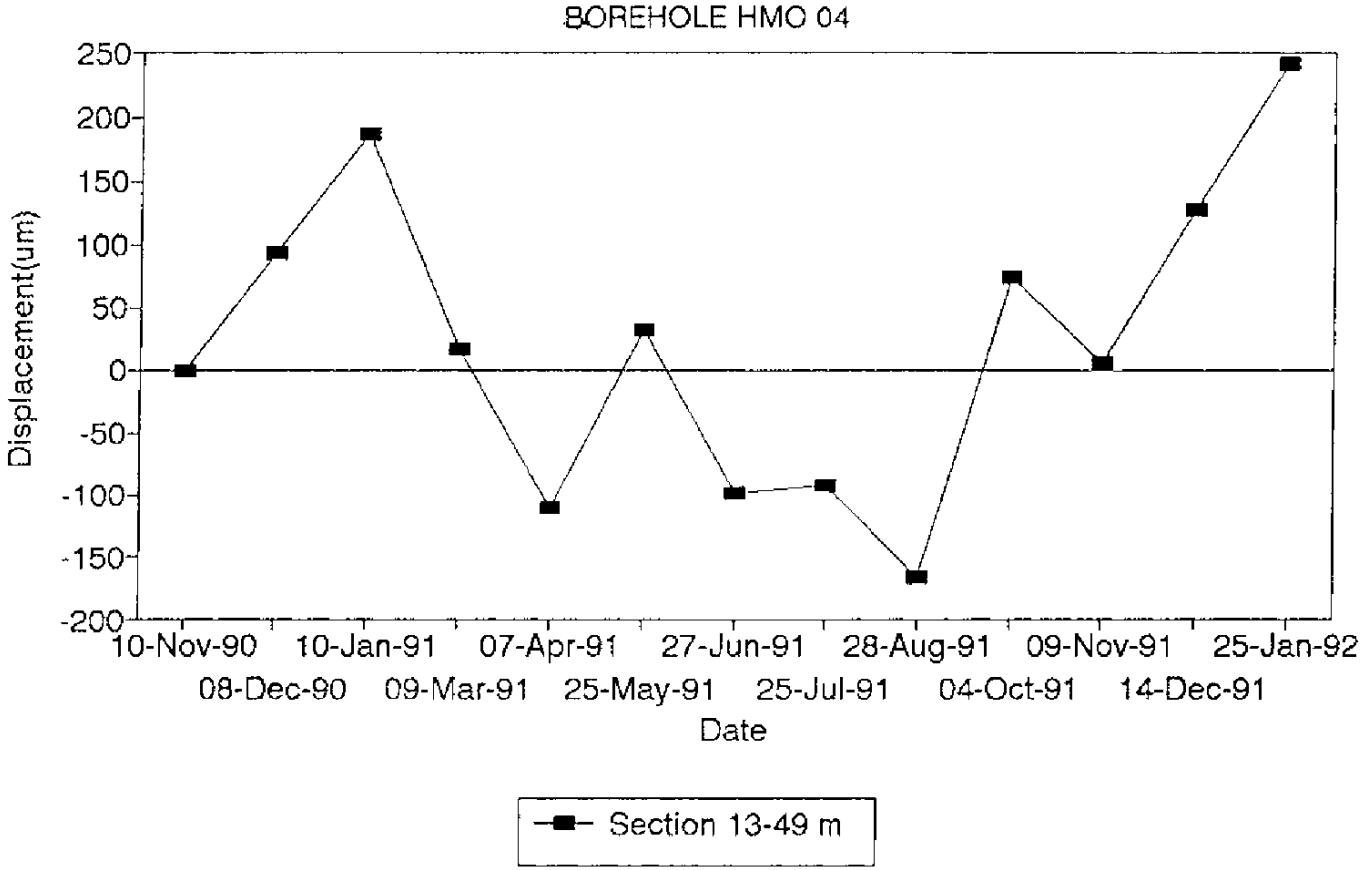

Figure 4.4 Measured displacement versus time, borehole section 13-49 meter (the displacement of the 49 meter measuring mark relative the 13 meter measuring mark).

5. CONCLUSIONS AND RECOMMENDATIONS

In this study measurements of rock movements in a post-glacial fault at the Molberget site have been reported. Between November-90 and January-92 rock displacement measurements were conducted in two boreholes. The result of these measurements can be summarized as follows:

The two boreholes HMO03 and HMO04 represents two out of the three axis in an orthogonal coordinate system. In figures 4.1 and 4.3 it can be seen that the upper part of the rock near surface, an approx. 2 meter thick section is expanding. The maximum vertical expansion is 120 μm, and the maximum horizontal expansion is 330 μm in N-S direction, in this upper 2 meter section.

After excluding the movements in the rock near the surface (the movements in the upper 2 meter thick section) the sum of the total movements varies on a annual cycle in the near horizontal direction. The maximum difference is 410 μm between the lowest and highest value recorded in the near horizontal borehole over the 36 meter long borehole section.

In the near vertical borehole HMO03 there has been a compression of 230 μm in a 5 meter long section located in the western (lower) block of the post-glacial fault, the bottom of the borehole.

It is not possible with today's knowledge and the available data set to exclude the existence of on-going movements in the PGF-fault at the Molberget site. This result is supported by the over one day repeated measurements and the tested and proved accuracy of the measurement system.

Further investigations to resolve the unanswered questions and explain actual displacement data obtained are needed:

* Continue the measurements with the Sliding Micrometer in the existing boreholes, at two months interval for an additional two years.

* Establish of a reference borehole located outside the fault in solid rock, in order to obtain information about any existence of natural rock movements/displacements over time.

* Measurement of the groundwater level variation versus time over a period of one year, in order to establish the site specific variations of the groundwater level in existing core drilled open holes. It is necessary to correlate the groundwater variations with the rock displacement recordings. Measurements should be recorded automatically to get a continuously curve over a period of one year.

6 REFERENCES

Bäckblom, G., Stanfors, R., 1989. Interdisciplinary study of post-glacial faulting in the Lansjärv area, Northern Sweden 1986-1988. TR 89-31

Eliasson, T., Smellie, J., Tullborg, E-T,. 1991. Mineralogical studies of the "post-glacial" fault exposed at Molberget, Lansjärv Area, Northern Sweden. AR 91-14.

Lagerbäck, R., 1990. Late Quaternary faulting and paleoseismicity in northern Fennoscandia, with particular reference to the Lansjärv area, northern Sweden. Geolog. Fören. Stockholm Förh. 112:333-354.

APPENDICES

1. PLOTS FROM 1 M-SECTIONS FROM READINGS IN BOREHOLE HMO03.

2. PLOTS FROM 1 M-SECTIONS FROM READINGS IN BOREHOLE HMO04.

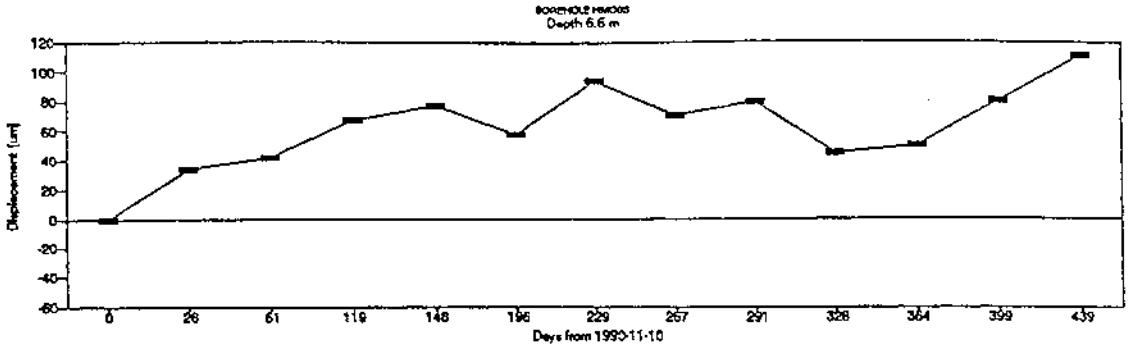
Depth 6.6 m
Displacement [um]
Days from 1990-11-10

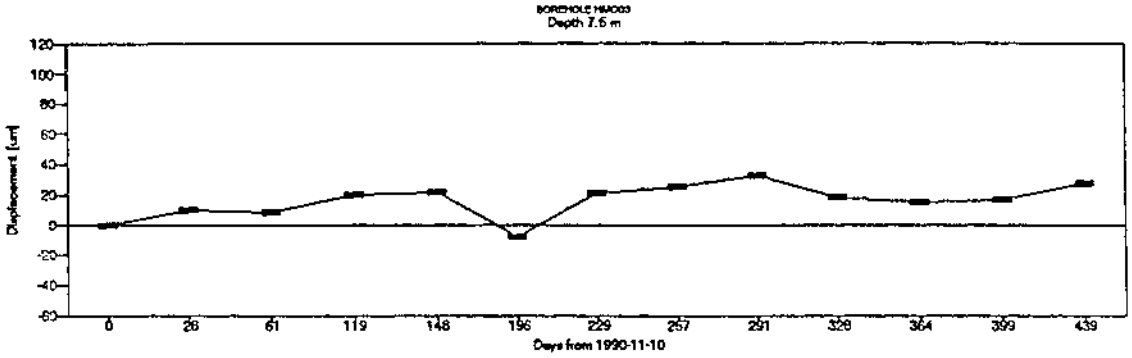
Depth 7.6 m
Displacement [um]
Days from 1990-11-10

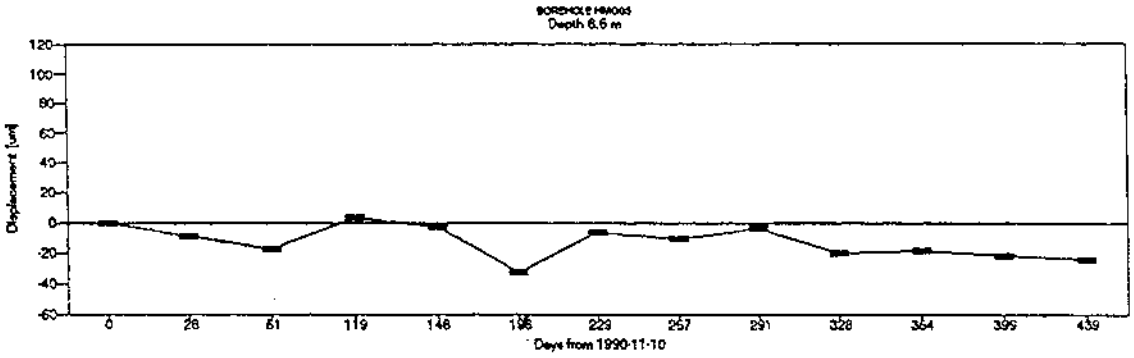
Depth 8.6 m
Displacement [um]
Days from 1990-11-10

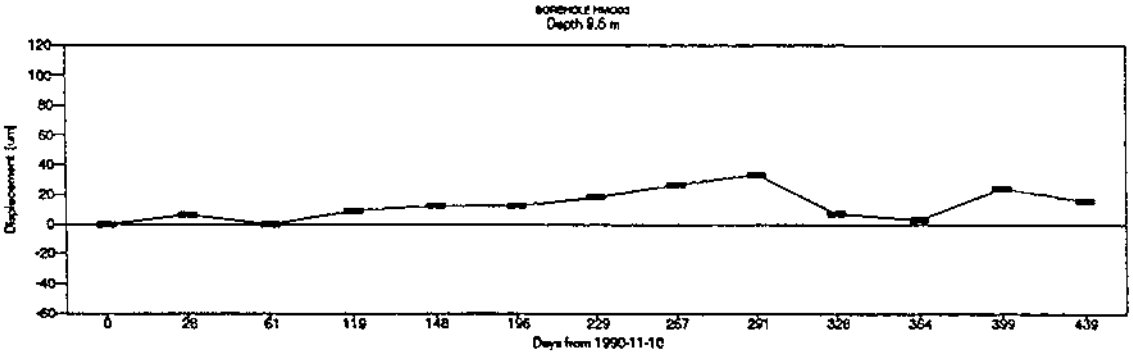
Depth 9.6 m
Displacement [um]
Days from 1990-11-10

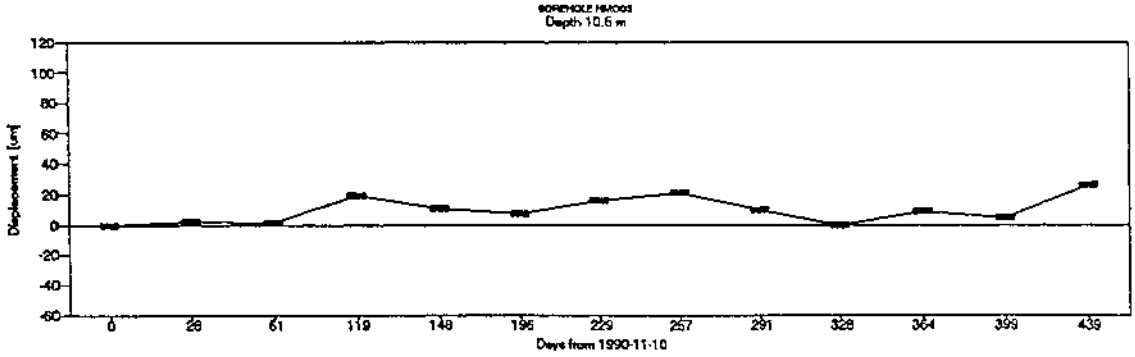
Depth 10.6 m
Displacement [um]
Days from 1990-11-10

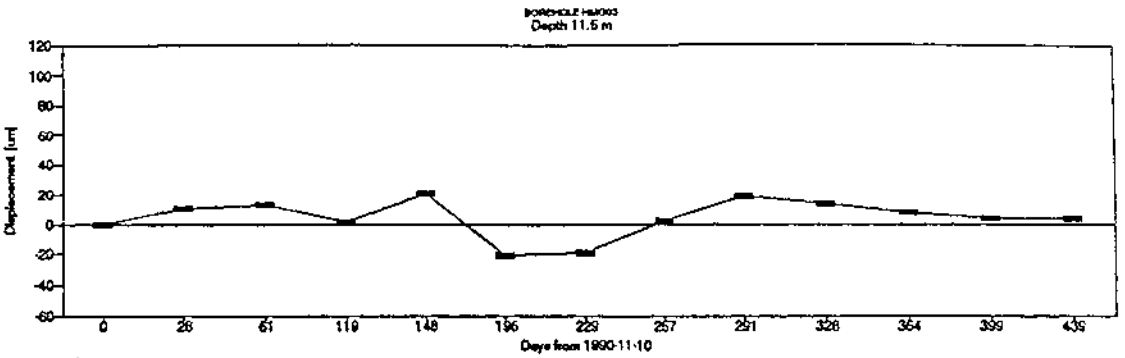
Depth 11.5 m
Displacement [um]
Days from 1990-11-10

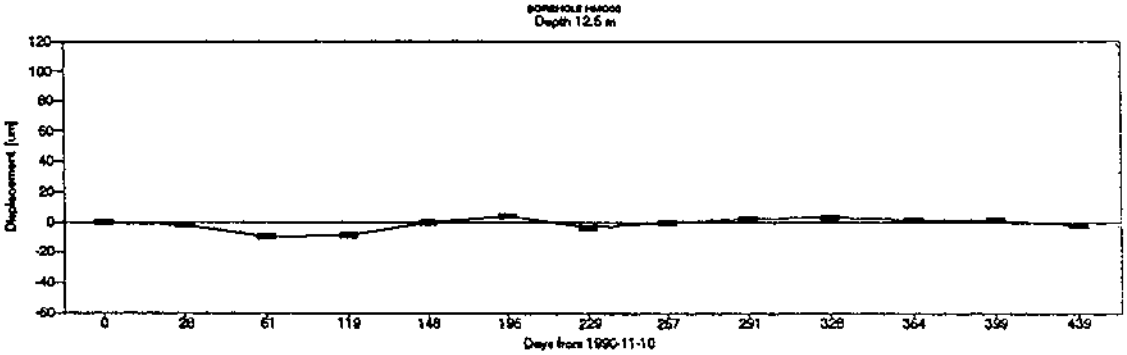
Depth 12.5 m
Displacement [um]
Days from 1990-11-10

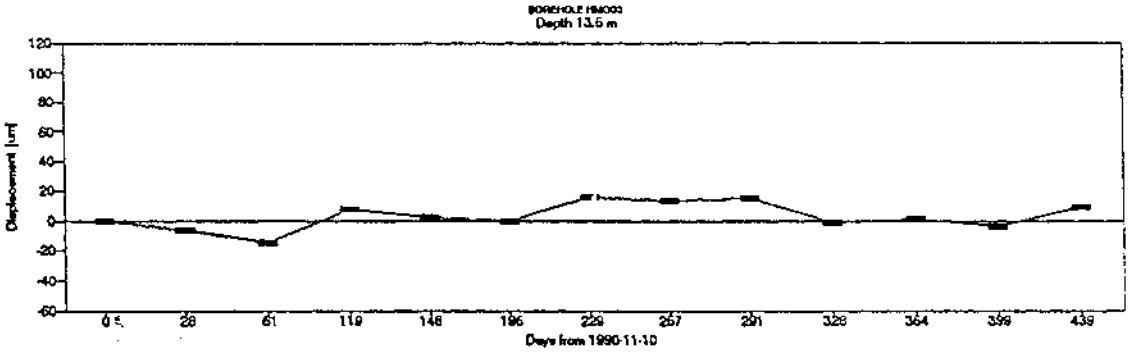
Depth 13.5 m
Displacement [um]
Days from 1990-11-10

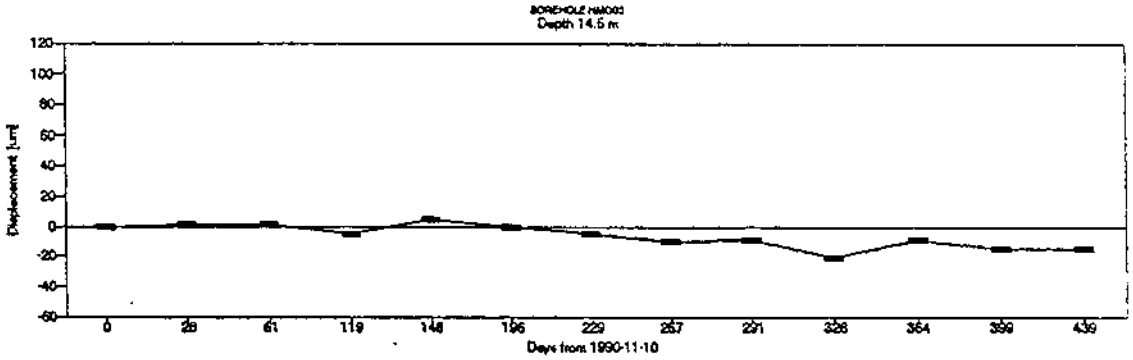
Depth 14.5 m
Displacement [um]
Days from 1990-11-10

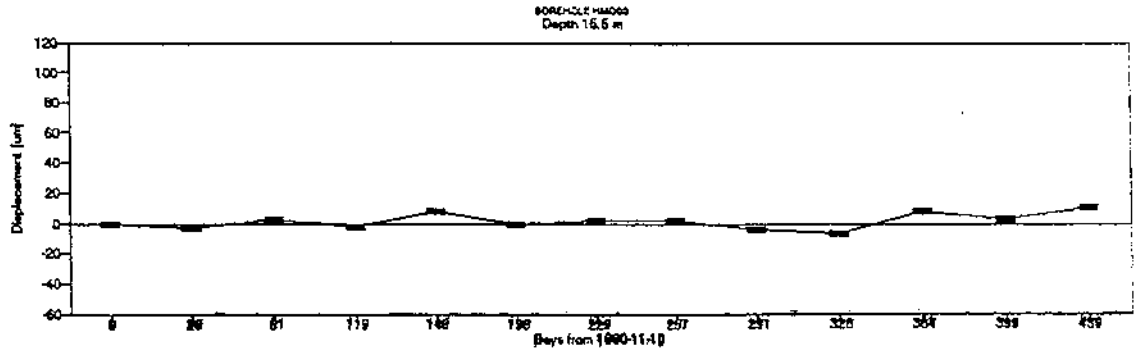
Depth 15.5 m
Displacement [um]
Days from 1990-11-10

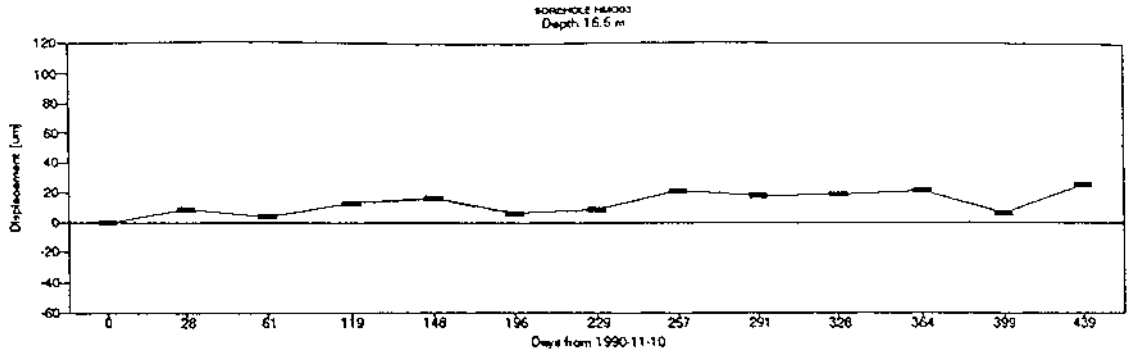
BOREHOLE HM003
Depth 16.6 m
Displacement [um]
Days from 1990-11-10

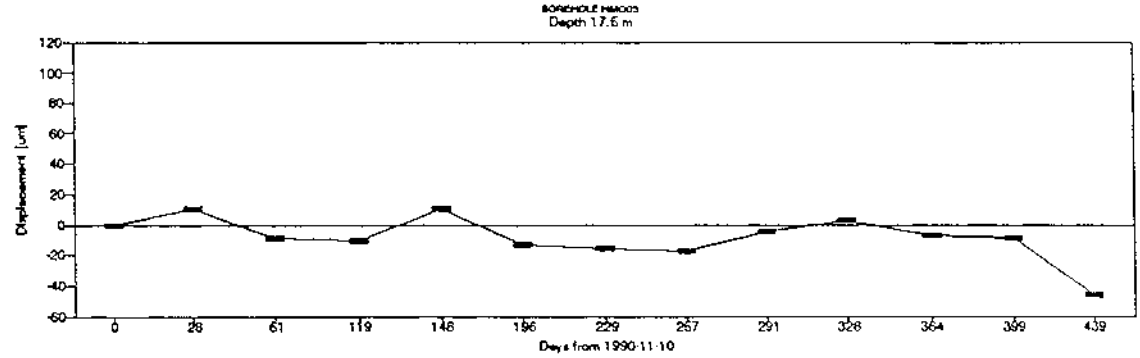
BOREHOLE HM003
Depth 17.6 m
Displacement [um]
Days from 1990-11-10

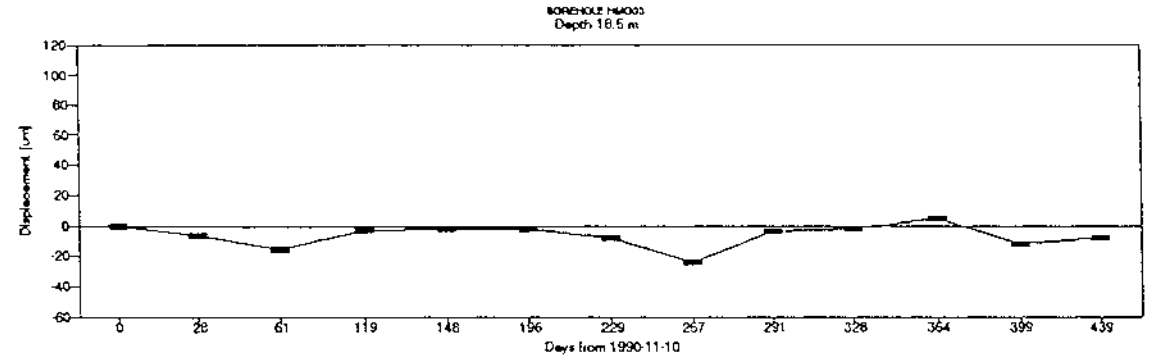
BOREHOLE HM003
Depth 18.6 m
Displacement [um]
Days from 1990-11-10

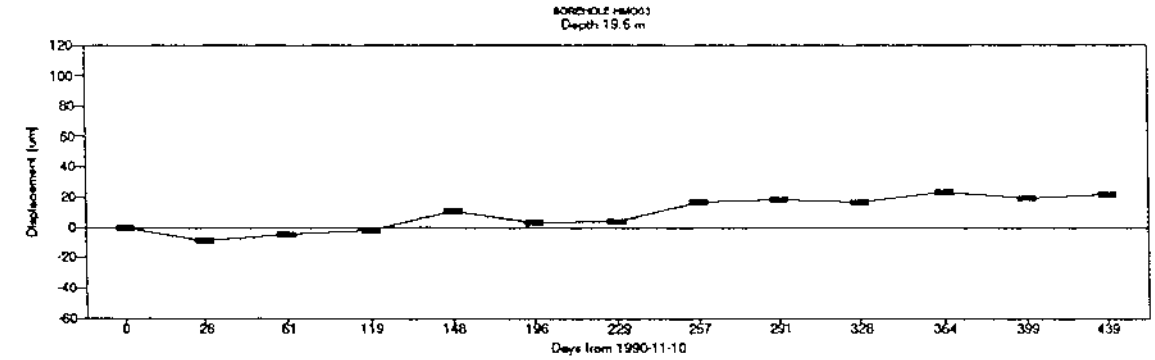
BOREHOLE HM003
Depth 19.6 m
Displacement [um]
Days from 1990-11-10

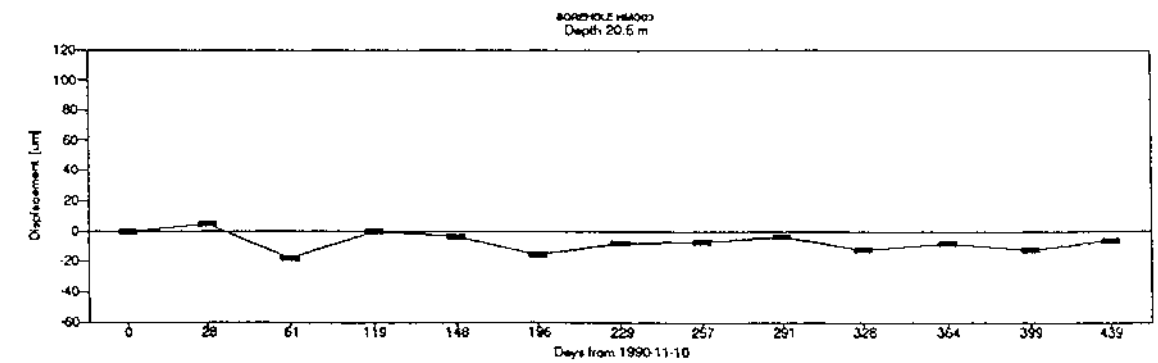
BOREHOLE HM003
Depth 20.6 m
Displacement [um]
Days from 1990-11-10

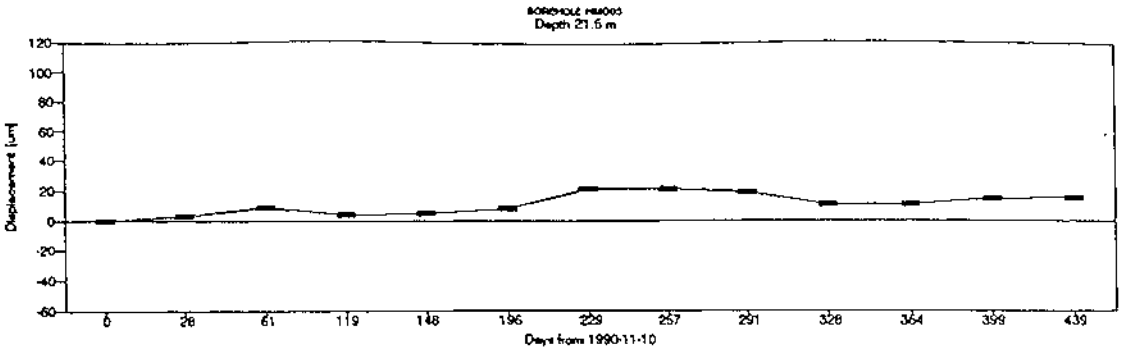
BOREHOLE HM003
Depth 21.5 m
Displacement [um]
120
100
80
60
40
20
0
-20
-40
-60
0
28
61
119
148
196
229
257
291
328
364
399
439
Days from 1990-11-10

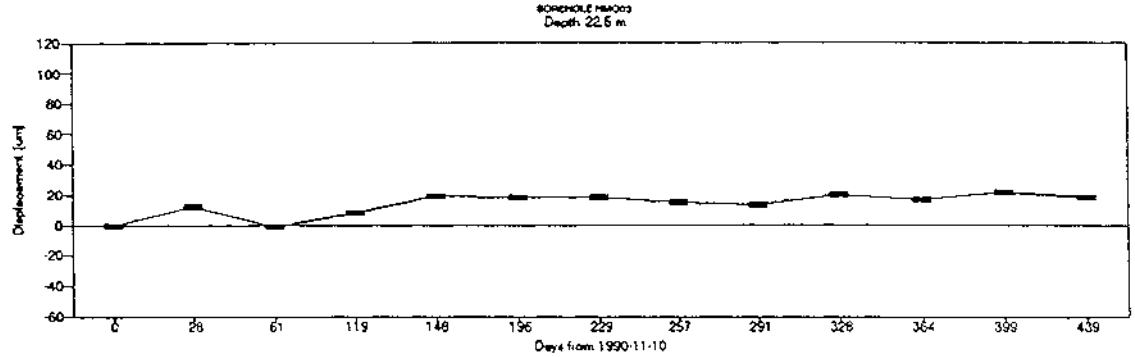
BOREHOLE HM003
Depth 22.5 m
Displacement [um]
120
100
80
60
40
20
0
-20
-40
-60
0
28
61
119
148
196
229
257
291
328
364
399
439
Days from 1990-11-10

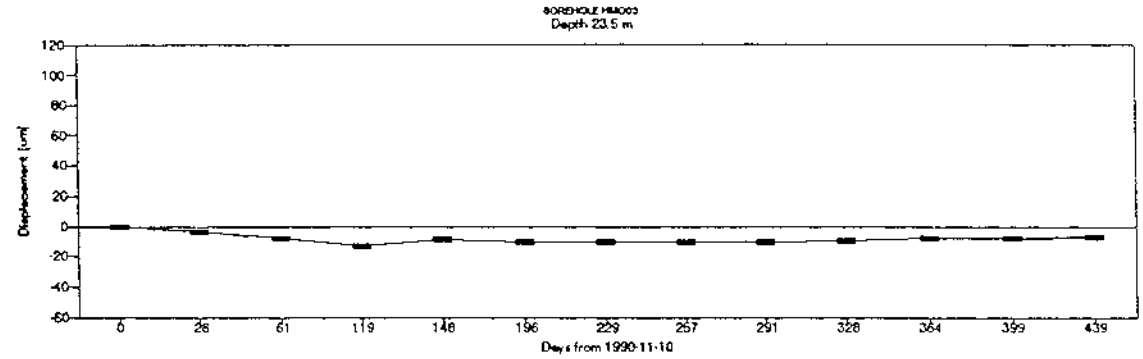
BOREHOLE HM003
Depth 23.5 m
Displacement [um]
120
100
80
60
40
20
0
-20
-40
-60
0
28
61
119
148
196
229
257
291
328
364
399
439
Days from 1990-11-10

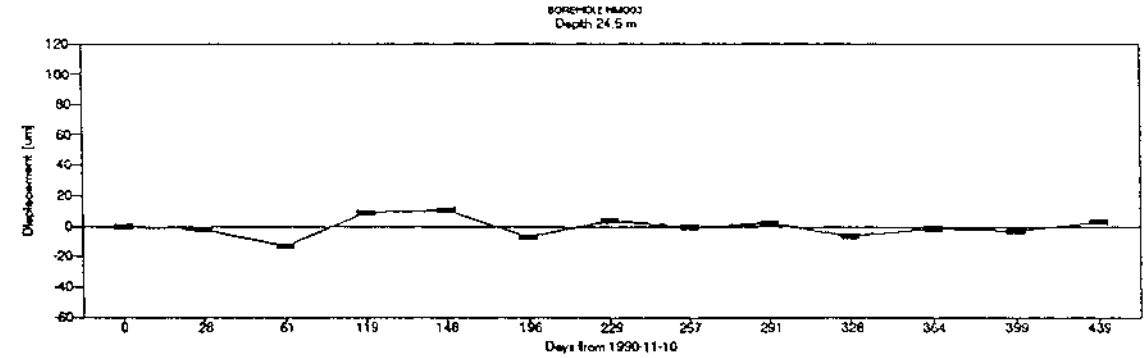
BOREHOLE HM003
Depth 24.5 m
Displacement [um]
120
100
80
60
40
20
0
-20
-40
-60
0
28
61
119
148
196
229
257
291
328
364
399
439
Days from 1990-11-10

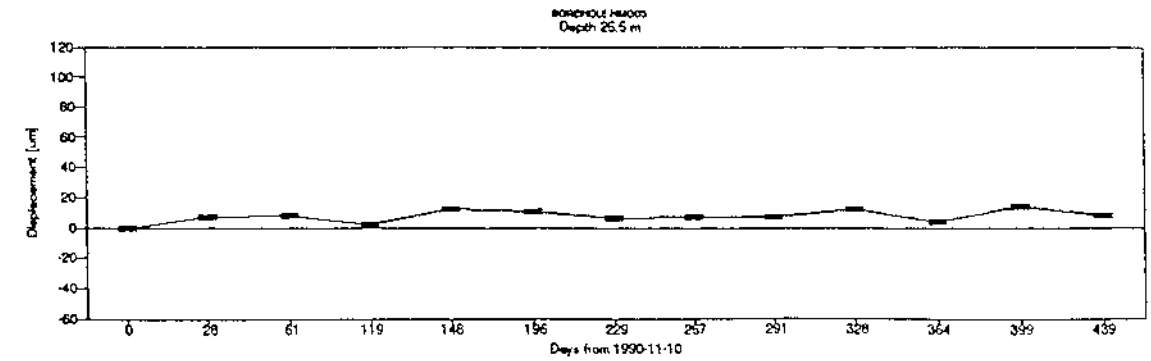
BOREHOLE HM003
Depth 25.5 m
Displacement [um]
120
100
80
60
40
20
0
-20
-40
-60
0
28
61
119
148
196
229
257
291
328
364
399
439
Days from 1990-11-10

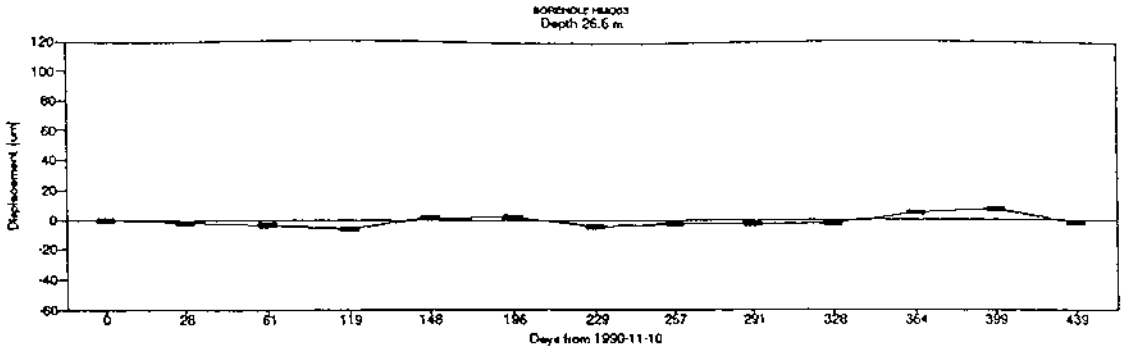
BOREHOLE HM003
Depth 26.6 m
Displacement [um]
Days from 1990-11-10

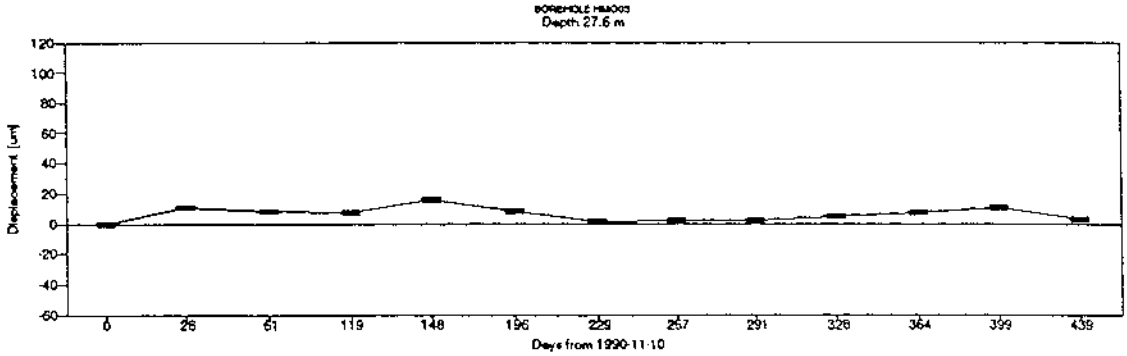
BOREHOLE HM003
Depth 27.6 m
Displacement [um]
Days from 1990-11-10

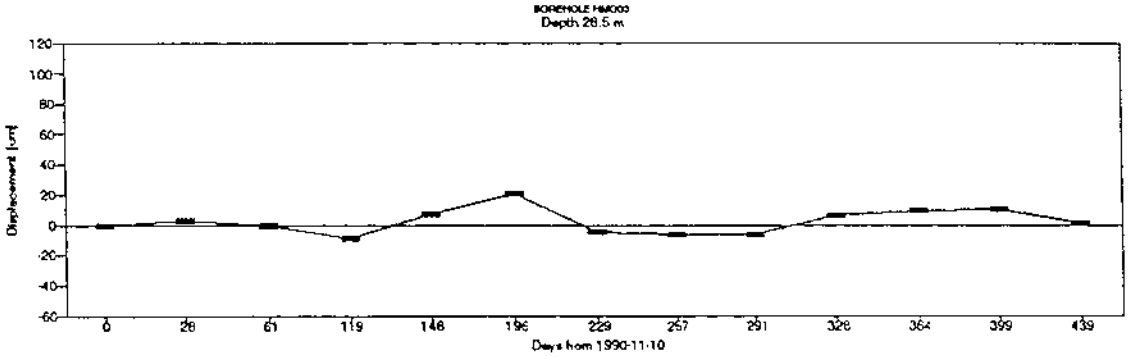
BOREHOLE HM003
Depth 28.5 m
Displacement [um]
Days from 1990-11-10

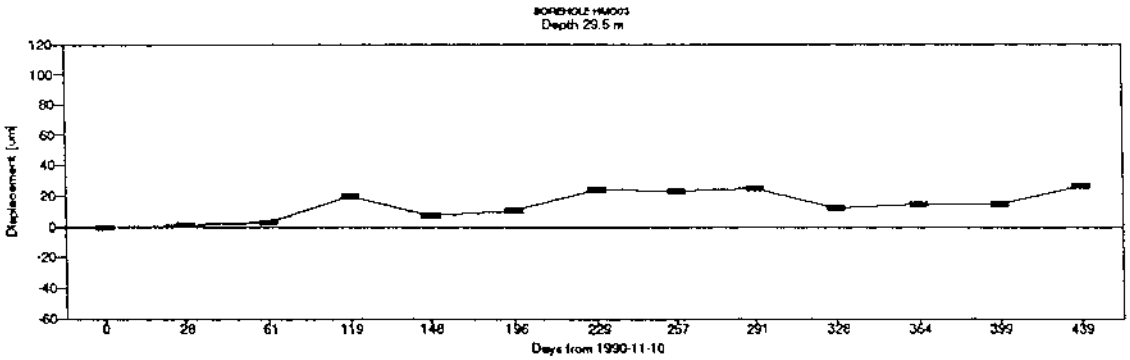
BOREHOLE HM003
Depth 29.5 m
Displacement [um]
Days from 1990-11-10

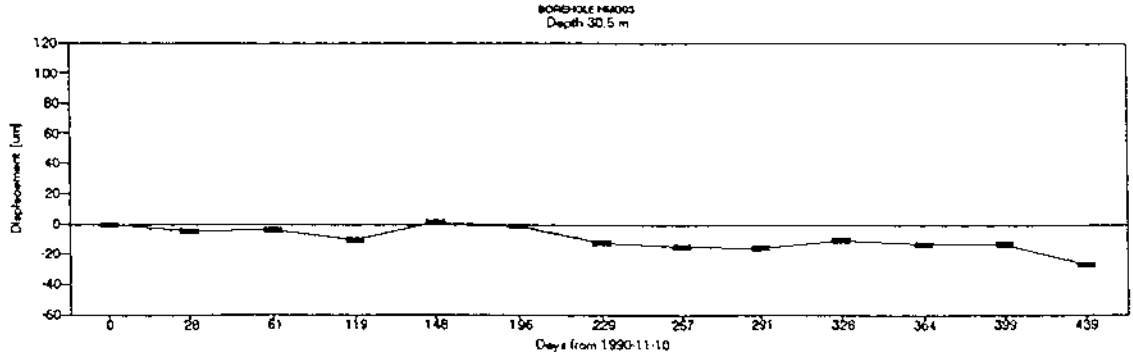
BOREHOLE HM003
Depth 30.5 m
Displacement [um]
Days from 1990-11-10

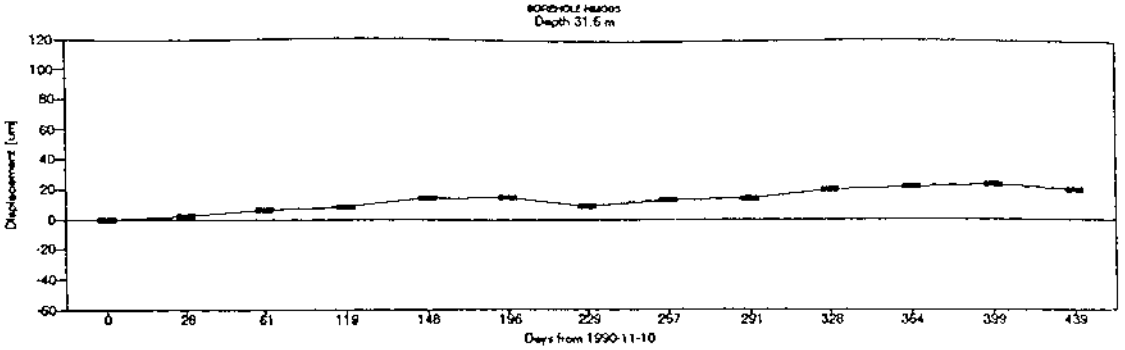
BOREHOLE HM003
Depth 31.6 m
Displacement [um]
Days from 1990-11-10

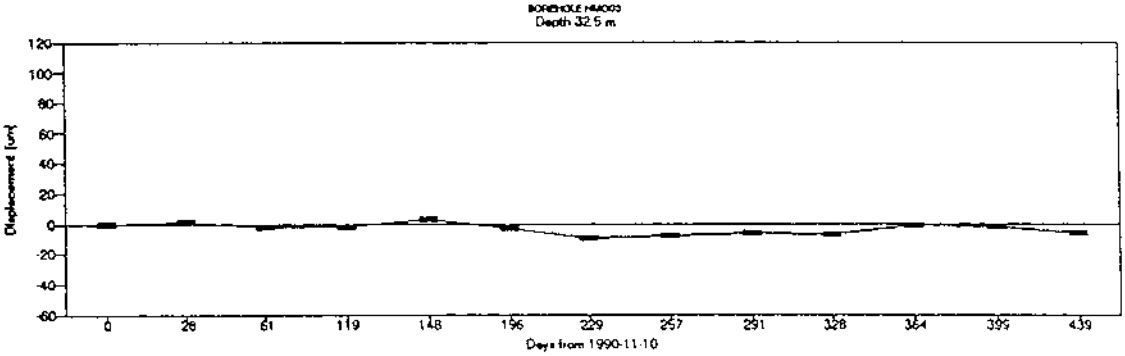
BOREHOLE HM003
Depth 32.5 m
Displacement [um]
Days from 1990-11-10

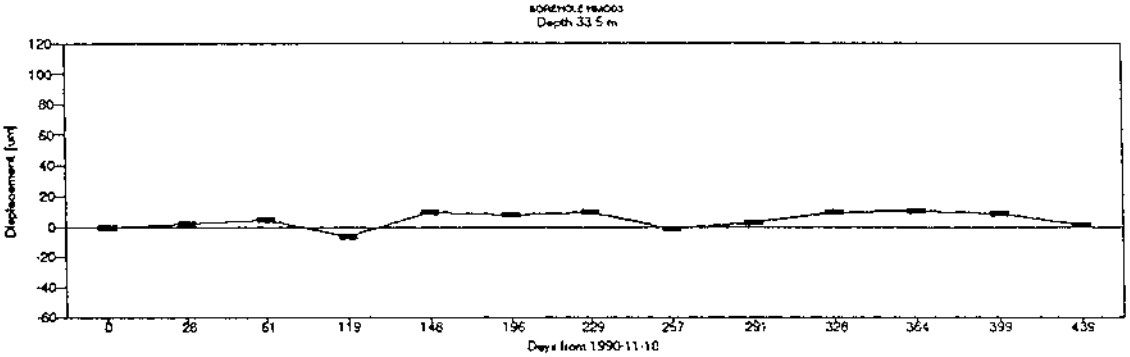
BOREHOLE HM003
Depth 33.5 m
Displacement [um]
Days from 1990-11-10

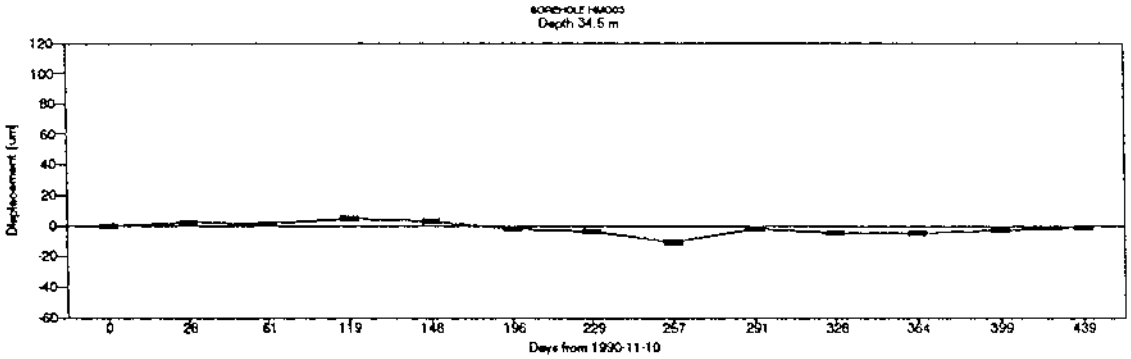
BOREHOLE HM003
Depth 34.5 m
Displacement [um]
Days from 1990-11-10

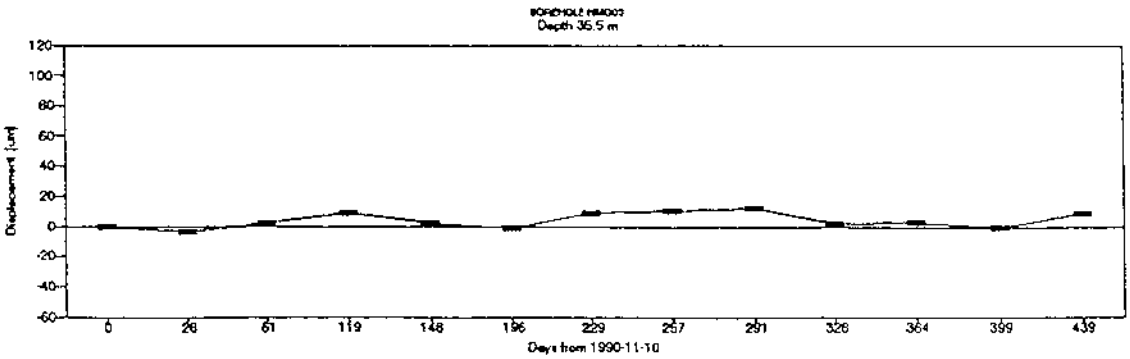
BOREHOLE HM003
Depth 35.5 m
Displacement [um]
Days from 1990-11-10

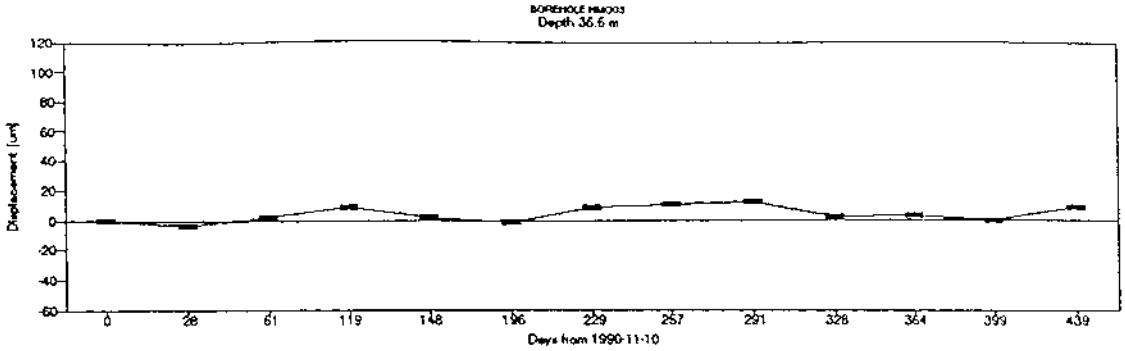
BOREHOLE HM003
Depth 36.6 m
Displacement [um]
Days from 1990-11-10

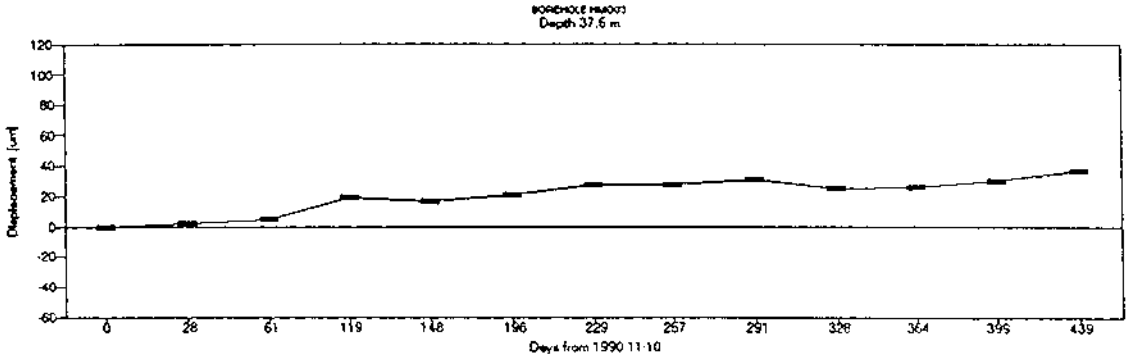
BOREHOLE HM003
Depth 37.6 m
Displacement [um]
Days from 1990-11-10

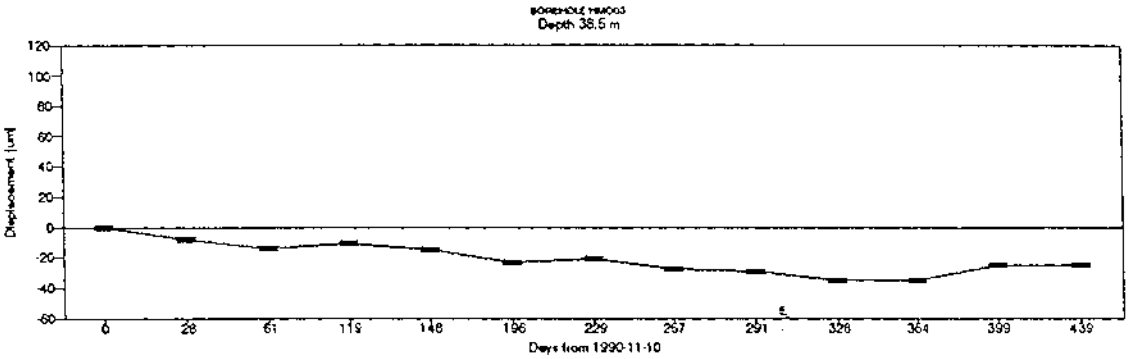
BOREHOLE HM003
Depth 38.5 m
Displacement [um]
Days from 1990-11-10

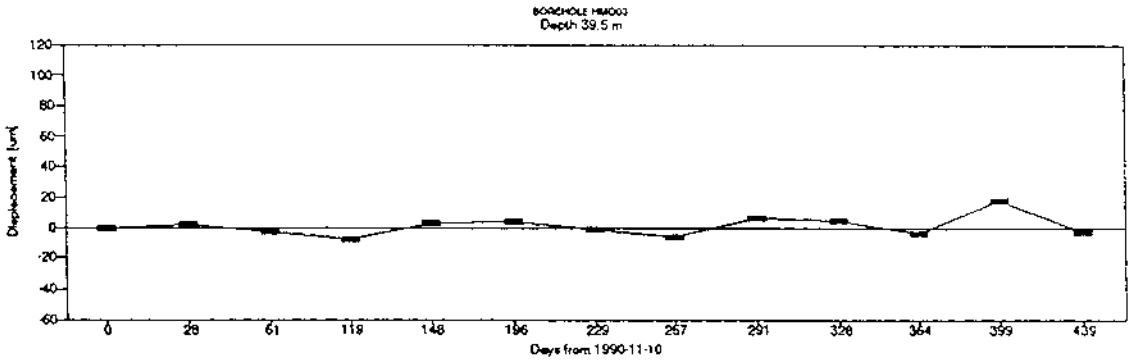
BOREHOLE HM003
Depth 39.5 m
Displacement [um]
Days from 1990-11-10

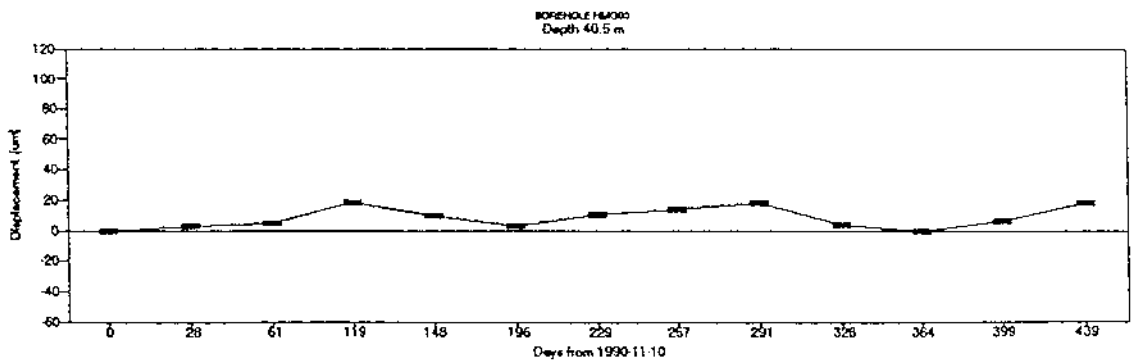
BOREHOLE HM003
Depth 40.5 m
Displacement [um]
Days from 1990-11-10

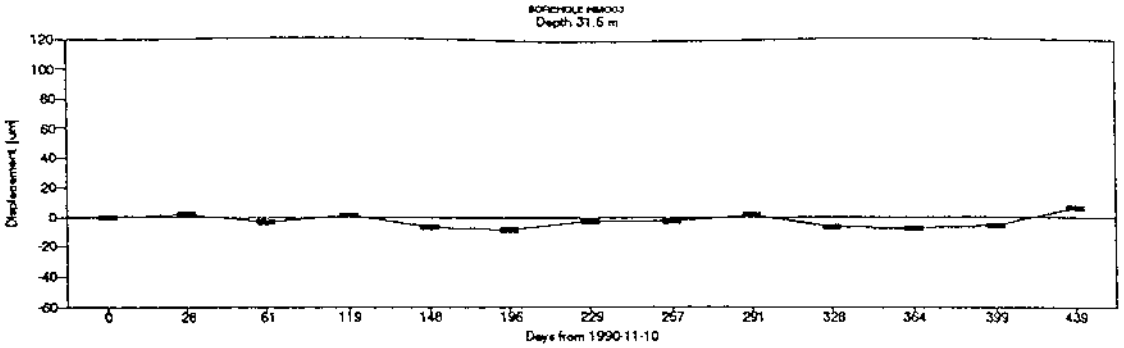
BOREHOLE HM003
Depth 31.5 m
Displacement [um]
Days from 1990-11-10

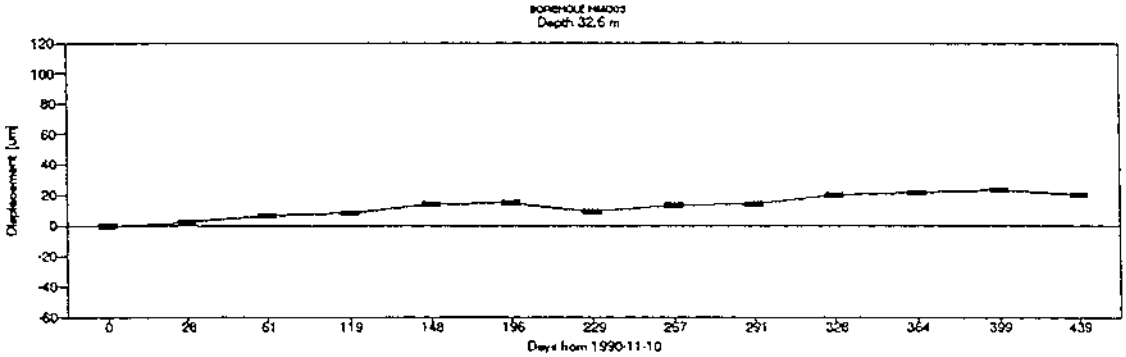
BOREHOLE HM003
Depth 32.5 m
Displacement [um]
Days from 1990-11-10

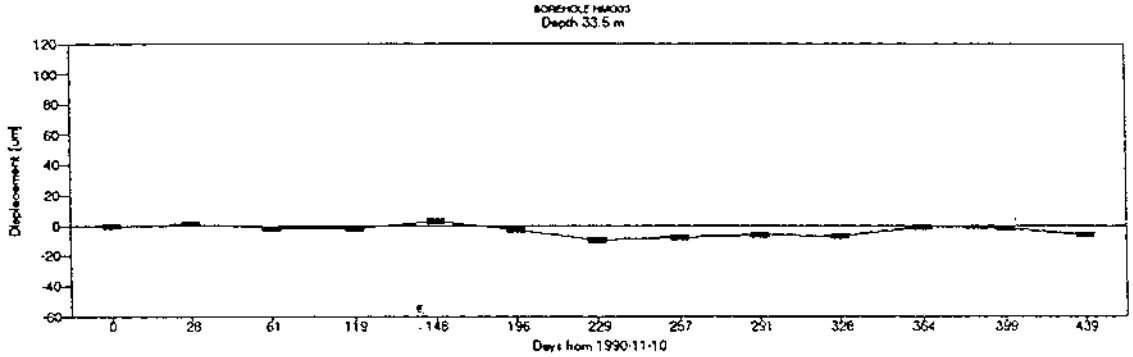
BOREHOLE HM003
Depth 33.5 m
Displacement [um]
Days from 1990-11-10

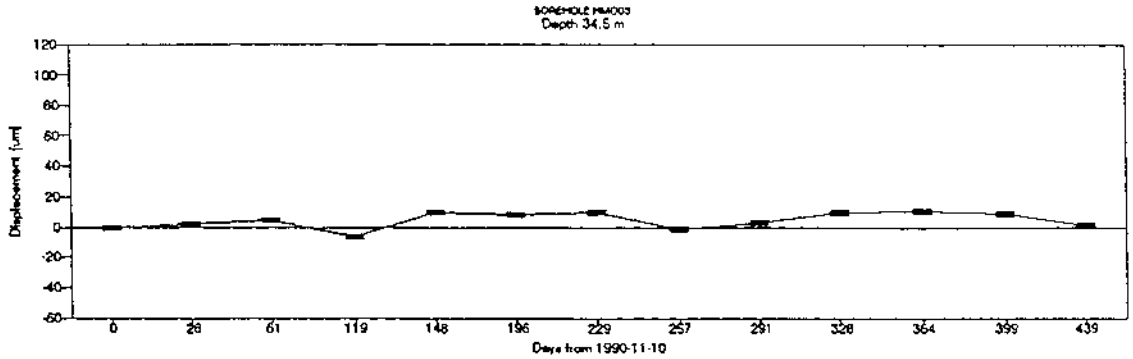
BOREHOLE HM003
Depth 34.5 m
Displacement [um]
Days from 1990-11-10

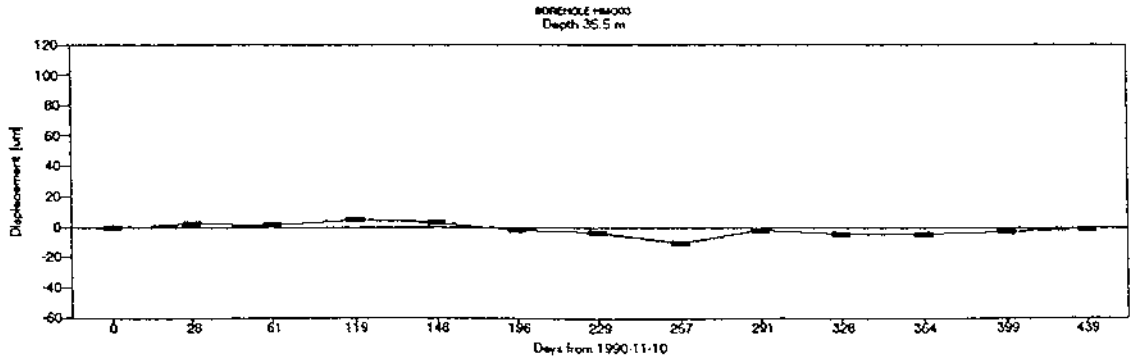
BOREHOLE HM003
Depth 35.5 m
Displacement [um]
Days from 1990-11-10

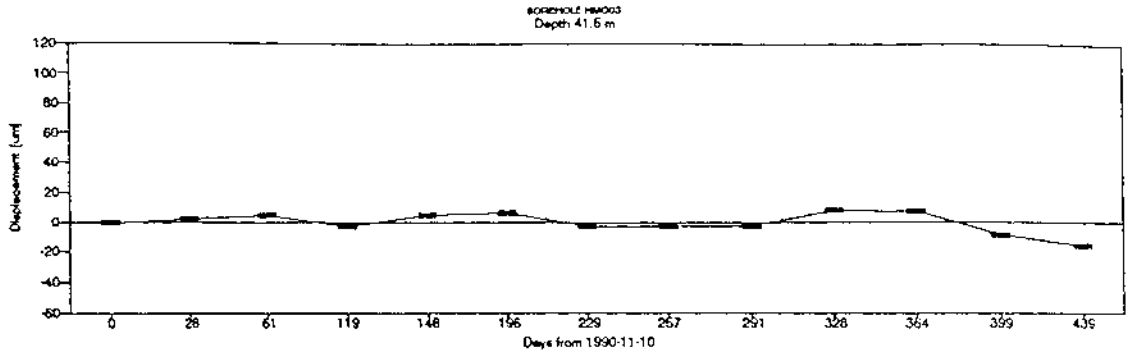
BOREHOLE HM003
Depth 41.5 m
Displacement [unit]
120
100
80
60
40
20
0
-20
-40
-60
0
28
61
119
148
196
229
257
291
328
364
399
439
Days from 1990-11-10

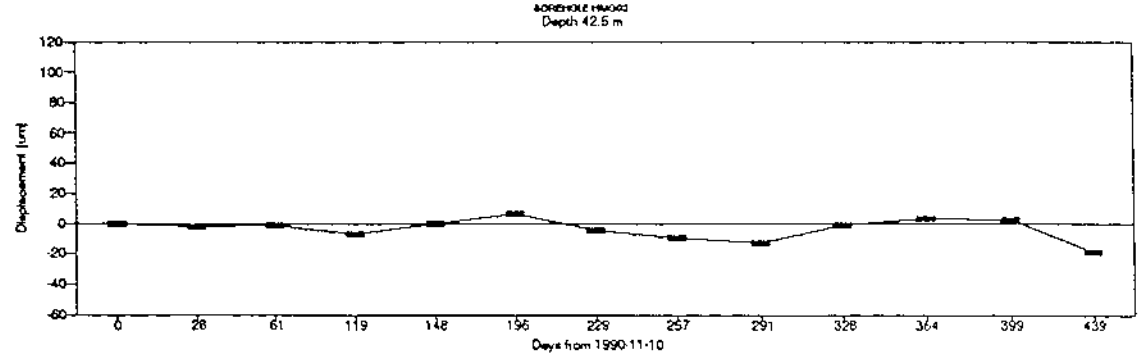
BOREHOLE HM003
Depth 42.5 m
Displacement [unit]
120
100
80
60
40
20
0
-20
-40
-60
0
28
61
119
148
196
229
257
291
328
364
399
439
Days from 1990-11-10

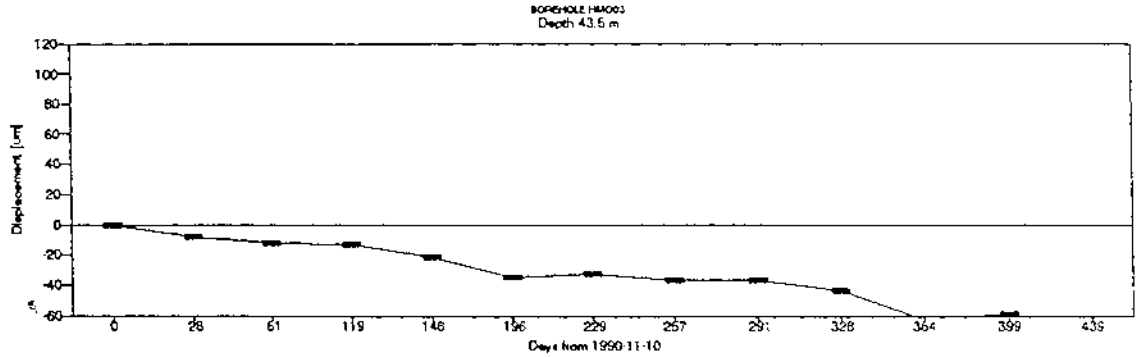
BOREHOLE HM003
Depth 43.5 m
Displacement [unit]
120
100
80
60
40
20
0
-20
-40
-60
0
28
61
119
148
196
229
257
291
328
364
399
439
Days from 1990-11-10

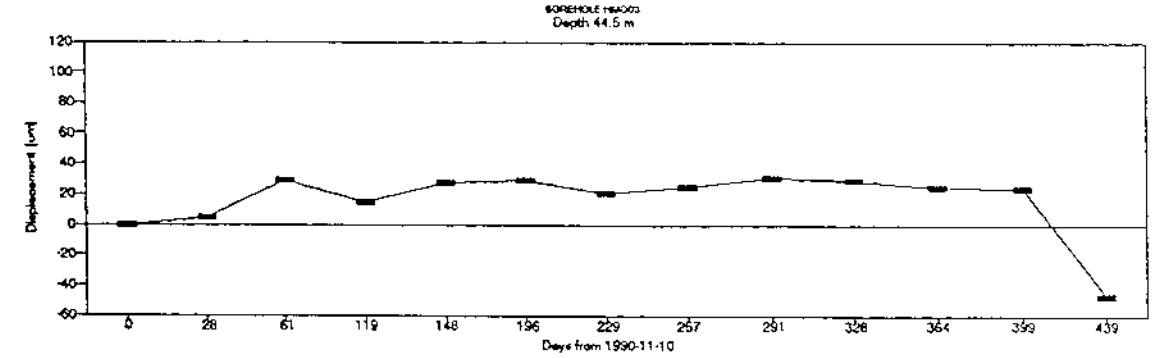
BOREHOLE HM003
Depth 44.5 m
Displacement [unit]
120
100
80
60
40
20
0
-20
-40
-60
0
28
61
119
148
196
229
257
291
328
364
399
439
Days from 1990-11-10

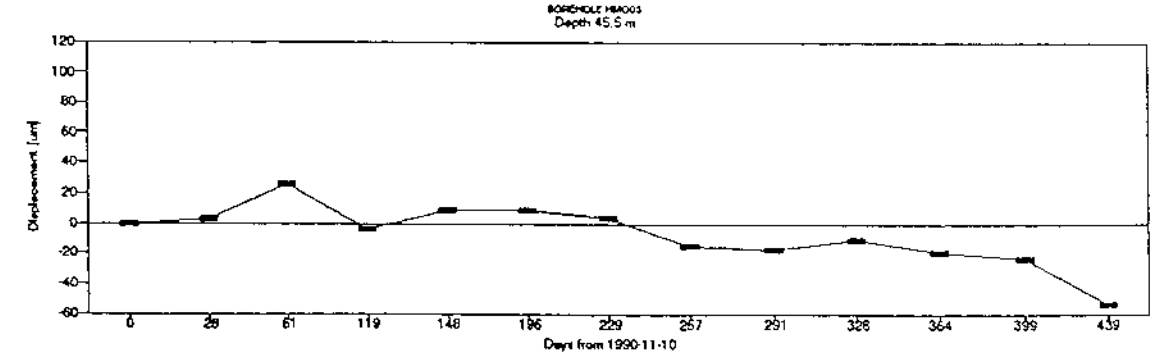
BOREHOLE HM003
Depth 45.5 m
Displacement [unit]
120
100
80
60
40
20
0
-20
-40
-60
0
28
61
119
148
196
229
257
291
328
364
399
439
Days from 1990-11-10

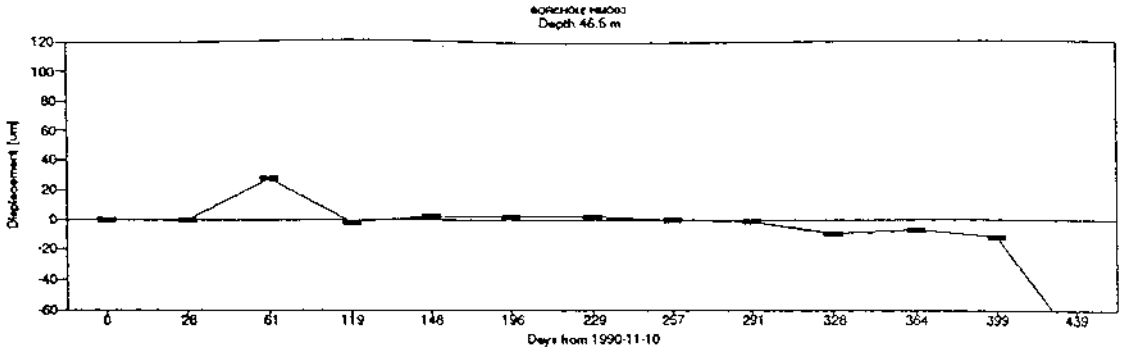
Depth: 46.5 m
Displacement [um]
120
100
80
60
40
20
0
-20
-40
-60
0
28
61
119
148
196
229
257
291
328
364
399
439
Days from 1990-11-10

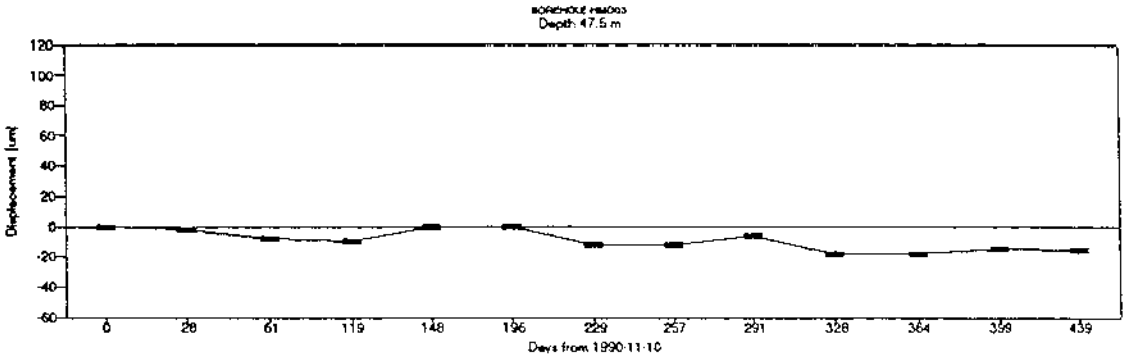
Depth: 47.5 m
Displacement [um]
120
100
80
60
40
20
0
-20
-40
-60
0
28
61
119
148
196
229
257
291
328
364
399
439
Days from 1990-11-10

Readings from borehole HMO03 nov-90 – jan-92.

6.5	981	1015	1023	1048	1058	1039	1075	1052	1061	1026	1031	1062	1092
7.5	1026	1036	1034	1046	1048	1018	1047	1051	1058	1044	1041	1043	1054
8.5	1007	998	990	1010	1004	974	1001	996	1003	987	989	985	983
9.5	910	916	910	919	922	922	928	937	943	917	913	934	926
10.5	841	843	842	860	852	848	857	862	851	841	850	846	867
11.5	899	910	912	900	920	878	880	901	918	913	907	903	903
12.5	1035	1033	1025	1026	1035	1039	1031	1035	1037	1038	1036	1036	1033
13.5	1042	1036	1027	1049	1044	1042	1058	1055	1057	1041	1043	1038	1051
14.5	1056	1057	1057	1051	1061	1056	1051	1046	1047	1035	1047	1041	1041
15.5	1046	1043	1049	1044	1054	1046	1048	1048	1042	1040	1054	1049	1057
16.5	666	675	670	679	683	672	675	688	684	685	688	672	692
17.5	929	940	920	918	940	916	913	912	924	932	922	920	883
18.5	755	749	739	752	753	753	747	731	751	753	760	743	747
19.5	1078	1069	1073	1076	1089	1081	1082	1095	1096	1095	1101	1097	1100
20.5	749	754	731	749	745	733	741	742	745	737	741	737	743
21.5	823	826	832	827	828	831	845	845	842	834	834	838	839
22.5	831	843	830	839	850	849	849	846	844	851	848	853	849
23.5	1068	1064	1060	1055	1059	1057	1057	1057	1057	1058	1060	1060	1061
24.5	1006	1004	993	1015	1017	999	1010	1006	1008	1000	1005	1003	1009
25.5	1076	1083	1084	1078	1088	1087	1082	1083	1083	1088	1080	1090	1084
26.5	1049	1047	1045	1043	1050	1051	1044	1046	1046	1046	1054	1056	1047
27.5	1182	1193	1190	1189	1198	1190	1183	1184	1184	1187	1189	1193	1185
28.5	1072	1075	1072	1063	1079	1093	1067	1066	1066	1078	1082	1083	1073
29.5	1070	1071	1073	1090	1077	1081	1094	1093	1095	1082	1085	1085	1097
30.5	1046	1041	1042	1035	1047	1045	1034	1031	1030	1035	1033	1033	1019
31.5	1038	1040	1034	1039	1031	1029	1035	1035	1039	1031	1030	1032	1044
32.5	988	990	994	996	1002	1003	997	1001	1002	1008	1010	1011	1008
33.5	1196	1197	1194	1194	1199	1193	1186	1188	1190	1189	1195	1194	1190
34.5	1032	1034	1037	1026	1042	1040	1042	1031	1035	1042	1043	1041	1033
35.5	986	988	987	991	989	984	982	975	984	981	981	983	985
36.5	1091	1087	1093	1100	1093	1090	1100	1102	1103	1093	1094	1091	1100
37.5	1095	1097	1100	1114	1112	1116	1123	1123	1126	1120	1121	1125	1132
38.5	1185	1177	1171	1174	1170	1162	1164	1157	1156	1150	1150	1160	1160
39.5	1276	1278	1273	1268	1279	1280	1275	1270	1262	1281	1272	1294	1273
40.5	1167	1170	1172	1185	1177	1170	1178	1161	1185	1171	1167	1173	1185
41.5	1333	1335	1338	1330	1338	1339	1330	1330	1330	1341	1340	1324	1317
42.5	1467	1465	1466	1460	1467	1473	1462	1457	1454	1466	1470	1469	1448
43.5	1009	1001	997	996	987	974	976	972	972	965	947	950	922
44.5	1295	1300	1324	1310	1323	1324	1316	1320	1326	1324	1320	1319	1248
45.5	1385	1388	1411	1381	1394	1394	1389	1370	1368	1374	1366	1362	1331
46.5	1304	1304	1332	1302	1306	1306	1306	1304	1303	1294	1297	1292	1222
47.5	1322	1320	1314	1312	1322	1322	1310	1310	1316	1304	1304	1307	1306

Readings from borehole HMO03 nov-90 – jan-92.

6.5	0	34	42	67	77	58	94	71	80	45	50	81	111
7.5	0	10	8	20	22	-8	21	25	32	18	15	17	28
8.5	0	-9	-17	3	-3	-33	-6	-11	-4	-20	-18	-22	-24
9.5	0	6	0	9	12	12	18	27	33	7	3	24	16
10.5	0	2	1	19	11	7	16	21	10	0	9	5	26
11.5	0	11	13	1	21	-21	-19	2	19	14	8	4	4
12.5	0	-2	-10	-9	0	4	-4	0	2	3	1	1	-2
13.5	0	-6	-15	7	2	0	16	13	15	-1	1	-4	9
14.5	0	1	1	-5	5	0	-5	-10	-9	-21	-9	-15	-15
15.5	0	-3	3	-2	8	0	2	2	-4	-6	8	3	11
16.5	0	9	4	13	17	6	9	22	18	19	22	6	26
17.5	0	11	-9	-11	11	-13	-16	-17	-5	3	-7	-9	-46
18.5	0	-6	-16	-3	-2	-2	-8	-24	-4	-2	5	-12	-8
19.5	0	-9	-5	-2	11	3	4	17	18	17	23	19	22
20.5	0	5	-18	0	-4	-16	-8	-7	-4	-12	-8	-12	-6
21.5	0	3	9	4	5	8	22	22	19	11	11	15	16
22.5	0	12	-1	8	19	18	18	15	13	20	17	22	18
23.5	0	-4	-8	-13	-9	-11	-11	-11	-11	-10	-8	-8	-7
24.5	0	-2	-13	9	11	-7	4	0	2	-6	-1	-3	3
25.5	0	7	8	2	12	11	6	7	7	12	4	14	8
26.5	0	-2	-4	-6	1	2	-5	-3	-3	-3	5	7	-2
27.5	0	11	8	7	16	8	1	2	2	5	7	11	3
28.5	0	3	0	-9	7	21	-5	-6	-6	6	10	11	1
29.5	0	1	3	20	7	11	24	23	25	12	15	15	27
30.5	0	-5	-4	-11	1	-1	-12	-15	-16	-11	-13	-13	-27
31.5	0	2	-4	1	-7	-9	-3	-3	1	-7	-8	-6	6
32.5	0	2	6	8	14	15	9	13	14	20	22	23	20
33.5	0	1	-2	-2	3	-3	-10	-8	-6	-7	-1	-2	-6
34.5	0	2	5	-6	10	8	10	-1	3	10	11	9	1
35.5	0	2	1	5	3	-2	-4	-11	-2	-5	-5	-3	-1
36.5	0	-4	2	9	2	-1	9	11	12	2	3	0	9
37.5	0	2	5	19	17	21	28	28	31	25	26	30	37
38.5	0	-8	-14	-11	-15	-23	-21	-28	-29	-35	-35	-25	-25
39.5	0	2	-3	-8	3	4	-1	-6	6	5	-4	18	-3
40.5	0	3	5	18	10	3	11	14	18	4	0	6	18
41.5	0	2	5	-3	5	6	-3	-3	-3	8	7	-9	-16
42.5	0	-2	-1	-7	0	6	-5	-10	-13	-1	3	2	-19
43.5	0	-8	-12	-13	-22	-35	-33	-37	-37	-44	-62	-59	-87
44.5	0	5	29	15	28	29	21	25	31	29	25	24	-47
45.5	0	3	26	-4	9	9	4	-15	-17	-11	-19	-23	-54
46.5	0	0	28	-2	2	2	2	0	-1	-10	-7	-12	-82
47.5	0	-2	-8	-10	0	0	-12	-12	-6	-18	-18	-15	-16

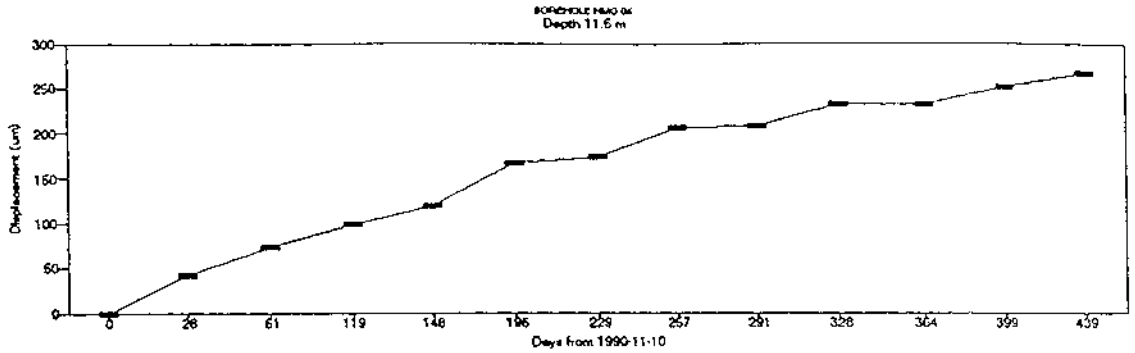
BOREHOLE HMO 04
Depth 11.6 m
Displacement (um)
Days from 1990-11-10

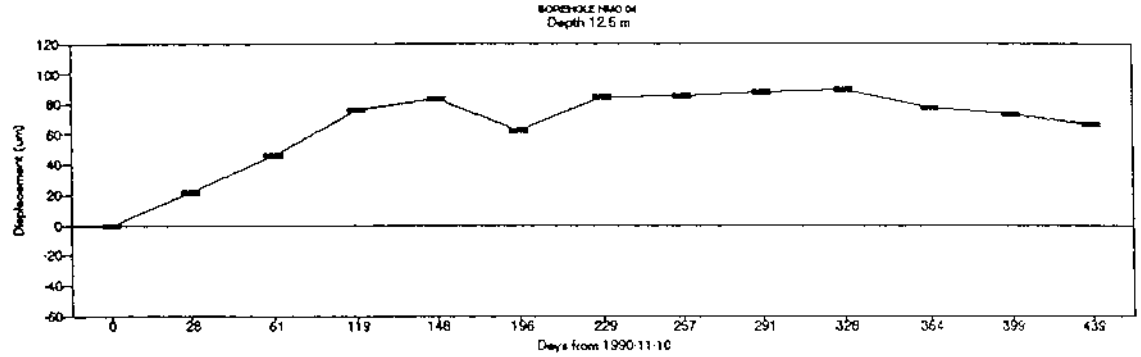
BOREHOLE HMO 04
Depth 12.5 m
Displacement (um)
Days from 1990-11-10

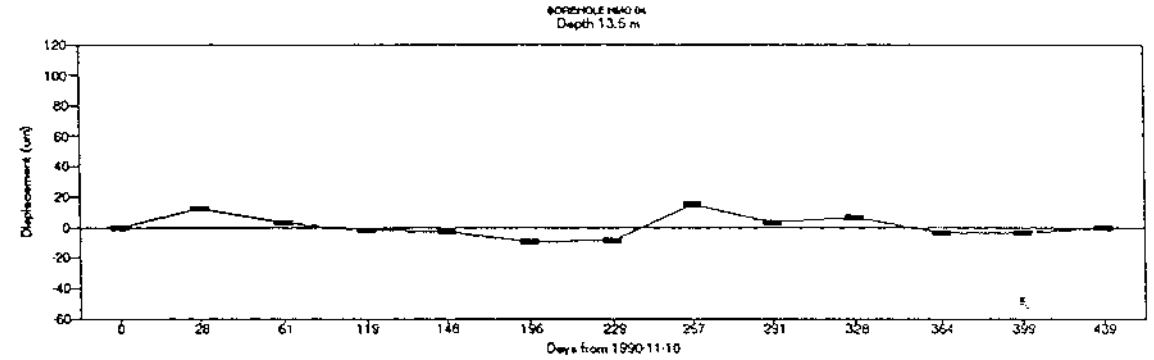
BOREHOLE HMO 04
Depth 13.5 m
Displacement (um)
Days from 1990-11-10

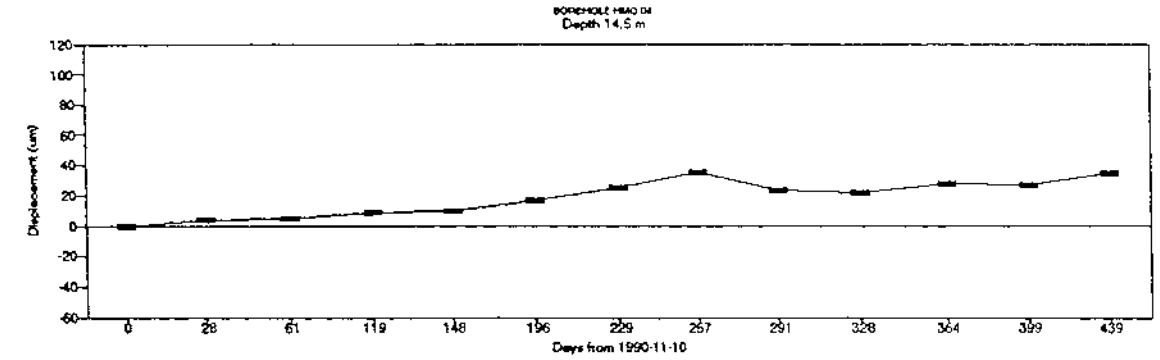
BOREHOLE HMO 04
Depth 14.5 m
Displacement (um)
Days from 1990-11-10

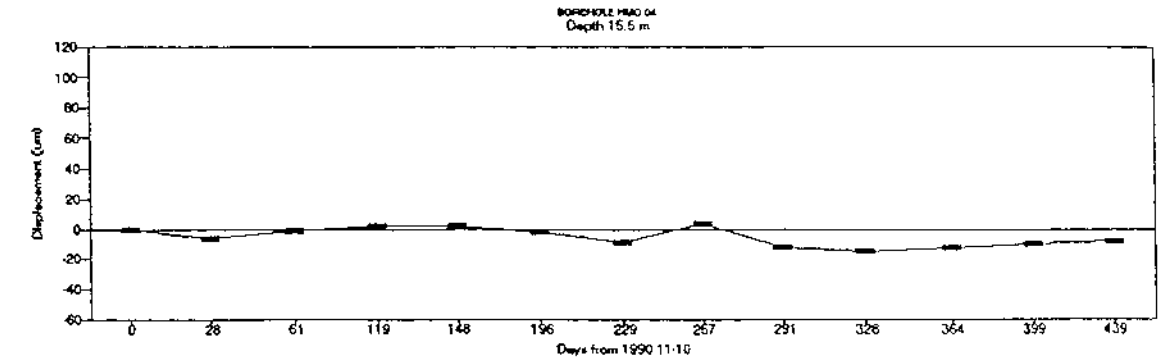
BOREHOLE HMO 04
Depth 15.5 m
Displacement (um)
Days from 1990-11-10

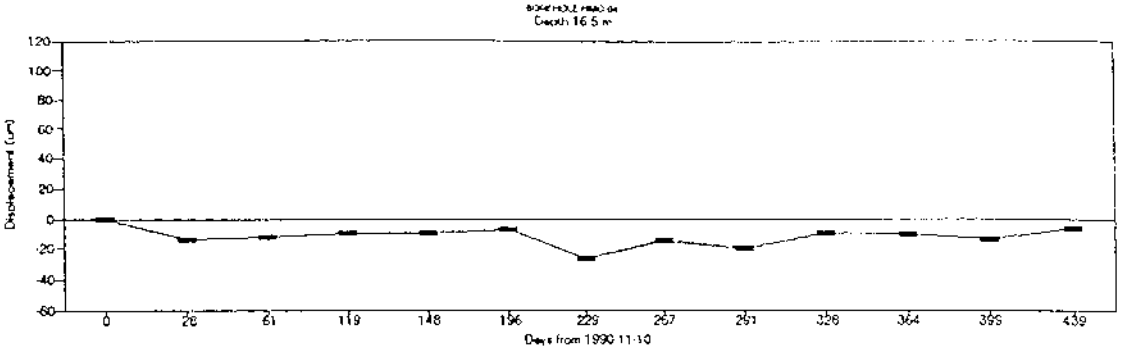
Depth 16.5 m
Displacement (um)
Days from 1990-11-10

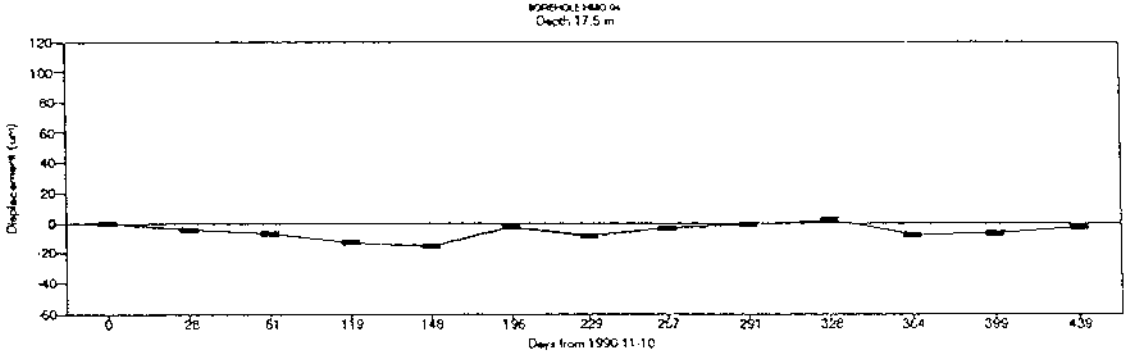
Depth 17.5 m
Displacement (um)
Days from 1990-11-10

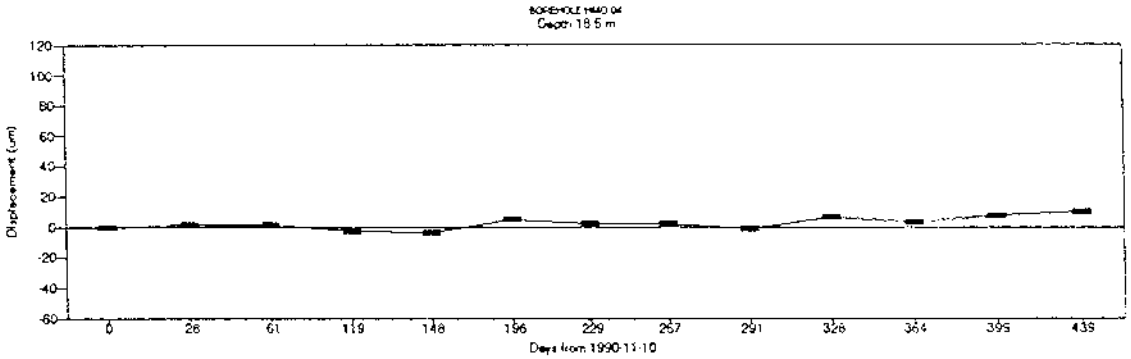
Depth 18.5 m
Displacement (um)
Days from 1990-11-10

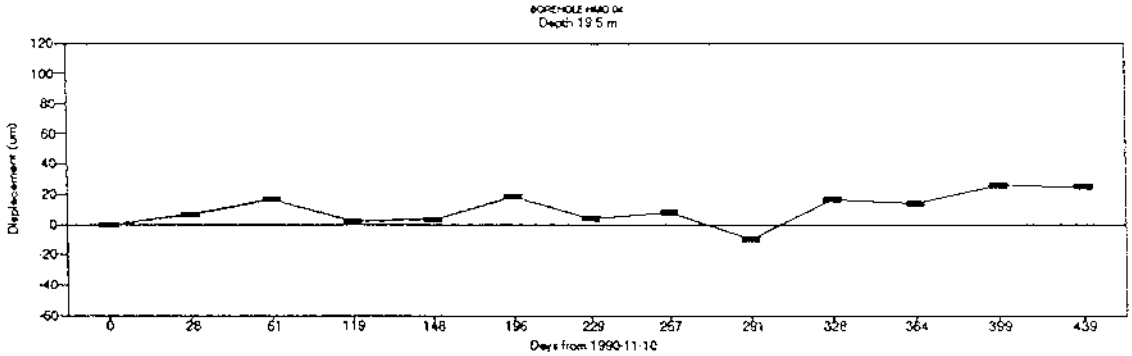
Depth 19.5 m
Displacement (um)
Days from 1990-11-10

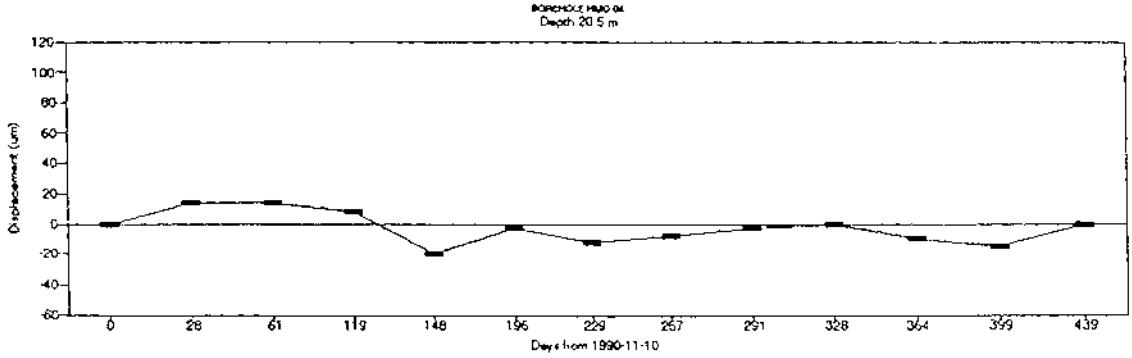
Depth 20.5 m
Displacement (um)
Days from 1990-11-10

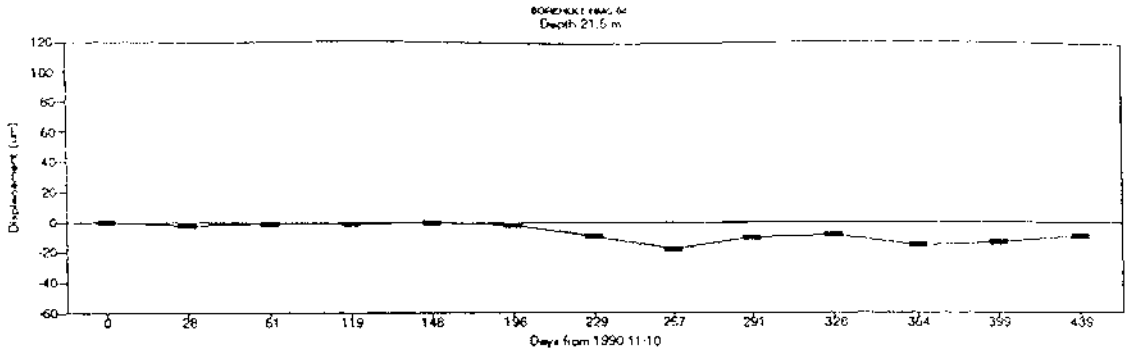
Depth 21.5 m
Displacement (um)
Days from 1990-11-10

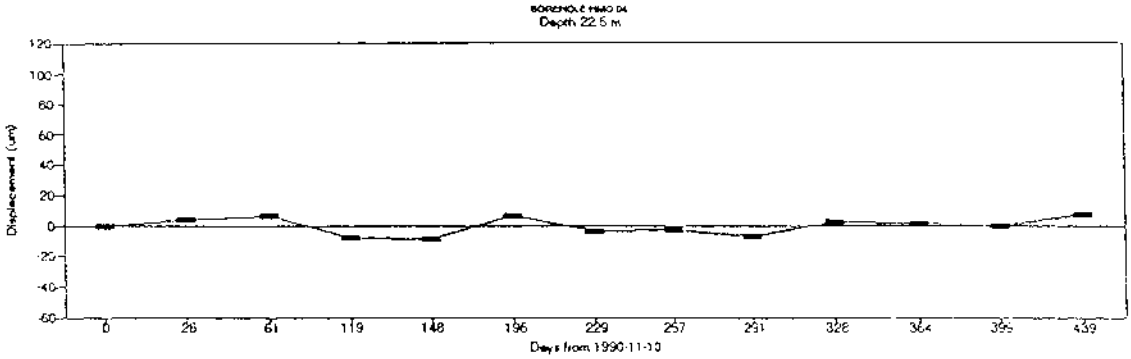
Depth 22.5 m
Displacement (um)
Days from 1990-11-10

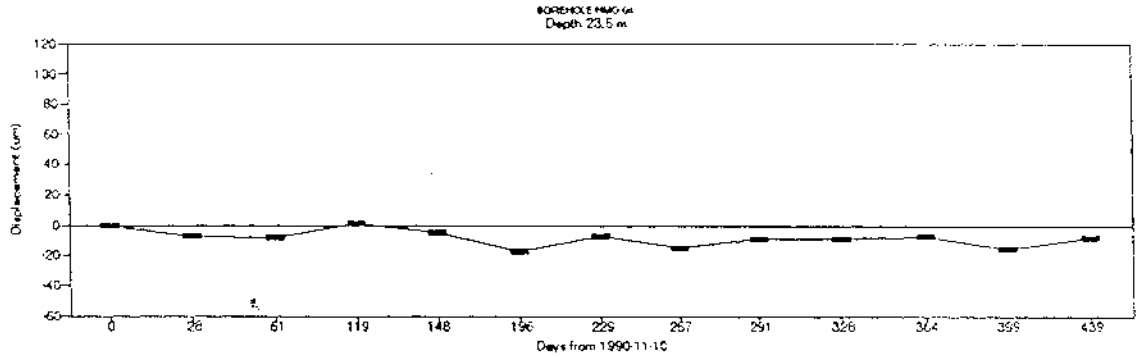
Depth 23.5 m
Displacement (um)
Days from 1990-11-10

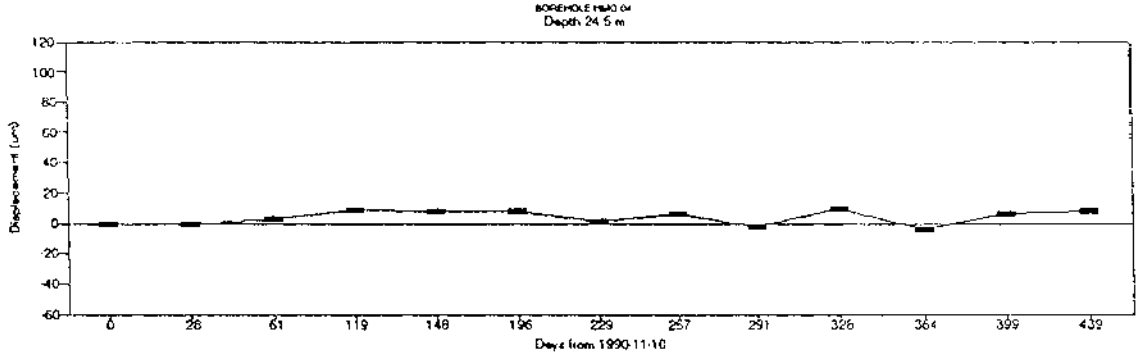
Depth 24.5 m
Displacement (um)
Days from 1990-11-10

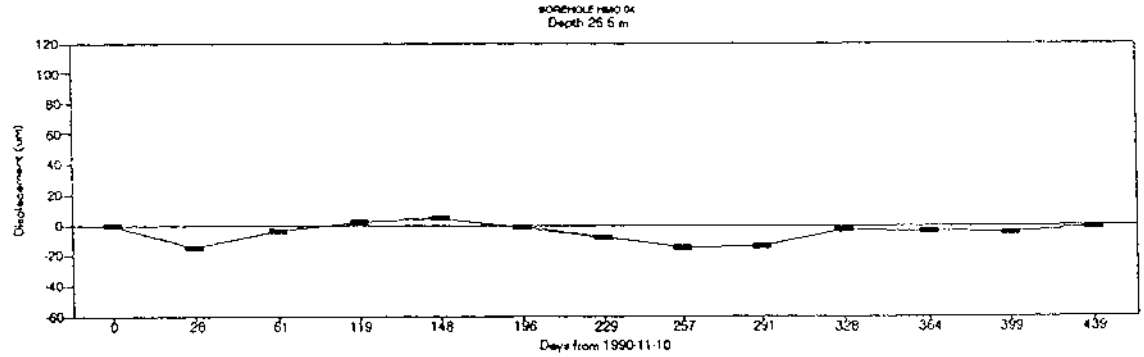
Depth 25.5 m
Displacement (um)
Days from 1990-11-10

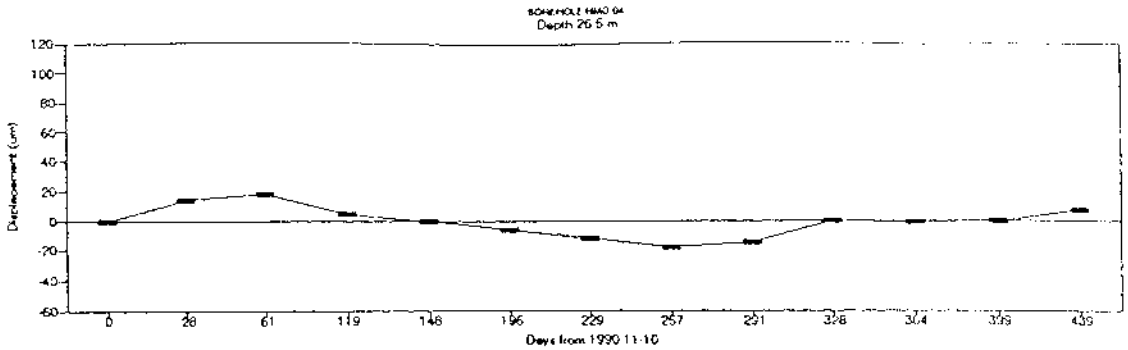
Depth 26.5 m
Displacement (um)
Days from 1990-11-10

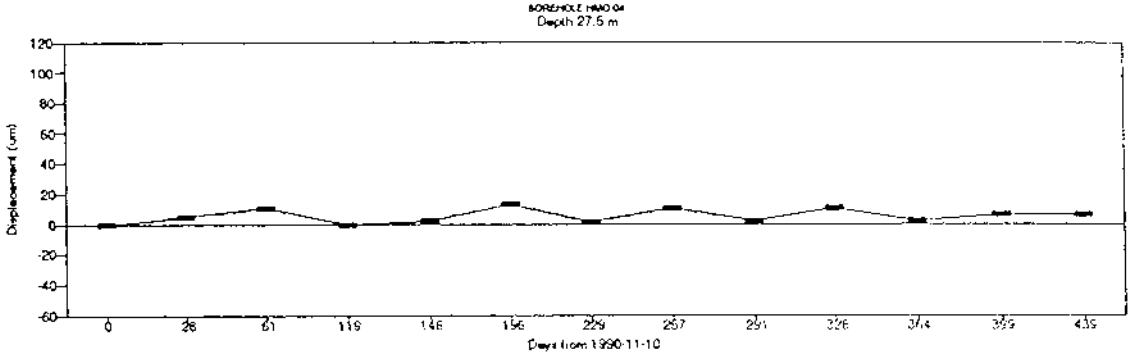
Depth 27.5 m
Displacement (um)
Days from 1990-11-10

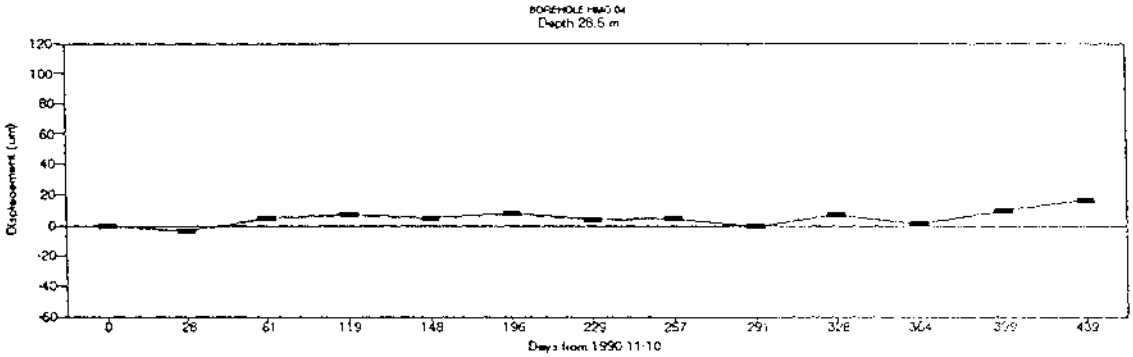
Depth 28.5 m
Displacement (um)
Days from 1990-11-10

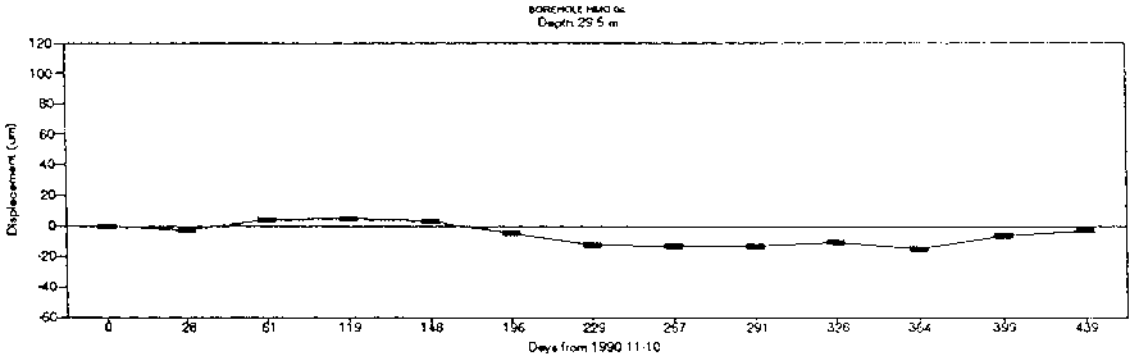
Depth 29.5 m
Displacement (um)
Days from 1990-11-10

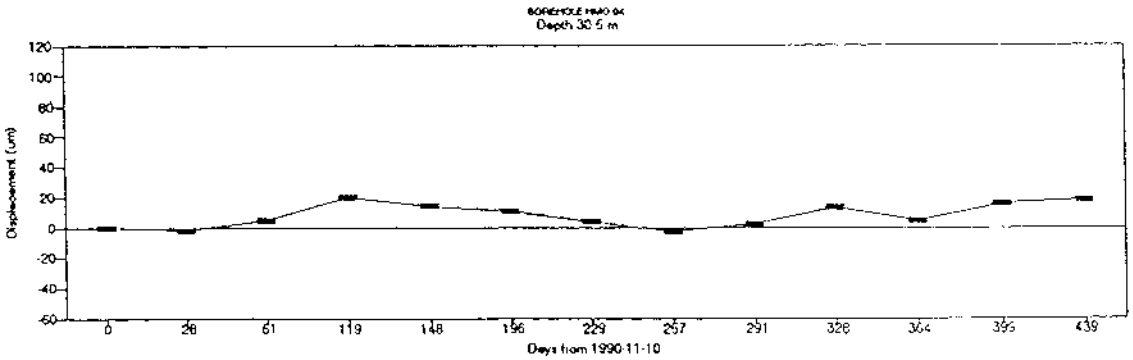
Depth 30.5 m
Displacement (um)
Days from 1990-11-10

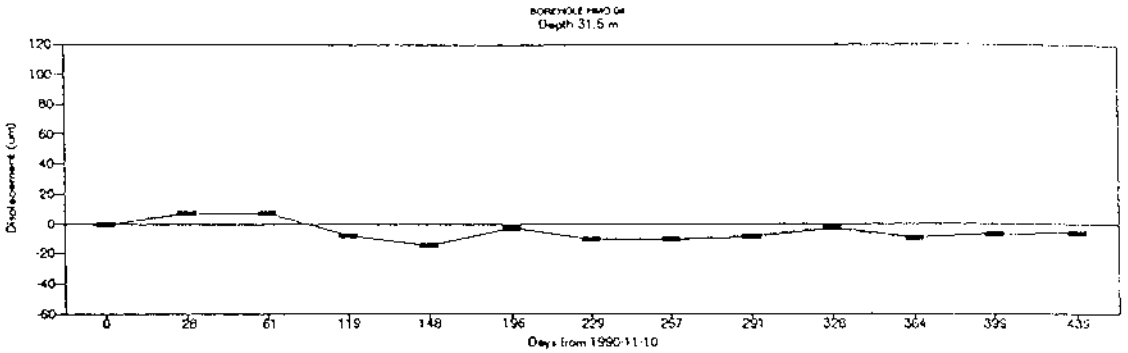
Depth 31.5 m
Displacement (um)
Days from 1990-11-10

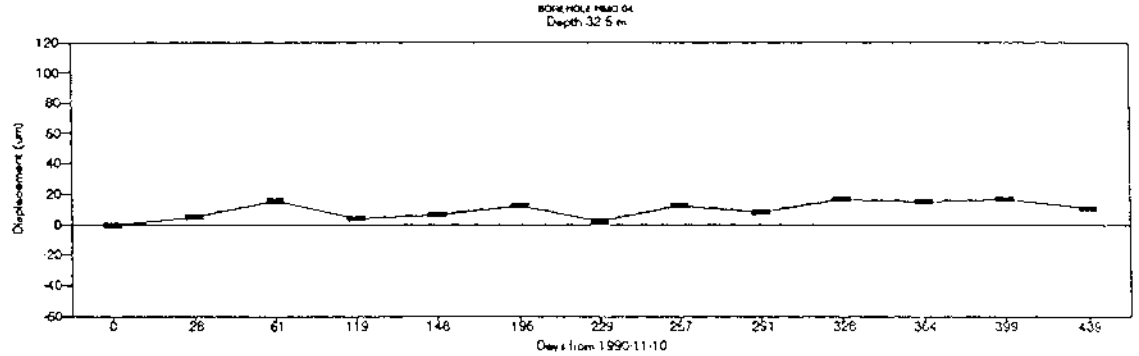
Depth 32.5 m
Displacement (um)
Days from 1990-11-10

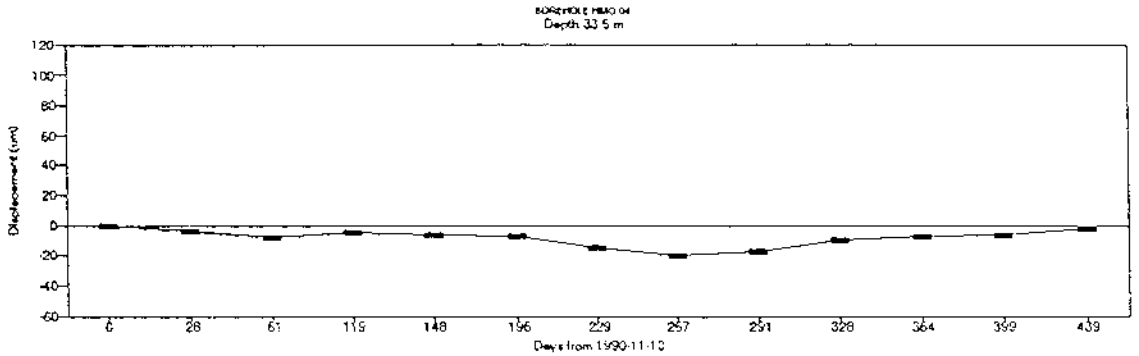
Depth 33.5 m
Displacement (um)
Days from 1990-11-10

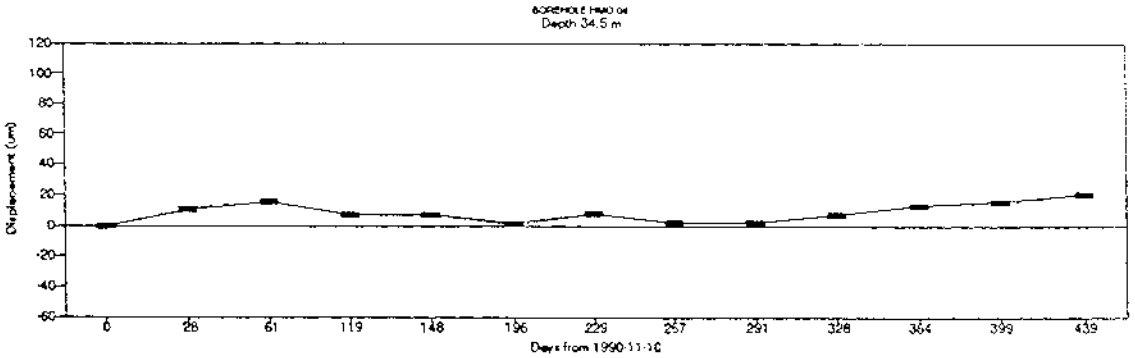
Depth 34.5 m
Displacement (um)
Days from 1990-11-10

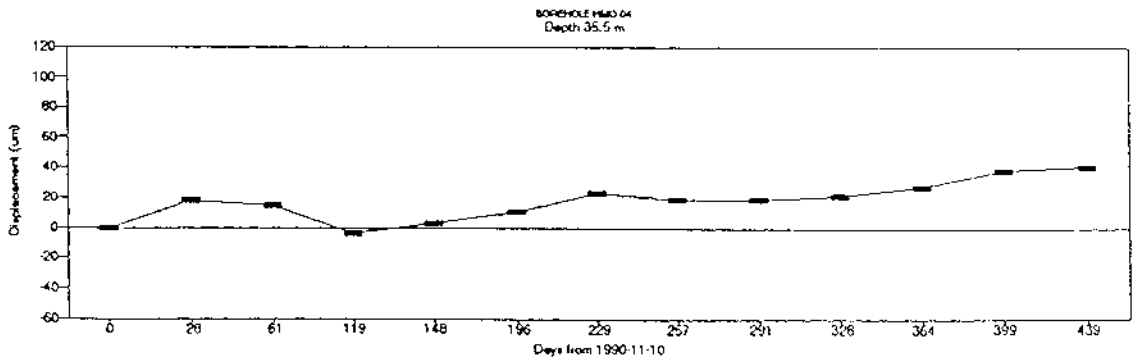
Depth 35.5 m
Displacement (um)
Days from 1990-11-10

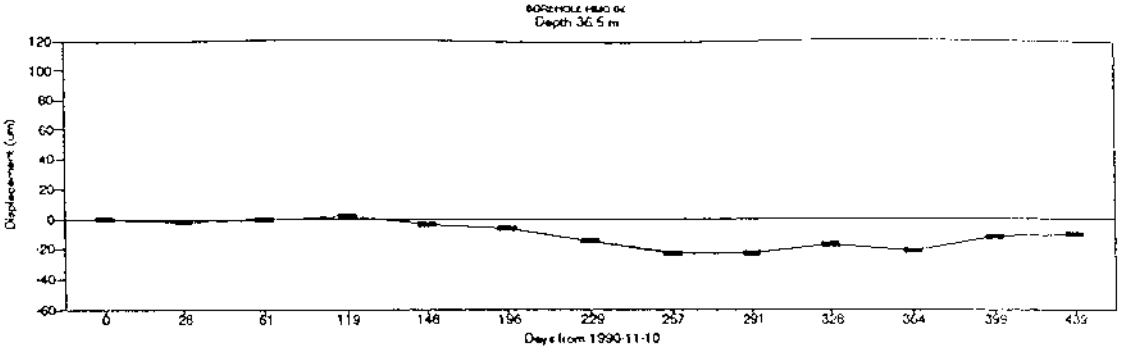
BOREHOLE HMO 04
Depth 36.5 m
Displacement (um)
Days from 1990-11-10

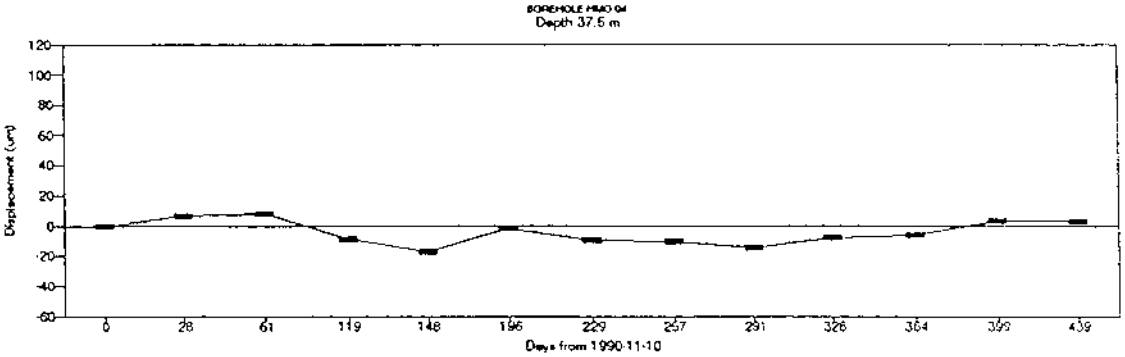
BOREHOLE HMO 04
Depth 37.5 m
Displacement (um)
Days from 1990-11-10

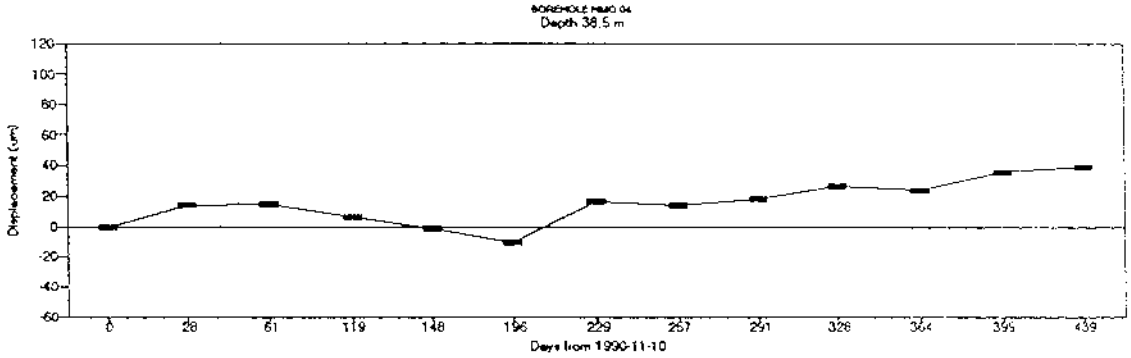
BOREHOLE HMO 04
Depth 38.5 m
Displacement (um)
Days from 1990-11-10

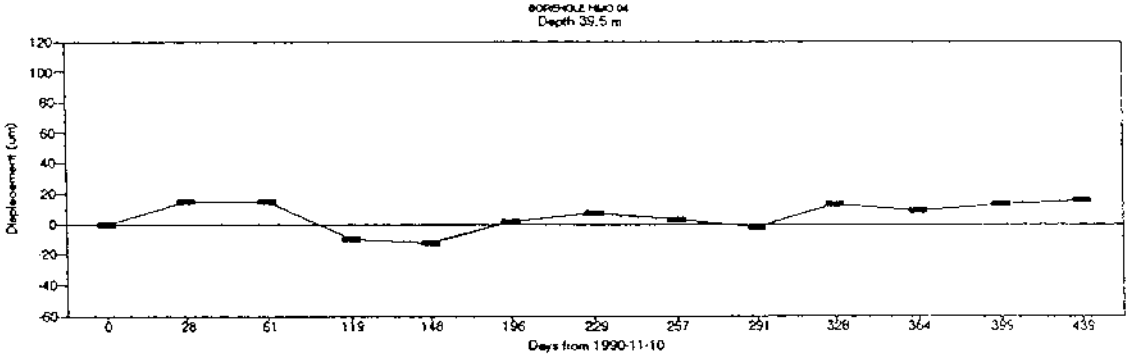
BOREHOLE HMO 04
Depth 39.5 m
Displacement (um)
Days from 1990-11-10

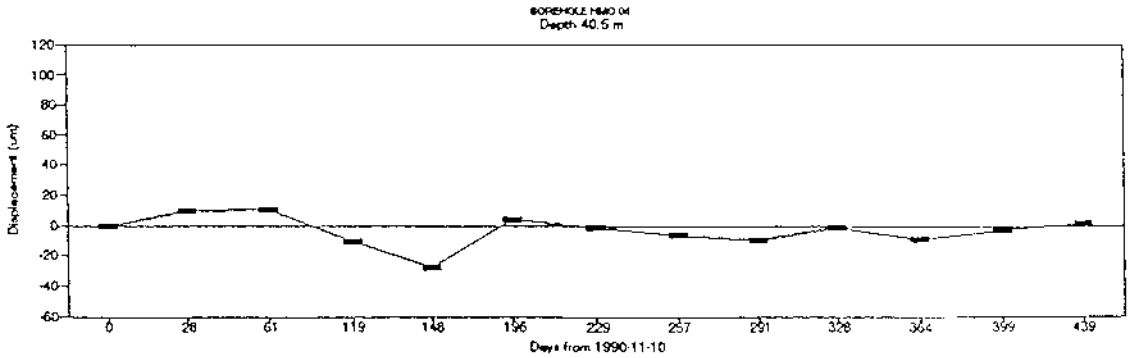
BOREHOLE HMO 04
Depth 40.5 m
Displacement (um)
Days from 1990-11-10

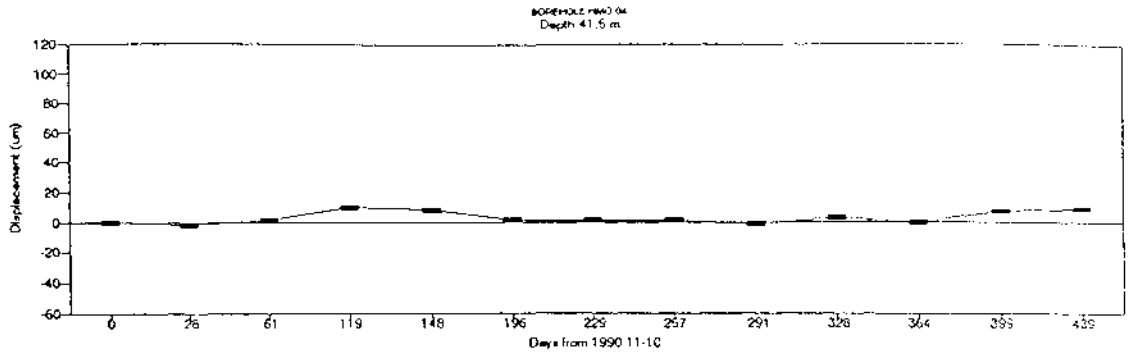
BOREHOLE HMD 04
Depth 41.5 m
Displacement (um)
Days from 1990-11-10

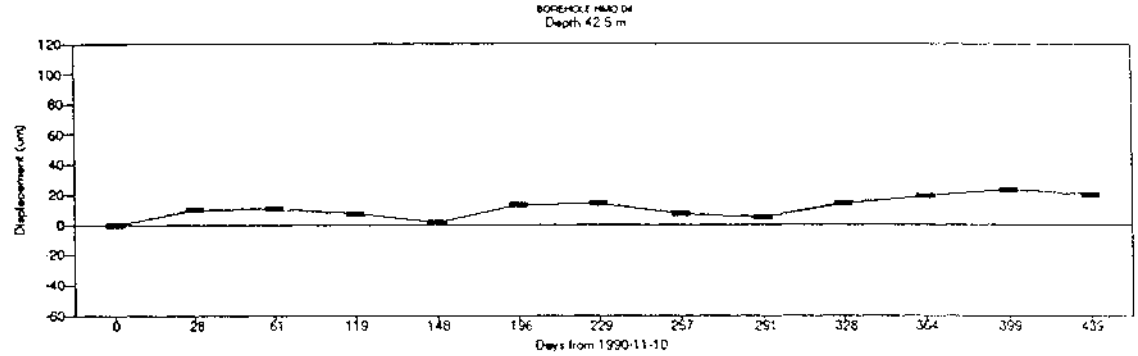
BOREHOLE HMD 04
Depth 42.5 m
Displacement (um)
Days from 1990-11-10

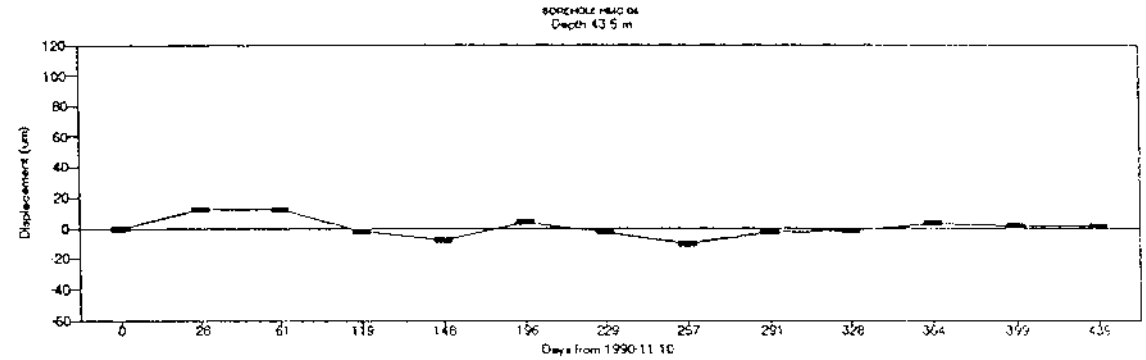
BOREHOLE HMD 04
Depth 43.5 m
Displacement (um)
Days from 1990-11-10

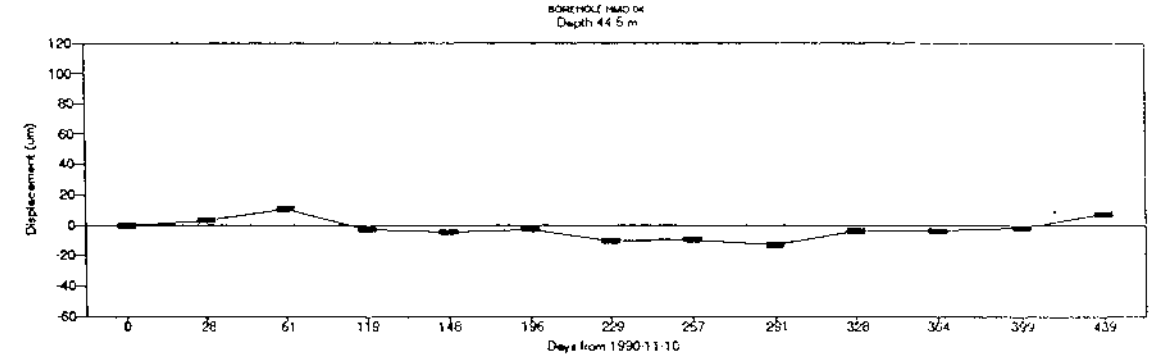
BOREHOLE HMD 04
Depth 44.5 m
Displacement (um)
Days from 1990-11-10

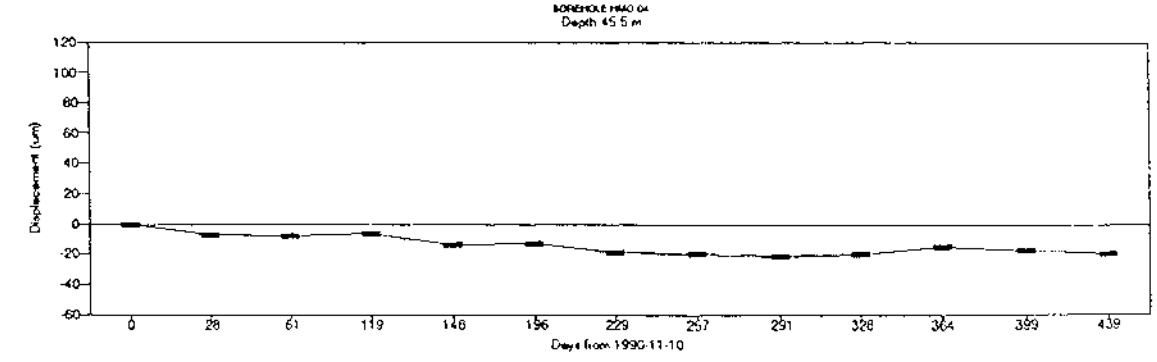
BOREHOLE HMD 04
Depth 45.5 m
Displacement (um)
Days from 1990-11-10

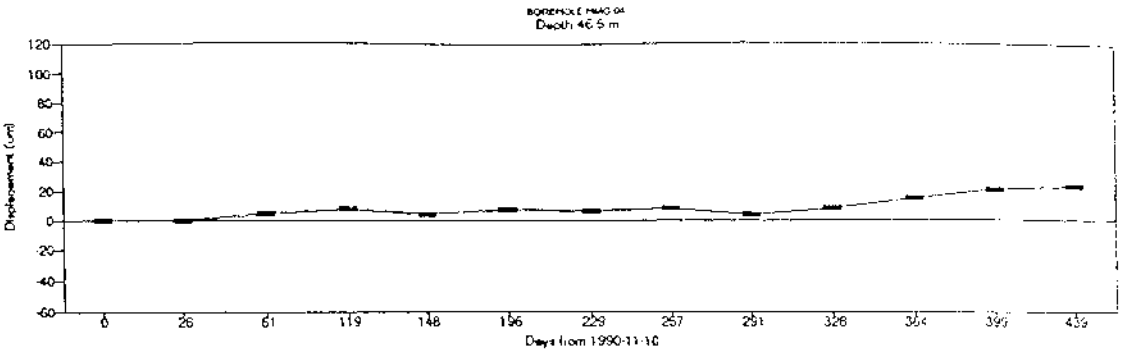
BOREHOLE HMO 04
Depth 46.5 m
Displacement (um)
120
100
80
60
40
20
0
-20
-40
-60
0
28
61
119
148
196
229
257
291
328
364
399
435
Days from 1990-11-10

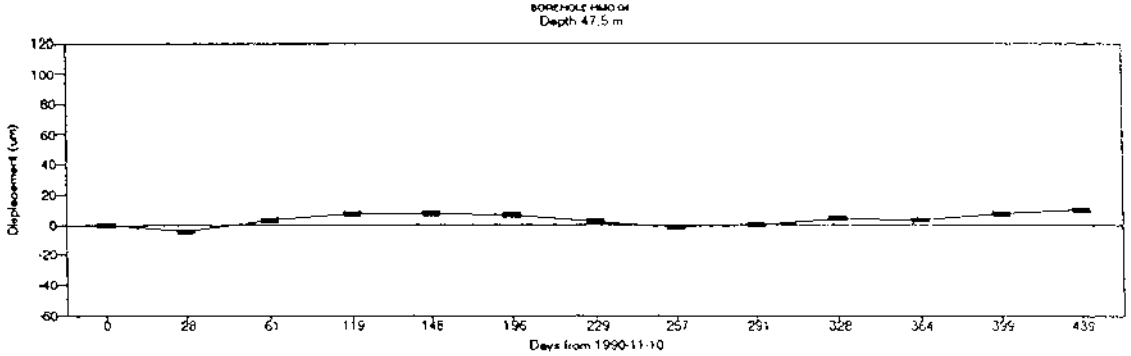
BOREHOLE HMO 04
Depth 47.5 m
Displacement (um)
120
100
80
60
40
20
0
-20
-40
-60
0
28
61
119
148
196
229
257
291
328
364
399
435
Days from 1990-11-10

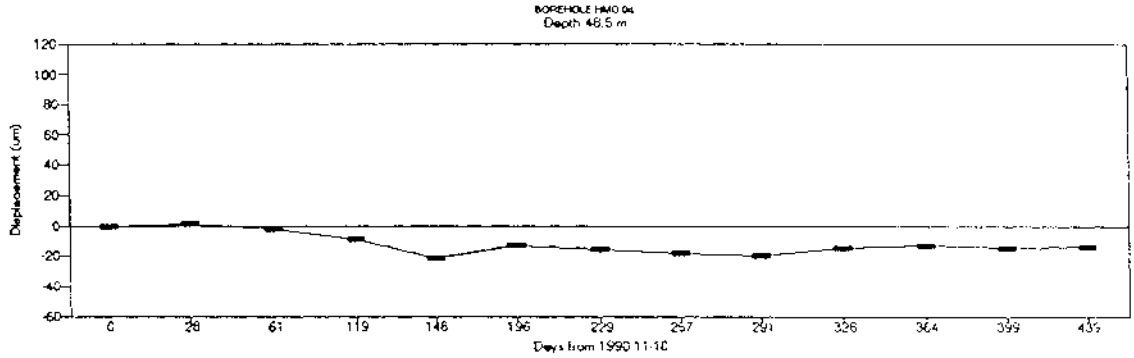
BOREHOLE HMO 04
Depth 48.5 m
Displacement (um)
120
100
80
60
40
20
0
-20
-40
-60
0
28
61
119
148
196
229
257
291
328
364
399
435
Days from 1990-11-10

Readings from borehole HM0 04 nov-90 – jan-92

11.5	747	788	820	845	869	914	921	954	955	979	979	999	1034
12.5	808	830	854	884	891	870	892	893	896	897	885	881	874
13.5	775	787	778	773	772	765	766	790	778	781	771	771	775
14.5	753	757	758	762	763	770	778	788	776	775	781	780	787
15.5	927	921	926	929	929	925	918	931	915	912	915	917	915
16.5	814	800	802	804	804	807	787	799	794	804	803	800	808
17.5	749	744	742	736	733	746	740	745	748	751	741	742	746
18.5	847	848	848	844	843	852	849	849	846	853	850	854	857
19.5	803	809	820	805	806	821	807	811	793	820	817	829	826
20.5	770	784	784	778	750	767	758	762	767	770	760	755	770
21.5	827	824	826	826	827	825	817	809	816	818	811	813	817
22.5	962	966	968	954	953	968	958	959	955	964	963	962	969
23.5	512	505	504	513	507	495	505	497	503	503	505	496	504
24.5	717	717	720	726	725	725	718	723	715	727	713	723	725
25.5	828	813	824	830	833	827	820	813	814	825	824	823	827
26.5	745	759	763	750	745	739	733	727	730	745	744	745	752
27.5	392	397	403	392	394	405	393	403	394	403	394	398	398
28.5	563	559	568	570	568	571	567	568	563	570	564	573	569
29.5	767	764	771	772	770	762	755	754	754	756	752	761	764
30.5	498	496	503	518	512	509	502	495	500	511	503	514	516
31.5	690	697	697	682	675	687	679	679	681	687	680	683	684
32.5	812	817	828	816	818	824	814	824	820	829	827	829	823
33.5	514	510	506	509	508	507	499	494	497	504	507	509	512
34.5	845	856	861	852	852	846	853	847	847	852	858	861	866
35.5	871	889	886	867	874	882	894	890	890	893	899	909	912
36.5	912	910	912	914	908	906	897	889	889	895	890	900	901
37.5	1149	1155	1157	1140	1132	1147	1139	1138	1134	1141	1143	1152	1152
38.5	908	922	923	914	907	897	925	922	926	935	932	944	947
39.5	1093	1108	1108	1083	1081	1094	1100	1096	1091	1106	1102	1106	1109
40.5	1559	1569	1570	1548	1531	1563	1558	1553	1549	1558	1550	1556	1560
41.5	1206	1204	1207	1216	1214	1207	1207	1207	1205	1209	1206	1213	1215
42.5	1436	1446	1447	1443	1437	1449	1450	1443	1441	1450	1455	1459	1456
43.5	1847	1859	1859	1845	1839	1851	1844	1836	1844	1845	1850	1848	1848
44.5	1223	1226	1234	1220	1218	1220	1212	1213	1210	1219	1219	1221	1230
45.5	1260	1273	1272	1274	1266	1267	1261	1260	1258	1260	1265	1263	1260
46.5	1432	1432	1437	1440	1436	1439	1438	1440	1436	1440	1447	1453	1455
47.5	950	945	953	957	957	956	952	948	950	954	953	957	960
48.5	1008	1009	1006	999	986	995	992	990	988	993	995	993	994

Readings from borehole HMO 04 nov-90 -- jan-92

11.5	0	41	73	98	119	167	174	207	208	231	232	252	267
12.5	0	22	46	76	83	62	84	85	88	89	77	73	66
13.5	0	12	3	-2	-3	-10	-9	15	3	6	-4	-4	0
14.5	0	4	5	9	10	17	25	35	23	22	28	27	34
15.5	0	-6	-1	2	2	-2	-9	4	-12	-15	-12	-10	-5
16.5	0	-14	-12	-10	-10	-7	-27	-15	-20	-10	-11	-14	-6
17.5	0	-5	-7	-13	-16	-3	-9	-4	-1	2	-8	-7	-3
18.5	0	1	1	-3	-4	5	2	2	-1	6	3	7	15
19.5	0	6	17	2	3	18	4	8	-10	17	14	26	25
20.5	0	14	14	8	-20	-3	-12	-8	-3	0	-10	-15	0
21.5	0	-3	-1	-1	0	-2	-10	-18	-11	-9	-16	-14	-10
22.5	0	4	6	-8	-9	6	-4	-3	-7	2	1	0	7
23.5	0	-7	-8	1	-5	-17	-7	-15	-9	-9	-7	-16	-8
24.5	0	0	3	9	8	8	1	6	-2	10	-4	6	8
25.5	0	-15	-4	2	5	-1	-8	-15	-14	-3	-4	-5	-1
26.5	0	14	18	5	0	-6	-12	-18	-15	0	-1	0	7
27.5	0	5	11	0	2	13	1	11	2	11	2	6	6
28.5	0	-4	5	7	5	8	4	5	0	7	1	10	17
29.5	0	-3	4	5	3	-5	-12	-13	-13	-11	-15	-6	-3
30.5	0	-2	5	20	14	11	4	-3	2	13	5	16	18
31.5	0	7	7	-8	-15	-3	-11	-11	-9	-3	-10	-7	-6
32.5	0	5	16	4	6	12	2	12	8	17	15	17	11
33.5	0	-4	-8	-5	-6	-7	-15	-20	-17	-10	-7	-6	-2
34.5	0	11	16	7	7	1	8	2	2	7	13	16	21
35.5	0	18	15	-4	3	11	23	19	19	22	28	38	41
36.5	0	-2	0	2	-4	-6	-15	-23	-23	-17	-22	-12	-11
37.5	0	6	8	-9	-17	-2	-10	-11	-15	-8	-6	3	3
38.5	0	14	15	6	-1	-11	17	14	18	27	24	36	39
39.5	0	15	15	-10	-12	1	7	3	-2	13	9	13	16
40.5	0	10	11	-11	-28	4	-1	-6	-10	-1	-9	-3	1
41.5	0	-2	1	10	8	1	1	1	-1	3	0	7	9
42.5	0	10	11	7	1	13	14	7	5	14	19	23	20
43.5	0	12	12	-2	-8	4	-3	-11	-3	-2	3	1	1
44.5	0	3	11	-3	-5	-3	-11	-10	-13	-4	-4	-2	7
45.5	0	-7	-8	-6	-14	-13	-19	-20	-22	-20	-15	-17	-20
46.5	0	0	5	8	4	7	6	8	4	8	15	21	23
47.5	0	-5	3	7	7	6	2	-2	0	4	3	7	10
48.5	0	1	-2	-9	-22	-13	-16	-18	-20	-15	-13	-15	-14

Analys av borrhålsdata från mätningar i Lansjärv

Kent Lindblad, Peter Lundman
Avd. För Bergmekanik, Tekniska Högskolan i Luleå

December 1993

SAMMANFATTNING

För att studera ev pågående neotektoniska rörelser i postglaciala förkastningar har ett område i Lansjärv, Norrbotten undersökts.

Under perioden 901110-920125 utfördes mätningar i två borrhål, ett brantstående och ett flackt, med Sliding Micrometer, denna rapport utvärderar de uppmätta rörelserna och analyserar orsakerna till de uppmätta rörelserna.

Mätningarna uppvisar anomalier på vissa sektioner i borrhålen. För att finna orsakerna till dessa har olika möjliga påverkande faktorer analyserats. Eftersom de flesta anomalierna uppträder i ytberget verkar det troligt att orsakerna är att finna i yttre faktorer, såsom temperaturvariationer, grundvattenförändringar samt tidvattnets effekt.

Den yttre temperaturvariationens påverkan på bergmassan har studerats genom att använda Fouriers värmeledningsekvation för att finna de teoretiska temperaturväxlingarna i bergmassan på skiftande djup. Det visar sig att det endast är på mycket ringa djup som de yttre temperaturerna ger upphov till temperaturväxlingar i bergmassan, på djup under 10 m är temperaturvariationen obetydlig. Dessa teoretiska temperaturväxlingar har sedan använts för att beräkna hur stora rörelser som kan förväntas i bergmassan under antagandet att denna är homogen och linjärelastisk. Resultaten visar att rörelserna orsakade av de yttre temperaturvariationerna är av underordnad betydelse.

Grundvattnets variationer och dess effekt på bergmassan har studerats genom tre olika modeller. I den första modellen antas det att grundvattenförändringarna ger upphov till en förändring av porvattentrycket. I det andra beräkningsfallet betraktas grundvattenförändringen som en utbredd last. Slutligen har en empirisk modell ställts upp som är kalibrerad mot faktiska grundvattenförändringar. Utav dessa modeller är det den sistnämnda som ger den bästa överensstämmelsen med faktiska rörelser. Med den empiriska modellen kan stora delar av rörelserna i det vertikala borrhålet, under sommarhalvåret, förklaras med grundvattenförändringarna. Det föreligger dock stora osäkerheter att klassificera rörelserna som årstidsberoende, då mätningarna endast täcker en årscykel.

Ytterligare en faktor som kan påverka de uppmätta rörelserna är det anlagda diket för kvartärgeologisk kartering. Effekterna av detta har simulerats med olika datorbaserade beräkningsmodeller, resultaten av dessa visar att stora delar av de horisontella rörelserna i riktning mot förkastningszonen kan tillskrivas det anlagda diket.

Det förekommer även rörelser i den nedre delen av det

brantstående borrhålet, dessa rörelser kan inte förklaras med några ytfenomen. Rörelserna i denna sektion får istället tillskrivas tektoniska rörelser i förkastningzonen. Det måste dock påpekas att de uppmätta rörelserna är små, även för de sektioner som uppvisar de största anomalierna (0.5 mm/m).

Totalt sett så visar vår analys att delar av de uppmätta rörelserna kan förklaras med ovanstående modeller, det finns naturliga förklaringar som inte är att hänföra till neotektonik. Del av rörelserna kan emellertid mycket väl vara orsakade av neotektoniska rörelser i förkastningen.

Slutsatsen och vår rekommendation från detta arbete är att mätningarna bör fortgå under en längre tidsperiod, 3-5 år, för att man med större säkerhet skall kunna uttala sig om vad som orsakar de uppmätta rörelserna i Lansjärvsförkastningen. Dessutom rekommenderar vi att mätningarna kompletteras med ytterligare två borrhål. Det ena 150-200 m långt, motiveras av att HM003 troligen inte övertvärar förkastningen vilket vore önsvärt för att möjliggöra mätning på båda sidor om förkastningen. Det andra bör vara ett kort vertikalt hål för grundvattennivåregistrering.

Innehållsförteckning

1 INLEDNING

I de norra delarna av Sverige, Norge och Finland förekommer det flera förkastningszoner som åldersmässigt kan klassas som postglaciala. I Lansjärv, Norrbotten har en förkastning daterats och den visar på en ålder av 9000 år (Lagerbäck, 1991). Förkastningarnas längd kan vara upp till 150 km och den vertikala förskjutningen varierar från någon meter upp till 30 m.

Som ett led i undersökningar av den svenska berggrundens stabilitet har SKB detaljstuderat en del av en 17 km lång förkastning i Molberget nära Lansjärv i Norrbotten, se Figur 1. Under 1987 grävdes ett dike över förkastningszonen detta kompletterades 1990 med ytterligare två diken och tre diamantborrhål (Eliasson m.fl, 1991). Vertikala förskjutningar på 3-5.6 m kunde konstateras, vidare konstaterades att förkastningszonen var en äldre rörelsezon som reaktiverats flera gånger under en lång period, även mätt med geologiskt mått. I den centrala delen består zonen av en starkt skjuvad mylonit, omgiven av en utåt avtagande uppkrossad omvandlingszon. Berget är i stort sett opåverkat 20 m ut från förkastningen.

För att få en uppfattning om rörelser fortfarande förekommer borrades 4 st hammarborrhål mot förkastningen. I två av dessa gjordes regelbundna deformationsmätningar i borrhålets riktning under perioden nov 1990 - jan 1992 (Nilsson, 1992).

Som uppföljning av dessa mätningar gjordes nedanstående studie med syftet att analysera borrhålsdata från mätningarna i Molberget, Lansjärv. Ett antal möjliga konceptuella modeller har provats för att förklara mätresultaten.

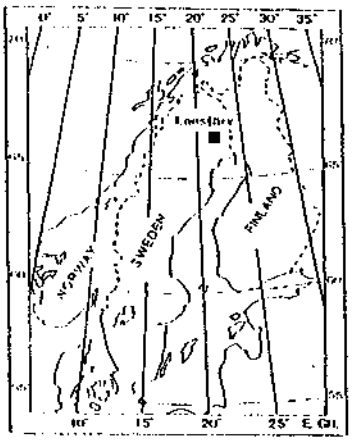

Figur 1. Lansjärvs läge.

2. BORRHÅLSDATA

För att mäta rörelserna i Lansjärvsförkastningen användes en Sliding micrometer. Sliding Micrometern är ett portabelt precisions instrument som mäter den relativa rörelsen mellan två mätklackar. Rörelsen, axiellt borrhålet registreras med hjälp av LVDT-givare placerad i mätsonden, se Figur 2.

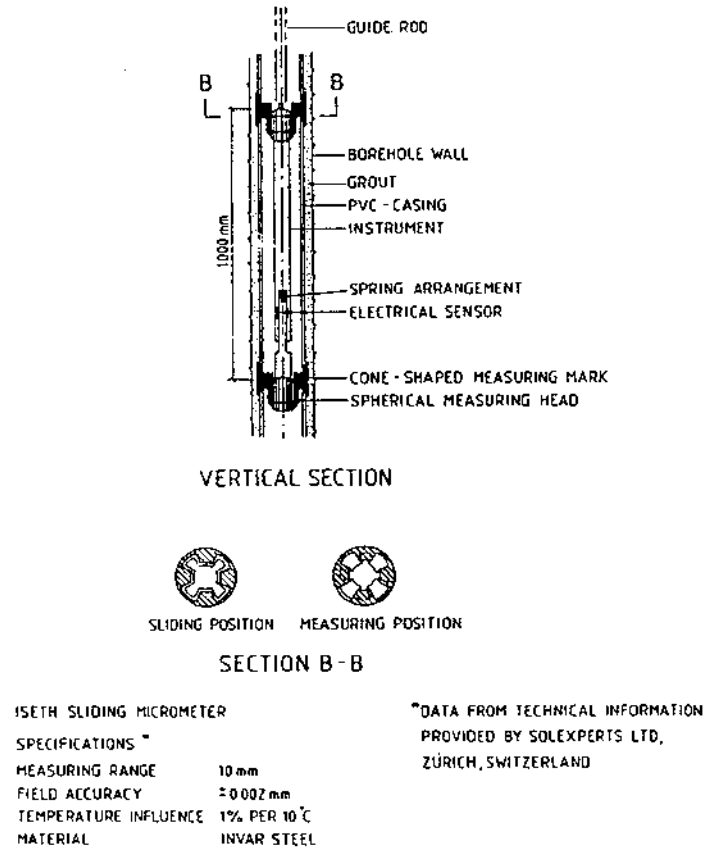

Figur 2. Beskrivning av Sliding Micrometer.

Mätklackarna är lokaliserade i följande borrhålssektioner:

Borrhål HMO 03 6.5-47.5
Borrhål HMO 04 11.5-48.5

Borrhålens placering framgår av figurerna 3-5.

Riktningen på respektive borrhål är följande:

HMO 03 292/70
HMO 04 1/30

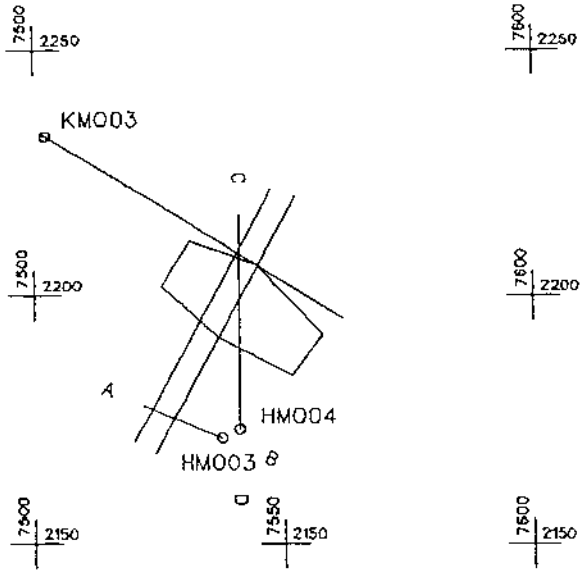

Figur 3. Borrhålens placering, horisontell vy.

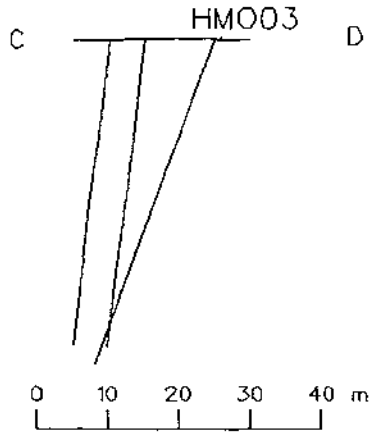

Figur 4. Vertikalprojektion, HMO03 med förkastningszon.
Höjdskala = längdskala.

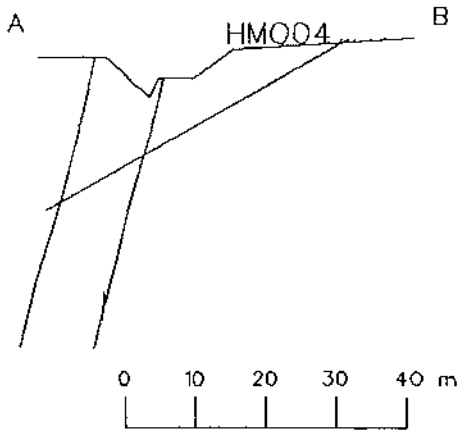

Figur 5. Vertikalprojektion, HMO04 med förkastningszon.
Höjdskala = längdskala.

De två borrhål i vilka deformationsmätningar är utförda övertvärar troligen inte förkastningszonen. HMO03 kan tom i sin helhet ligga utanför den centrala delen av förkastningszonen. Det innebär att en rörelse längs förkastningen ej med säkerhet kan registreras i de två borrhålen.

Mätningarna utfördes vid tretton tillfällen enligt tidsschema nedan:

Tidpunkt	Ordningsnr. dag
10 november 1990	0
8 december 1990	28
10 januari 1991	61
9 mars 1991	119
7 april 1991	148
25 maj 1991	196
27 juni 1991	229
25 juli 1991	257
28 augusti 1991	291
4 oktober 1991	328
9 november 1991	364
14 december 1991	399
25 januari 1992	439

Delar av mätresultaten redovisas i figurerna 6-7. Kompletta mätvärden redovisas i Bilaga 1-2. Som framgår är det främst i ytan som rörelser sker, men även i botten av HMO 03. Det är därför naturligt att det främst är dessa anomalier som bör förklaras.

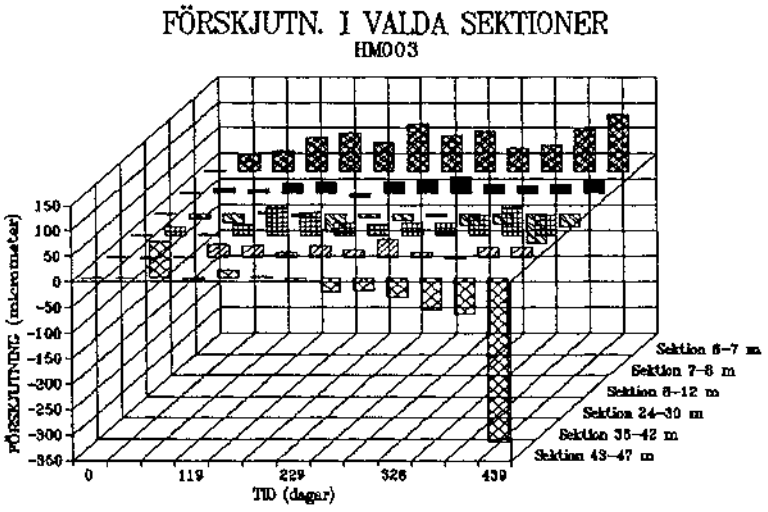

Figur 6. Grafisk presentation av deformationsmätningarna i HMO03. Ackumulerade belopp, första mättillfället (dag 0) är satt till referensnivå.

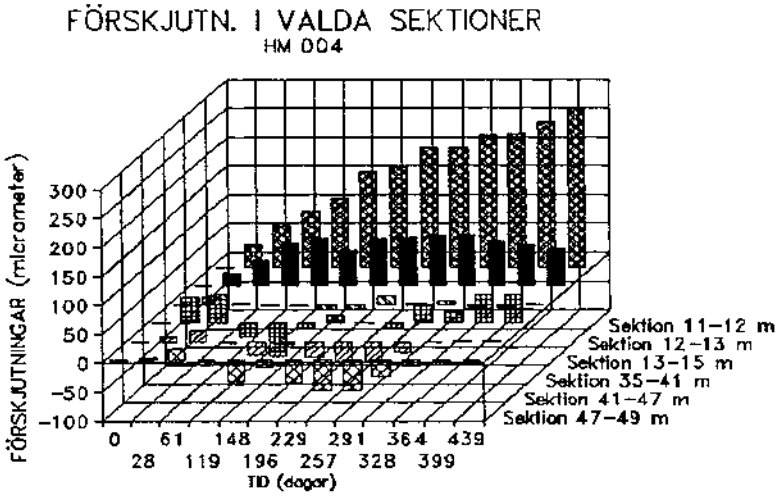

Figur 7. Grafisk presentation av deformationsmätningarna i HMO04. Ackumulerade belopp, första mättillfället (dag 0) är satt till referensnivå.

I tillägg till dessa mätningar har korttidsvariationerna studerats under en dag med ett mätintervall på ca 2 timmar, se Bilaga 3.

Vid granskning av mätresultaten finner man 3 påtagliga anomalier:

- I den ytnära delen av HMO04 är det mycket stor utvidgning under hela mätperioden.
- I den ytnära delen av HMO03 förekommer stora rörelser, både kompression och utvidgning.
- I HMO03, sektion 42.5-47.5m (dvs längst ned) är det en mycket stor kompression i slutet av mätperioden.

3. MODELLANSATS

Rörelser har uppmätts i borrhålen. Frågan är om det är verkliga rörelser i förkastningszonen orsakade av neotektonik eller om rörelserna är orsakade av temperatur- och/eller variationer i grundvattennivån? Beror de på dikesgrävning i närheten eller kanske på mätfel/instrumentfel? Några modeller har provats för att utröna om dessa yttre faktorer kan förklara mätresultaten.

- Den första modellen studerar vilken effekt en temperaturförändring i berget har på deformationer i berget. Eftersom lufttemperaturen varierar periodiskt, dels under ett dygn och dels under ett år, beräknas bergtemperaturens variation på olika djup, som en funktion av lufttemperaturens variationer.

- I den andra modellen undersöks vattnets påverkan. Bland annat innefattar detta variationer i porvattentrycket beroende på vattenståndsförändringar. Tidvatteneffekter och nederbörd beaktas också.

- I den tredje modellen beräknas deformationer som beror på förflyttningar av jordmassor i samband med dikesgrävning och dikets återställande.

De deformationer som beräknas i ovanstående modeller elimineras om möjligt från de totalt uppmätta deformationerna. Den restdeformation som kvarstår kan vara orsakad av neotektonik i förkastningszonen, d.v.s jordskorpan är fortfarande aktiv i detta område.

4. TEMPERATURENS EFFEKT

Vilka effekter har de normala temperaturväxlingarna på bergmassan i Lansjärv? Det kan omedelbart konstateras att dessa har mycket liten effekt på bergets mekaniska egenskaper. Vid tester i samband med anläggandet av Avesta värmelager kunde det påvisas att det krävs mycket stora temperaturvariationer för att dessa skall påverka bergets mekaniska egenskaper. Av försöken framgår att bergets E-modulen sjunker vid stora Δ T. En temperaturhöjning på 100° gör att bergets E-modul ändras från 65 till 55 GPa, samt att ett Δ T på 600° ger förändringar i tryckhållfastheten med ca. 50 %. För fallet Lansjärv är det aldrig frågan om dessa enorma temperaturvarianser, där kan det i extrema fall röra sig om skillnader på 5° i bergmassan.

Bergtemperaturen varierar bl a på grund av luftens temperaturvariation. Temperaturen som funktion av djupet innehåller både dämpning och fasförskjutning vilket beror på bergets fysikaliska egenskaper, djupet och perioden på variationen (Jessop, 1990). Temperaturen kan beräknas med hjälp av värmeledningsekvationen (också kallad Fouriers ekvation).

$$\frac{\partial u}{\partial t} = c^2 \frac{\partial^2 u}{\partial x^2} \qquad \text{(ekv 1)}$$

Genom att förenkla formeln till att gälla för ett homogent halvrum vars yttemperatur (luften) varierar periodiskt erhålls uttrycket:

$$A_z = A_0 e^{-\sqrt{\frac{\omega}{2\alpha}} z} = A_0 e^{-\sqrt{\frac{\pi}{\alpha P}} z} \qquad \text{(ekv 2)}$$

där A_z =temperatur-amplituden på djupet z
A_0 =temperatur-amplituden på ytan
P =perioden
ω =vinkelfrekvens= $2\pi/P$
α =termisk diffusivitet

T (temperaturen på djupet z) är ej i fas med T_0 (temperaturen på ytan) utan är fasförskjuten enligt ekv 3.

$$fasförskj = z\sqrt{\frac{\omega}{2\alpha}} \qquad \text{(ekv 3)}$$

4.1 FÖRENKLINGAR VID BERÄKNING.

Frysning (tjälbildning) samt snötäckets isolerande effekt beaktas inte. Dessa faktorer gör båda att amplituden blir mindre och fasförskjutningen större i verkligheten än vid beräkningen, beräkningarna ger alltså ett konservativt värde på temperatureffekten.

Vidare antas all värmeöverföring ske genom diffusion.

Eftersom dessa förenklingar mest gör sig gällande i de översta jordlagren görs två jämförelser.

4.2 JÄMFÖRELSE 1

För att få en uppfattning om beräkningsmodellens överensstämmelse med verkligheten gjordes en beräkning av temp-amplituden och fasförskjutningen på 0.5 m respektive 1.0 m:s jorddjup. Beräkningarna jämfördes med de av SMHI faktiskt uppmätta temperaturerna i morän i Abisko, se Figur 8. Som ingångsvärde i modellen användes temp-amplituden i luft (A_0) motsvarande det som kan utläsas ur temp-registreringar i närbelägna Torneträsk, se Figur 8 (Väder och vatten, SMHI).

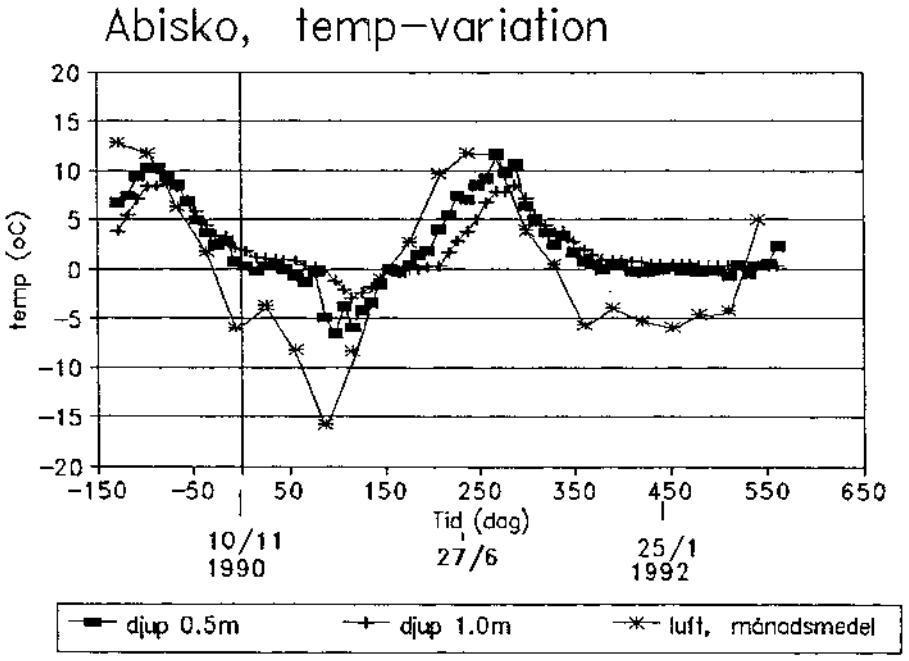

Figur 8. Temperaturmätningar i morän i Abisko samt lufttemperatur i närbelägna Torneträsk (källa SMHI).

Vi har då följande ingångsvärden:

A_0 =12 grader (motsvarar faktiskt värde i Torne-träsk)
P =1 år= 31536000 s
ω =1.99 E-7
α =4.0E-7 (antaget)

Dessa värden insatt i ekv (2) och (3) ger resultat enligt Tabell 1.

Eftersom diffusiviteten är svårbestämd och kan variera kraftigt för olika jordtyper görs en enkel känslighetsanalys på diffusivitetens påverkan på temperaturen i morän. Resultaten redovisas också i Tabell 1.

	Djup (m)	beräknad temp (°C)	uppmätt temp (°C)	ber.fas-förskj. (dagar)	uppm. fas-förskj. (dagar)
Morän Abisko	0.5	9	8	15	18(osäker)
Morän Abisko	1.0	7	5	29	28(osäker)
alterna-tivt α					
α=1.5E-7	1.0	5	5	47	28(osäker)
α=5.0E-7	1.0	8	5	26	28(osäker)

Tabell 1. Beräknad och uppmätt temperaturamplitud och fasförskjutning i morän.

4.3 JÄMFÖRELSE 2

På samma sätt som ovan gjordes ytterligare en modellberäkning. I denna jämfördes de av SMHI faktiskt uppmätta temperaturerna i sandjord i Flahult, Småland (se Figur 9), med teoretiskt beräknade temperaturer. Som ingångsvärde i modellen användes temp-amplituden i luft (A_0) motsvarande det som kan utläsas ur temp-registreringar i närbelägna Jönköping, se Figur 9.

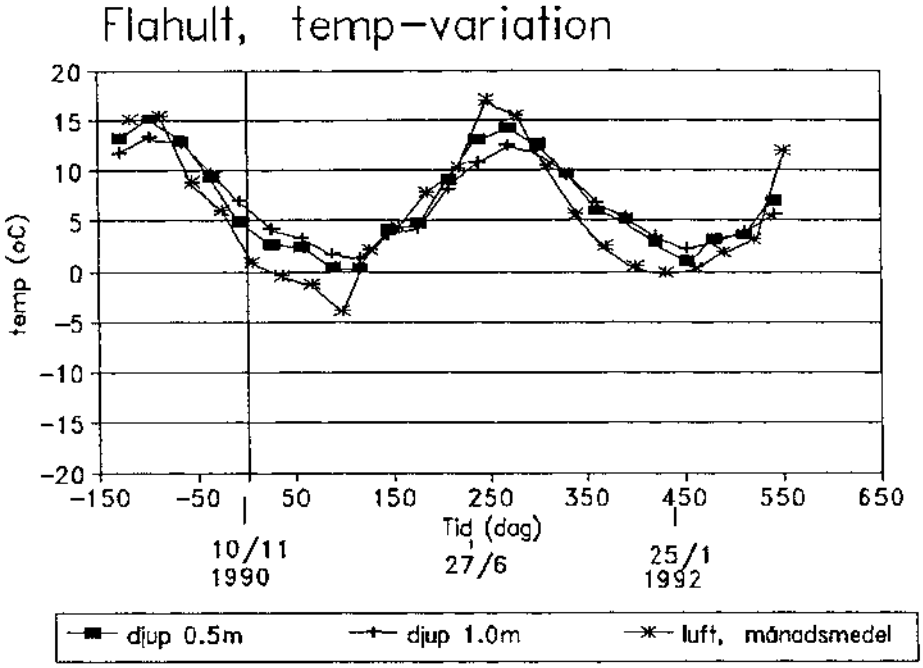

Figur 9. Temperaturmätningar i sandjord i Flahult, Småland samt lufttemperatur i Jönköping (källa SMHI).

Vi har då följande ingångsvärden:

A_0 =10 grader (motsvarar faktiskt värde i Jönköping)
P =1 år= 31536000 s
ω =1.99E-7
α =4.0E-7 (antaget)

Dessa värden insatt i ekv (2) och (3) ger resultat enligt Tabell 2.

	Djup (m)	beräknad temp (°C)	uppmätt temp (°C)	ber.fas-förskj. (dagar)	uppm. fas-förskj. (dagar)
Sandjord Flahult	0.5	8	7	15	11(osäker)
Sandjord Flahult	1.0	6	5.5	29	16(osäker)

Tabell 2. Beräknad och uppmätt temperaturamplitud och fasförskjutning i sandjord.

Dessa två jämförelser visar att beräkningsmodellen överensstämmer med verkligheten. Det var vissa svårigheter att utifrån tillgängliga data avläsa den verkliga fasförskjutningen men storleksordningen på felen är acceptabla (<40%). Modellen går att använda för vår undersökning och gjorda förenklingar påverkar ej resultaten på något avgörande sätt.

4.4 2-LAGERMODELL

En 2-lagermodell antas med morän i första lagret och granodiorit i det andra, se Figur 10.

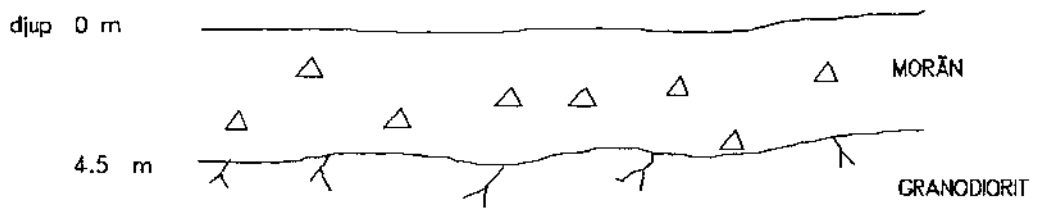

Figur 10. Antagen 2-lagersmodell.

Amplituden och fasförskjutningen vid gränsskiktet beräknas med hjälp av ekv (2) och(3). Dessa värden blir sedan ingångsvärden för beräkning av amplitud och fasförskjutning på olika djup i det andra lagret.

Vidare antas att temperaturen varierar sinusformat över året.

Antagen temperaturvariation i luften grundar sig på månadsmedelvärde i Pålkem, 20 km från Lansjärv, se Figur 11.

Nu kan temperaturen beräknas på olika djup vid olika tidpunkter med varierande ingångsparametrar, se Figur 12. Det framgår att på 10 m:s djup är temperaturvariationen bara 0.1 ^{0}C.

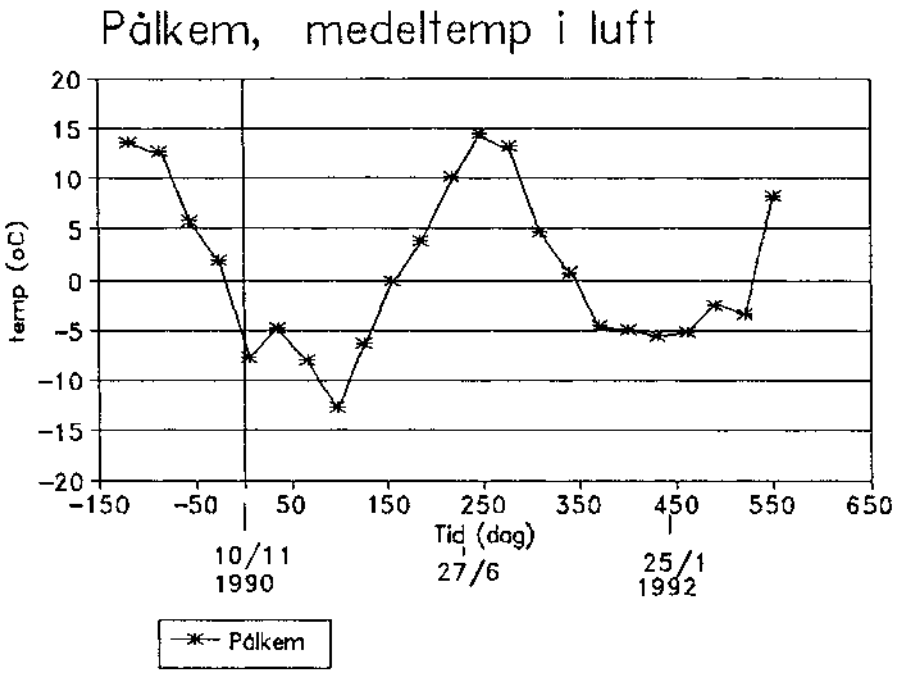

Figur 11. Luftens medeltemperatur i Pålkem, nära Lansjärv.

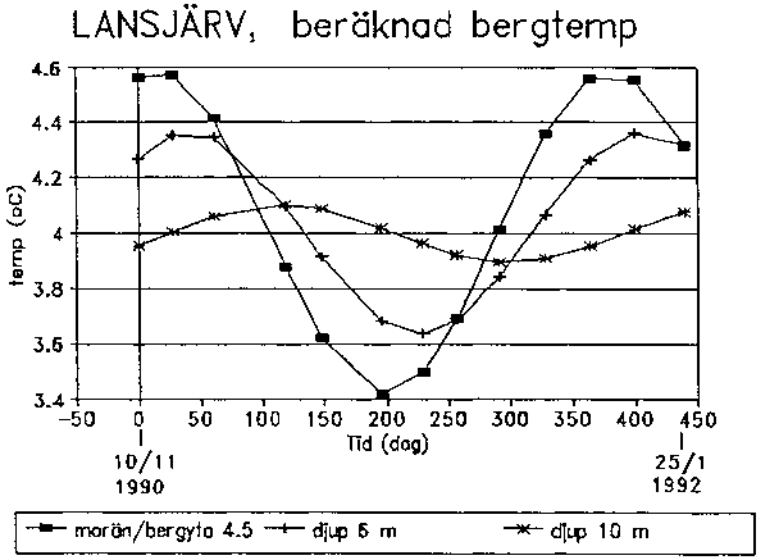

diffusivitet morän =4.0E-07 m^2/s
diffusivitet berg =1.0E-07 m^2/s
A_0 =11 grader

Figur 12. Beräknad temperaturvariation på olika djup.

4.5 TEMPERATURENS EFFEKT PÅ BERGMASSAN.

För att koppla de framräknade temperaturvariationerna till töjningarna i bergmassan antas följande.
Den studerade sektionen är (se Figur 13) fast inspänd radiellt kring hålet men har möjlighet att röra sig längs borrhålet. Till grund för detta antagande är mätsektionens läge. Sektionen är belägen i det ytnära berget, vilket ger att det finns möjligheter för berget att utvidgas i z-riktning. Sektionen är dock placerad så långt ifrån förkastningen att den kan anses som fast inspänd i horisontalled. Vidare antas att spänningarna i vertikalled ~ 0. Dessa antaganden leder till följande:
Mätsektionen kommer enbart att vara utsatt för rörelser i vertikalled. Dessa är orsakade av temperaturutvidgningen i bergmassan, samt indirekt av spänningsförändringen radiellt borrhålet som uppstår p.g.a temperaturvariationen.
Eftersom temperaturen är likformigt fördelad gäller att töjningarna är likformiga om det antas att berget är isotropt samt ej fastspänt i någon riktning.

$$\varepsilon_T=\varepsilon_{zz}=\varepsilon_{xx}=\varepsilon_{yy}$$

Temperaturutvidgningen ges av (Brady m.fl, 1985):

$$\varepsilon_{zz}=\beta\Delta T \qquad \text{(ekv.4)}$$

där ß=längdutvidgningskoefficienten

Den indirekta längdutvidgningen orsakad av tryckökningen radiellt borrhålet på grund av fast inspänning blir (Bjurström m.fl,1977):

$$\varepsilon_{zz}=\frac{\nu}{E}(\Delta\sigma_{yy}+\Delta\sigma_{xx})$$

där ν = tvärkontraktionstalet (Poissons tal)
E = elasticitetsmodulen
σ_{xx} och σ_{yy}= huvudspänningsriktningar

$$\Delta\sigma_{yy}=\Delta\sigma_{xx}=E\varepsilon_t$$

$$\varepsilon_{zz}=2\nu\varepsilon_T \qquad \text{(ekv. 5)}$$

Totala töjningen orsakad av temperaturvariationerna fås

genom att addera bidraget från temperaturökningen (ekv.4) och bidraget från tryckökningen (ekv.5):

$$\varepsilon_{tot}=(1+2\nu)\beta\Delta T \qquad \text{(ekv.6)}$$

De tidigare beräkningarna m.h.a värmeledningsekvationen visar att temperaturvariationen på 6 m djup är $\pm$ 0.4°. Längdutvidgningskoefficienten (ß) varierar mellan 5-10 μm/°K för bergarter liknande de som finns i Lansjärv (Division of Rock Mechanics,1986). Om betraktelsen sker under idealiserade förhållanden så ger detta att magnituden på de teoretiska rörelserna pga temperaturvariationerna skulle kunna vara i storleksordningen 5-10 μm. Genom att räkna om de teoretiska temperaturvariationerna enligt ekv. 3 erhålls värden enligt Figur 13. I Figur 13 har graferna olika amplituder, vilket möjligen kan förklaras av de idealiserade förhållanden som har antagits. Men även om en mer komplex modell av berget antas, som ger större rörelser pga temperaturdifferensen, så kvarstår faktum att kurvorna ligger ur fas. Utav detta kan temperaturens inverkan på rörelserna anses vara av underordnad betydelse, möjligen kan den ha någon form av underordnad störning under sommarhalvåret.

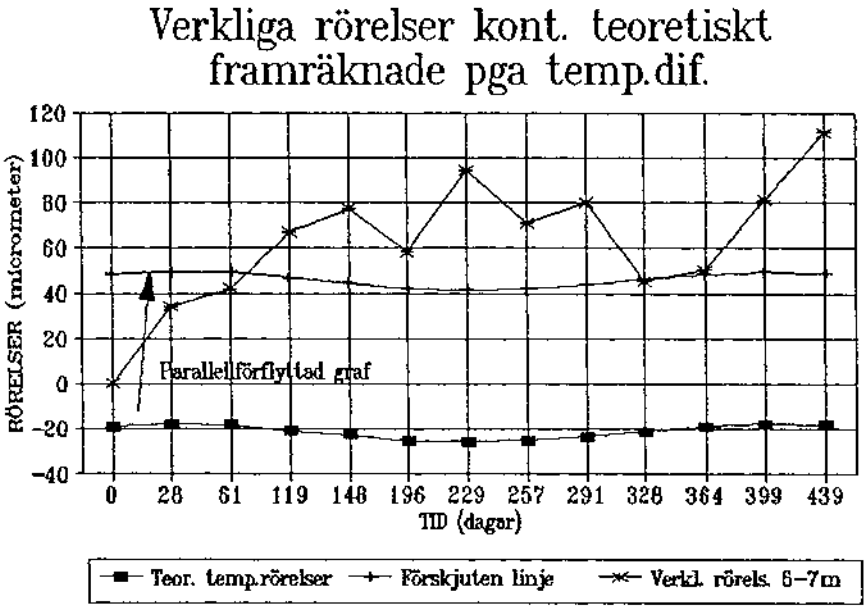

Figur 13. Rörelser på grund av temperaturförändringar i bh HMO03.

5. GRUNDVATTNETS EFFEKT

Fakta angående grundvattenvariationerna är hämtade ur SGU:s grundvattenmätningar i Pålkem, beläget ca. 20 km från Lansjärv, se Bilaga 4.

Det är möjligt att betrakta vattnets effekt på bergmassan på tre olika sätt beroende på vilken struktur bergmassan har.

- Första belastningsfallet antar förändringar i porvattentrycket pga den skiftande grundvattennivån.

- Andra belastningsfallet betraktar vattnet som en utbredd last.

I ovanstående fall antas bergmassan vara isotrop och linjärelastisk.

- Tredje hypotesen antar att grundvattnets nivåförändringar äger rum i gränsområdet morän och ytberg.

5.1 FÖRÄNDRING I PORVATTENTRYCKET.

Eftersom ovanstående antagande gör att Hooke's lag gäller kan töjningarna beräknas enligt nedan (Brady m.fl,1985):

$$\varepsilon_{xx}=\frac{1}{E}[\sigma_{xx}-\nu(\sigma_{yy}+\sigma_{zz})] \qquad \text{(ekv. 1)}$$

Förändringarna i porvattentrycket sker hydrostatiskt enligt:

$$\Delta\sigma_{xx}=\Delta\sigma_{zz}=\Delta\sigma_{yy}=\Delta\sigma$$

$$\Delta\varepsilon_{xx}=\frac{1}{E}[\sigma_{xx}-\nu(\sigma_{yy}+\sigma_{zz})]-\frac{1}{E}[\sigma_{xx}+\Delta\sigma-\nu(\sigma_{yy}+\sigma_{zz}+2\Delta\sigma)]$$

$$\Delta\varepsilon_{xx}=-\frac{1}{E}[\Delta\sigma-\nu(-2\Delta\sigma)] \qquad \text{(ekv. 2)}$$

Enligt grundvattenmätningarna så sker största variationen i vattenståndet under april och maj.

Max. g.r.v nivå 40 cm under rör, överkant (maj).
Min. g.r.v nivå 240 cm under rör, överkant (april).

Δ g.r.v nivå = 200 cm detta skulle medföra en ökning av porvattentrycket motsvarande 0.02 MPa.

Ett antagande av E= 60 GPa ν= 0.2 insatt i ekv. 2 ger töjningar på 0.2 μstrain.
Detta ger marginella töjningar, värden som ligger inom felgränserna för instrumentets mätnoggrannhet, även sett på en 10 meters sträcka. Även om det antas att E-modulen är mycket låg så är de teoretiskt framräknade värdena alltför låga för att förklara de verkliga rörelserna.

5.2 VATTNET SOM UTBREDD LAST

Detta fall är inte realistiskt då det förutsätter ett antagande om mycket låg permeabilitet i ytberget. Dessutom skulle spänningsförändringarna orsakade av detta endast verka på σ_{zz} vilket i sin tur endast skulle ge töjningar motsvarande:

$$\varepsilon_{zz}=\frac{1}{E}\Delta\sigma_{zz}$$

Detta visar att även för det här antagandet ligger de teoretiska töjningarna inom felgränserna för instrumentets mätnoggrannhet.

Resultatet visar att oavsett om en betraktelse sker enligt alternativ 1 eller 2, så pekar det på att de här framräknade teoretiska töjningarna är för små för att förklara de uppmätta rörelserna i Lansjärv.

5.3 RÖRELSER I SVAGHETSPLAN

Den mest troliga hypotesen är, att grundvattnets variation mellan min och max värden sker i ytberget. Om man antar att berget är uppsprucket vid ytan gäller inte längre Hooke's lag eftersom bergmassan inte längre är att betrakta som isotrop. Enligt denna teori kommer de förhärskande rörelserna att ske längs sprickplan och andra svaghetszoner. Eftersom lägen och storlekar på svaghetsplanen är okända måste det göras en koppling mellan grundvattenförändring och de uppmätta rörelserna.

En lämplig ansats är att studera hur grundvatten förändringen på 200 cm mellan april och maj återspeglar sig i mätresultaten, eftersom temperaturvariationen är relativt liten under dessa två månader. Under samma period ger mätresultaten att sektionen är utsatt för en liten kompres-

sion. Det verkar dock mer troligt att den verkliga effekten av grundvattenförändringen gör sig gällande under nästa mätning, då sektionen uppvisar en töjning. Studerad sektion är 6 - 7 m i HM003 där rörelsen var 36 μm under maj - juni. Detta skulle då ge en rörelse på 18 μm/(m grundvattenförändring). Detta kan sedan räknas om till förväntade rörelser orsakade av de varierande grundvattenrörelserna, enligt Figur 14.

Som visas i figuren så följer de förväntade rörelserna pga grundvattenvariationerna de uppmätta värdena relativt bra i den region vilken kalibreringen har skett. En möjlig förklaring kan vara att vattnet har större möjlighet att söka sig ner i sprickor och andra svaghetsplan under den tid av året som marken är tjälfri. Under denna tid av året är även mängden fritt vatten också stor, emedan det under vinterhalvåret måste ske en infiltration från omgivande berg.

Genom att eliminera de förväntade rörelserna orsakade av grundvattenvariationerna, visar det sig att sektionen 6-7 m verkar vara utsatt för en kontinuerlig utvidgning som framförallt sker under vinterhalvåret. Denna utvidgning ser ut att variera en del år från år. Om en betraktelse

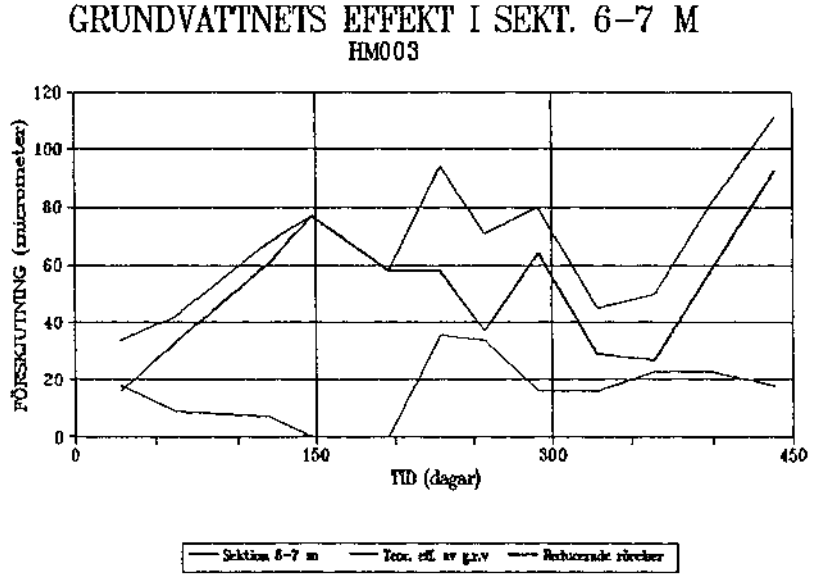

Figur 14. Grundvattnets effekt i HM003, sektion 6-7 m.

sker från dec 90 - jan 91 samt dec 91 - jan 92, visar det sig att rörelserna varierar från 8 µm för det förstnämnda till 30 µm i den andra tidsperioden. Detta sker trots att temperaturvariansen och grundvattenförändringen är i det närmaste identisk för de båda perioderna.

Liknande variationer borde rent teoretiskt uppstå även i HMO04, trots att det hålet i det närmaste att beakta som horisontellt. Utav de mätningar som finns tillgängliga är det dock mycket svårt att avgöra om det förekommer några variationer i de uppmätta rörelserna som är direkt kopplad till grundvattenförändringarna. En annan sak som är värt att poängtera är skillnaden i rörelser i samma månader år från år.

Mätningarna är gjorda under en tidsperiod av 14 mån, Det är således svårt att dra slutsatser om vad som är årstidsberoende och vad som beror på andra faktorer. Ett mätprogram över en längre tidsperiod krävs.

5.4 TIDVATTEN

Solens och månens inbördes förhållande ger upphov till tidvatteneffekter i haven.
Vid mätning av vattennivåer i brunnar har man i Sverige kunnat iaktta en variation på grund av tidvattnet. Amplituden på dessa variationer är ca 0.1 m som mest och detta maximum uppnås ca 2 gånger per dygn (Eriksson m.fl,1970).

För att återkoppla till mätningarna i Lansjärv kan man säga att tidvattenfasen vid mättillfällena var okänd. Därför får tidvattenvariationen anses som ett mätfel motsvarande effekten av 0.2 m:s förändring av grundvattennivån, dvs 4 µm/m. Detta överensstämmer med de uppmätta korttidsvariationerna, se Bilaga 3.

6. YTTRE BELASTNING

I närheten av HM004 anlades ett dike med syfte att kartera de översta jordlagren. Vilken effekt har detta på rörelserna i berget ?

För att studera vilka rörelser som kan förväntas i berggrunden har en modell i UDEC (2D -distinct element program) tagits fram, se Figur 15. Modellen är som många andra numeriska modeller, inte en exakt kopia av verkligheten. Syftet med denna är istället att studera vilken storlek de olika materialparametrarna måste ha, för att de uppmätta värdena skall verifieras i modellen. Utifrån detta går det att bedöma om det är ett rimligt antagande att diket är orsak till delar av de faktiska rörelserna.

Det kan vara svårt att dra några slutsatser av mätningarna och de beräknade rörelserna, vilket framförallt beror på svårigheterna att avgöra om alla uppmätta rörelser som sker härrör från en pågående rörelse mot diket. Alternativt om denna rörelse har nått sitt maximala belopp under året eller om rörelserna därefter har sin förklaring i andra orsaker.

Med den numeriska modellen går det att få fram ett absolutbelopp på rörelserna orsakad av diket, se Figur 16. Detta absolutbelopp är direkt kopplat till materialparametrarna. Eftersom det är osäkert hur mycket av rörelserna som härrör från det anlagda diket, är det naturligtvis med stor osäkerhet som material-parametrarna kan kalibreras. Om sprickparametrarna i förkastningszonen sätts mycket låga (Kohesionen = 0 och Friktionsvinkeln 20°) och om E-modulen

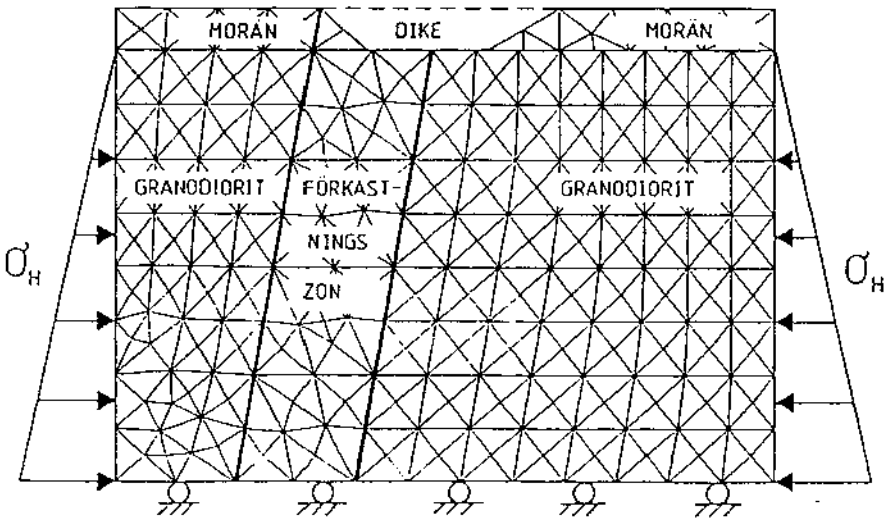

Figur 15. UDEC-modell.

enbart varieras inom acceptabla intervall för resp. område så kan de teoretiska absolut-beloppen för töjningarna variera från 20-200 μm.

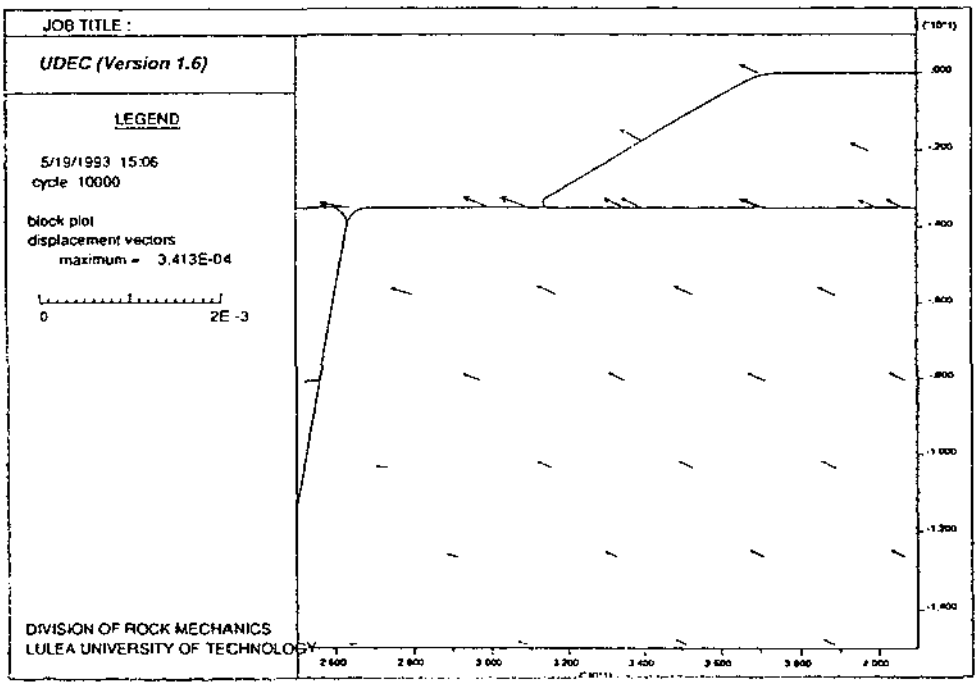

Figur 16. Beräknade rörelser enligt UDEC-modell.

Trots osäkerheterna i de framräknade absolutbeloppen kan man dra slutsatsen att delar av rörelserna i sektion 11-12 m HM004 kan tillskrivas det anlagda diket, däremot är det svårt att med säkerhet säga hur stor denna del är av de totala rörelserna. Ett rimligt antagande är att E-modulen för bergmassan är relativt låg, eftersom det är i ytberget som mätningarna har skett. Om så är fallet kan delar av de faktiska rörelserna bero på diket.

7 DISKUSSION

Generellt kan sägas att det är svårt att avgöra om förändringarna är periodiska eller ej. Särskilt gäller detta årsvariationer eftersom den totala mättiden endast har varit 14.5 månader.

Enligt våra beräkningar varierar temperaturen i berget på 6 m:s djup inom ett intervall på 0.8 grader sett över 1 års tid. Detta ger upphov till en deformation på högst 10 μm/m. Temperaturvariationerna avtar snabbt nedåt för att vid 10 m vara nästan obefintliga.
Årsvariationen kan inte spåras i de uppmätta värdena eftersom deformationen på grund av temperaturförändringar är så liten i förhållande till den totala deformationen. Dessutom har mätningarna bara skett över en period av 14.5 mån vilket medför att slutsatser om variationer på årsbasis kan vara förhastade.

Vissa osäkerheter föreligger i den antagna grundvattenmodellen för HMO03 då rörelsemönstret ej återspeglas i HMO04. Orsaken kan vara de stora ytliga deformationerna i HMO04 som gör att grundvatteneffekterna döljs.
Om en jämförelse görs mot korttidsvariationerna, troligen orsakade av tidvattnet, verifierar detta att 1 m vattenpelare orsakar 18 μm:s rörelse/m. Resultaten pekar entydigt på svårigheterna att ställa upp en teoretisk modell av grundvatteneffekterna. Dessa effekter bör istället analyseras empiriskt genom en längre mätserie.

Som tidigare sagts är det troligt att huvuddelen av rörelserna i den första mätsektionen av HMO04 härrör från dikesgrävningen. Storleksordningen är svårbedömd då det är omöjligt att avgöra den absoluta töjningen. Enda sättet att verifiera detta är återigen att mäta huruvida rörelserna fortgår eller inte.

En sektion som uppvisar rörelser, men ej är kopplad till yteffekter, är den nedersta delen av HMO03. Rörelserna här kan endast förklaras med verkliga rörelser i förkastningen. Värt att notera är att alla sektioner har totala rörelser understigande 0.5 mm (500 μm), där flertalet sektioner understiger 0.05 mm (50 μm). Med andra ord är de uppmätta rörelserna mycket små.

8 REKOMMENDATION OM FORTSATTA ARBETEN

Slutsatsen, och vår rekommendation utifrån detta arbete är att mätningarna bör fortgå under en längre tidsperiod, 3-5 år, för att man med större säkerhet skall kunna uttala sig om vad som orsakar de uppmätta rörelserna i Lansjärvsförkastningen. Dessutom rekommenderar vi att mätningarna kompletteras med ytterligare två borrhål. Det ena 150-200 m långt, motiveras av att HMO03 troligen inte övertvärar förkastningen vilket vore önsvärt för att möjliggöra mätning på båda sidor om förkastningen. Det andra bör vara ett kort vertikalt hål för grundvattennivåregistrering.

9 REFERENSER

Bjurström, S., 1977. Lagring och transport av vattenburen värme i berg, Fältförsök, BeFo Nr 11:14/77.

Brady, B.H.G, & Brown, E.T, 1985. Rock mechanics for underground mining.

Division of rockmechanics, 1986. Heat induced fracturing of rock in an existing uniaxial stress field, Resarch report 1986:02, LuTH.

Eliasson, T., Smellie, J., Tullborg, E-T., 1991. Mineralogical studies of the "post-glacial" fault exposed at Molberget, Lansjärv area, Northern Sweden. SKB AR 91-14.

Eriksson, E., Gustafsson, Y., Nilsson, K., 1970. Grundvatten.

Jessop, A.M., 1990. Termal geophysics.

Lagerbäck, R., 1991. Seismically deformed sediments in the Lansjärv area, Northern Sweden. SKB TR 91-17.

Nilsson, G., 1992. Displacement measurments in the post-glacial fault at the Molberget site, Lansjärv area. SKB ej publicerad rapport.

Rehbinder, G., 1985. Stresses and strains around a heated sperical cavity in an elastic medium, Rock mechanics and rock engineering 18 (1985) p. 213-218, litt.

Väder och Vatten, juli 1990 - maj 1992, SMHI.

BILAGA 1 Borrhålsdata HMO03

Readings from borehole HMO03 nov-90 - jan-92.

6.5	981	1015	1023	1048	1058	1039	1075	1052	1061	1026	1031	1062	1092
7.5	1026	1036	1034	1046	1048	1018	1047	1051	1058	1044	1041	1043	1054
8.5	1007	998	990	1010	1004	974	1001	996	1003	987	989	985	983
9.5	910	916	910	919	922	922	928	937	943	917	913	934	926
10.5	841	843	842	860	852	848	857	862	851	841	850	846	867
11.5	899	910	912	900	920	878	880	901	918	913	907	903	903
12.5	1035	1033	1025	1026	1035	1039	1031	1035	1037	1038	1036	1036	1033
13.5	1042	1036	1027	1049	1044	1042	1058	1055	1057	1041	1043	1038	1051
14.5	1056	1057	1057	1051	1061	1056	1051	1046	1047	1035	1047	1041	1041
15.5	1046	1043	1049	1044	1054	1046	1048	1048	1042	1040	1054	1049	1057
16.5	666	675	670	679	683	672	675	688	684	685	688	672	692
17.5	929	940	920	918	940	916	913	912	924	932	922	920	883
18.5	755	749	739	752	753	753	747	731	751	753	760	743	747
19.5	1078	1069	1073	1076	1089	1081	1082	1095	1096	1095	1101	1097	1100
20.5	749	754	731	749	745	733	741	742	745	737	741	737	743
21.5	820	826	832	827	828	831	845	845	842	834	834	838	839
22.5	831	843	830	839	850	849	849	846	844	851	848	853	849
23.5	1068	1064	1060	1055	1059	1057	1057	1057	1057	1058	1060	1060	1061
24.5	1006	1004	993	1015	1017	999	1010	1006	1008	1000	1005	1003	1009
25.5	1076	1083	1084	1078	1088	1087	1082	1083	1083	1088	1080	1090	1084
26.5	1049	1047	1045	1043	1050	1051	1044	1046	1046	1046	1054	1056	1047
27.5	1182	1193	1190	1189	1198	1190	1183	1184	1184	1187	1189	1193	1185
28.5	1072	1075	1072	1063	1079	1093	1067	1066	1066	1078	1082	1083	1073
29.5	1070	1071	1073	1090	1077	1081	1094	1093	1095	1082	1085	1085	1097
30.5	1046	1041	1042	1035	1047	1045	1034	1031	1030	1035	1033	1033	1019
31.5	1038	1040	1034	1039	1031	1029	1035	1035	1039	1031	1030	1032	1044
32.5	988	990	994	996	1002	1003	997	1001	1002	1008	1010	1011	1008
33.5	1196	1197	1194	1194	1199	1193	1186	1188	1190	1189	1195	1194	1190
34.5	1032	1034	1037	1026	1042	1040	1042	1031	1035	1042	1043	1041	1033
35.5	986	988	987	991	989	984	982	975	984	981	981	983	985
36.5	1091	1087	1093	1100	1093	1090	1100	1102	1103	1093	1094	1091	1100
37.5	1095	1097	1100	1114	1112	1116	1123	1123	1126	1120	1121	1125	1132
38.5	1165	1177	1171	1174	1170	1162	1164	1157	1156	1150	1150	1160	1160
39.5	1276	1278	1273	1268	1279	1280	1275	1270	1282	1281	1272	1294	1273
40.5	1167	1170	1172	1185	1177	1170	1178	1181	1185	1171	1167	1173	1185
41.5	1333	1335	1338	1330	1338	1339	1330	1330	1330	1341	1340	1324	1317
42.5	1467	1465	1466	1460	1467	1473	1462	1457	1454	1466	1470	1469	1448
43.5	1009	1001	997	996	987	974	976	972	972	965	947	950	922
44.5	1295	1300	1324	1310	1323	1324	1316	1320	1326	1324	1320	1319	1248
45.5	1385	1388	1411	1381	1394	1394	1389	1370	1368	1374	1366	1362	1331
46.5	1304	1304	1332	1302	1306	1306	1306	1304	1303	1294	1297	1292	1222
47.5	1322	1320	1314	1312	1322	1322	1310	1310	1316	1304	1304	1307	1306

BILAGA 2 Borrhålsdata HMO04

Readings from borehole HMO 04 nov-90 – jan-92

11.5	747	788	820	845	866	914	921	954	955	978	979	999	1034
12.5	808	830	854	884	891	870	892	893	896	897	885	881	874
13.5	775	787	778	773	772	765	766	790	778	781	771	771	775
14.5	753	757	758	762	763	770	778	788	776	775	781	780	787
15.5	927	921	926	929	929	925	918	931	915	912	915	917	919
16.5	814	800	802	804	804	807	787	799	794	804	803	800	808
17.5	749	744	742	736	733	746	740	745	748	751	741	742	746
18.5	847	848	848	844	843	852	849	849	846	853	850	854	857
19.5	803	809	820	805	806	821	807	811	793	820	817	829	828
20.5	770	784	784	778	750	767	758	762	767	770	760	755	770
21.5	827	824	826	826	827	825	817	809	816	818	811	813	817
22.5	962	966	968	954	953	968	958	959	955	964	963	962	969
23.5	512	505	504	513	507	495	505	497	503	503	505	496	504
24.5	717	717	720	726	725	725	718	723	715	727	713	723	725
25.5	828	813	824	830	833	827	820	813	814	825	824	823	827
26.5	745	759	763	750	745	739	733	727	730	745	744	745	752
27.5	392	397	403	392	394	405	393	403	394	403	394	398	398
28.5	563	559	568	570	568	571	567	568	563	570	564	573	580
29.5	767	764	771	772	770	762	755	754	754	756	752	761	764
30.5	498	496	503	518	512	509	502	495	500	511	503	514	516
31.5	690	697	697	682	675	687	679	679	681	687	680	683	684
32.5	812	817	828	816	818	824	814	824	820	829	827	829	823
33.5	514	510	506	509	508	507	499	494	497	504	507	508	512
34.5	845	856	861	852	852	846	853	847	847	852	858	861	866
35.5	871	869	886	867	874	882	894	890	890	893	899	909	912
36.5	912	910	912	914	908	906	897	889	889	895	890	900	901
37.5	1149	1155	1157	1140	1132	1147	1139	1138	1134	1141	1143	1152	1152
38.5	908	922	923	914	907	897	925	922	926	935	932	944	947
39.5	1093	1108	1108	1083	1081	1094	1100	1096	1091	1106	1102	1106	1109
40.5	1559	1569	1570	1548	1531	1563	1558	1553	1549	1558	1550	1556	1560
41.5	1206	1204	1207	1216	1214	1207	1207	1207	1205	1209	1206	1213	1215
42.5	1436	1446	1447	1443	1437	1449	1450	1443	1441	1450	1455	1459	1456
43.5	1847	1859	1859	1845	1839	1851	1844	1836	1844	1845	1850	1848	1848
44.5	1223	1226	1234	1220	1218	1220	1212	1213	1210	1219	1219	1221	1230
45.5	1260	1273	1272	1274	1266	1267	1261	1260	1258	1260	1265	1263	1260
46.5	1432	1432	1437	1440	1436	1439	1438	1440	1436	1440	1447	1453	1455
47.5	950	945	953	957	957	956	952	948	950	954	953	957	960
48.5	1008	1009	1006	999	986	995	992	990	988	993	995	993	994

BILAGA 3 Korttidsvariation, mätdata

Mätresultat från de övre delarna av HMO04.
Mätningarna är gjorda samma dag.

djup	kl 08.00	09.45	11.38	13.25	15.35	17.45
11,5	1034	1034	1033	1034	1036	1038
12,5	874	878	876	877	877	875
13,5	775	776	777	779	779	780
14,5	787	788	788	788	789	789
15,5	919	920	922	922	921	920
16,5	808	807	805	806	809	806
17,5	746	745	747	748	749	746
18,5	857	856	854	858	854	858
19,5	828	828	831	829	830	827
20,5	770	766	764	765	765	765
21,5	817	820	819	820	820	821
22,5	969	972	968	972	971	973
23,5	504	504	506	504	508	509
24,5	725	727	728	726	725	724
25,5	827	828	827	828	827	827

BILAGA 4 **Grundvattenmätning i Pålkem**

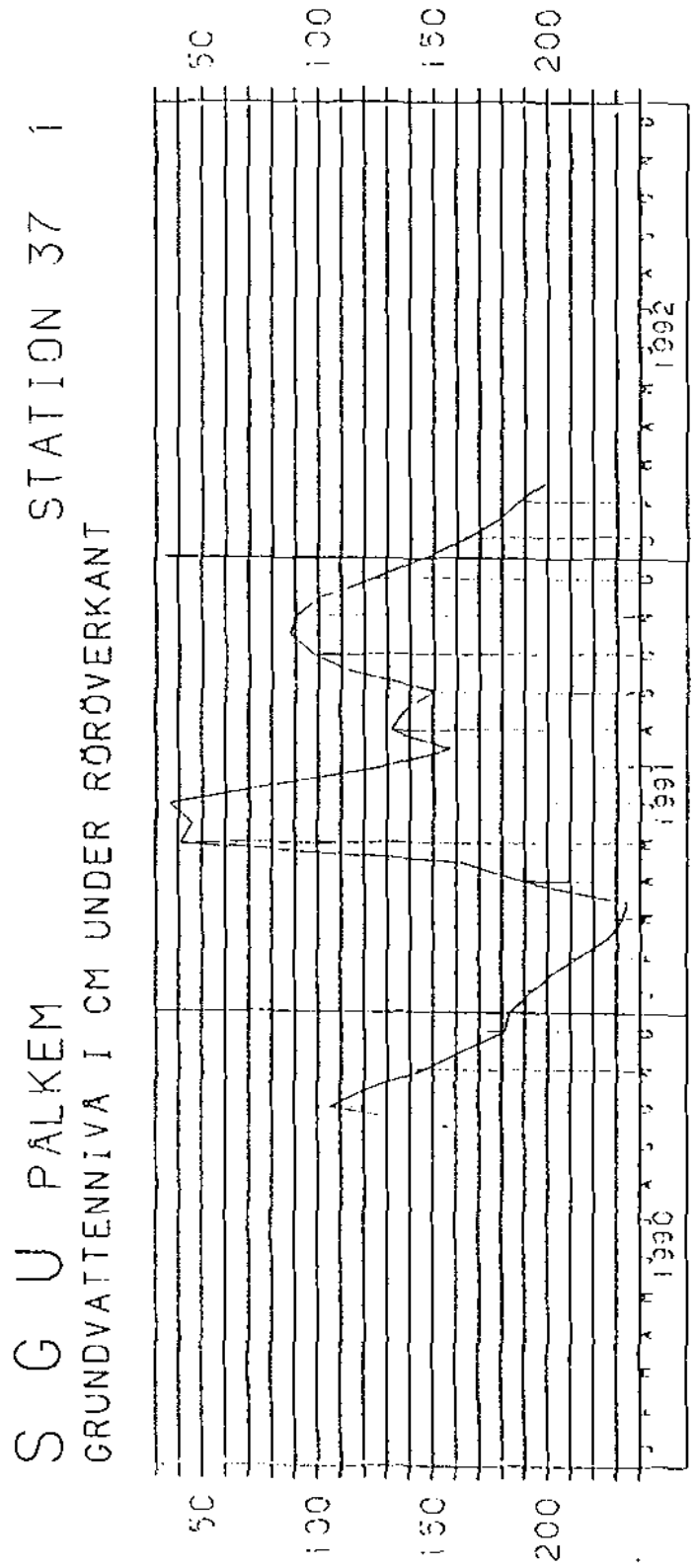

BILAGA 5 Indatafil till UDEC

```
*LANSJÄRVS FÖRKASTNING
block 0 0 55 0 55 -40 0 -40
*KROSSZON
crack 17 0 10 -40
crack 27 0 20 -40
*MORÄNLAGER
crack 0 -3.5 55 -3.5
*DIKE
crack 18 0 21 -3.5
crack 37 0 31 -3.5
*SPRICKOR I FÖRKASTNINGEN
jreg 17 0 27 0 20 -40 10 -40
jset 80 10 20 10 5 3 10 5 10 -40
*ZON GENERERING
*set edge 0.5
gen edge 5
*MTRL EGENSKAPER
*MAT 1 (GRANODIORIT) (E=10 GPa v=0.20)
prop mat 1 k=4.16e9 g=5.56e9 dens=2700 kn=1e11 ks=1e11
*FÖRKASTNINGSZON (E=1 GPa v=0.20)
prop mat 2 k=0.42e9 g=0.56e9 dens=2600 kn=1e11 ks=1e11
*MORÄN (E=1 GPa v=0.20)
prop mat 3 k=0.42e9 g=0.56e9 dens=2500 kn=1e11 ks=1e11
*SPRICKOR
prop jmat 1 jkn 1e11 jks 1e11 jfric 0.2 jcoh 0.0
prop jmat 2 jkn 1e11 jks 1e11 jfric 0.2 jcoh 0.0
prop jmat 3 jkn 1e11 jks 1e11 jfric 0.5 jcoh 2.0e6
*MTRL BESTÄMNING
*FÖRKASTNINGSZON
change region 17 -4 26 -4 20 -40 9 -40 mat 2
change region 17 -4 26 -4 20 -40 9 -40 jmat 2
*MORÄNEN
change region 0 0 55 0 55 -3.5 0 -3.5 mat 3
change region 0 0 55 0 55 -3.5 0 -3.5 jmat 3
damp auto
*RANDVILLKOR
bound stress 0 0 0 ygrad 0.075e6 0 0.027
insitu stress 0 0 0 ygrad 0.075e6 0 0.027
gravity 0 -9.81
bound -1 56 -41 -39 yvel 0.0
*HISTORIES
hist n=100 ydisp 40 -7.5 ydisp 22 -10
hist n=100 ydisp 22 -30 xdisp  22 -30
hist n=100 xdisp 40 -7.5 xdisp 22 -10
cycle 5000
save kons.sav
del bl 1028 del bl 1528 del bl 388 reset disp
cycle 5000 save dike.sav
```

Mineralogical studies of the “post-glacial” fault exposed at Molberget, Lansjärv area, northern Sweden

Thomas Eliasson
Geologiska Institutionen, Göteborgs Universitet och
Chalmers Tekniska Högskola

John Smellie, Conterra AB

Eva-Lena Tullborg, Sveriges Geologiska AB

May 1991

ABSTRACT

The inferred post-glacial fault at Molberget is orientated in N20-30°E/80°W. Mineralogical and textural investigations adjcent to, and within the fault zone, show that the faulting took place along an old shear zone, probably of Proterozoic age. Thin protomylonites/mylonites occur parallel and discordant to old ductile foliation structures within the host granite. High-temperature hydrothermal alterations accompany this early dynamic metamorphism. Subsequent and repeated episodes of cataclastic fracturing have transected and brecciated the previous ductile deformation structures. Low-temperture fracture fillings such as Fe-oxyhydroxides and zeolites occur in the most recent cross-cutting microfractures.

Contents

MINERALOGICAL STUDIES OF THE "POST-GLACIAL" FAULT EXPOSED AT MOLBERGET, LANSJÄRV AREA, NORTHERN SWEDEN

1. INTRODUCTION

Following a recent major study of post-glacial faulting in the Lansjärv area in northern Sweden (Fig. 1) (Bäckblom and Stanfors, 1989) it was decided to excavate and drill two profiles across the fault at Molberget in the near-vicinity of the trench (now infilled) earlier described by Lagerbäck (Bäckblom and Stanfors, op. cit.).

The trenches at Molberget are located at the southern end of a 17 km long NE trending fault scarp. This fault, together with four major and several minor fault scarps, forms a 50 km long SSW-NNE trending fault set (Lagerbäck, 1990). The location of the two profiles (Profiles 1 and 3) are demarcated in Figure 2; transverse sections showing the positions of the three boreholes drilled (KMO01-KMO03) are illustrated in Figures 3 and 4. The subvertical bedrock scarp is about 7 m high in profile 1 and about 3 m in profile 3. The profiles show the the major fault to be trending N20-30°E and dipping approx. 80°W.

Drilling has been difficult through the fault zone because of the highly fractured and crushed nature of the bedrock, and core recovery has therefore been disappointing. Because of bedrock instability one of the boreholes (KMO01) had to be plugged with cement following drilling, and has not been recored.

The primary purpose of the present study is to investigate whether the post-glacial fault zone coincides with the reactivation of a pre-existing fracture or weakness zone in the bedrock. The aim of the investigation is to identify and describe textural and mineralogical alterations in the wall rock and within the fracture zone. The character of the alterations (i.e. low- or high temperature, brittle or ductile deformation structures etc.) will provide information on the thermotectonic history of the fault zone.

1.1 General Geology

Preliminary mapping of the two trenches and associated drillcores

(Nilsson, Kullman and Strâhle) shows the dominant rock to be a medium- to coarse-grained biotite-hornblende grey-coloured slightly foliated granite/granodiorite (Figs. 3, 4 and 5). Small, ellipsoidal xenoliths less than 1m thick, composed of foliated fine- to medium-grained intermediate volcanites (e.g. samples 1:3), are commonly seen in the granitoid rocks. When approaching the central fault zone from either direction there is a gradual change to a red colouration due to an increase in fracture intensity coupled to iron staining resulting from hydrothermal alteration.

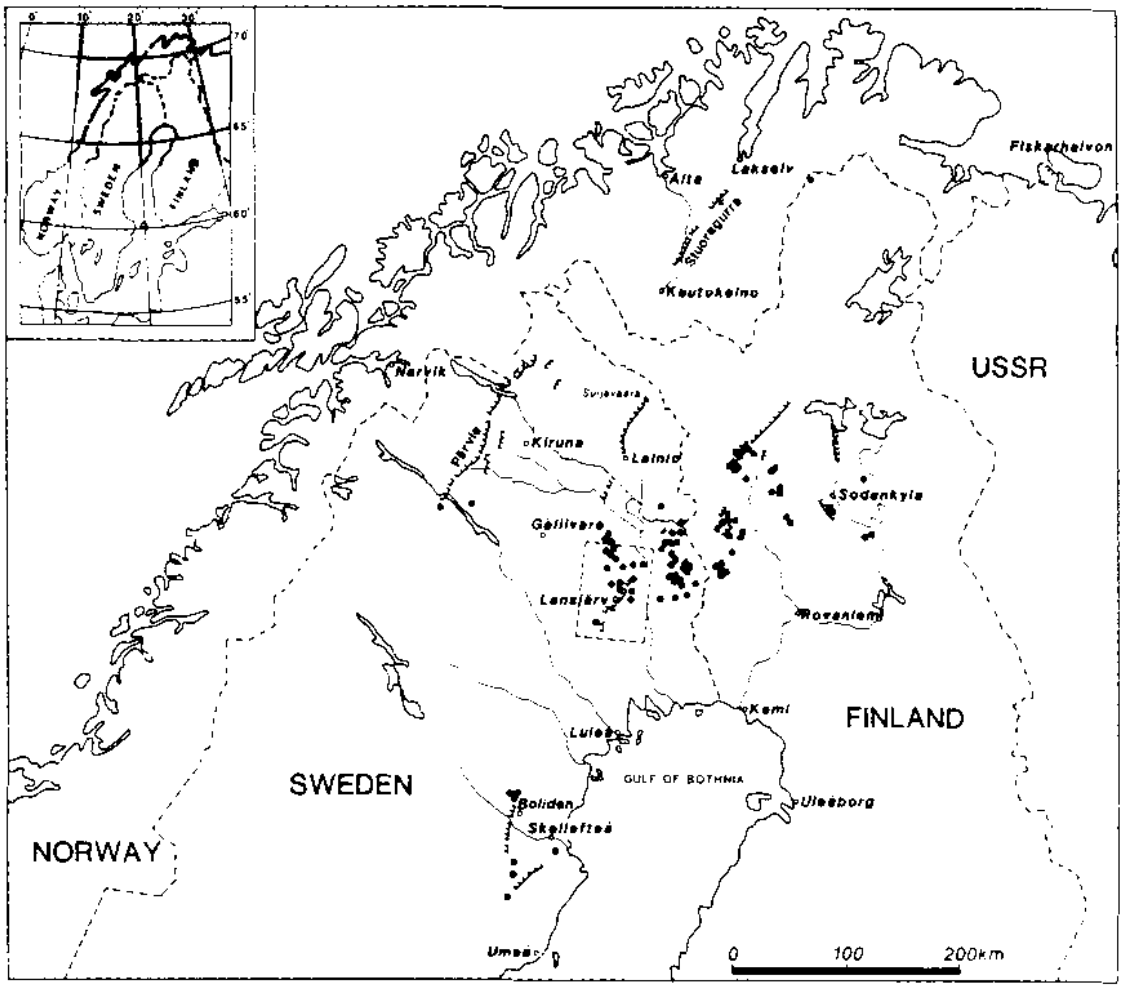

FIGURE 1. Map of northern Fennoscandia showing locations of landslides (black dots) and fault scarps interpreted as being of late- or postglacial age (from Lagerbäck, 1990).

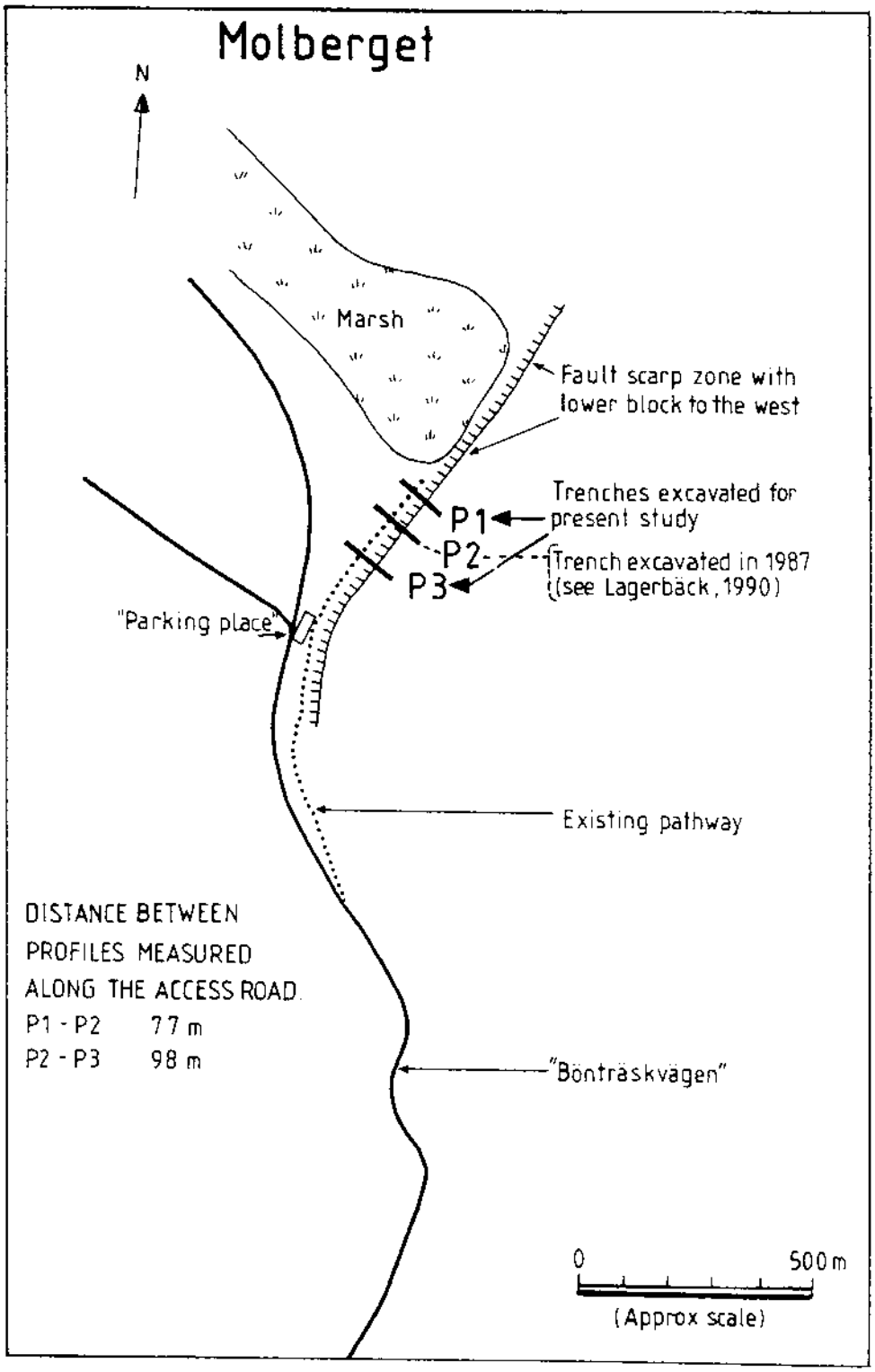

FIGURE 2. Schematic map showing the localities of trenched profiles P1, P2 and P3 at Molberget in the Lansjärv area.

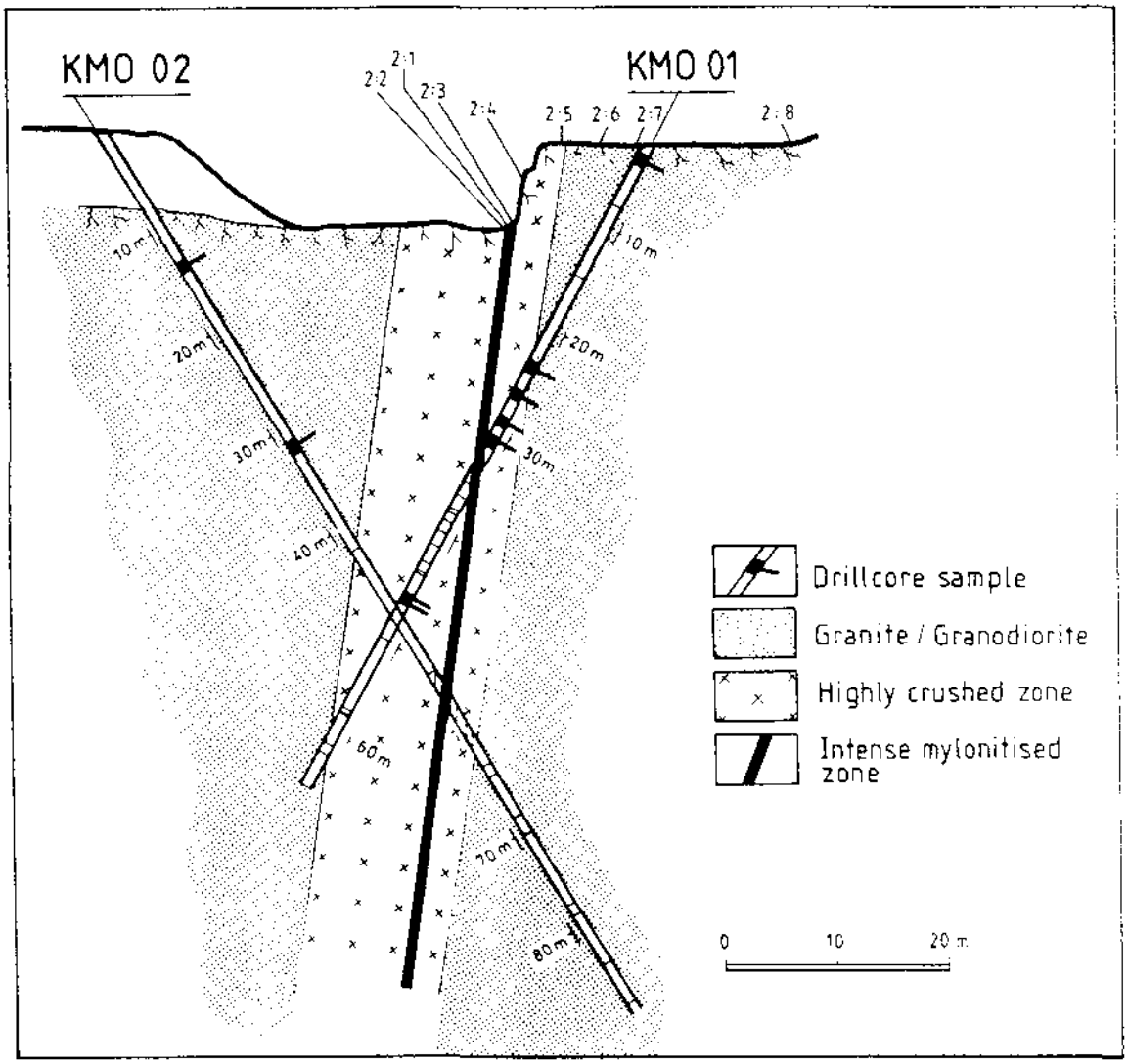

FIGURE 3. Profile 1 (P1 in Fig. 2) showing the location of boreholes KMO01 and KMO02 and the sampling positions.

Shearing and iron staining is most intense across an approx. 5-10 metre wide crush zone which extends west from the fault scarp. This zone is further delineated by two marginal major shear zones (heavily mylonitised): one approx. 2 metres wide at the scarp junction and the other approx. 40 cm wide located along the western margin of the crush zone. Within this crush

zone, and in its near-vicinity, several sheared dolerite intrusions were observed (e.g. samples 1:12 and 1:9 from profile 3, see also appendices) ranging in width from a few centimetres to tens of centimetres. These varied in texture from fairly coarse-grained to fine-grained, the latter type (highly altered and tectonised) forming the junction between the fault scarp and the major crush zone shown in Profile 3. A somewhat younger pegmatite crosscuts zones of intensive foliation in the granite/granodiorite, but is not observed to penetrate the shear zone.

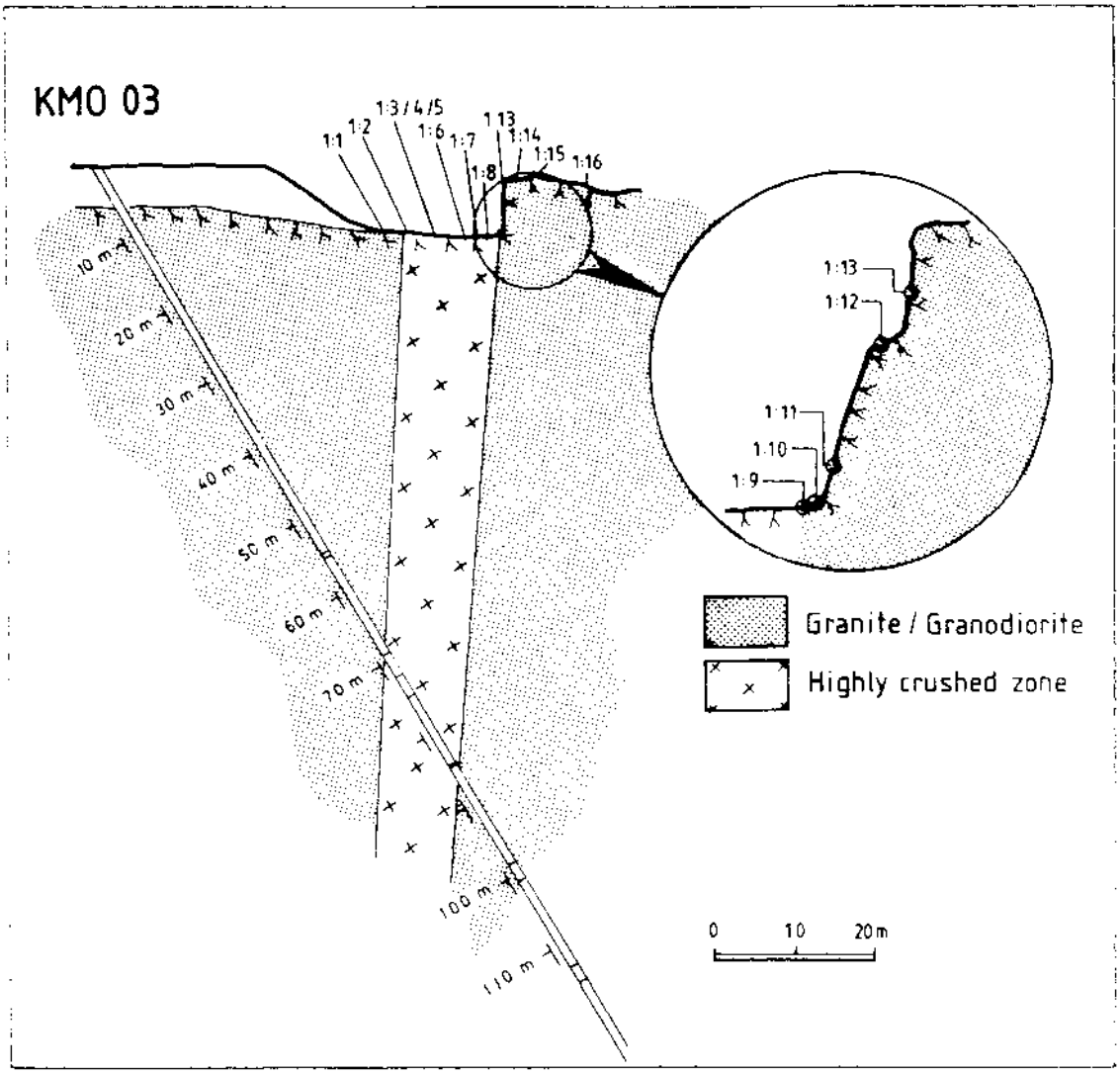

FIGURE 4. Profile 3 (P3 in Fig. 2) showing the location of borehole KMO03 and the sampling positions.

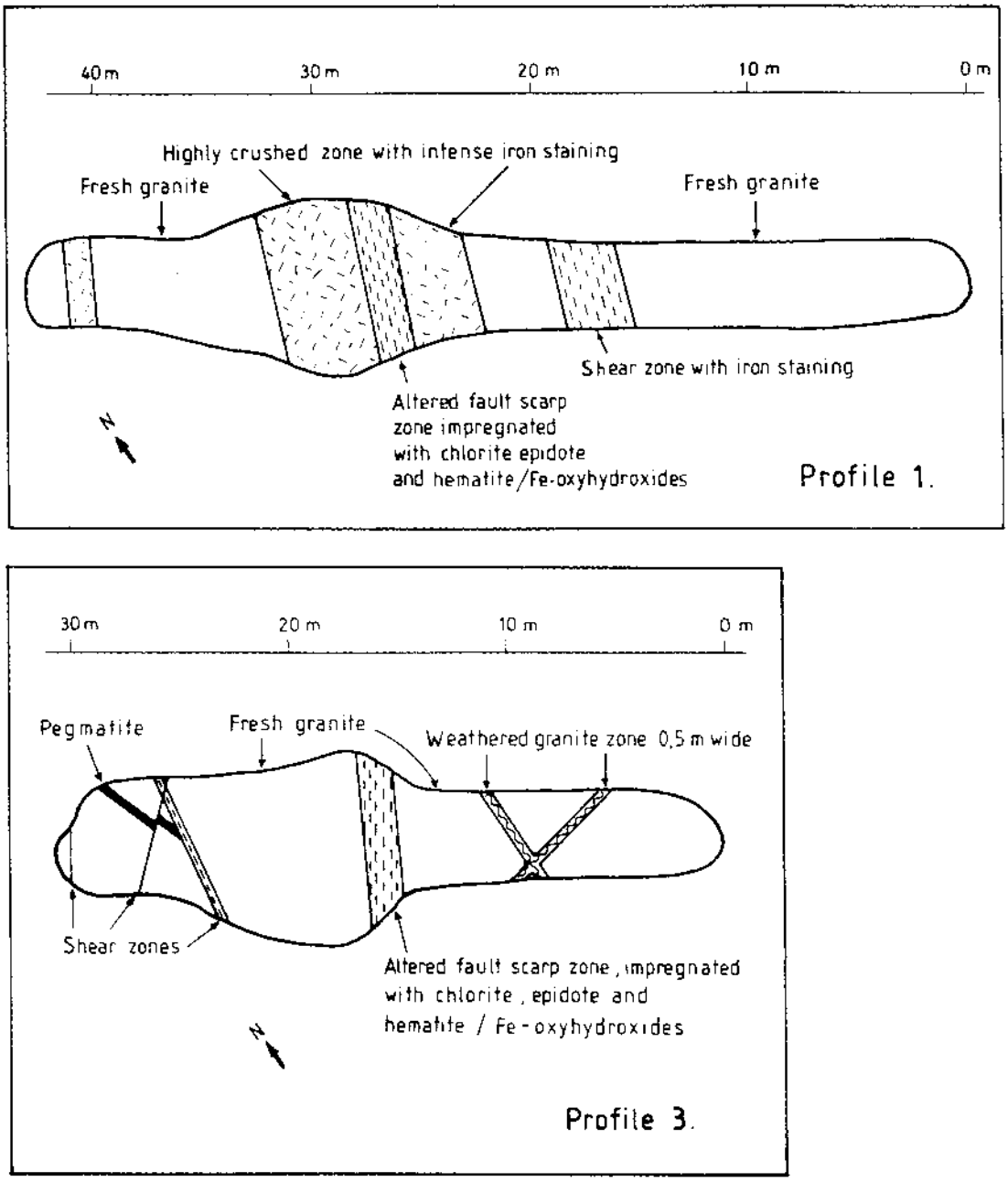

FIGURE 5. Schematic geological maps of the trenched outcrops (after Nilsson and Kullman).

Along the cataclastic/mylonitic zones there are considerable amounts of epidote, chlorite, clay mineral aggregates and a heavy permeation of Fe-oxyhydroxides. From the clay mineral content (red-coloured hematitic clay) Lagerbäck (1990) has reported the presence of vermiculite and expandable mixed-layer minerals, and from a similar residue in the raised block of the fault he reports vermiculite, expandable mixed-layer minerals, illite, plagioclase and K-feldspar.

The youngest fault movements (yielding observable and preserved stuctures on the fault planes) are considered to be strike slip movements as interpreted from horizontal striae etched on the fault plane.

2. SAMPLING

Rock samples were selected from the uncovered outcrops of the trench floors and from drillcore material. A preference to sample the fault and shear zones was made, but representative samples from unfractured "fresh" granite/granodiorite and the hydrothermally altered iron stained varieties were also selected to ensure a representative background assessment. The sampling localities, both outcrop and drillcore, are shown in Figures 3 and 4. Sampling of the drillcores was facilitated by the drillcore logging profiles (Appendices 1-3) (Stråhle & Arnefors, SGAB). Rock types, alterations, fracture fillings, skin features, fracture frequency and RQD of the drillcores are summarised in Figures A1.1, A2.1 and A3.1 (apps. 1-3). Figures A1.2, A2.2 and A3.2 in more detail show the respective distributions of the main fracture infilling and coating minerals (calcite, Fe-oxyhydroxide, chlorite, epidote and hematite) within crush zones and sealed and open fractures.

The term hematite at places includes, as seen from the mineralogical studies (below), Fe-rich minerals such as limonite, goethite and Fe-oxyhydroxides. As borehole KMO03 was in the process of being drilled at the time of sampling, no samples have been studied from this source.

The drillcore logs show that the heavily crushed zones are characterised by Fe-oxyhydroxides, epidote and chlorite; subordinately calcite has been observed.

The main difference between the sealed and the open fractures is the almost complete absence of epidote and Fe-oxyhydroxides in the former, and the predominance of chlorite in the latter; the amount of calcite is

roughly similar in both although with a slight excess bias in the sealed fractures. The presence of Fe-oxyhydroxides suggests that these fractures are water conducting, although there are no hydraulic data to substantiate this. The additional presence of epidote indicates that these same fractures represents earlier pathways for hydrothermal solutions and/or formed later in association with mylonitisation.

The greater bias of calcite in the sealed fractures may indicate its dissolution and removal in the open conducting fractures. In this respect it is also interesting to note that, within open fractures, calcite is found near to the surface in all three boreholes; 9 m in KMO01, 11 m in KMO02 and 31 m in KMO03. This would seem to suggest that the fault zone represents a discharge area; in a recharge area calcite would be expected to be removed by incoming low pH groundwaters, only to be reprecipitated later at greater depths when the groundwaters achieve supersaturation with respect to calcite.

Polished thin sections were prepared perpendicular to the main foliation trend from each sample; when relevant, some additional samples were taken perpendicular to the dominant fracture trends for micro-tectonic studies. Textural relationships and alteration features were studied and microphotograps were taken of the thin sections with a polarizing microscope. Identification and investigation of opaque minerals were carried out using reflected light. Fracture fillings from samples 1:11 and KM002:59.5 m were submitted for XRD analysis at SGU in Uppsala.

It should be stressed that clays may be more common than thought; complete removal of clay material from such fracture zones may have resulted during water-flush drilling. This would result in a gross underrepresentation of such material during drillhole logging and subsequent mineralogical studies.

The feasibility of radiometeric dating of the fault gouge (that has been formed or affected by the latest movements) at Lansjärv by electron spin resonance spectroscopy (ESR) has been investigated in collaboration with Dr R. Grün, Cambridge Univeristy. The method is based on the detection of paramagnetic centres in minerals (in this case quartz) which accumulate over time due to natural radioactivity. The method can be applied to date faults provided that any previously acquired ESR signals in the samples are deleted during the last fault movement. When studying the fault zone at Lansjärv together with Dr Grün it was concluded that it was premature to

conduct an ESR study of the fault gouge. This was partly due to the problem of identifying fault gouge that may have been affected by the last fault movement and partly due to insufficient amounts of fault gouge material in the cores (about 2 to 3 g of quartz is required for one study).

3. MINERALOGICAL STUDIES

Descriptions of the rock samples and their semiquantitative mineralogical compositions are given in Tables 1 and 2; the mineralogical contents in vol. % for eight relatively fresh samples are given in Table 3.

The host granite/granodiorite, which is largely medium- to coarse-grained, is somewhat variable in composition. Plagioclase (An 22-34) dominates with generally somewhat less quartz and microcline. Interstitially located are aggregates comprising magnetite, hornblende and biotite with subordinate amounts of sphene, apatite and accessory zircon; sporadic allanite and pyrite also occur. In some apparently unaltered samples two generations of sphene can be identified. In these cases euhedral/subhedral crystals have overgrowths of anhedral sphene. The content of the primary mafic phases range from about 8 to 27 vol %.

The weakly foliated fine- to medium-grained dolerite, sample 1:12, consits essentially of plagioclase and hornblede. The sampled volcanite (1:3), is a fine- to medium grained mesocratic to mafic foliated and weakly banded tracyandesite. Thus, the rather diverse rock types present imply that the respective mineralogies resulting from the dynamic and hydrothermal metamorphism will also be variable.

In Figure 6 eight samples are plotted in the modal classification diagram after Streckeisen (1976). The samples plot in the field of granite, granodiorite and monzonite. The grayish colour and mineralogical composition thus suggest that the host granites belong to the Haparanda suite as described by Lagerbäck (1990). The volcanite plots almost in the tracyandesite (monzodiorite) field.

From XRD investigations of sample 1:11, quartz, chlorite, hematite and possibly some goethite, were identified. The chlorite contained interlayered sheets of chlorite/vermiculite and chlorite/smectite. Microcline and/or sphene were also possibly present. The sample from 59.5 m depth in drillcore KMO02 yeilded reflections for quartz, chlorite, albite, microcline and hematite. The chlorite contained one iron atom per six octahedral

sites and equal amounts of iron in the octahedral- and hydroxide-sheets. The albite may thus represent residual parts of completely decomposed plagioclase (oligoclase) grains. The presence of clay minerals within the fault zone shows that low temperature alteration/weathering has occurred and/or is occurring along the hydraulically conducting fault zone.

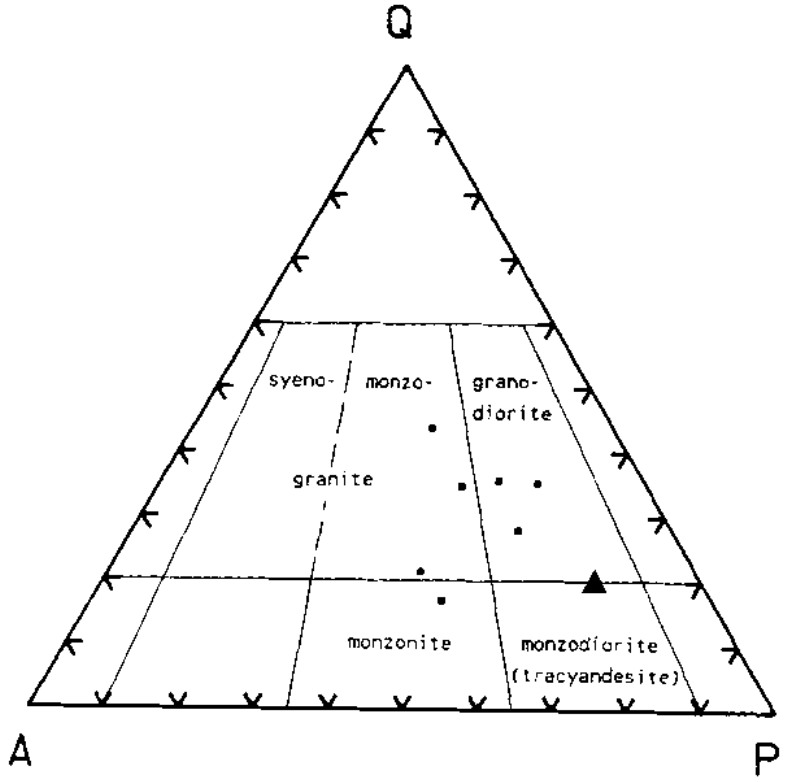

FIGURE 6. Modal classification diagram after Streckeisen (1976). Closed triangle represents intermediate volcanite (sample 1:3). A=alkali feldspar (microcline), Q=quartz, P=plagioclase. Data from table 3.

3.1 Alteration Features

From Tables 1-3 the alteration trends can be clearly seen as the crush zone is approached. There is an increase in the amount of secondary minerals in samples from the crushed zone. Alteration is believed to be mainly hydrothermal resulting from the circulation of fluids along the heavily fractured fault zone. Very characteristic is the decomposition and disapparence of biotite and hornblende (cf. Tables 1 and 2).

Table 1. Rock description and mineralogical data on samples from profile 1 (see Fig. 3 for sample loctions)

Sample	Qz	Mi	Pl	Bi	Hbl	Mn[a]	Sph	Zr	Ap	Py	Ser	Chl	Ep[b]	Hm	Li	Goe	Fex	Leu	Cc	Ana	[c]
2:8	X	X	X	♦	♦	♦	♦	+	+	+	·		o								
KM001:2.7	X	♦	X	♦	♦	♦	♦	+	+	+	·	·	o				o				
2:7	X	♦	X	♦	♦	♦	♦	+	+	+	·	o	o	o							
2:6	X	X	X		♦	+	+		+		·	o	o							·	
2:5	X	♦	X		♦	♦	♦	+	+		o	o	·	o	·						▓
KM001:25.3	♦	♦	X			+	♦	+	+		o	o	·	o	·	·	o		o		▓
KM001:27.1	♦	♦	X			+	+		+		o	o	·	·		·	o	o			▓
KM001:29.0	X	♦	X	+		+	+	+	+		o	o	·	·	·		o	o			▓
2:4	X	♦	X			+	+	+	+		Θ	o	·	o	·			o			▓
K1:31.5	X	♦	+								o	Θ	o			·	o				▓
2:3	X	♦	+		♦						·	o	Θ		o	·	o	·			▓
2:2	X	♦	+								·	·	o		o	·	o				▓
2:1	♦	♦	+				+		+		o	Θ	Θ	·	o	o	o	o			▓
KM001:45.6	X	X	X			+	+		♦		Θ	o	·	o	·		o	·			▓
KM001:47.5	X	X	X			+	+		♦		o	o	·	o	Θ		Θ				▓
KM002:32.0	X	♦	X	+	+	+	+		+		Θ	o	Θ	o	o	·	Θ		o	·	
KM002:14.4	X	X	X	+	+	+	+	+	+		Θ	o	o	o	o		o	·			

[a] Sample KM002:32.0 and KM002:14.4 containes very small residual cores within Hm-altered grains.
[b] Sample 2:8, KM001:2.7, 2.7 and KM002:14.4 contains late magmatic epidote.
[c] ▓= Highly crushed zone (cf. Fig. 3).

ABBREVIATIONS AND MINERAL CLASSIFICATION:

Essential:	Accessory:	Secondary:	
Qz=quartz	Sph=sphene	Ser=sericite	Fex=Fe-oxyhydroxide
Mi=microcline	Zr=zircon	Chl=chlorite	Leu=leucoxene
Pl=plagioclase	Ap=apatite	Ep=epidote	Cc=calcite
Bi=biotite	All=allanite	Hm=hematite	Ana=analcime
Hbl=hornblende	Py=pyrite	Li=limonite	
Mn=magnetite		Goe=goethite	

X,Θ =major phase, ♦,o =minor phase, +,· =accessory phase

ROCK DESCRIPTION:

2:8	Gray, medium-grained, weakly foliated and lineated granodiorite.
KM001:2.7	Gray, medium-grained, weakly foliated granite.
2:7	Reddish-gray, medium-grained, weakly foliated and sparsely porphyritic granite.
2:6	Red stained, ±foliated granite; Qz-Ep healed fractures (6 and 1 mm, respectively).
2:5	Red, fine- to medium-grained, slightly hydrothermally altered biotite granodiorite.
KM001:25.3	Fine-grained, foliated, slightly hydrothermally altered mafic dolerite.
KM001:27.1	Fractured protomylonitic (foliated) granodiorite.
KM001:29.0	Red stained foliated granodiorite.
2:4	Red medium-grained foliated granite.
KM001:31.5	Brecciated and brittled fractured mylonite; pervasive FeOOH impregnation.
2:3	Reddish, tectonised and fractured granite with thin mylonitic zones.
2:2	Greenish-red mylonite cut by extensional microfractures with 1) Qz and 2) Fex + Goe.
2:1	Grayish black mylonite; microfractures with FeOOH + Goe and Qz.
KM001:45.6	Thin Qz-Ep coated fracture in grayish-red, fine-grained foliated granite.
KM001:47.5	Brecciated and microfractured (±Qz and Fex impregnation) protomylonitic granite.
KM002:32.0	±Foliated granite cut by complex fracture (repeatedly activated) partly mylonitic.
KM002:14.4	Water-bearing FeOOH coated fracture in gray, medium grained, weakly foliated granite.

Table 2. Rock description and mineralogical data on samples from profile 3 (see Fig. 4 for sampled locations)

Sample	Qz	Mi	Pl	Bi	Hbl	Mn	Sph	Zr	Ap	All	Ser	Chl	Ep	Hm	Li	Goe	Fex	Leu	Cc	[a]
1:16	X	X	X	♦	+	♦	+	+	+	+	·	·	·	·			·	·		
1:15	X	X	X	+	♦	+	♦	+	+		o	o	·	·	·			o		
1:14	X	X	X	♦	♦	♦	♦	+	+		·	·								
1:13	X	X	X			♦	+	+	+		·	o	·				·	·		▓
1:12	+	+	X		X	♦	+		+		·	o		·			·			▓
1:11	♦	♦	+				♦	+			o	Θ	Θ	·	o	Θ	o			▓
1:10	♦	♦	+				+		+		o	o	Θ		o	·	o			▓
1:9	+	♦	X			♦	♦				Θ	Θ	·	o	·	o	·			▓
1:8	X	♦	X	+		+	♦		+	+	Θ	Θ	o	·	o	·	·			▓
1:7	X	♦	X			+	♦		+		Θ	Θ	Θ	o	o		·			▓
1:6	X	X	X			+	♦	+			Θ	Θ	Θ	·	·		o			▓
1:5	X	X	X	+			♦	+	+		Θ	o	·		·	·	o			▓
1:4	X	X	X	♦	♦	♦	♦		+		·	o	·	o			·			▒
1:3	+	♦	X	♦	X	♦	+	+	+		·		·							▒
1:2	X	♦	X	♦		♦	+		+		o	o	o	o	·		o			▒
1:1	X	♦	X	♦		♦	♦	+	+		·	·	·	·						▒

[a] ▓= Highly crushed zone, ▒=more or less crushed rock (cf. Fig. 4).

ABBREVIATIONS AND MINERAL CLASSIFICATION:

Essential;	Accessory;	Secondary;
Qz=quartz	Sph=sphene	Ser=sericite
Mi=microcline	Zr=zircon	Chl=chlorite
Pl=plagioclase	Ap=apatite	Ep=epidote
Bi=biotite	All=allanite	Hm=hematite
Hbl=hornblende	Py=pyrite	Li=limonite
Mn=magnetite		Goe=goethite
		Fex=Fe-oxyhydroxide
		Leu=leucoxene
		Cc=calcite

X,Θ =major phase, ♦,o =minor phase, +,· =accessory phase

ROCK DESCRIPTION:

1:16 Gray, medium-grained, somewhat bleached granodiorite.
1:15 Grayish-red, medium-grained bleached ±fractured lineated granite.
1:14 Gray, medium-grained, weakly foliated granodiorite. (similar to 1:4)
1:13 Reddish-gray, fractured and foliated hydrothermally altered granite.
1:12 Fine-grained, weakly foliated, rather fresh dolerite dyke.
1:11 Fe-oxyhydroxide impregnated mylonite/protomylonite.
1:10 Greenish-black, mylonite.
1:9 Fine-grained, foliated, altered mafic dyke.
1:8 Red, fine to medium-grained, foliated and lineated granite.
1:7 Red, fractured and brecciated granite.
1:6 Red, medium-grained, foliated granite cut by thin mylonites.
1:5 Red, fine to medium-grained, foliated granite.
1:4 Gray, medium-grained, foliated and somewhat lineated granodiorite (sparsely porphyritic).
1:3 Dark-gray, fine- to medium-grained, foliated, intermediate-mafic volcanite.
1:2 Red, medium-grained fractured granodiorite.
1:1 Gray, medium-grained, very weakly foliated granodiorite.

TABLE 3. Modal data for some representative samples from Molberget. For rock description see Tables 1 and 2

Sample	Qz	Kfsp	Plag	Bi	Hbl	Chl[a]	Op	Sph	Ap	Zr	Ep	Acc	no
1:16	38.7	21.6	28.2	7.6	1.4	0.1	1.2	0.6	+	+	+	0.5	1488
1:8	30.7	22.1	35.9			10.8	0.1	+	+		0.3	0.1	1557
1:4	13.5	29.1	37.3	0.2	10.3	8.0	0.3	0.3	+		0.5	0.2	2226
1:3	12.5	9.4	41.3	10.0	22.1	1.1	1.0	1.0	+	+	0.7	0.6	1289
1:2	24.5	18.3	45.6	0.7	1.0	7.1	0.3	0.3	+		1.5	0.4	1382
1:1	31.9	17.4	40.3	6.2		2.1	0.7	0.4	0.3	+	+	0.4	1680
2:8	18.2	31.4	35.4	5.2	6.1	0.3	0.6	0.4	0.3	+	1.5	0.4	1057
KMO01:2.7	20.7	8.4	37.9	16.4	9.3	0.5	1.1	1.0	0.3	+	3.8	0.4	1196

[a] Altered biotite/hornblende

ABBREVIATIONS:
For most mineral abbreviations see Table 1. Op =opagues, Acc =accessory and secondary minerals (includes minerals noted in trace amounts), + =trace, no =points counted over thin section.

Microfracturing in sample 1:15 (outside the major crush zone), accompanied by hydrothermal alteration, has caused an increased decomposition of biotite and plagioclase to chlorite and sericite respectively. The relatively high epidote content in the undeformed and rather fresh samples 2:8, KMO01:2.7, 2:7 and KMO02:14.4 from profile 1 (c.f. Table 1) is due to late magmatic (deuteric) formation of epidote at the expense of hornblende (Hbl + K + H_2O → epidote + biotite + sphene). In contrast, the plagioclase principally are unaltered in these samples. Thus, the sericitic alteration of the plagioclase (cf. Tables 1 and 2) is due to movement of hydrothermal fluids within and adjacent to the major shear/cataclastic zone.

The dynamic/cataclastic metamorphism is more localised were severe straining has resulted in complete recrystallisation/fragmentation of the rock. Some recent weathering also occurs near the bedrock surface and to some depth along conductive fracture zones, but these latter effects are difficult to quantify mineralogically. In general, the hydrothermal and cataclastic alterations show the following characteristics :

a) Plagioclase quickly breaks down to a fine-grained mica (dominantly sericite). In the mylonitic and strongly hydrothermally altered zones

plagioclase decomposes completely to a extremely fine-grained saussurite mixture of epidote ± sericite ± albite ± calcite. The illites identified in the fracture zone are low temperature (<200-300°C) alteration (weathering) products of feldspars. The analcime identified is probably formed from albite (Ab + H_2O = Anc·H_2O + SiO_2) at temperatures below 200°C (Winkler, 1979).

b) Microcline, in contrast to the plagioclase, remains relatively fresh until maximum alteration occurs, when it too eventually becomes impregnated with Fe-oxyhydoxides and breaks down to fine-grained micas and possibly clay minerals. Microcline as well as plagioclase behaved relatively competently during the cataclastic episodes, developing microfractures and crush features.

c) Quartz, contrary to the feldspars, easily recrystallised to subgrains with polygonal texture. Quartz was also mobilised during several tectonic events being localised to fractures.

d) Biotite and hornblende alters to chlorite, sometimes accompanied by small magnetite clusters and hydrous Fe-oxides, particularly from hornblende breakdown. Continued alteration, probably at temperatures below 100-200°C (Hower, 1981), produced interstratified chlorite/smectite.

e) In the slightly altered and foliated granite types magnetite alters to hematite. Continued oxidation and weathering has produced goethite/limonite and other hydrous Fe-oxides. There is a pronounced increase in secondary iron minerals in the cataclastic and hydrothermally altered rocks (cf. Table 1 and 2). Thus iron is highly mobile, and it appears as Fe-oxyhydroxides filling fractures and staining felsic minerals in the altered rocks.

f) Sphene sometimes shows peripheral breakdown to Ti-oxide phases such as rutile and leucoxene. In highly strained zones, sphene is generally completely recrystallised to small subhedral elliptical grains.

In many cases, depending on the availability of Ca, epidote commonly forms in association with the breakdown of biotite, hornblende, plagioclase and to a lesser extent from magnetite alteration. These epidotes tend to be well-developed euhedral to subhedral grains, consisting both of Fe-rich epidote types (usually in association with biotite/hornblende breakdown) and Ca-rich clinozoisite varieties (often accompanying matrix plagioclase breakdown).

The increase in red colouration of the rocks is due to the presence of finely dispersed Fe-oxyhydroxides, particularly within the altered plagioclases (see Plate 1), less with the microcline, and more concentrated amounts (commonly including limonite) located along micro-fractures and interstitially within the crystal rock fabric.

Apart from localised alteration of the magnetite grains, no hematite has been microscopically observed in any of the sections as fracture fillings. Thus, a large part of the hematite, macroscopically identified during of the drill core examination, may in fact be Fe-oxyhydroxides. This is due to the difficulty to oculary distinguish between hematite and well crystallised Fe-oxyhydroxides such as goethite and limonite.

3.2 Tectonic Features

On a regional scale the Lansjärv fault system is interpreted to be a thrust gently dipping towards the east within a zone striking NNE to NE (Henkel, 1989; Talbot et al., 1989). In contrast, at Molberget the fault is nearly vertical dipping 80° to the west with a strike of N25-30°E. Thus, as Lagerbäck (1990) points out, it appears that the fault planes along the Lansjärv fault system have different dips. He also stresses that the long extension of the fault scarps indicates that the faults extend deep into the crust. Talbot et al. (1989) point out, the thrusts are surface manifestations of transpression along a steep NNE-trending shear zone. This implies, that sections of the fault zone may exhibit thrust planes with variable dips.

Observations in the trenches show the granite/granodiorite to have a gently dipping foliation which becomes increasingly intensified and parallel, the nearer the major fault zone is approached. This foliation deflection is not smooth, but tends to be irregular forming a pattern of anastomosing foliations distorted by minor shears in different directions. These distortions of the early foliation suggest the presence of a much earlier intense shear zone parallel to the fault scarp. Maximum shear is reflected by narrow zones of mylonitisation or cataclasis characterised by chlorite/epidote veins; younger faults tend to be coated in Fe-oxyhydroxides and show horizontal striae.

The microscopic studies support the above observations. The general regional foliation in the granite/granodiorite is seen as a weak alignement

of matrix biotite/chlorite with some elongation of the quartz/feldspar (due to limited recrystallisation) becoming more apparent as the shearing intensity increases towards the major fault. As a result of this ductile stage the rock becomes more gneissose in texture. Thin mylonite horizons occur parallel to, as well as cruss-cuting the gneissosity. Within the highly strained parts of the rock and in the early high temperature mylonites quartz and partly the feldspars have annealed and formed polygonala subgrains. Thus, the in hand specimens apparent mineral orientation is microscopically seen as granular bands with slight variation in mineralogy.

Following foliation, all major changes are dominated by the mechanical crushing and shearing (cataclasis) of the rock fabric, accompanied by the introduction of low-temperature Ca-rich hydrothermal solutions (which may also be somewhat Ti-rich).

The cataclastites comprise broken up granite/granodiorite fragments (size range: 1-10 mm) set in a clay matrix (mostly chlorite) highly charged with Fe-rich granular epidote, Fe-oxyhydroxides and to a lesser extent sphene (see Plate 2). The plagioclase is in an advanced state of alteration to sericite, and some of the quartz is partly recrystallised, irregular in form and cloudy due to dustings of Fe-oxyhydroxides. Within these cataclastic zones a large proportion of the chlorite has recrystallised to form unstrained, randomly oriented grains. Magnetite is generally completely oxidised to hematite and/or Fe-oxyhydroxides. As mentioned above, clay material removed from similar cataclastic/mylonitic zones (Lagerbäck, 1990) showed the presence of vermiculite and expandable mixed-layer minerals.

The textures vary from coarse, where the crushed host-rock fragments comprise some 60% of the rock, to fine, where clays become dominant, to material which contains mostly impregnations of epidote, chlorite and sphene, later charged with Fe-oxyhydroxides. Notable is the occurence of unsheared anastomosing extensional microfractures filled with quartz and FeOOH which cut the cataclasites and mylonites.

Fine parallel to subparallel schistosity textures, seen as string-like concentrations of Fe-oxyhydroxides (including limonite), are observed to traverse mylonite zones; other distinctive veinlets also occur. One thin section in particular illustrates the general sequence of events within these highly sheared zones (Plate 3). Here a fine-grained mylonite is traversed parallel to the schistosity by a compound "veinlet" (10 mm wide)

PLATE 1. Microphotograph of sample 1:15 illustrating the staining and sericitic alteration of plagioclase. Note the unaltered appearance of microcline and quartz. View about 3.5 mm. Plane-polarized light.

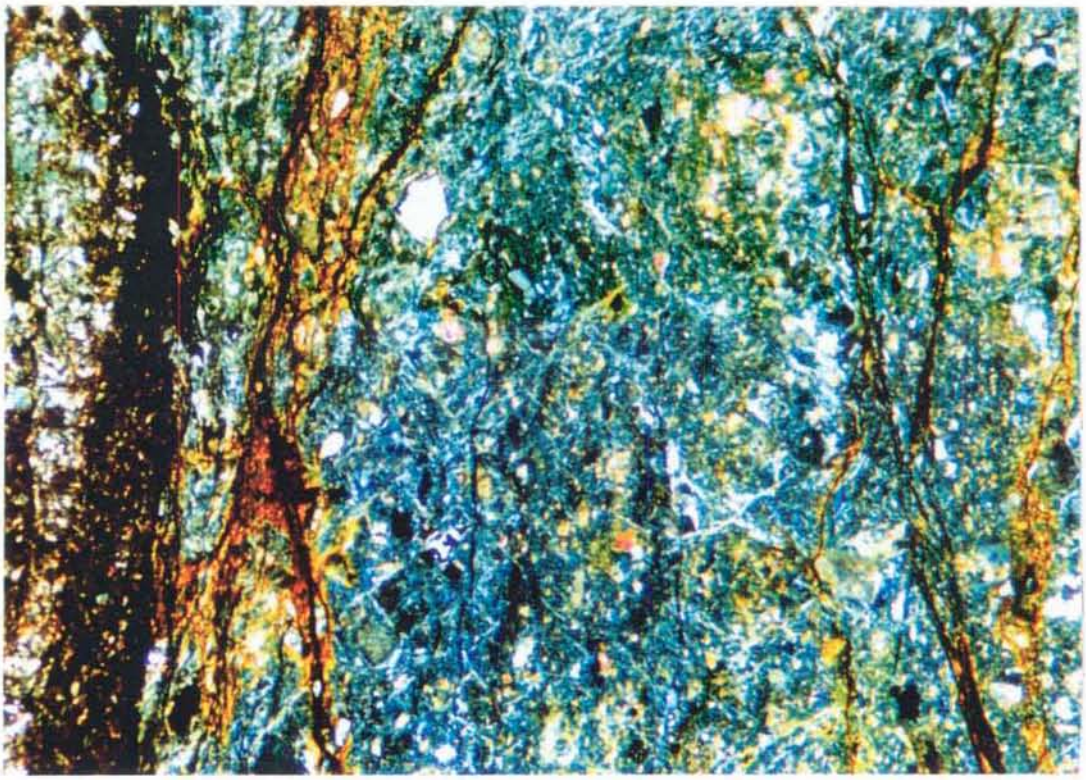

PLATE 2. Mylonite/cataclastic rock (sample 1:11) with microcline fragments and minute epidote grains in a matrix of crushed silicates. The microfractures are filled with goethite/limonite (dark) and rusty Fe-oxyhydroxides (reddish-brown). View is about 3.5 mm (cross-polarized light).

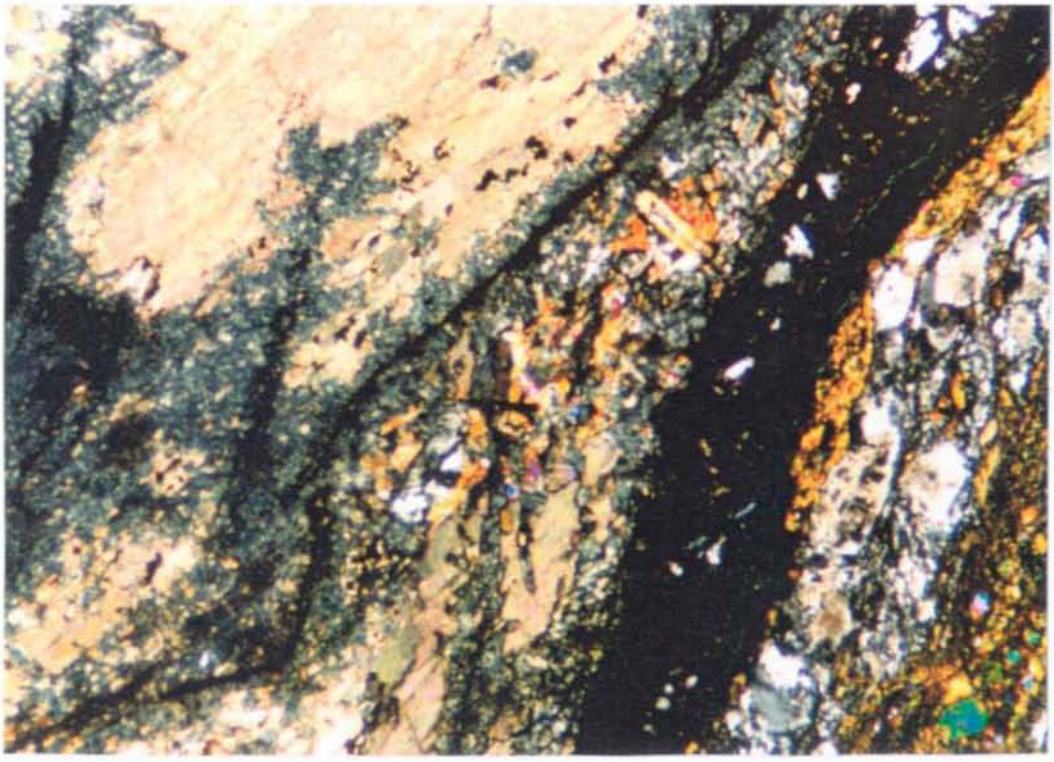

PLATE 3. Complex fracture in sample KMO02 at 32.0 m depth. At the lower right part of the field granular epidote and rock fragments. To the left occur large calcite crystals corroded along microfractures due to analcime and Fe-oxyhydroxide formation/precipitation. View is about 3.5 mm wide (cross-polarized light).

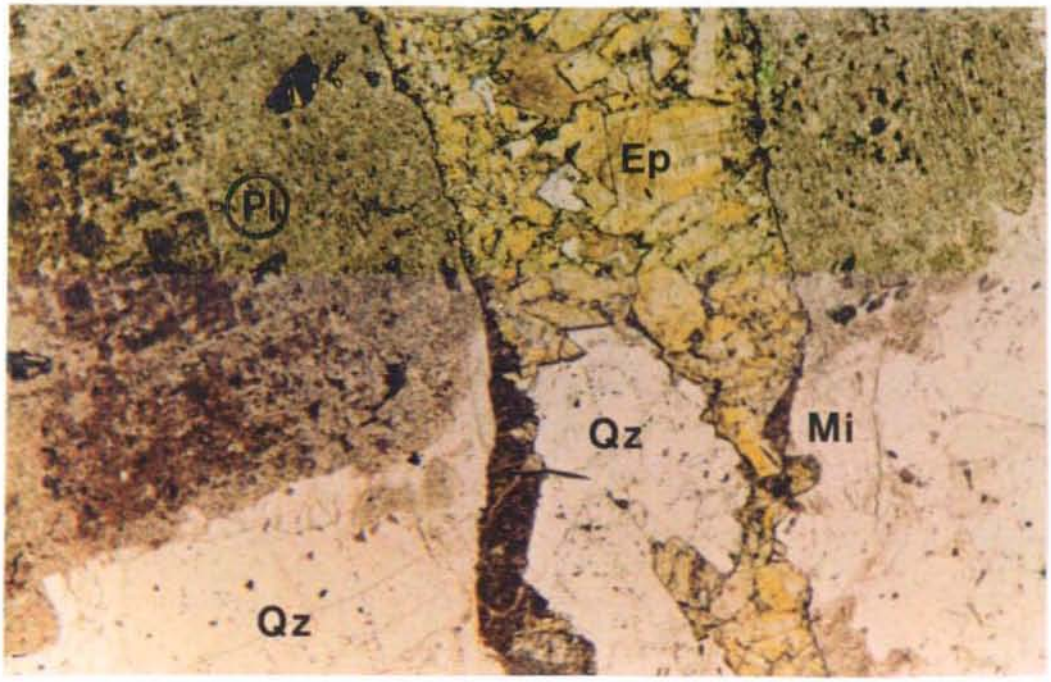

PLATE 4. Quartz + epidote ± analcime filled extensional fracture in weakly foliated granite (sample 2:6). The Na-zeolite (analcime) occur as light brownish crystals in the central part of the fracture and as dark brown crystals at the lower left margin of the fracture. Plane-polarized light.

representing three paragenetic stages. The first stage is the introduction of Ca(Ti?)-rich hydrothermal solutions resulting in aggregates of granular Fe-rich epidote with dispersed sphene and subordinate magnetite. Included in this are preserved rock (microcline ± quartz) fragments and sometimes clays (chlorite). This stage is later traversed by veinlets (infilled fractures?) containing mostly calcite. The final stage is the presence of micro-fractures and associated formation of zeolite (analcime) and Fe-oxyhydroxides precipitation which cross-cut the rock fabric often displacing the earlier textures.

Another section (Plate 4) shows that zeolite (analcime) formed coevally or slightly later than quartz-epidote precipitation. The section also shows a notable alteration of the plagioclase. The section aslo show that the late generations of epidote and quartz form euhedral to subhedral crystals growing out from the rim into the fracture cavity.

4. SUMMARY AND CONCLUSIONS

Field observations coupled to the microscopic studies have shown the following sequence of events:

1. More than 20 metres from the Molberget fault zone the host granite/ granodiorite is relatively fresh and exhibits primary magmatic textures. There is, however, a hint of a regional tectonic foliation seen mainly as a weak alignement of biotite.
2. Towards the fault zone the host-rock becomes more gneissic due to the stronger alignement of the altered biotite (now chlorite) and the partial recrystallisation of the quartz/ feldspar matrix. The rock also becomes reddish in colour due to an increase in the number of small narrow shear zones stained by Fe-oxyhydroxides; this staining is considered hydrothermal in origin. Hydrothermal effects have also resulted in the staining (principally plagioclase), alteration and breakdown of many of the primary magmatic rock-forming minerals.
3. Along the fault scarp and 5-10 metres to the west, two zones of intensely sheared mylonite occur which delineate a central highly crushed or shattered zone which is heavily impregnated by Fe-oxyhydroxides. This zone represents a more crushed and hydrothermally altered version of the above point (2).

4. The mylonitic and cataclastic zones post-date the ductile distortions represented by point (2), and have also contributed to the increased fracturing of the shattered zone of point (3). This is evidenced by the occurrence of numerous narrow mylonitic zones (cms wide) present throughout this shattered zone. The mylonites/cataclastites are characterised by crushed granitic fragments (extremely altered) and clays (mostly chlorite with some vermiculite and expandable mixed-layer varieties).
5. Reactivation has occurred, perhaps repeatedly, along these major cataclastic/mylonite zones, which have been later impregnated by Ca-hydrothermal solutions. This has resulted in the heavy impregnation of parts of these zones by epidote $\pm$ goethite and limonite. Mobilisation of Ti has resulted in crystallisation of sphene.
6. A further stage is represented by calcite-rich infillings/ veins which have often penetrated along the same zones of weakness as the mineral assemblages described in point (5). Coeval, or slightly later than calcite, zeolite occurs usually as a central (final) infilling in the fracture cavities.
7. The youngest stage is the cross-cutting of all previous textures/fabrics by microfissures containing concentrations of Fe-oxyhydroxides.

Quartz-infilled extensional fractures/veinlets occur throughout the above sequence of events, being a very late stage (see point (6)) as well as being cross-cut by mylonite, which in turn is cut by the final microfractures (see point (7)).

The overall conclusion is that reactivation has repeatedly occurred along the Molberget fault zone throughout a long period of geological time. The latest of these movements, with preserved structural markers, is indicated to be horizontal. It should be noted that vertical striae formed as a result of the post-glacial faulting advocated by Lagerbäck (1990) can probably be preserved in the most "soft" fault gouge. Carefull excavation and detailed investigations of all possible fault planes are thus necessary to identify these kinematic indicators. In the absence of any quantitative isotopic dating potential, coupled with no obvious structural evidence to the contrary, it is not possible to conclude that major post-glacial movement has taken place.

5. REFERENCES

Bäckblom, G. & Stanfors, R., 1989: Interdisciplinary study of post-glacial faulting in the Lansjärv area, northern Sweden, 1986-1988. SKB Tech. Rep. (TR 89-31), Stockholm.

Henkel, H., 1989: Tectonic studies in the Lansjärv region. In: G. Bäckblom, & R. Stanfors, (eds): Interdisciplinary study of post-glacial faulting in the Lansjärv area, northern Sweden, 1986-1988. SKB Tech. Rep. (TR 89-31), Stockholm.

Hower, J., 1981: Shale diagenesis. In: F.J. Longstaffe (ed), Short Course in Clays and the Resource Geologist. Mineralogical Assoc. of Canada, Toronto.

Lagerbäck, R., 1990: Late Quaternary faulting and paleoseismicity in northern Fennoscandia, with particular reference to the Lansjärv area, northern Sweden. Geol. Fören. Stockholm Förh. 112:333-354.

Streckeisen, A., 1976: To each plutonic rock its proper name. Earth Sci. Rev., 12: 1-33.

Talbot, C., Munier, R. & Riad, L., 1989: Reactivation of Proterozoic shear zones. In: G. Bäckblom, & R. Stanfors, (eds): Interdisciplinary study of post-glacial faulting in the Lansjärv area, northern Sweden, 1986-1988. SKB Tech. Rep. (TR 89-31), Stockholm.

Winkler, H.G.F., 1979: Petrogenesis of Metamorphic Rocks. Fifth ed. Springer Verlag. New York.

APPENDICES

LEGEND FOR FIGURES: A1.1, A2.1 AND A3.1

FIGURE A1.1

HOLE : KM001
GEOLOGIST: STR
DATE : 900918
SCALE 1:200

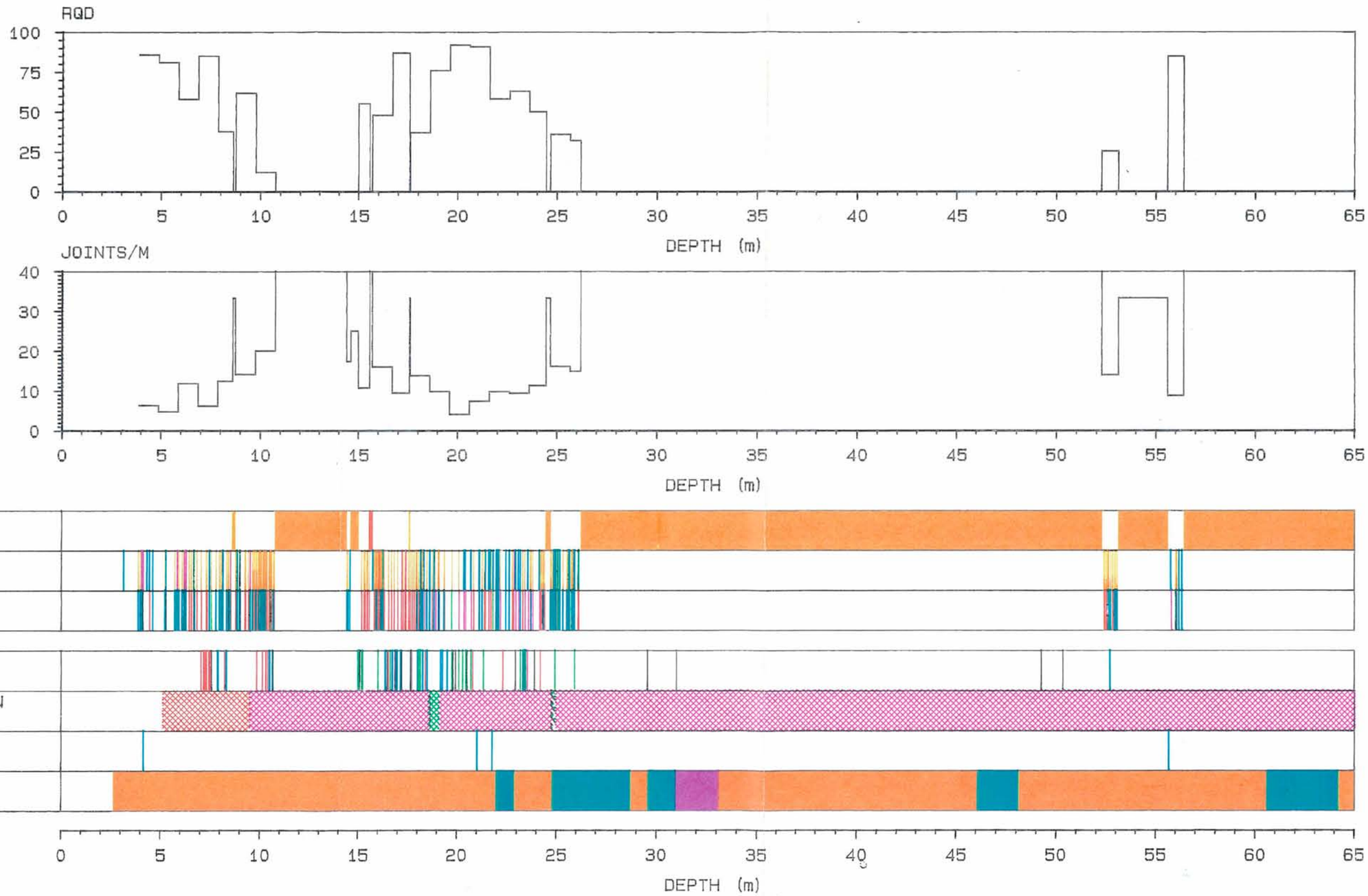

HOLE : KM001
GEOLOGIST: S SEHLSTEDT
DATE : 910110
SCALE 1:500

KA = calcite
FE = Fe-oxyhydroxides
KL = chlorite
EP = epidote
HM = hematite

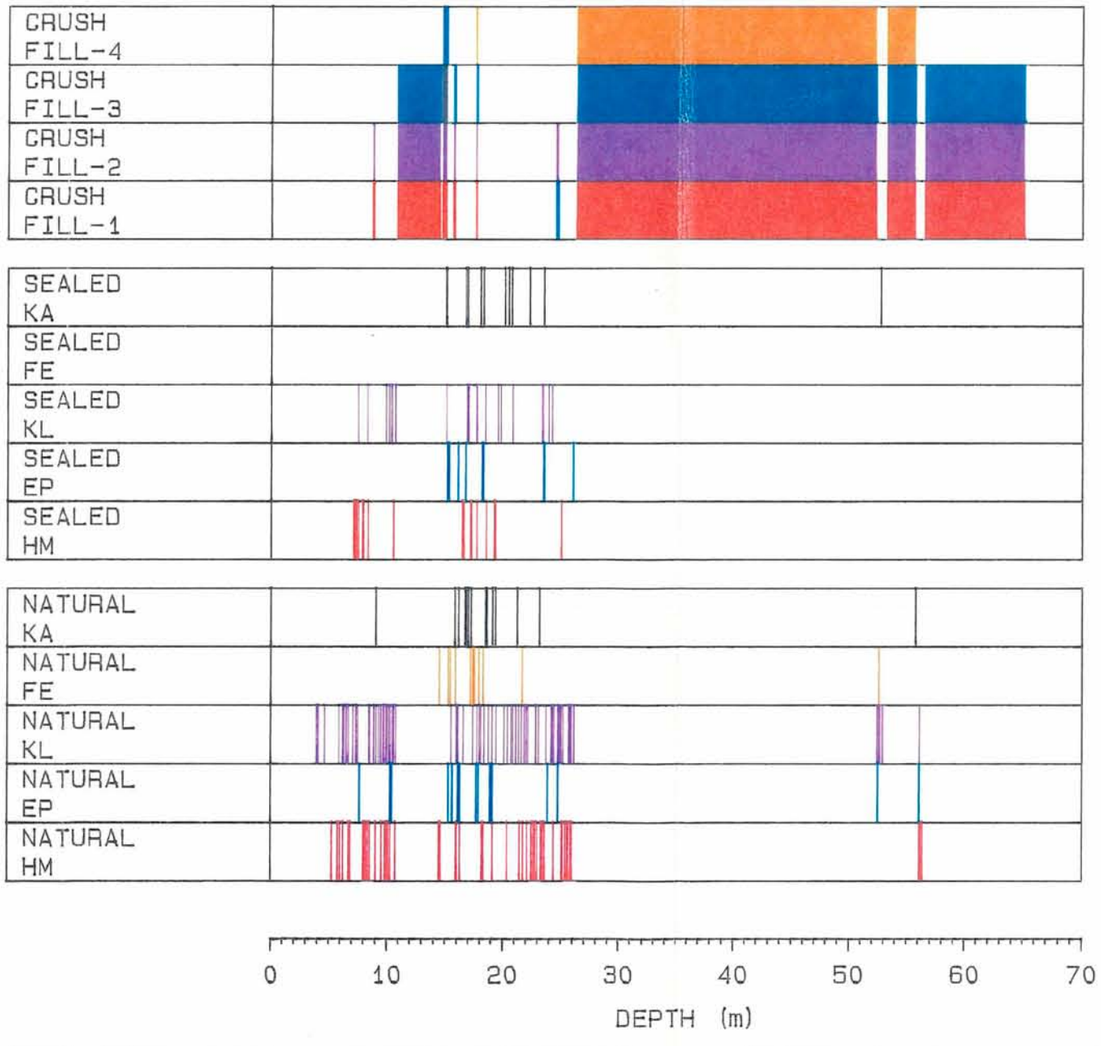

FIGURE A2.1

HOLE : KM002
GEOLOGIST: STR
DATE : 900918
SCALE 1:200

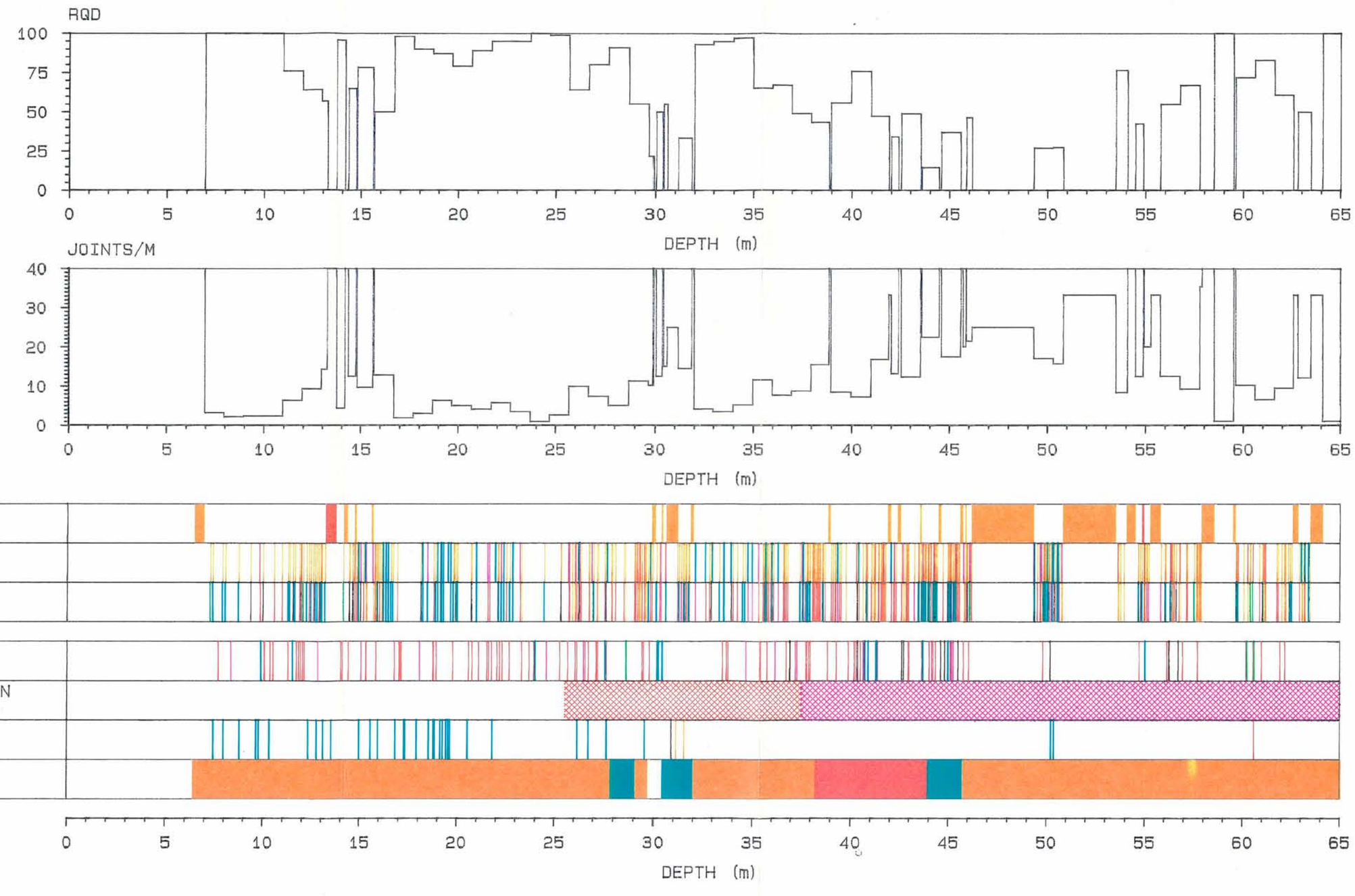

HOLE : KM002
GEOLOGIST: STR
DATE : 900918
SCALE 1:200

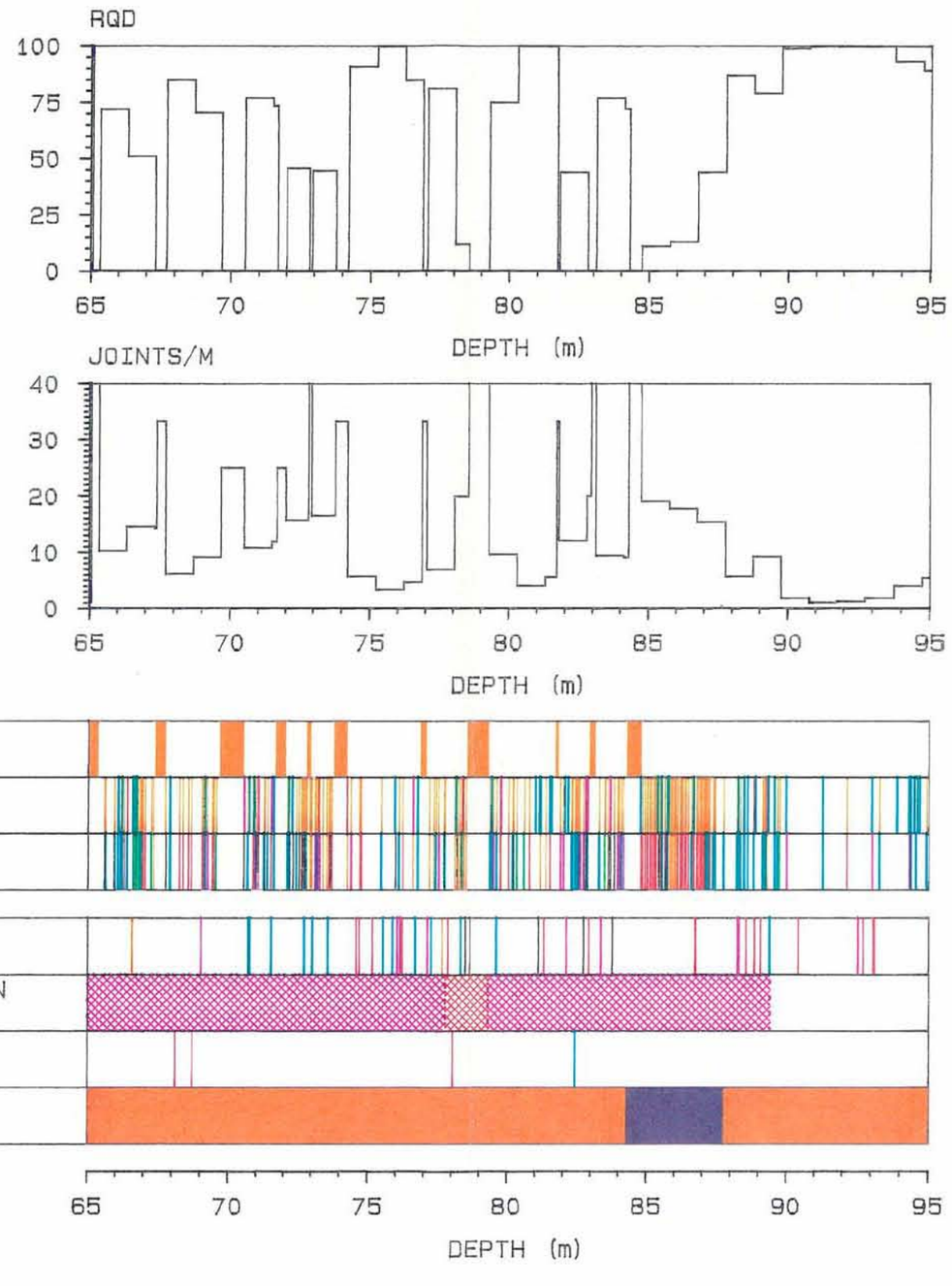

FIGURE A2.2

HOLE : KM002
GEOLOGIST: S SEHLSETDT
DATE : 910111
SCALE 1:500

KA = calcite
FE = Fe-oxyhydroxides
KL = chlorite
EP = epidote
HM = hematite

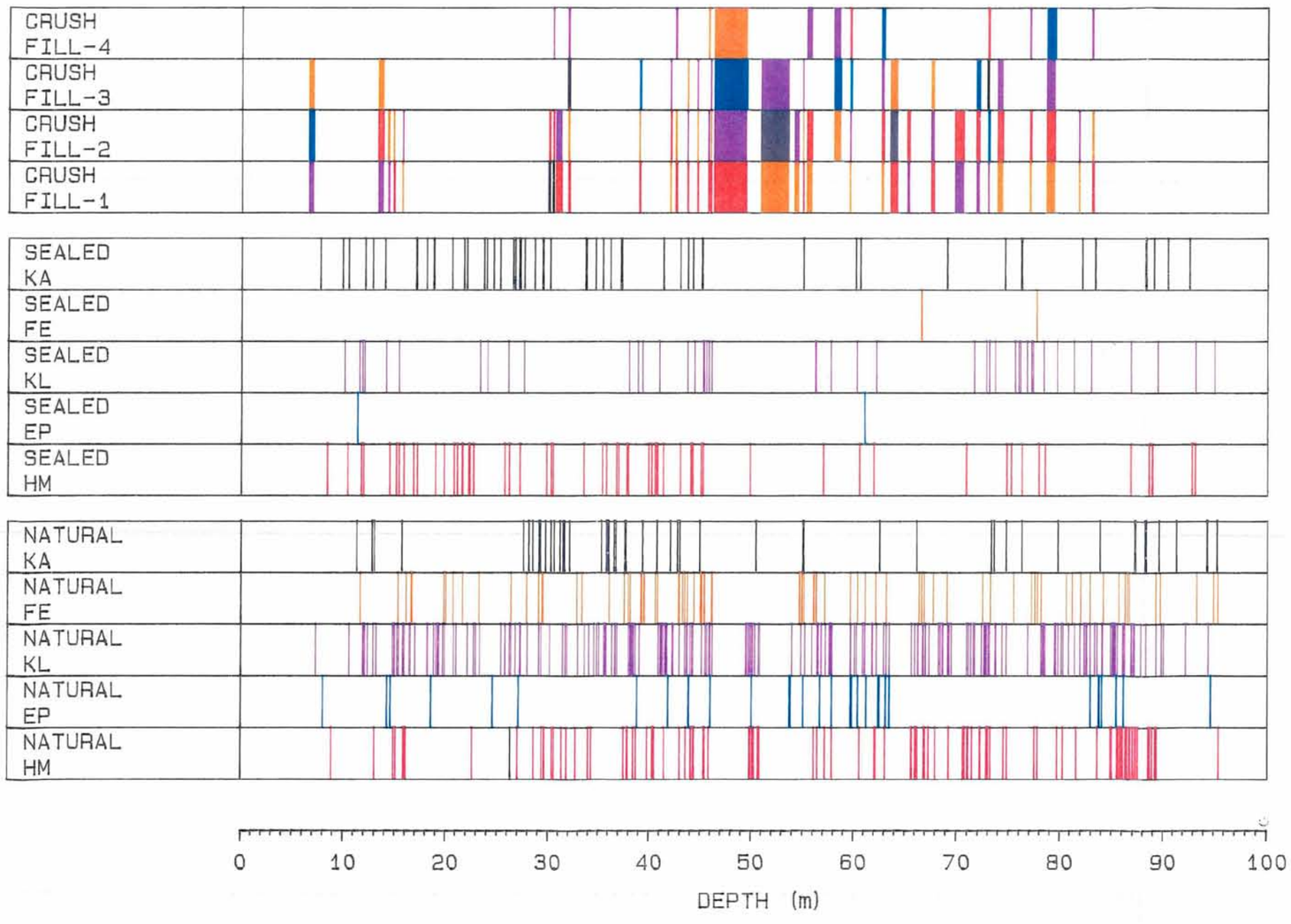

FIGURE A3.1

HOLE : KM003
GEOLOGIST: STR
DATE : 900919
SCALE 1:200

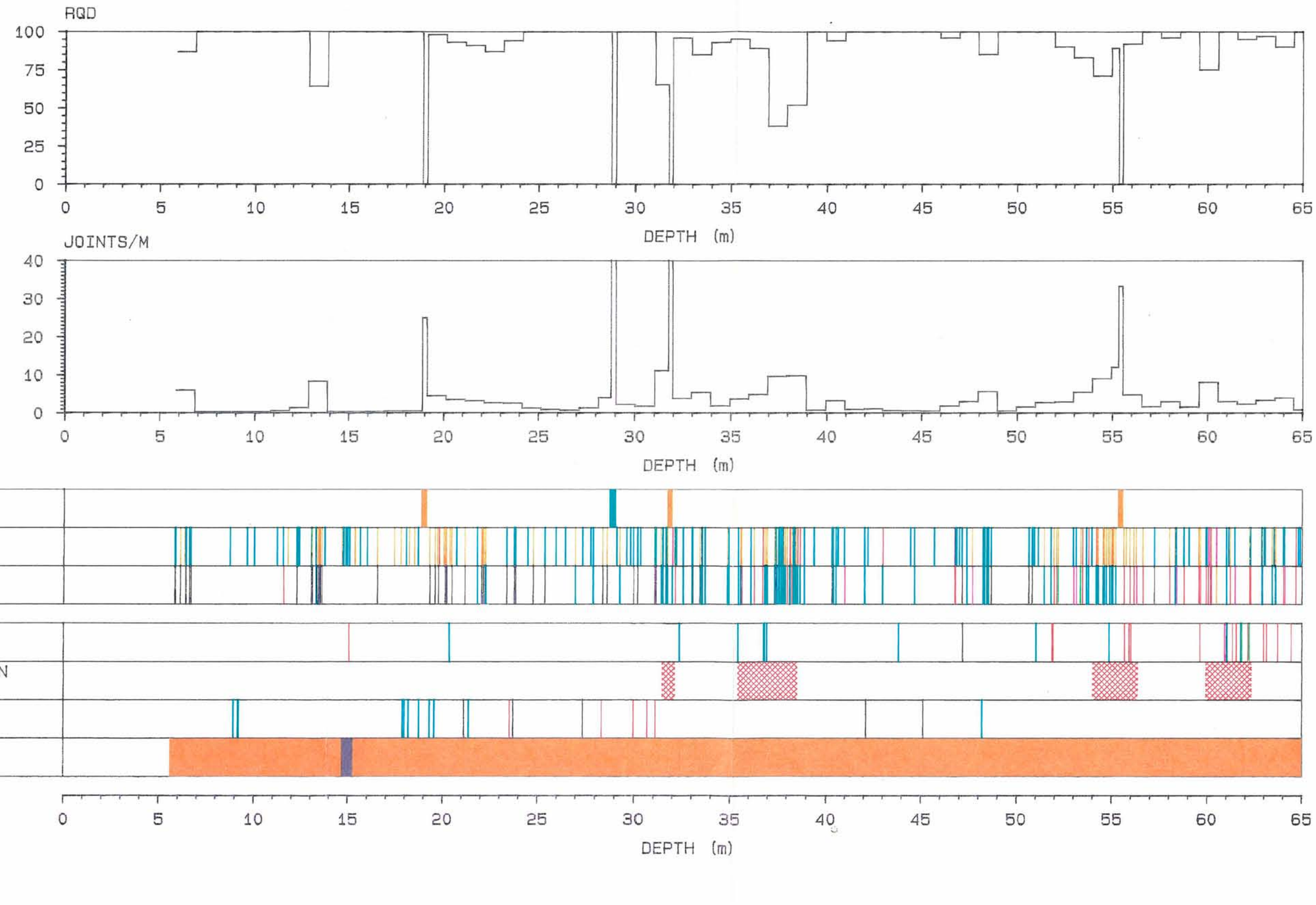

HOLE : KM003
GEOLOGIST: STR
DATE : 900919
SCALE 1:200

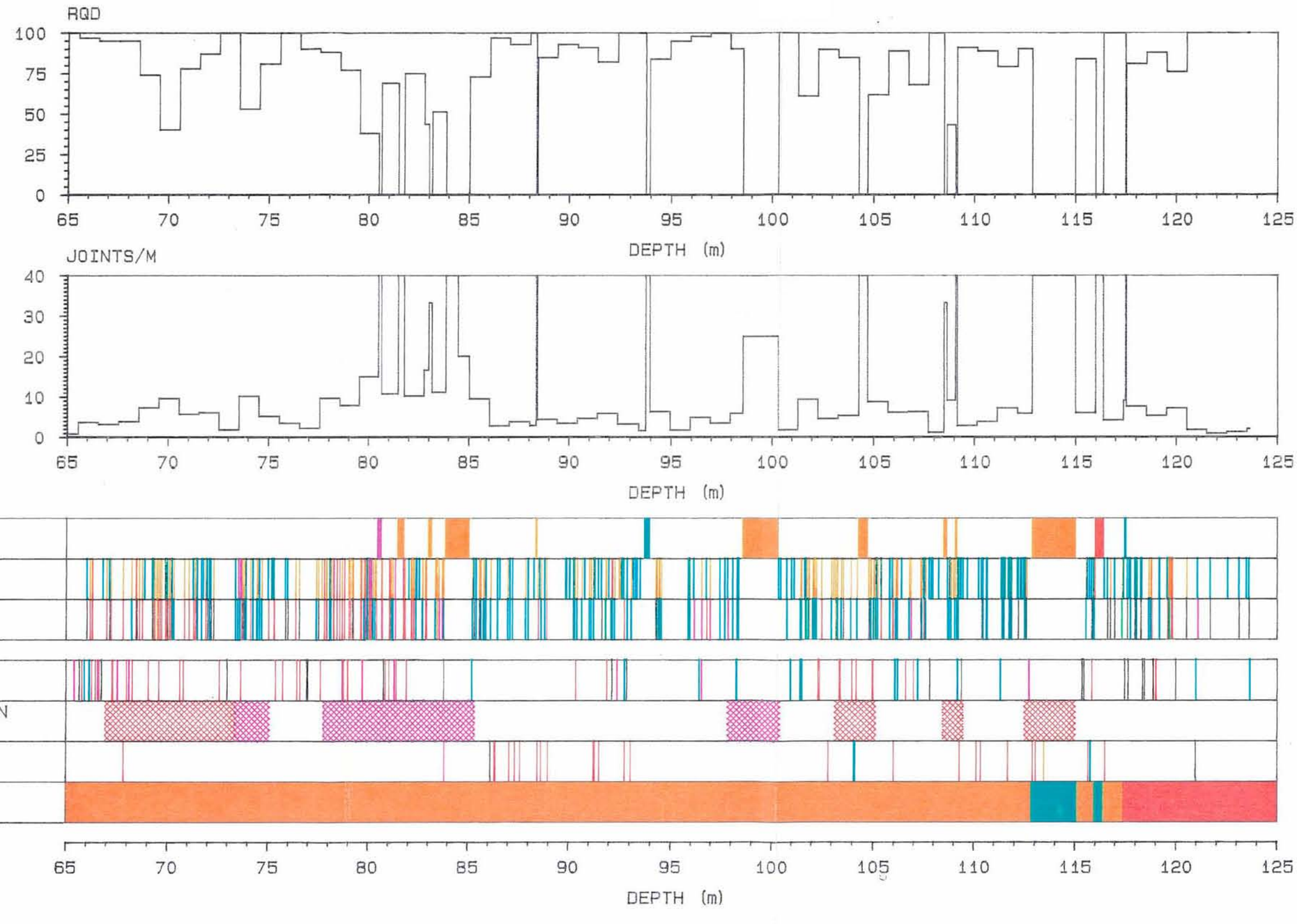

FIGURE A3.2

HOLE : KM003
GEOLOGIST: S SEHLSTEDT
DATE : 910111
SCALE 1:500

KA = calcite
FE = Fe-oxyhydroxides
KL = chlorite
EP = epidote
HM = hematite

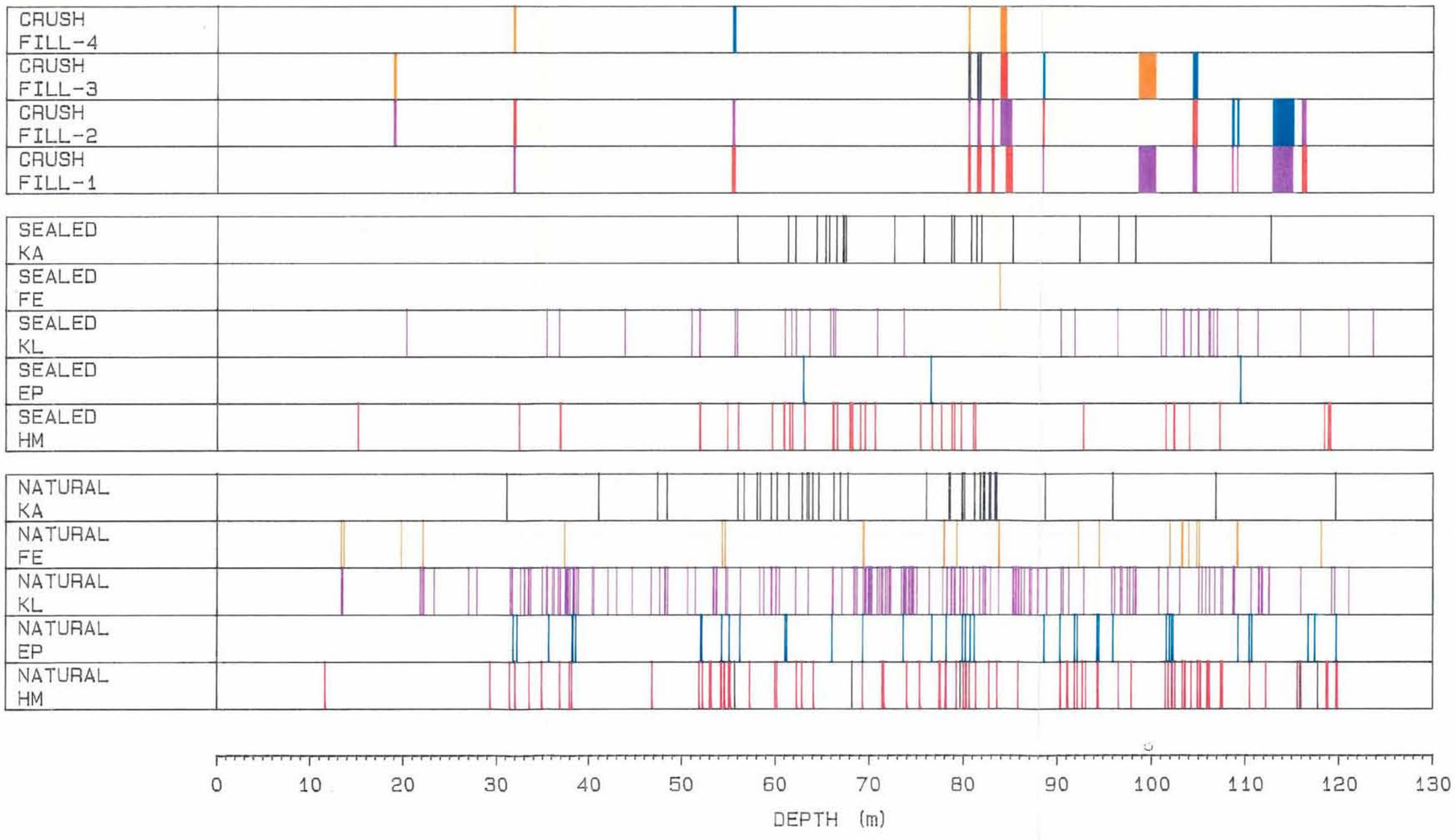

Hydrogeological investigations in the Lansjärv area

Kent Hansson, Swedish Geological Co

February 1989

Contents

1. BACKGROUND

Within the SKB project "Stability of the rock in a long-range perspective", an investigation of the rock properties in Lansjärv has been conducted, primarily with respect to geological, seismic and hydraulic conditions. The work has been focused on a fracture zone which is considered to show signs of postglacial activity, a so called postglacial fault (PGF). A core borehole, KLJ01, of depth 500 m penetrating a large fracture zone at a depth of approximately 150 m, was drilled during the year 1987. Due to technical problems during the penetration of the zone grouting was required. The grouting was preceded by hydraulic testing to a depth of 150 m.

On commision from SKB, SGAB has performed hydraulic testing in the upper 150 m as well as the remainder of the borehole KLJ01. The hydraulic tests have been performed in 10 m sections down to 150 m, and in 30 m and 3 m sections in the rest of the borehole. In addition, the work has included geodetic surveying of boreholes in the Lansjärv area, observations of groundwater levels in boreholes, and compilation of topographic and groundwater level maps.

2. GENERAL

The Lansjärv area is located 150 km north of Luleå in Norrbotten County in the north of Sweden, see Figure 1. Three percussion boreholes and one core borehole have been drilled in the area, see Figure 2. Two of the percussion holes were drilled 100-150 m southeast of where the fracture zone penetrates the ground surface. The boreholes were surveyed during June, 1988, and their positions in the RAK-network is given in Table 1.

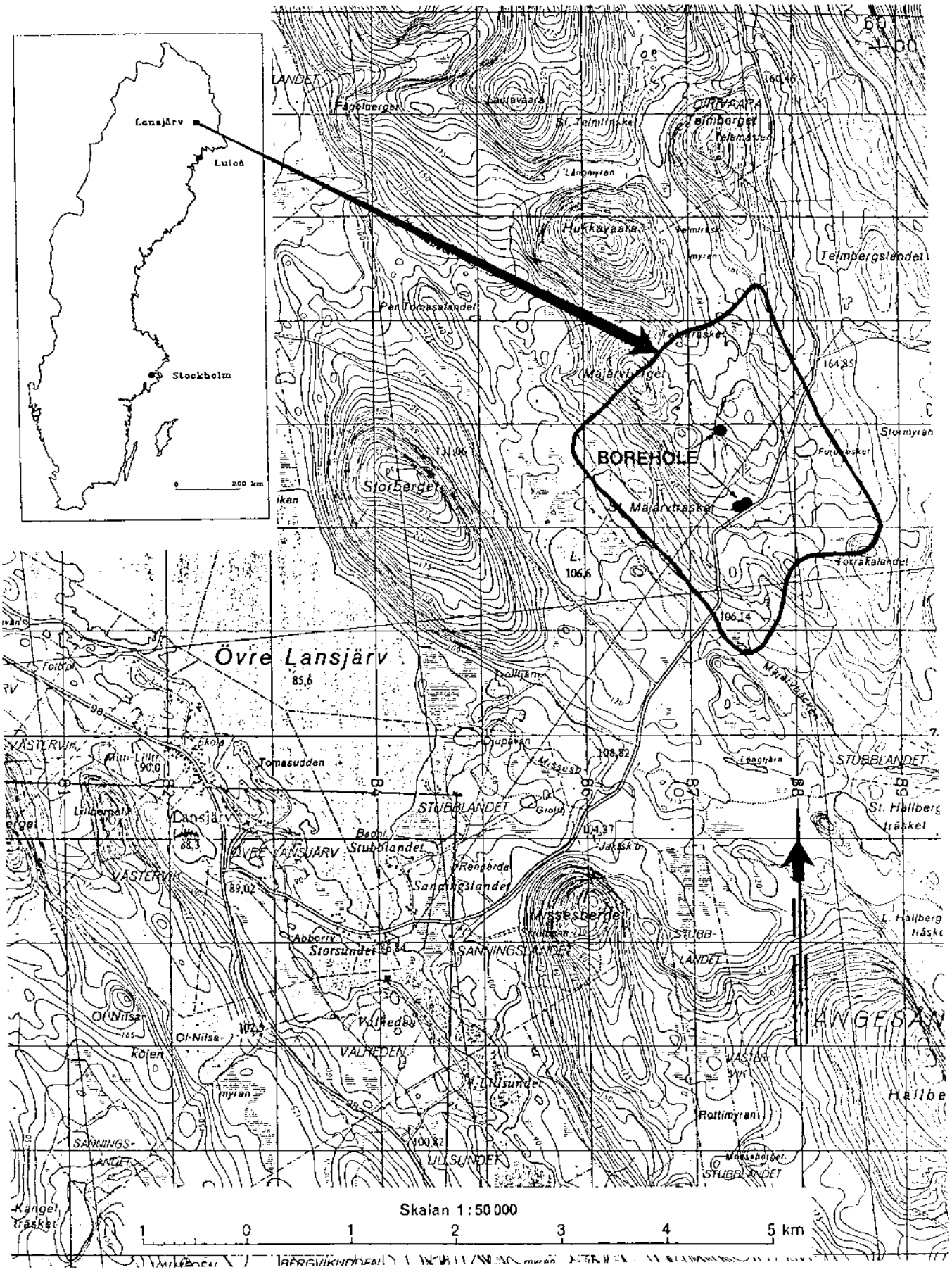

Figure 1 Location of the Lansjärv area.

Figure 2 Local topographical map of the Lansjärv site.

Table 1 Coordinates in the RAK-network for boreholes in Lansjärv (Z = upper casing).

Bore-hole	X	Y	Z (m a s l)
KLJ01	7412160,24	1787484,73	+153,98
HLJ01	7412175,43	1787510,43	+154,23
HLJ02	7412926,13	1787276,77	+177,91
HLJ03	7412925,87	1787275,87	+172,74

In three of the boreholes the casing was extended to the Z-coordinates given in Table 1. These extensions are presented in Table 2 together with dates. During the core logging and the hydraulic testing, carried out in September 1987 and September 1988, the reference levels of the boreholes used were the ones obtained in connection with the drilling, i.e. before the casing extension.

Table 2 Extensions of borehole casing relative to the reference level measured during drilling.

Bore-hole	Extension	Date
KLJ01	+0,46	870204
HLJ01	+0,50	871130
HLJ02	±0	-
HLJ03	+0,50	880117

3. HYDRAULIC TESTING IN BOREHOLE KLJ01

The hydraulic testing in borehole KLJ01 was performed at two occasions, September 1987 and September 1988. Considerable problems with caving in the borehole arose after approximately 150 m of drilling. The upper part of the hole was then subjected to hydraulic testing prior to any attempts to stabilize the caved section.

3.1 TESTS IN THE DEPTH INTERVAL 39 - 151 m.

Ten water injection tests were performed during September 1987. The tests were performed as double packer measurements in 10 m intervals. In addition, two single packer measurements were conducted in the part between the lowermost test section and the bottom of the borehole; one injection test and one pumping test were performed.

The equipment for the water injection tests is shown in Figure 3. The tests were conducted with a steel pipe tube attached to a drilling rig. The flow meters were registered manually, while the pressure in the tested section was monitored by pressure transducers and registered on a pen recorder. The packers were of the type Dt 53. Hydraulic communication between the steel pipe tube and the measured section was opened and closed with a test valve. The test sequence comprised 15 min of packer inflation followed by 15 min of water injection.

The tests were evaluated assuming stationary conditions according to Moye (1967):

$$K = C \cdot Q/L \cdot H_o \qquad (1)$$

where

$C = (1 + \ln(L/2r_w))/2\pi$

K = hydraulic conductivity (m/s)

Q = water flow (m^3/s)

L = length of test section (m)

H_o = injection pressure (m)

r_w = radius of the borehole (m)

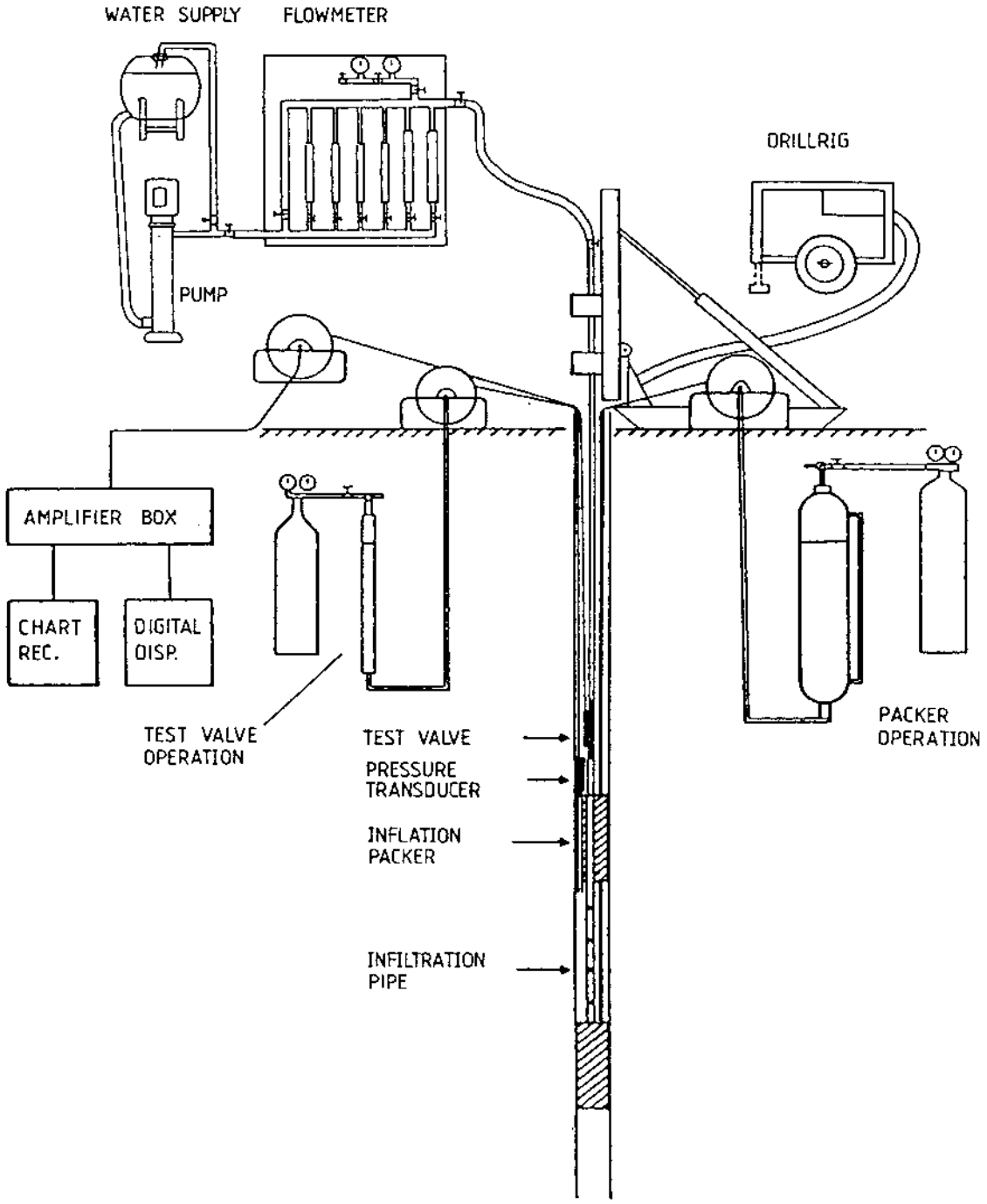

Figure 3 Principal layout of the equipment for water injection tests.

The pumping test was performed as gas-lift pumping. Gas was injected in the steel pipe tube at a depth of approximately 100 m. The water discharge was measured at several times during pumping using a tank and stop watch. The pumping test was evaluated for both stationary and transient conditions.

The results of the tests, calculated according to Eq. 1, are presented in Figure 4 and Table 3. All of the test sections have a hydraulic conductivity greater than 10^{-7} m/s. The greatest value (2.0×10^{-5} m/s) was found in the section 128-138 m.

Table 3 Hydraulic conductivity for the interval 39-151.2 m in borehole KLJ01, Lansjärv.

Section (m)	Hydraulic conductivity K (m/s)	Remark
39 - 49	7.9 x E-7	
49 - 59	2.2 x E-7	
59 - 69	6.4 x E-7	
69 - 79	5.9 x E-7	
79 - 89	1.0 x E-6	
89 - 99	4.6 x E-6	
98 - 108	6.4 x E-6	
108 - 118	4.5 x E-7	
118 - 128	1.2 x E-6	
128 - 138	2.0 x E-5	
139 - 151.2	5.2 x E-7	single packer
139 - 151.2 P s-s	9.5 x E-8	"
139 - 151.2 P trans	4.8 x E-7	"

P = pumping test
s-s = steady state evaluation
trans = transient evaluation
E-7 = 10^{-7}

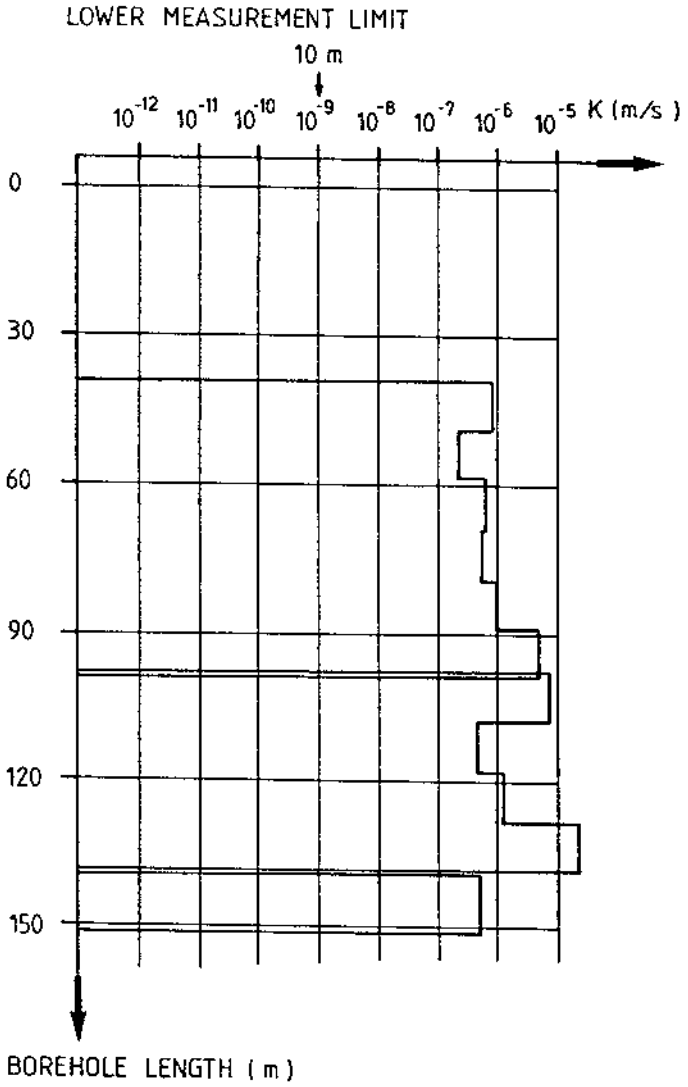

Figure 4 Hydraulic conductivity from 39-151 m in KLJ01.

3.2 TESTS IN THE DEPTH INTERVAL 154 - 490 m.

Following grouting at the 150 m level and casing to a depth of 153 m, the drillings were resumed to a depth of 500 m. After drilling was completed, some minor cavings occurred, probably at the 250 m level, where the borehole on several occasions was blocked during borehole measurements. An additional complication, with consequences for the choice of equipment for the hydraulic testing, was the great depths to the groundwater level in the boreholes, indicating levels between 20-70 m below the ground surface (c.f. section 4). This would effect the packer deflation after each test.

A set of equipment was designed to be able to handle the above mentioned facts. The equipment at the ground surface is identical to the one in Figure 3, while the equipment in the borehole has a decreased outer diameter (from ø 53 mm to ø 45 mm). This enables it to be inserted through a temporary casing (54/47 mm) if needed. The casing would be applied (or drilled) down to the area where problems might arise. The packers are of the type Pb 2-42 with an outer diameter of 43 mm and packer inflation starts at a pressure of approximately 20 bar. In order to minimize changes in dimension of the down-hole tool, the injection pipe was also constructed with a diameter of ø 43 mm. However, all tests could be completed without the aid of the temporary casing.

The stationary injection tests were conducted according to the following sequence :

	30 m-sections	3 m-sections
Packer inflation	30 min	15 min
Pressure adjustment	15-60 min	10-15 min
Water injection	15 min	10 min
Packer deflation	10 min	10 min
Change of section	20 min	3 min

The reason for the long times of pressure adjustment was that there were indications that the groundwater pressure in the deeper parts of the borehole was rather low. The water injection was performed using an excess pressure of approximately 0.2 MPa, relative to the adjusted pressure in the measured section.

The evaluation of the tests was performed assuming steady state conditions according to Eq. 1 where C is set to 1 for both 30 m and 3 m sections (in Eq. 1, C=1.15 for 30 m and C=0.79 for 3m). The reason for this is that the summed transmissivities of 3 m sections and the corresponding 30 m section are compared. Otherwise, since the most conductive part or parts of a 30 m section has the largest impact on the total transmissivity of the section, these parts are given different weight in the comparison, i.e. different radius of influence. Also, the use of different constants C may not be justified according to non-porous behavior in fractured medium. The results of the tests are shown in Figure 5 and Table 4.

The T-quotient in Table 4 is defined as the ratio of transmissivities of 30 m sections to the sum of the transmissivities of corresponding 3 m sections or reciprocally in such manner that the T-quotient is greater than unity.

The agreement between 30 m sections and summed 3 m sections are very good. The larges T-quotient is 2.7 and most sections have a ratio $\leq$ 1.5.

In the sections 154-190 m the hydraulic conductivity is high, especially in the fracture zone between 181-190 m ($\geq 10^{-6}$ m/s). From 190 to 300 m the hydraulic conductivity decreases successively to the lower measurement limit of 3 m tests (1×10^{-10} m/s). Below 300 m, most of the tests yield values close to lower measurement limit. However, even in this area sections with hydraulic conductivity greater than 10^{-8} m/s can be found.

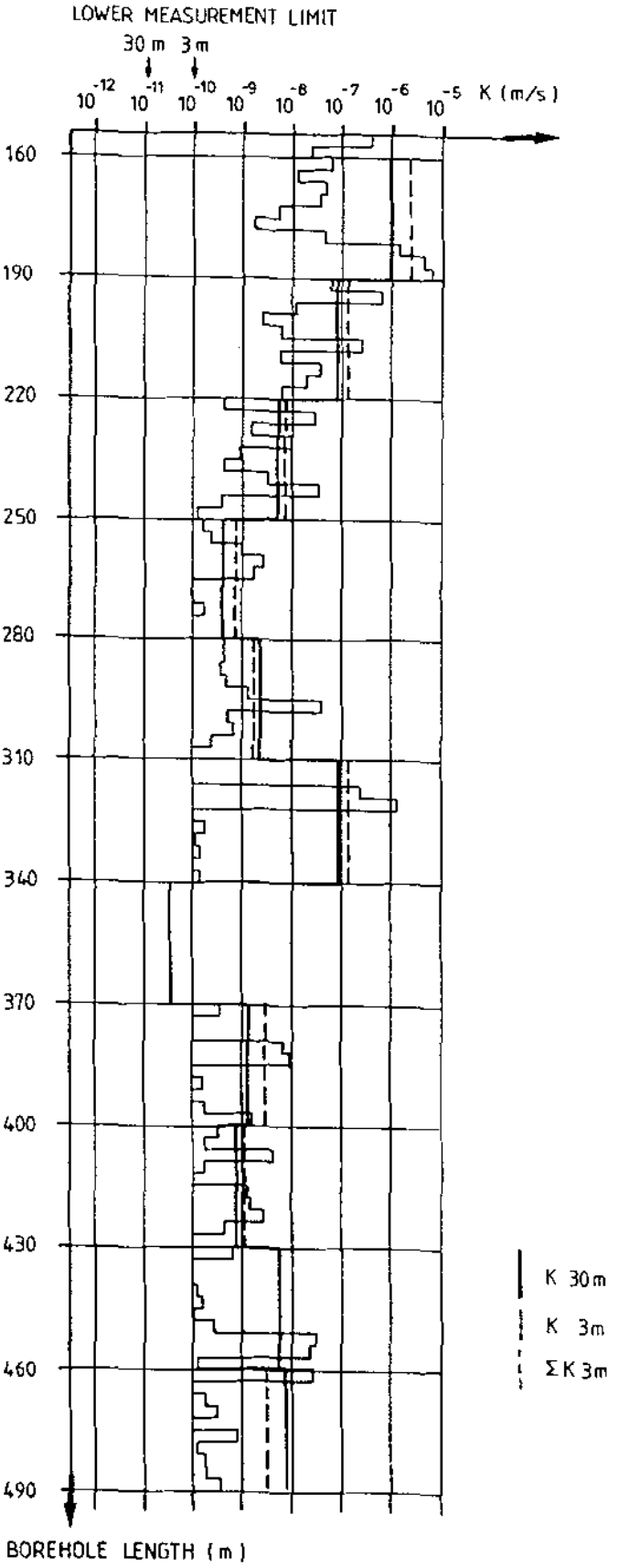

Figure 5 Hydraulic conductivity from 154-490 m in KLJ01.

Table 4 Hydraulic conductivity (K) in borehole KLJ01 from 154 m to 490 m. The T-quotient is defined to be ≥ 1.

Section (m)	Hydr cond 3 m (m/s)	Hydr cond (30 m) calculated from 3 m values (m/s)	Hydr cond 30 m (m/s)	T-quotient
154-157	3.9 E-7	-	-	
157-160	2.2 E-8			
160-163	6.2 E-8			
163-166	1.1 E-8			
166-169	4.9 E-8			
169-172	3.9 E-8			
172-175	5.4 E-9	1.2 E-6	9.8 E-7	1.2
175-178	1.7 E-9			
178-181	4.8 E-8			
181-184	1.4 E-6			
184-187	4.1 E-6			
187-190	6.2 E-6			
190-193	6.2 E-8			
193-196	6.6 E-7			
196-199	1.1 E-8			
199-202	2.2 E-9			
202-205	6.1 E-9	1.1 E-7	9.6 E-8	1.1
205-208	2.6 E-7			
208-211	5.9 E-9			
211-214	4.1 E-8			
214-217	2.0 E-8			
217-220	6.3 E-9			
220-223	4.5 E-10			
223-226	3.0 E-8			
226-229	1.6 E-9			
229-232	6.9 E-9			
232-235	1.0 E-9	8.2 E-9	5.3 E-9	1.5
235-238	4.3 E-10			
238-241	3.3 E-9			
241-244	3.8 E-8			
244-247	4.4 E-10			
247-250	1.2 E-10			
250-253	1.4 E-10			
253-256	2.3 E-10			
256-259	1.1 E-9			
259-262	2.5 E-9			
262-265	1.9 E-9	6.5 E-10	4.3 E-10	1.5
265-268	1.1 E-10			
268-271	1.2 E-10			
271-274	1.5 E-10			
274-277	9.4 E-11*			
277-280	9.9 E-11*			

Table 4 cont.

Section (m)	Hydr cond 3 m (m/s)	Hydr cond (30 m) calculated from 3 m values (m/s)	Hydr cond 30 m (m/s)	T-quotient
280-283	4.8 E-10			
283-286	4.9 E-10			
286-289	4.1 E-10			
289-292	5.1 E-10			
292-295	1.1 E-9	1.9 E-9	2.2 E-9	1.2
295-298	1.4 E-8			
298-301	1.6 E-10			
301-304	1.7 E-10			
304-307	2.8 E-10			
307-310	7.5 E-11*			
310-313	<1.7 E-12*			
313-316	5.8 E-11*			
316-319	2.6 E-7			
319-322	1.2 E-6			
322-325	4.1 E-11*	1-5 E-7	9.6 E-8	1.6
325-328	1.8 E-10			
328-331	1.2 E-10			
331-334	1.5 E-10			
334-337	9.8 E-11*			
337-340	1.4 E-10			
340-343				
343-346				
346-349				
349-352				
352-355		-	3.6 E-11	-
355-358				
358-361				
361-364				
364-367				
367-370				
370-373	3.8 E-10			
373-376	8.2 E-11*			
376-379	3.4 E-11*			
379-382	7.1 E-9			
382-385	9.8 E-9	2.0 E-9	1.3 E-9	1.5
385-388	6.1 E-11*			
388-391	1.4 E-10			
391-394	6.9 E-11*			
394-397	1.8 E-10			
397-400	1.7 E-9			
400-403	3.5 E-10			
403-406	1.8 E-10			
406-409	4.2 E-9			
409-412	1.7 E-10			
412-415	6.7 E-11*	1.0 E-9	8.1 E-10	1.2
415-418	1.2 E-9			
418-421	1.3 E-9			
421-424	2.8 E-9			
424-427	2.4 E-10			
427-430	4.6 E-11*			

Table 4 cont.

Section (m)	Hydr cond 3 m (m/s)	Hydr cond (30 m) calculated from 3 m values (m/s)	Hydr cond 30 m (m/s)	T-quotient
430-433	7.0 E-10			
433-436	7.8 E-11*			
436-439	7.8 E-11*			
439-442	1.2 E-10			
442-445	1.5 E-10	5.6 E-9	5.6 E-9	1.0
445-448	1.0 E-10			
448-451	2.4 E-10			
451-454	3.0 E-8			
454-457	2.4 E-8			
457-460	1.1 E-10			
460-463	2.8 E-8			
463-466	9.9 E-11*			
466-469	1.2 E-10			
469-472	2.9 E-10			
472-475	8.0 E-11*	3.0 E-9	8.0 E-9	2.7
475-478	7.5 E-10			
478-481	1.1 E-10			
481-484	1.7 E-10			
484-487	1.8 E-10			
487-490	3.4 E-10			

* uncertain value (i.e. below measurement limit 1.0 E-10 m/s)

4. GROUNDWATER LEVELS

4.1 GROUNDWATER LEVEL MAP

As a basis for future modeling of groundwater flow in the Lansjärv area a groundwater level map was constructed, c.f. Figure 6. There are no boreholes in the area that only penetrate the surficial parts, and therefore a general relationship between topography and the depth to the groundwater table has been used. Further, it is assumed that wetlands and streams are groundwater tables and that the groundwater level under isolated high areas is about 10 to 15 m below the ground level.

According to the map, the general direction of the surficial groundwater flow in the area appears to be towards SE, but in the western part the gradient is steep in the SW direction.

4.2 PIEZOMETRIC HEAD IN THE BEDROCK

The location of the boreholes are shown in Figure 6. The ground water level in the boreholes was measured 1988-06-11 and 1988-10-17 and are presented in Table 5.

Table 5 Altitude of the groundwater level in Lansjärv.

Bore-hole	Borehole length (m)	Borehole incl (°)	Ground level (m a s l)	Groundwater level 88-06-11 (m a s l)	88-10-17 (m a s l)
KLJ01	500	85	+153,5	+134,0	135,3
HLJ01	75	70	+153,7	-	151,1
HLJ02	84	85	+177,9	-	121,0*
HLJ03	92	85	+172,2	+102,5	105,7

* uncertain value

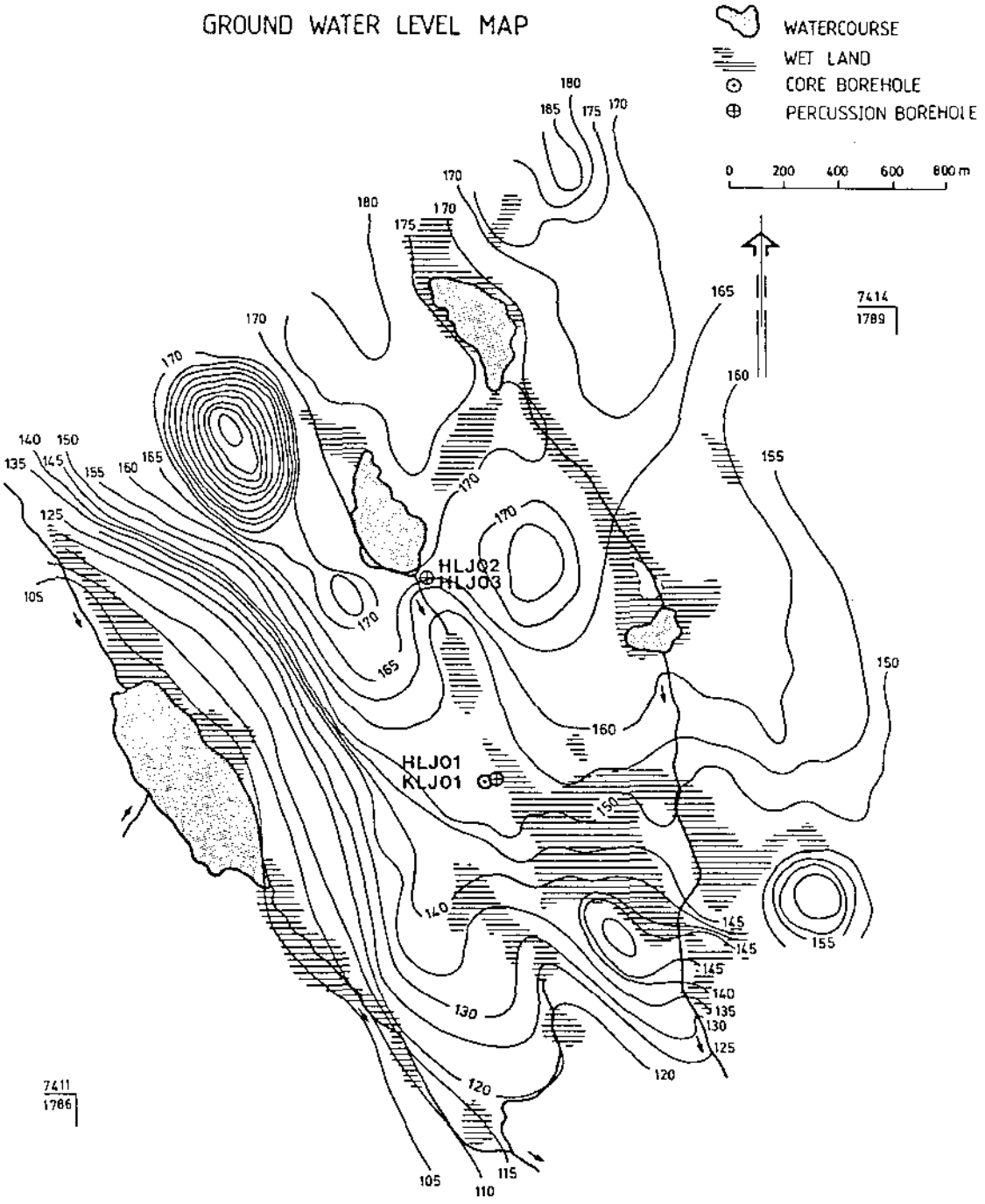

Figure 6 Groundwater level map of the Lansjärv area.

As can be seen in Table 5 the two percussion holes (HLJ02 and HLJ03) located close to the intersection of the fracture zone with the ground surface, have groundwater levels approximately 55 - 65 m below the ground surface.

In connection with the hydraulic tests performed in 30 m sections during August 1988 the groundwater pressure was registered in the isolated sections both during packer inflation (including open communication to the pipe string during 30 min), and after the section was shut off from the pipe string for an additional 60 min.

Figure 7 shows hydraulic conductivity and calculated groundwater pressures (from the pressure transducer) as metre water column plotted versus the borehole length (crosses). Only pressure values from sections with a hydraulic conductivity $\geq 10^{-9}$ m/s have been plotted. These values are obtained from the end of the pressure adjustment period. For the two lowermost sections extrapolated pressures (to one week) are also presented (dots). The hydrostatic pressure in the open borehole is shown as a solid line.

The groundwater pressures measured at different depths in the borehole were checked against groundwater level in the open borehole and vertical depth of the pressure transducer (based on borehole deviation data). The average (absolute) error of pressure readings is $\pm$ 0.1% (i.e. $\leq$ 1.0 m). The salinity in the borehole is very low, approx. 50 ppm, and errors caused by density differences are negligible.

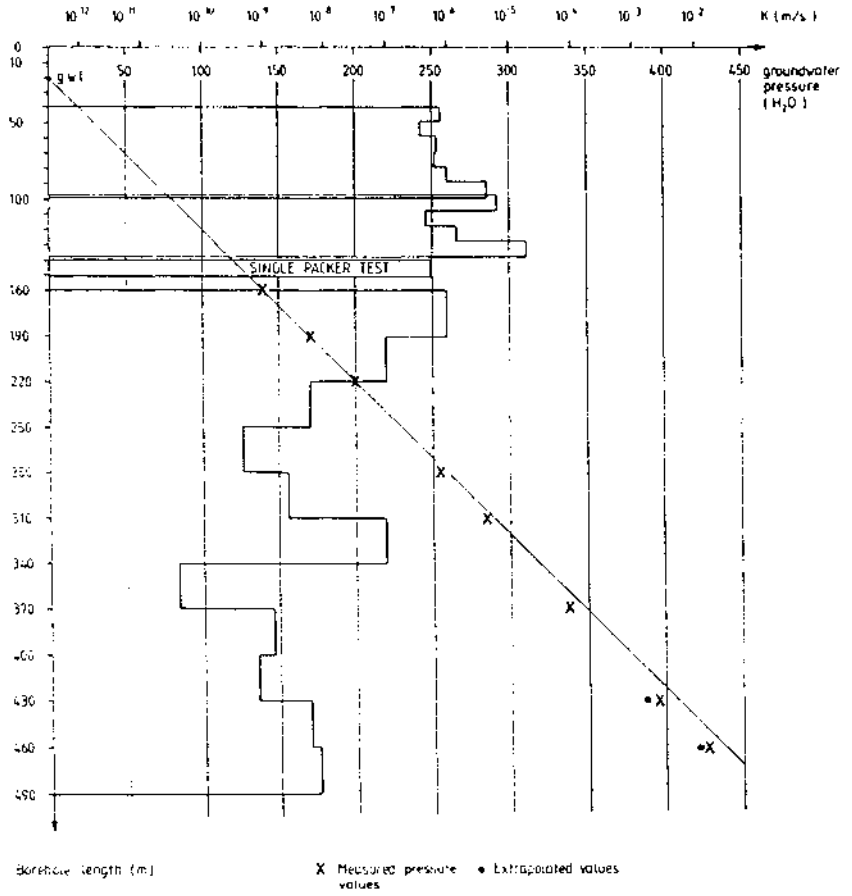

Figure 7 Hydraulic conductivity and groundwater pressure in KLJ01.

The groundwater level in KLJ01 is located about 20 m below the ground surface. The pressure levels from 280 m and downwards show values that are an additional 10 - 20 m lower, with decreasing pressure levels towards the bottom of the borehole. This pressure distribution indicates that there probably exists a hydraulic conductor with low pressure level below the bottom of KLJ01. Alternatively, the thin zones and the single fractures in the lower part of the borehole may be interconnected with some depression in the surrounding landscape without having a hydraulic connection with the highly conductive fracture zone which lower parts extend to a depth of approximately 190 m.

The measured pressure values presented in Figure 7 have been used to predict the pressure in a hypothetical fracture zone, located some 600 m and 700 m below the ground surface. This was made by using first- and second-order polynomials. For the first-order polynomial the pressure level at 600 m was 38 m below the ground surface and at 700 m it was 44 m below the surface. Corresponding values for the second degree polynomial were 47 m and 56 m.

5. CONCLUSIONS

Three percussion boreholes and one cored borehole were drilled in the Lansjärv area, located in the northern part of Sweden, in order to investigate a fracture zone with signs of postglacial activity. The core borehole KLJ01 has been tested hydraulically. The upper part of the borehole (39 - 190 m) has a high hydraulic conductivity ($> 10^{-7}$ m/s). The greatest value was found in the sections 128 - 138 m and 181 - 190 m. From 190 m to 300 m the hydraulic conductivity (3 m sections) decreases successively to the lower measurement limit of 3 m tests (10^{-10} m/s). Below 300 m, most of the tests yield values around the lower measurement limit. However, even in this region, hydraulic conductivities exceeding 10^{-8} m/s can be found.

The direction of the surficial groundwater flow in the area seems to be towards SE in general, but in the western part of the area the hydraulic gradient is steep towards SW.

The measured groundwater tables in the percussion boreholes HLJ02 and HLJ03, located close to the intersection of the fracture zone with the ground surface, have groundwater tables about 55 - 65 m below the surface.

The groundwater level in corehole KLJ01 is located about 20 m below the ground surface. The pressure levels from 280 m and downwards show values an additional 10 - 20 m lower, with decreasing pressure levels towards the bottom of the borehole. This pressure pattern indicates that there probably exists a hydraulic conductor with low pressure level below the bottom of KLJ01. Alternatively, the thin zones and the single fractures in the lower part of the borehole may be interconnected with some depression in the surrounding landscape without having a hydraulic connection with the highly conductive fracture zone which lower parts extend to a depth of approximately 190 m.

6. REFERENCES

Henkel, H., 1988: Tectonic studies in the Lansjärv region. SKB TR 88-07.

Moye, D.G., 1967: Diamond drilling for Foundation Exploration. Civil Eng. Trans., Inst. Eng. Australia, April 1967, pp 95-100.

Hydrofracturing stress measurements in borehole KLJ01, Lansjärv

Bjarni Bjarnason, Luleå University of Technology

March 1989

ABSTRACT

Rock stress measurements have been conducted by the hydrofracturing method in the 500 m deep borehole KLJ01 in the Lansjärv area in Northern-Sweden. The borehole intersects the gently dipping plane of a post-glacial fault at approximately 150 m depth. Results were obtained within a 200 m section of the borehole, between 300-500 m depth, but high fracture frequency precluded stress determination at other levels. Between 400 m and 500 m the maximum horizontal stress and the theoretical vertical stress are nearly equal in magnitude whereas the minimum horizontal stress is only half that value. The orientation of hydrofractures turns approximately 90° over a depth interval of less than 200 m, from N30°W at 300 m to N60°E at 500 m depth.

Contents

SUMMARY

The rock stress measurements at Lansjärv form a part of a larger research project on the tectonic stability of the swedish bedrock, initiated and run by SKB. It is a further step in the overall research into the suitability of the precambrian swedish bedrock as a hostrock for a nuclear waste repository. The measurements were not intended to show the regional stress state at Lansjärv but rather to throw some light on possible stress anomalies associated with the post-glacially active faults in the are.

The stress measurements were conducted in a 500 m deep vertical borehole, KLJ01, near the village of Lansjärv in Northern Sweden. The borehole is located in an area of recent tectonic activity and it is believed to intersect the plane of a gently dipping post-glacial fault at a depth of 150 m. Casing in the borehole down to 150 m depth and high fracture frequency below the casing precluded stress measurements at shallower levels than 300 m.

The results show magnitudes and orientations of maximum and minimum stress components in the horizontal plane, at depths from 300 m to 500 m depth. The minimum horizontal stress is lower in magnitude than the lithostatic vertical stress at all depths. Near the bottom of the borehole the minimum horizontal stress is extremely low, showing only half the value of the vertical overburden stress. The maximum horizontal stress is from 1.6 to 2.0 times larger in magnitude than the minimum horizontal stress. The orientations of hydrofractures in the borehole turn more than 90° over a depth interval of less

than 200 m, from N39°W at 323.5 m to N60°E at the bottom of the borehole. The stress state at 400-500 m can be described as:

SH = Sv = 2Sh

with SH oriented N50-60°E.

It is most probable that principal stress orientations are influenced by the immediate vicinity of the fault plane and that SH, Sh and Sv are not principal tresses.

1 INTRODUCTION

1.1 BACKGROUND

The rock stress measurements presented in this report form a part of a larger research project on the tectonic stability of the swedish bedrock. The field studies within the bedrock stability project have been concentrated to the neotectonic active Lansjärv area in Northern Sweden. The bedrock stability project, initiated by SKB, is a further step in the overall research into the suitability of the precambrian swedish bedrock as a hostrock for an intended nuclear waste depository.

1.2 GEOGRAPHICAL AND GEOLOGICAL SETTING

The Lansjärv area is located in the northernmost part of Sweden, near to the Bay of Bothnia, approximately at 66°N and 22°E. The geographical location of the study area is shown in Figure 1-1.

The choice of the Lansjärv site for the bedrock stability research project is primarily based on the occurrence of about 45 km of post glacial fault scarps within an area of 150 x 200 km. Furthermore, it offers good road access, a large amount of detailed geophysical data and the occurrence of several regionally extending fault systems, Henkel 1988.

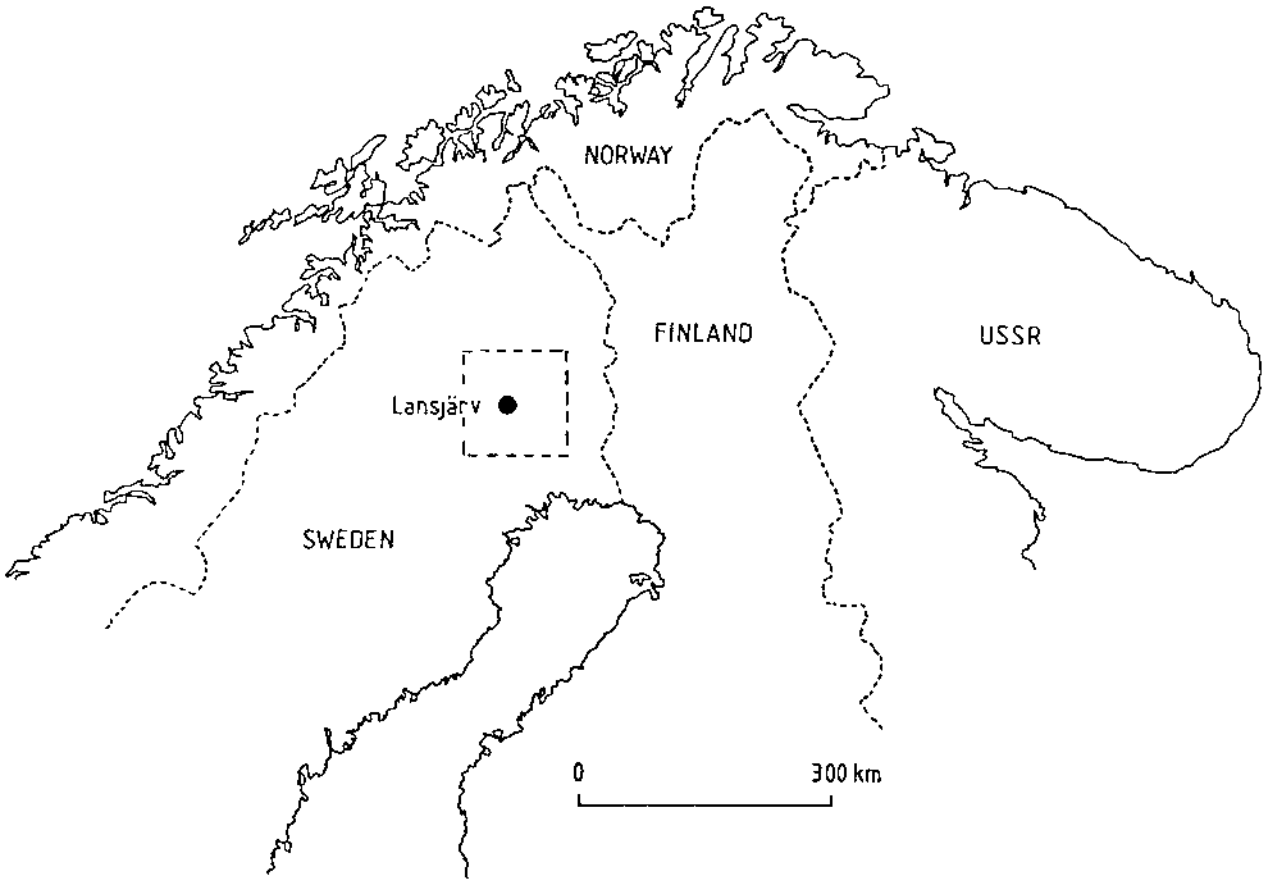

Figure 1-1 Geographical location of the Lansjärv study area.

2 THEORY, INSTRUMENTATION AND TESTING PROCEDURE

A detailed description of the hydrofracturing method and the instrumentation used lies outside the scope of this study. The interested reader is referred to a thorough presentation given in Bjarnason, 1986, and Bjarnason and Stephansson, 1986. The sections below give an introduction to the subject.

2.1 THEORY

The stress calculations for the crystalline rocks tested at Lansjärv follow the classical theory for hydraulic fracturing in almost impermeable, isotropic and linear elastic medium, Hubbert and Willis, 1957. The vertical stress Sv is calculated from the weight of the overlying rock mass in each test point according to:

$$Sv = gz \qquad (1)$$

where;

Sv = vertical stress
g = unit weight of the rock mass
z = depth from the ground level

The minimum and maximum horizontal stresses are calculated using data from the pressure records obtained from vertical hydrofractures, (coplanar with the borehole axis), according to the following equations:

$$Sh = Ps \qquad (2)$$
$$SHI = 3Sh - Pb + T \quad \text{or} \qquad (3)$$
$$SHII = 3Sh - Pr \qquad (4)$$

where;

Sh = minimum horizontal stress
Ps = shut-in pressure on the fracture plane
SHI = maximum horizontal stress by the first breakdown method
SHII = maximum horizontal stress by the second breakdown method

Pb = breakdown pressure (fracture initiation pressure)
T = tensile strength of intact rock under hydraulic fracturing conditions
Pr = reopening pressure of the hydrofracture

The first breakdown method,SHI applies a fixed value for the hydrofracturing tensile strength of the rock, T. The value of T is determined by laboratory tests on core samples from the borehole. A central axial borehole, drilled through the core sample is pressurized internally by water until fracturing occurs. The values of T are obtained from fracturing tests in boreholes of 10 mm diameter in the core samples. A scale factor of 0.62 is used to extrapolate the laboratory results to apply for the 56 mm borehole in the field, according to Parish and Sih,1965 and Doe et al.1983.

For the second breakdown method the difference between the breakdown pressure and the reopening pressure, Pb - Pr,is used as a measure of the hydrofracturing tensile strength of the rock at each test point. (See Figure 2-1 and Table 4-2).

The crystalline rock matrix is considered as being impermeable to water and a pore pressure term has not been included in equations (3) and (4) to determine SH.

Shut-in pressures from the field curves are selected by the tangent method at the point of intersection between two tangent lines. One is drawn to the immediate pressure drop following shut-down, and the other is drawn to the almost linear part of the post-shut-in part of the curve. A typical pressure-time record from the measurements at Lansjärv is shown in Figure 2-1.

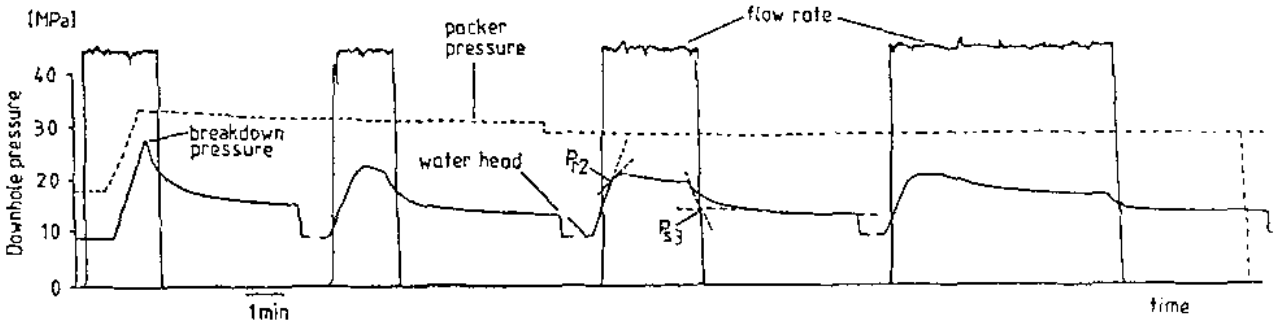

Figure 2-1 A typical hydrofracturing record from the stress measurements in Lansjärv. Borehole KLJ01, depth 469.3 m. Different vertical scales, the scale shown on the vertical axis is for the downhole test pressure.

Breakdown and reopening pressures are defined as the points for each cycle where the pressure-time curve during pressurization begins to deviate from linearity (Figure 2-1).

The orientation of the horizontal stresses is determined from the strike of the hydrofractures created at each test point. In isotropic rock material the orientation of hydrofractures will be controlled by the stress directions in the rock mass surrounding the borehole. Under ideal circumstances the hydrofracture will initiate in a vertical plane, perpendicular to the minimum horizontal stress. The orientation of the hydrofractures is determined by an impression packer coupled to a single-shot magnetic compass.

2.2 INSTRUMENTATION

Field measurements were conducted by the hydrofracturing instrumentation at the Division of Rock Mechanics at Luleå University of Technology. A detailed description of the instrumentation is given in Bjarnason and Torikka, 1989. Downhole tools are run in the borehole and operated by a 1000 m long multihose, containing hydraulic tubing and signal cables for downhole communication. Flow rates and pressures are

water and the packers is measured by pressure transducers at the manifold. Water flow rates to the test section are measured by in-line turbine flow meters at the outlet from the manifold. The downhole pressure in the test section is measured by a pressure transducer located within the straddle packer unit, giving direct readings to surface through the signal cable. This eliminates corrections for flow dependent pressure drops in the pressure line and for the water head at the test depth. The main components of the instrumentation are:

- Downhole packer assemblies: A straddle packer assembly for isolating the test section during fracturing of the rock and registration of pressure-time curves for evaluation of stress magnitudes. A single impression packer to orientate fractures in the borehole wall. A single-shot magnetic compass is attached to the impression packer to orientate it during the impression period.

- A water system including a 100 MPa water pump to fracture the rock and inject water to the fractures, and a manifold and an adjustable bypass valve to control pressure and flow during testing.

- A data acquisition system to record pressure and flow data during testing.

- A multihose to operate the downhole equipment from the surface. The multihose is composed of high pressure hoses, signal cable and a load wire, all included in a polyurethane outer jacket.

2.3 TESTING PROCEDURE

Test sections of intact rock are chosen from the detailed fracture log of the drill core. The straddle packer is lowered to the test depth and inflated by water. The straddle packer and the test interval are pressurized simultaneously to avoid high stress concentrations at the packer ends. The packers are controlled through a separate pressure line and the packer pressure is kept slightly above the test section pressure throughout the test cycle. A pressure transducer for the fracturing pressure is located within

the straddle packer assembly giving direct readings to surface through the signal cable. Packer pressures are read at surface together with a double check on the fracture test pressure.

Fracturing is conducted at constant flow rate, about 3.5 l/min, usually resulting in breakdown within 30 to 40 seconds. The test line is shut down immediately after breakdown is observed, and a first shut-in pressure is recorded. The shut-in curve is normally recorded 3 to 4 minutes after shut down. Venting of the test section after each pressurization cycle is normally conducted until pressure rebounds after repeated closing of the test line fade out. The first pressurization cycle is followed by three cycles where pressurization is conducted at the same constant flow rate. The pumping time after reopening the fracture is increased for each cycle. This causes a stepwise propagation of the fracture out from the borehole with the aim to record the change in shut-in pressure as a function of fracture extension or geometry.

Fracture impressions are taken at the test points after terminating fracturing and injections. The impression packer is inflated at the test point for 30-40 minutes. The orientation of the impression packer, recorded by magnetic compass during the impression period, enables the determination of the hydrofracture orientation.

3 SITE CONDTIONS AND FIELD WORK

3.1 SITE CONDITIONS

The borehole KLJ01 is lying about 10 km NE of the village of Lansjärv, Figure 3-1. It is located between two NW striking fault zone segments, the Ängesån segment to the north and the Lansån segment to the south. The escarpment of a postglacial fault trending NNE passes in a NS direction some 900 m to the west of the borehole (PGF in Figure 3-1). The original length of the borehole was 500.60 m of 56 mm diameter, dipping 85° to the NW (315°). It was expected to intersect the postglacial fault at a vertical depth of about 150 m.

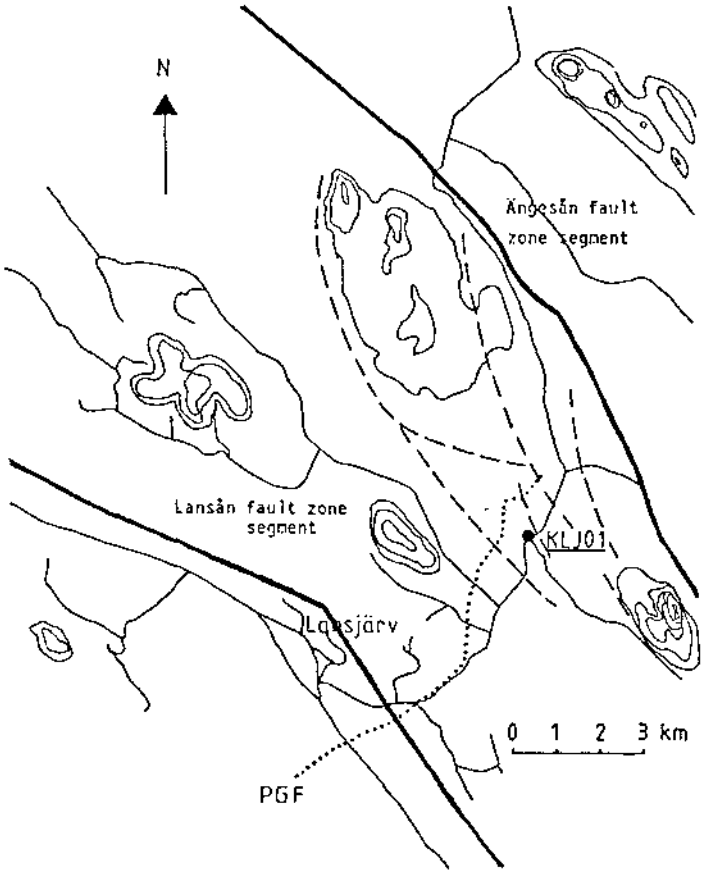

Figure 3-1 Location of borehole KLJ01 related to tectonics of the Lansjärv area.

It took 3 .5 months to complete the borehole due to severe stability problems in the heavily fractured and locally crushed rock mass. The hole had to be cased down to 152 m to manage to cross a crushed zone at 150 m. From surface down to approximately 300 m the fracture frequency in the drill core is generally very high, with a broad increase between 100-300 m, Figure 3-2. Zones of crushed rock are found throughout the borehole but most frequently between 100-250 m.

The most common rock in the borehole is granite, often occurring as recrystallized, gneissic or foliated with pegmatite rests.

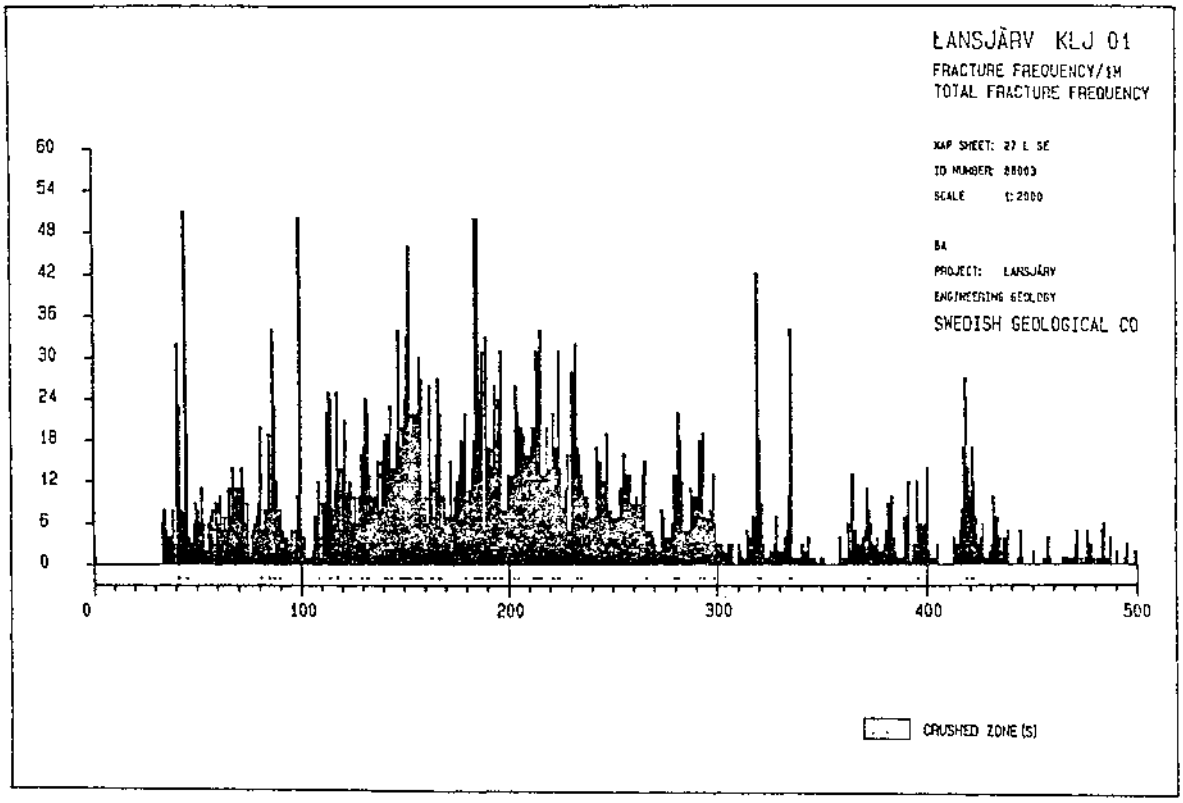

Figure 3-2 Fracture frequency in the rock core from borehole KLJ01 in Lansjärv.

3.2 FIELD WORK

The field work in Lansjärv was conducted from 10th of September till 3rd of October 1988. Difficulties were experienced in the borehole work from the beginning due to instability of the borehole walls within some of the crushed zones. The packer assemblies had to be run very slowly to avoid getting stuck. This resulted in excessively long running times during the fracture impression work.

The borehole is cased down to 152 m depth, which precluded measurements at shallower levels. The high fracture frequency in the rock (Figure 3-2) further precluded successful stress measurements from the end of the casing down to approximately 300 m depth.

After finishing half of the fracturing work and a few fracture orientations the borehole collapsed at 240 m depth. A 3 m long, thick-wall steel pipe of 50 mm OD weighing 80 kg, was prepared to fit the cable head of the multihose. It was hooked on by a tension link of approximately 20 kN pull-off strength, 1/3 of the breaking load of the multihose. The weight was lowered down to the collapse zone at 240 m and by repeated blows it was cleared out. The fragments from the collapse zone clogged the borehole at different depths below 240 m but successively the borehole could be cleared down to bottom. The borehole stayed open but tight for the rest of the measuring period.

4 RESULTS

4.1 TEST DATA

Measurements were conducted at totally 27 different levels in the borehole. Most of the test points are located within the relatively sound rock volume at depths greater than 300 m. Attempts were made to measure stresses in six points between 220-290 m but due to difficult wall conditions with preexisting fractures, none of these points gave successful results.

All borehole depths where hydrofracturing tests were attempted are listed in Table 4-1.

Table 4-1 Hydrofracturing test depths in Borehole KLJ01.

Completed measurements		Abandoned tests
Depth [m]	Depth [m]	Depth [m]
308,5	449,0	220,5
323,5	452,0	230,0
347,5	455,0	284,0
352,0	462,5	286,0
354,0	469,3	288,0
356,5	474,5	290,0
378,4	480,3	
410,3	489,3	
440,4	491,8	
442,5	494,0	
447,0		

Twenty points out of the 21 completed measuring points listed in Table 4-1 gave good results. Pressure data from these 20 points are presented in Table 4-2.

Table 4-2 Pressure data from hydrofracturing tests in borehole KLJ01.

Depth [m]	Pb [MPa]	Pr1 [MPa]	Pr2 [MPa]	Pr3 [MPa]	Ps1 [MPa]	Ps2 [MPa]	Ps3 [MPa]	Ps4 [MPa]
308,5	13,1	6,9	6,1	5,8	5,1	4,7	4,6	5,1
323,5	14,4	8,1	7,2	6,7	6,3	5,7	5,6	5,6
352,0	13,7	11,3	10,4	9,9	8,6	8,3	7,6	7,4
354,0	14,9	10,6	10,6	10,6	9,1	8,8	8,4	7,9
356,5	13,7	10,4	9,9	9,2	9,8	8,8	8,6	8,8
378,4	19,8	11,9	11,3	9,4	9,2	9,4	9,2	9,7
410,3	16,9	11,5	9,0	7,7	7,6	7,3	7,5	7,0
440,4	14,6	8,1	7,7	7,7	7,7	7,3	7,3	7,3
442,5	14,2	10,4	9,9	9,9	8,8	7,8	8,0	8,3
447,0	17,3	7,2	6,3	5,9	6,6	6,4	6,3	6,3
449,0	14,2	9,2	6,9	5,9	6,8	6,3	6,2	6,0
452,0	16,6	10,3	6,2	5,8	7,0	5,6	5,5	5,6
455,0	18,7	12,4	11,0	5,6	8,7	6,6	6,0	5,5
462,5	14,6	8,6	7,5	6,8	6,6	5,9	5,7	5,8
469,3	13,5	9,9	9,5	9,0	8,8	7,5	7,2	6,9
474,5	17,1	9,6	7,7	6,5	7,1	5,9	5,8	5,8
480,3	13,4	9,6	8,1	7,2	8,1	7,6	7,3	6,6
489,3	16,0	12,2	7,7	7,2	8,3	6,6	6,1	6,1
491,8	14,7	10,1	7,7	7,5	7,9	6,4	6,2	6,2
494,0	13,7	7,0	6,5	6,1	6,9	6,6	6,4	6,4

Pb = Breakdown pressure (fracture initiation pressure).
Pr1 = First reopening pressure of the fracture.
Pr2 = Second reopening pressure etc.
PS1 = First shut-in pressure etc.

Results from laboratory tests on core samples from KLJ01 are listed in Table 4-3. The value of the applied tensile strength, T, has been obtained by reducing the results of the laboratory tests in Table 4-3, with a scale factor of 0.62 to apply for the 56 mm borehole in the field. A separate mean value is obtained for each main rock type tested. The hydraulic tensile strength is applied to the field results according to rock type in each test point in the borehole. The T values applied are as follows:

Gneissic granite	T	=	7.6 MPa
Grey granite	T	=	6.2 MPa
Red granite, recrystallized	T	=	4.9 MPa
Grey granite with pegmatite	T	=	3.3 MPa

Pegmatite	T	=	3.3 MPa
Foliated grey granite	T	=	3.3 MPa

Table 4-3 Results from hydrofracturing laboratory tests on core samples from KLJ01.

Depth [m]	P_i [MPa]	Depth [m]	P_i [MPa]
351,6	5,9	439,6	10,3
351,7	4,9		
351,8	5,4	451,0	8,1
352,0	10,3	451,2	7,9
352,1	10,8	451,3	8,1
352,2	10,8	451,5	8,0
		451,6	7,6
322,5	10,3		
322,7	8,9	480,5	13,0
322,8	9,9	480,9	12,1
		481,0	11,8
439,3	8,8		
439,4	9,4	488,3	9,5
439,5	8,3	488,4	9,7
		488,5	10,6

Pi = Internal pressure at fracture initiation

4.2 STRESS MAGNITUDES AND STRESS RATIOS

Horizontal stress magnitudes for the test points listed in Table 4-2 are presented in Table 4-4. Two points, 308.5 m and 378.4 m, have been omitted in Table 4-4 as fracture impressions from these points showed no reliable vertical hydrofractures in the borehole wall.

The vertical stress, Sv,shown in the table is a theoretical value calculated from the weight of the overburden according to eq. (1). Horizontal and vertical stress ratios are also shown.

Table 4-4 Stresses and stress ratios from hydrofracturing tests in borehole KLJ01, Lansjärv.

Depth	Sv	Sh	SHI	SHII	SHI / Sh	SHII / Sh	Sh / Sv	SHI / Sv	SHII / Sv
[m]	[MPa]	[MPa]	[MPa]	[MPa]					
323,5	8,5	5,6	7,4	9,7	1,3	1,7	0,7	0,9	1,1
352,0	9,3	7,6	12,4	12,5	1,6	1,6	0,8	1,3	1,3
354,0	9,3	8,4	13,6	14,5	1,6	1,7	0,9	1,5	1,6
356,5	9,4	8,8	15,9	16,4	1,8	1,9	0,9	1,7	1,7
410,3	10,8	7,5	10,4	13,4	1,4	1,8	0,7	1,0	1,2
440,4	11,6	7,3	15,0	14,4	2,0	2,0	0,6	1,3	1,2
442,5	11,7	8,0	13,0	14,0	1,6	1,8	0,7	1,1	1,2
447,0	11,8	6,3	7,8	12,6	1,2	2,0	0,5	0,7	1,1
449,0	11,8	6,2	10,7	11,7	1.7	1.9	0,5	0,9	1,0
452,0	11,9	5,5	6,0	10,4	1,1	1,9	0,5	0,5	0,9
455,0	12,0	6,0	5,3	6,9	0,9	1,2	0,5	0,4	0,6
462,5	12,2	5,7	8,7	9,6	1,5	1,7	0,5	0,7	0,8
469,3	12,4	7,2	14,2	12,0	2,0	1.7	0,6	1,1	1,0
474,5	12,5	5,8	6,2	9,5	1,1	1,7	0,5	0,5	0,8
480,3	12,7	7,3	16,2	13,9	2,2	1,9	0,6	1,3	1,1
489,3	12,9	6,1	8,6	10,6	1,4	1,7	0,5	0,7	0,8
491,8	13,0	6,2	9,8	10,8	1,6	1,7	0,5	0,8	0,8
494,0	13,0	6,4	11,4	12,6	1,8	2,0	0,5	0,9	1,0

Sv = Calculated vertical overburden stress
Sh = Minimum horizontal stress
SHI = Maximum horizontal stress according to eq. (3)
SHII = Maximum horizontal stress according to eq. (4)

The results of the stress measurements as presented in Table 4-4 are plotted in Figure 4-1 through 4-3. The assumed vertical stress is shown by a solid line in all the figures.

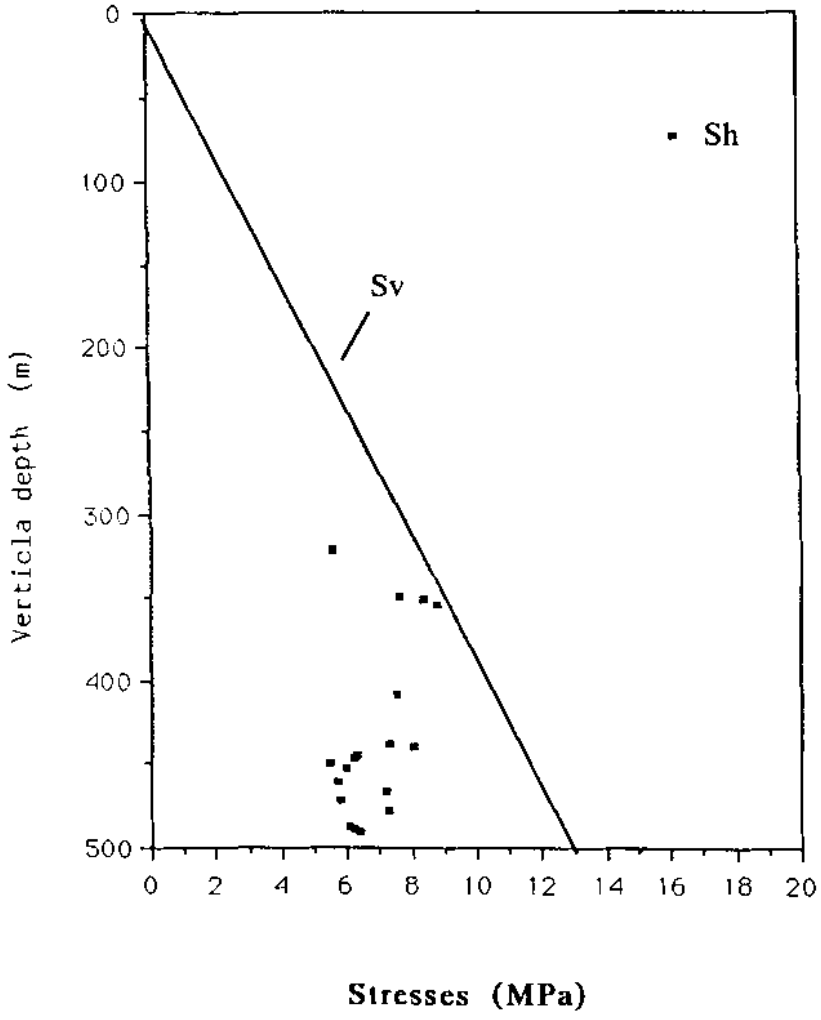

Figure 4-1 The minimum horizontal stress, Sh, as a function of depth in borehole KLJ01, Lansjärv. The vertical stress, Sv, is a theoretically assumed value.

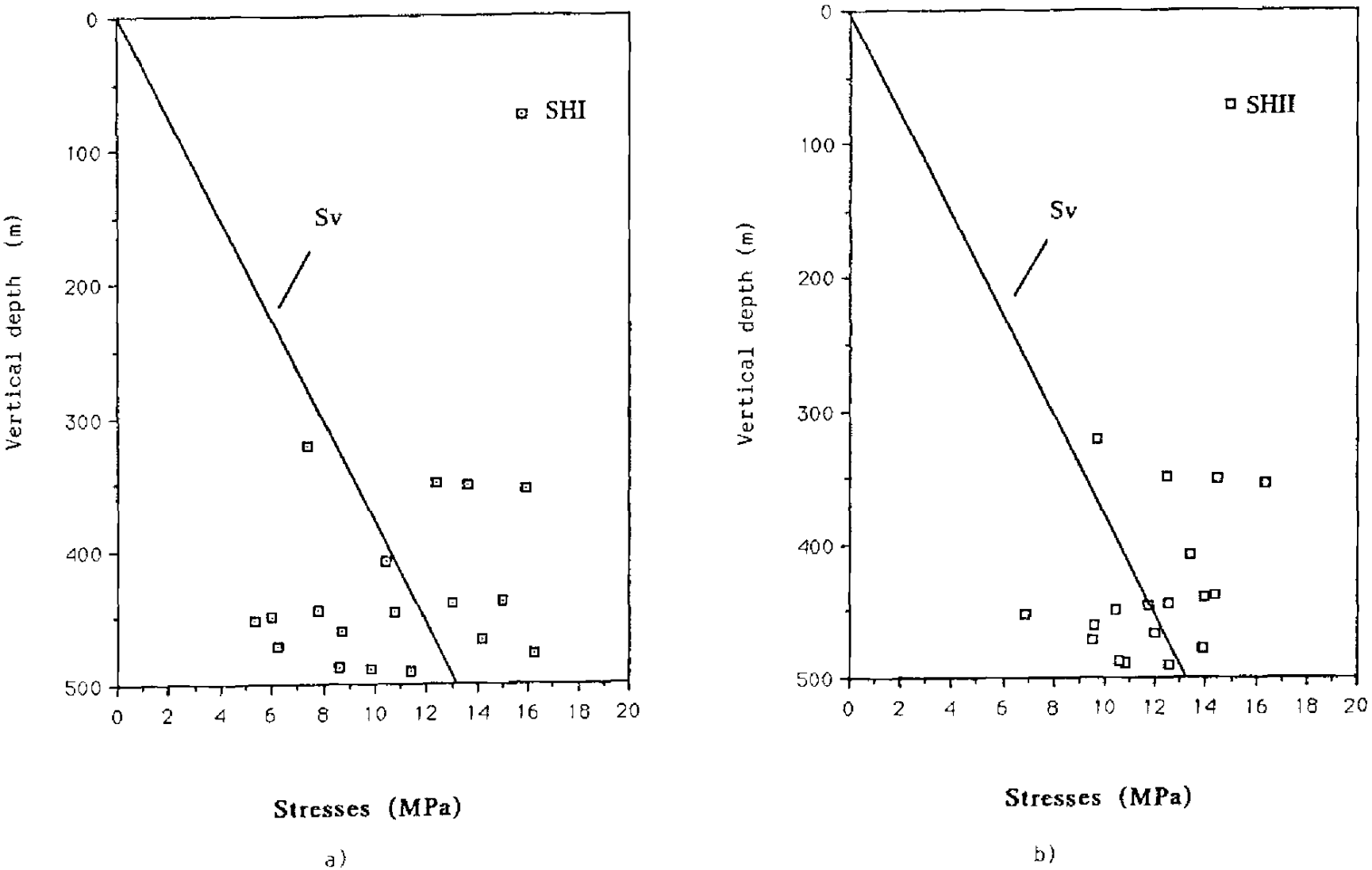

Figure 4-2 Maximum horizontal stress vs. depth in borehole KLJ01. The vertical stress, Sv, is a theoretically assumed value. a) SHI, maximum horizontal stress by the first breakdown method applying laboratory values for the hydraulic tensile strength, T. b) SHII, maximum horizontal stress by the second breakdown method applying field values for T, (T = Pb-Pr).

Results from both first- and second breakdown methods are presented here for the sake of completeness, as both methods are applied by researchers in the field of hydrofracturing stress measurements. However, as the second breakdown method (Figure 4-2,b) takes into account the actual rock conditions at each test point in the borehole it is believed to give a more realistic picture of the true stress field in the rock mass.

In Figure 4-3 both Sh and SHII are plotted together as a function of depth.

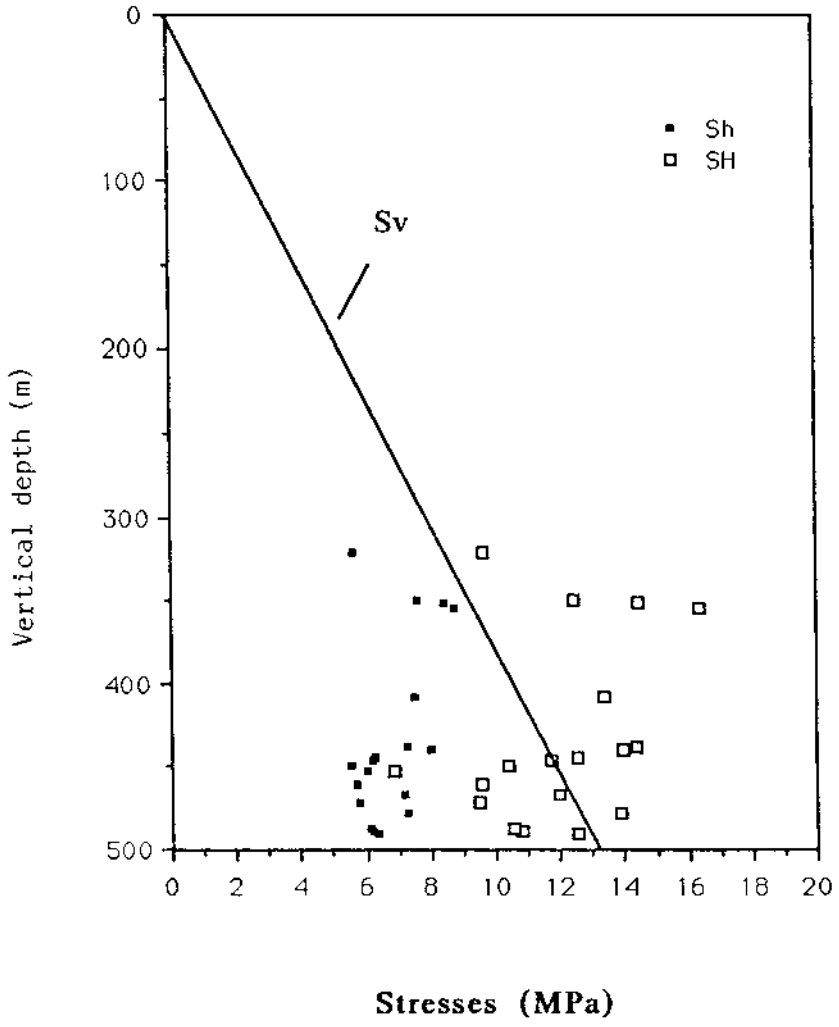

Figure 4-3 Minimum and maximum horizontal stresses as a function of depth in the rock mass. SH shows the second breakdown values. Sv is the assumed overburden stress.

4.3 ORIENTATION OF HORIZONTAL STRESSES

Fracture impressions were taken at 19 test points in the borehole. Results from all fracture impressions are presented in Table 4-5. Two of the impressions showed no vertical hydrofractures and gave no information on horizontal stress orientations. Furthermore, the test point at 494.0 m depth was too close to the bottom of the borehole to allow impression to be taken due to the length of the compass barrel.

Table 4-5 Orientation data for hydraulically created fractures in KLJ01.

Depth [m]	Toolface [°]	F1 [°]	F2 [°]	SH [°]
308,5	239	No reliable vertical fracture		
323,5	119	81	265	39W
347,5	185	168	337	17W
352,0	274	90	336	24W
354,0	37	4	181	3E
356,5	254	175	359	3W
378,4	295	No reliable vertical fracture		
410,3	51	53	171	(53E)
440,4	157	21	193	17E
442,5	237	22	201	22E
447,0	228	62	239	61E
449,0	77	50	233	52E
455,0	58	60	237	59E
462,5	19	60	208	44E
469,3	300	43	223	43E
474,5	48	48	223	46E
480,3	140	70	252	71E
489,3	117	56	236	61E
491,8	193	65	240	60E
494,0	No orientation, bottom of borehole			

Tool face = Orientation of reference line on packer referred to N. F1 = Orientation of fracture 1. F2 = Orientation of fracture 2. ( ) = Fracture orientation not reliable. SH = Orientation of maximum horizontal stress.

Orientations of the maximum horizontal stress, SH, are plotted versus depth in Figure 4-4. The figure shows rotation of SH with depth of approximately 90° over a depth interval of only 150 m.

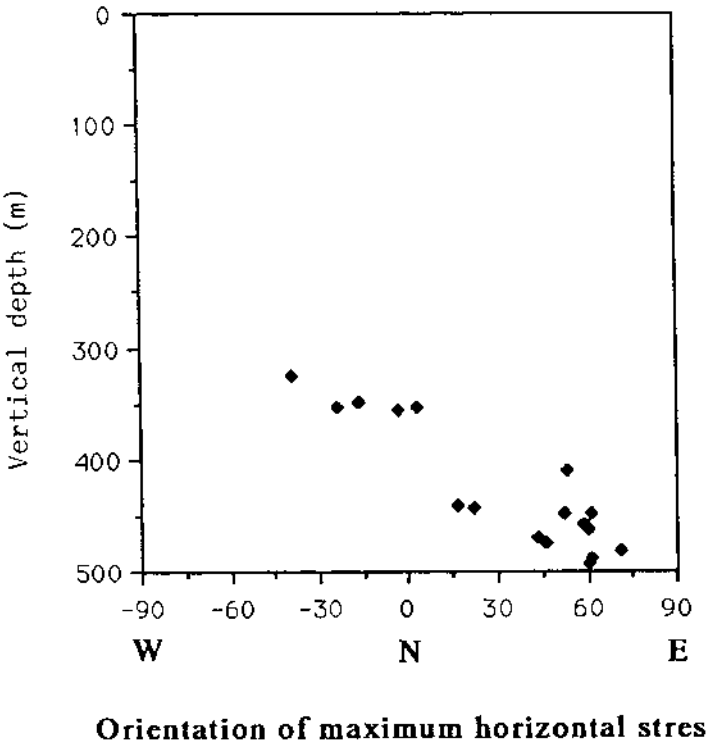

Figure 4-4 Orientation versus depth of the maximum horizontal stress, SH, as inferred from hydrofracture orientations.

5 DISCUSSION AND CONCLUSIONS

The stress measurements in borehole KLJ01 in Lansjärv differ from earlier hydrofracturing stress measurements in Sweden with respect to the tectonics of the research area. The Lansjärv region is situated at the southern extremity of the 600 x 200 km Senja tectonic lens, Henkel 1988. A post-glacial fault reaches ground surface only 900 m to the west of the borehole, Figure 3-1. The fault plane has a low ESE dip and the borehole is believed to intersect the fault plane at approximately 150 m depth.

The results of the stress measurements show magnitudes and orientations of maximum and minimum stress components in the horizontal plane, at depths between 300 - 500 m. Unfortunately, casing in the borehole down to 150 m depth and a very high fracture frequency below the casing precluded stress measurements at shallower levels than 300 m.

The minimum horizontal stress, Figure 4-1, has a magnitude which is lower than the lithostatic vertical stress at all depths. The stress ratio, Sh/Sv is 0.7 at 300 m, then increases rapidly with depth to reach a maximum value of 0.9 around 350 m depth. Between 400-500 m Sh shows no increase with depth but is roughly confined within the limits 6-8 MPa. Sh is extremely low near the bottom of the borehole where the average value between 450-500 m is only 6.2 MPa, compared to a theoretical value of 12.6 MPa for the vertical stress at 475 m depth. This is far the lowest horizontal stress measured at similar depths by the hydrofracturing method in Sweden.

The maximum horizontal stress, Table 4-4 and Figure 4-3, is from 1.6 up to 2.0 times larger in magnitude than the minimum horizontal stress. From 300 m down to approximately 450 m depth, SH is somewhat larger than the lithostatic vertical stress but at deeper levels the SH/Sv ratio is close to, or lower than, unity. Between 400-500 m the magnitude of SH is spread

between approximately 10 and 14 MPa but shows no increase with depth.

The vertical stress, Sv, as presented in this report is a pure estimate. Occasionally the validity of the vertical stress estimate can be checked in the field by hydraulic jacking tests on preexisting horizontal fractures. Where this has been successfully done in Sweden the jacking pressure on horizontal fractures has been in good agreement with the lithostatic estimate. In Lansjärv however, no such horizontal jacking results were obtained.

The SH orientations obtained in borehole KLJ01 are most unusual. At 323.5 m depth the SH direction is N39°W. It then turns rapidly with increased depth and reaches N60°E at the bottom of the borehole, turning approximately 90° over a depth interval of less than 200 m. Between 400 m and 500 m most of the SH orientations fall within N50-60°E.

The general assumption for hydrofracturing measurements in vertical boreholes in undisturbed areas is that principal stresses are horizontal and vertical. In the Lansjärv case such an assumption is not straight forward. It is most probable that principal stress orientations are influenced by the immediate vicinity of the fault plane and that SH, Sh, and Sv are not pure principal stresses. This is supported by the rapid change in orientation observed for the maximum horizontal stress.

The state of stress in the rock mass at depths between 400-500 m in KLJ01 can roughly be described as:

SH = Sv = 2Sh

with SH oriented N50-60°E.

The measurements were not intended to show the regional stress state at Lansjärv but rather to throw some light on possible stress anomalies associated with active faults.

6 REFERENCES

Bjarnason, B. 1986. Hydrofracturing rock stress measurements in the Baltic Shield. Licentiated Thesis 1986: 12 L. Luleå University, Luleå.

Bjarnason, B. and Stephansson, O. 1986. Hydraulic fracturing rock stress measurements in borehole Gi-1 Gideå study site, Sweden. SKB Technical Report 86-11. SKB (Swedish Nuclear Fuel and Waste Management Co.), Stockholm.

Bjarnason, B. and Torikka, A. 1989. Field instrumentation for hydrofracturing stress measurements. Documentation of the 1000 m hydrofracturing unit at Luleå University of Technology. SKB Technical Report (in press).

Doe T W, Ingevald K, Strindell L, Leijon B, Hustrulid W, Majer E and Carlsson H 1983. In Situ Stress Measurements at the Stripa Mine, Sweden. Report LBL-15009, SAC44. Swedish-American Cooperative Program on Radioactive Waste Storage in Mined Caverns in Cristalline Rock. 251 p.

Henkel, H. 1988. Tectonic studies in the Lansjärv region. SKB Technical Report, Stockholm, 88-07.

Hubbert M K and Willis D G 1957. Mechanics of hydraulic fracturing. Trans. A.I.M.E., 210, pp. 153-168.

Paris P and Sih G 1965. Stress analysis of a crack. In: Fracture Toughness and its Testing. American Society of Testing and Materials Special Publications 381, pp. 30-83.